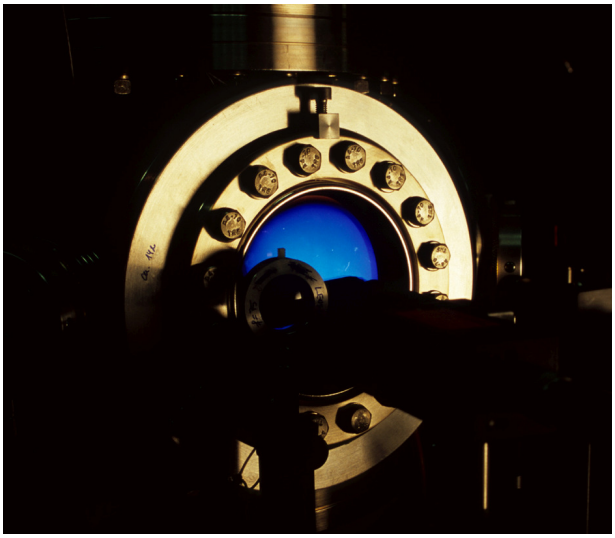

ICTP-SAIFR school 6.-17. of March 2023 on the

Interaction of Light with Cold Atoms

Lecture on

Atom-Light Interaction *and Basic Applications*

Ph.W. Courteille
Universidade de São Paulo
Instituto de Física de São Carlos
13/03/2023

2

.

.

Preface

The following notes have been prepared for the ICTP-SAIFR school on *'Interaction of Light with Cold Atoms'* held 2023 in São Paulo. They are conceived to support an introductory course on *'Atom-Light Interaction and Basic Applications'*. The course is divided into 5 lectures and a bonus.

Cold atomic clouds represent an ideal platform for studies of basic phenomena of light-matter interaction. The invention of powerful cooling and trapping techniques for atoms led to an unprecedented experimental control over all relevant degrees of freedom to a point where the interaction is dominated by weak quantum effects. This course reviews the foundations of this area of physics, emphasizing the role of light forces on the atomic motion. Collective and self-organization phenomena arising from a cooperative reaction of many atoms to incident light will be discussed.

The course is meant for graduate students and requires basic knowledge of *quantum mechanics* and *electromagnetism* at the undergraduate level. The lectures will be complemented by exercises proposed at the end of each lecture. The present notes are mostly extracted from some textbooks (see below) and more in-depth scripts which can be consulted for further reading on the website http://www.ifsc.usp.br/∼strontium/ under the menu item 'Teaching' ⟶ 'Cursos 2023-1' ⟶ 'ICTP-SAIFR pre-doctoral school'. The following literature is recommended for preparation and further reading:

Ph.W. Courteille, script on *Electrodynamics: Electricity, magnetism, and radiation* (2018)

Ph.W. Courteille, script on *Quantum mechanics applied to atomic and molecular physics* (2019)

H.J. Metcalf, P. van der Straten, *Laser Cooling and Trapping*, (Graduate Texts in Contemporary Physics, Springer, 1999)

J. Weiner and P-T. Ho, *Light-Matter Interaction: Fundamentals and Applications* (Springer-Verlag, Berlin, 2003)

Ch.J. Foot, *Atomic physics*, (Oxford Master Series in Atomic, Optical and Laser Physics, 2005)

R. Loudon, *The quantum theory of light* (Oxford Science Publications, Oxford, 1973)

Ch.C. Gerry and P.L. Knight, *Introductory Quantum Optics* (Cambridge University Press, 2005)

P. Meystre and M. Sargent III, *Elements of Quantum Optics* (Springer-Verlag, Berlin, 1990)

I.I. Sobelman, *Atomic Spectra and Radiative Transitions* (Springer Verlag, Berlin, 1977)

M. Weissbluth, *Photon-Atom Interactions* (Academic Press, Boston, 1989)

C. Cohen-Tannoudji, B. Diu, F. Laloe, *Quantum mechanics, vol. 1*, (Wiley Interscience, 1977)

D.J. Griffiths, *Introduction to Quantum mechanics*, Pearson Education Limited (2014)

L.I. Schiff, *Quantum mechanics* (McGraw-Hill Book Company, 1968)

J.J. Sakurai, J.J. Napolitano, *Modern Quantum Mechanics*, 2nd ed., (2011)

Content

1 Two-level atom in a radiation field **1**
1.1 Introduction . . . 1
1.1.1 Atoms and photons . . . 1
1.1.2 Definition of the research area . . . 3
1.2 Two-level systems in quantum mechanics . . . 6
1.2.1 Time-dependent perturbations . . . 7
1.2.2 Light-shift in the semi-classical picture . . . 10
1.2.3 Numerical simulations and quantum jumps . . . 11
1.3 Exercises . . . 14
1.4 Further reading . . . 16

2 The Bloch equations **17**
2.1 Density operator . . . 18
2.1.1 Matrix formalism . . . 19
2.1.2 Spontaneous emission . . . 21
2.1.3 Temporal evolution of the density operator . . . 25
2.2 Bloch equations for two-level atoms . . . 26
2.2.1 The matrix elements of the density operator . . . 26
2.2.2 Rotating wave approximation . . . 27
2.2.3 Pauli matrices and the atomic Bloch vector . . . 28
2.2.4 Manipulation of the state by sequences of radiation pulses . . . 30
2.3 Bloch equations with spontaneous emission and line broadenings . . . 31
2.3.1 Phenomenological inclusion of spontaneous emission . . . 31
2.3.2 Line broadening mechanisms . . . 33
2.4 Multi-level systems . . . 37
2.4.1 Liouville equation . . . 37
2.4.2 Bloch equations for three levels . . . 38
2.4.3 Numerical treatment of Bloch equations . . . 40
2.5 Quantization of the electromagnetic field . . . 42
2.5.1 Field operators . . . 43
2.5.2 Interaction of quantized fields with atoms . . . 45
2.5.3 Dressed states . . . 47
2.6 The Jaynes-Cummings model . . . 48
2.6.1 Dressed states representation . . . 49
2.6.2 Classical and quantum limits . . . 51
2.6.3 Observables and correlations of the Jaynes-Cummings dynamics 54
2.7 Exercises . . . 57
2.8 Further reading . . . 66

3 Atomic motion in electromagnetic fields **69**
3.1 Atomic level structure . . . 69
3.1.1 Level structure of alkali-metal atoms . . . 70
3.1.2 Angular momentum and selection rules . . . 73
3.1.3 Optical transitions in multilevel atoms . . . 75
3.1.4 Fine and hyperfine interactions . . . 77
3.1.5 Selection rules for emission in certain directions . . . 78
3.2 Magnetic traps . . . 78
3.2.1 Forces on magnetic dipole moments . . . 79
3.2.2 Quadrupolar traps and Majorana spin-flips . . . 80
3.2.3 Magnetic Ioffe-type traps . . . 82
3.2.4 Adiabatic potentials . . . 84
3.3 Optical forces . . . 85
3.3.1 The dipolar gradient force and the radiation pressure force . . . 87
3.3.2 Recoil- and Doppler-shift . . . 89
3.4 Exercises . . . 92
3.5 Further reading . . . 94

4 Manipulation of atomic gases **95**
4.1 The atomic motion . . . 96
4.1.1 The atom as a matter wave . . . 96
4.1.2 Characteristic velocities . . . 97
4.2 Optical cooling . . . 99
4.2.1 Optical molasses . . . 99
4.2.2 Sub-Doppler cooling . . . 100
4.2.3 Cooling trapped particles . . . 106
4.3 Optical and magneto-optical traps . . . 106
4.3.1 The magneto-optical trap . . . 106
4.3.2 Optical dipole traps . . . 110
4.4 Radiative coupling and evaporative cooling . . . 113
4.4.1 Evaporative cooling . . . 113
4.4.2 Sympathetic cooling . . . 119
4.5 Analysing techniques . . . 120
4.5.1 Time-of-flight imaging . . . 120
4.5.2 Absorption imaging . . . 121
4.5.3 Dispersive imaging . . . 123
4.5.4 Refraction of atoms by light and of light by atoms . . . 124
4.6 Exercises . . . 125
4.7 Further reading . . . 128

5 Coupling of atoms and optical cavities **129**
5.1 Light fields in cavities without atoms . . . 130
5.1.1 Master equation . . . 130
5.1.2 Characterization of the bare cavity . . . 133
5.2 Interaction of atoms with cavities . . . 136
5.2.1 Characterization of the atom-field coupling . . . 137
5.2.2 Normal mode splitting in linear cavities . . . 140

5.3 The Dicke model in the mean-field approximation . . . 143
5.3.1 Dicke states . . . 144
5.3.2 Coherent spin states . . . 148
5.3.3 Rotations, spin excitation and precession . . . 149
5.3.4 Uncertainties, quantum projection noise and spin squeezing . . 151
5.4 Super- and subradiance in open systems . . . 154
5.4.1 Models for open systems and phase transitions . . . 155
5.4.2 Superradiant Dicke phase transition . . . 158
5.4.3 Beyond mean-field . . . 158
5.5 Interacting atoms . . . 159
5.5.1 Rydberg blockade . . . 160
5.5.2 Dipole-dipole interactions in the non-linear optics regime . . . 161
5.5.3 Cavity-mediated spin-exchange interactions . . . 163
5.6 Exercises . . . 165
5.7 Further reading . . . 168

6 Bonus: Atomic motion in optical lattices and cavities 171
6.1 Atoms in an optical standing wave . . . 171
6.1.1 Bloch oscillations . . . 173
6.2 Cavity interacting with a single atom . . . 176
6.2.1 Derivation of the CARL equations . . . 177
6.2.2 Solutions of the CARL equations . . . 178
6.3 CARL: The collective atomic recoil laser . . . 180
6.3.1 Collective effects . . . 181
6.4 Quantization of the atomic motion in cavities . . . 182
6.4.1 Modal expansion of the motion . . . 182
6.5 Exercises . . . 184
6.6 Further reading . . . 184

Chapter 1

Two-level atom in a radiation field

Our perception of the macroscopic world is dominated by light and matter. Since ancient Greek philosophy our conceptions of light and matter follow a capricious evolution, culminating with the discovery of the atom and the formulation of the theories of *electrodynamics and quantum mechanics*. Combining those two theories and accepting that both, light and matter exhibit particle-like and wave-like features, we believe to have nowadays at hand a reasonably sound picture. This confidence is alimented by the predictive power of modern physics. Nevertheless, there remain many open questions, in particular, when it comes to cooperative effects in light scattering from ensembles of atoms: On one hand, Maxwell's equations tell us how light interacts with macroscopic bodies via reflection, refraction, emission of radiation, and even exerting radiative forces. On the other hand, atomic physics tells us to break down matter into indivisible atoms, with Niels Bohr teaching us, how light interacts with those atoms. Now, the transition from the microscopic quantum world to the classical macroscopic world is particularly tricky, and much can be learned extending the quantum concepts to collective effects gradually increasing the number of atoms and their density. Some of this will be done during this school. In this series of lectures, we will mostly concentrate on the interaction of light with individual atoms and only in the last lecture discuss an example of a collective effect in a dilute gas.

We start the first lecture in Sec. 1.1 with a brief historical survey and a definition of the area of research in physics covered by this lecture, which is the *interaction of light with cold atoms*. As already mentioned the correct framework of this area is provided by the theories of *electrodynamics and quantum mechanics*. We will review in Sec. 1.2 quantum mechanical time-dependent perturbation theory, which we apply to the Rabi problem of two levels interacting with a coherent radiation field. We will briefly introduce the notions of the dressed states and of quantum jumps.

1.1 Introduction

1.1.1 Atoms and photons

The fundamental idea of quantum mechanics is the assumption that there are entities which can not be subdivided beyond a certain limit. Examples are the mass of a body,

the speed of an electron orbiting an atom, or the intensity of a beam of light. This idea was first uttered by *Leucippus* 500 years a.c. and his student *Democritus*, who imagined matter being made of smallest particles which they called *atoms*. These atoms move freely, collide, combine, and separate: 'There is nothing else than atoms and free space' they claimed. The microscopic atoms would have the same characteristics as the macroscopic objects they form when they combine, for example, color and shape. The idea of the atom resurfaced and was refined in the course of the 18^{th} century (see Tab. 1.1 below). Today, we know that the basic idea was good, but reality is a little more complicated.

Table 1.1: *Historical time line of the quantization of matter.*

500 a.c.	Democritus	invention of the atom
1800	Avogadro, Dalton	reinvention of the atom
1897	Thomson	charge transport, raisin-in-a-cake model
1909	Rutherford, Geiger, Marsden	α-scattering, charge localized in nuclei
1911	Rutherford	planetary model
1900	Bohr	quantized orbitals
1923	de Broglie	matter has characteristics of waves
1927	Davisson, Germer, Stern	electron and atoms diffraction

Still, at the end of the 19^{th} century, the physical world seemed rather simple: matter and light was all that existed. Matter was made up of atoms and light was a wave. Therefore, to describe a real system, it was enough to calculate the trajectories of its elementary particles and the propagation of light between them. The way that light interacts with polarizable and magnetizable matter via electric and magnetic fields had been perfectly explained by laws discovered by Coulomb, Ampère, Faraday, and Maxwell.

However, new experimental observations, such as the ultraviolet divergence of black-body radiation, that appeared in the late 19^{th} century, were incompatible with these traditional concepts. New ideas were pioneered by *Max Planck* who, in 1905, with a little help from Einstein quantized the electromagnetic field, and therefore the light, into small harmonic oscillators. This was the starting point for the development of a new theory called 'quantum mechanics'. Soon, this theory was applied to explain the photoelectric effect. The second important step was initialized by *Niels Bohr*, who quantized the hydrogen atom in 1913 into discrete excitation levels.

Table 1.2: *Historical time line of the quantization of light.*

1801	Young	light is diffracted like a wave
1860	Maxwell	unified theory of electrodynamics including light
1888	Hertz	detection of radio waves
$\sim$ 1890		accurate measurements of black-body radiation spectra
1900	Planck	quantum hypothesis: $E = h\nu$
1905	Einstein	photoelectric effect, light behaves like a particle

Nowadays we know that our universe is not as simple as classical mechanics suggested, and that atoms are also waves and light also behaves like particles. This *duality principle* is one of the fundamental ideas of quantum mechanics. The appearance of an object as a wave or as a particle depends on the situation in which it is observed. While the wave nature of light was well established in classical physics since a long time, Louis de Broglie was the first in 1924 to apply the duality principle also to massive particles and to predict that particles, under certain conditions, behave like waves the wavelengths of which increase as their velocity decreases. Each particle (or body) is delocalized along a distance corresponding to this 'de Broglie wavelength'. This feature of matter was soon discovered experimentally in electron beams and is still used today in commercial devices, for example in electron microscopes.

1.1.2 Definition of the research area

Having decomposed our world into its elementary components, light and atoms, we may now recompose it by identifying the relevant degrees of freedom and gradually increasing the complexity of the systems we want to study.

In quantum mechanics we associate an energy to every degree of freedom and to its interaction with other degrees of freedom. Looking for example at a *single atom* we notice, that it has a mass and therefore mechanical degrees of freedom which may carry kinetic and potential energy,

$$\hat{H}_{cm} = \frac{\mathbf{P}^2}{2M} + V(\mathbf{R}) \ . \tag{1.1}$$

On the other hand, we learn in atomic physics, that atoms also have an internal structure, which is due to the motion of negatively charged electrons orbiting around a positively charged nucleus. The details of the internal structure, which is organized into discrete energy levels, are very complicated, and its derivation will not be the topic of this course. Instead we assume the structure of energy levels $\hbar\omega_i$ as given, we write it down as,

$$\hat{H}_{ele} = \sum_i \hbar\omega_i |i\rangle\langle i| \ , \tag{1.2}$$

and illustrate it in so-called Grotrian diagrams, which exhibit the energy structure in a compact way. An example is shown in Fig. 1.1. Every energy level corresponds to a particular configuration of the electrons and their spins within the electronic shell of the atom, and it is the 'compatibility' of two such configurations which determines, via so-called selection rules, whether a transition between them is easy or unlikely to occur.

Since Planck's treatment of blackbody radiation, we know that any radiation field is composed of quanta called *photons*. Since, in a radiation mode (denoted by its wavevector $\mathbf{k}$) all photons have equal energy $\hbar\omega_{\mathbf{k}}$, we may treat it like a harmonic oscillator and write the Hamiltonian of a radiation field in terms of photon creation and annihilation operators,

$$\hat{H}_{rad} = \sum_{\mathbf{k}} \hbar\omega_{\mathbf{k}} \left(\hat{a}^\dagger_{\mathbf{k}} \hat{a}_{\mathbf{k}} + \tfrac{1}{2} \right) \ . \tag{1.3}$$

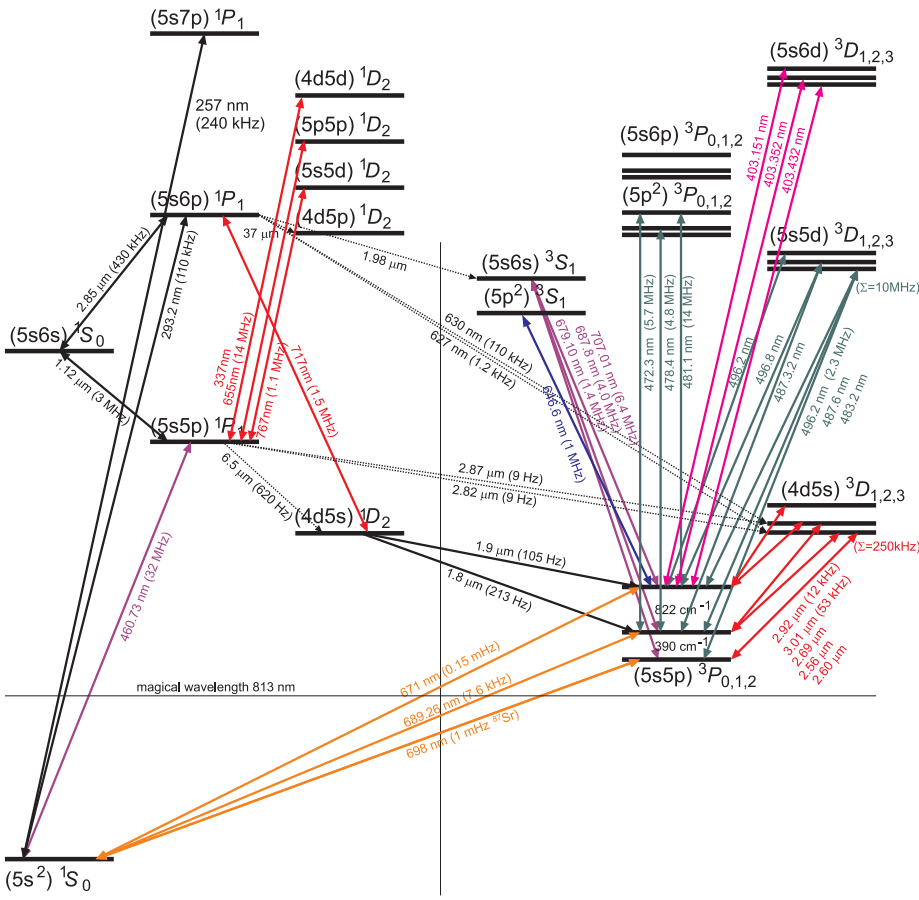

Figure 1.1: Grotrian diagram of strontium.

It is important to be aware that radiation fields do not only carry energy (via their intensity), but they also carry momentum (via their Poynting vector).

Fundamental laws of physics tell us, that the energy associated with every degree of freedom (atomic or radiative) is *conserved*, and this also holds for linear and angular momentum. Degrees of freedom may interact, where we understand any interaction in terms of collisions which must conserve energy, momentum, and angular momentum, as well. In quantum mechanics we describe a collision by a concatenation of creation, annihilation or transition operators acting on different degrees of freedom. For example, if $\hat{a}^\dagger_{\mathbf{k}}$ means the creation of a photon in mode $\mathbf{k}$ and $\hat{\sigma}^- \equiv |1\rangle\langle 2|$ the transition of an atom from an excited state $|2\rangle$ to a ground state $|1\rangle$, then the operator,

$$\hat{H}_{int} \propto \hat{a}^\dagger_{\mathbf{k}} \hat{\sigma}^- e^{\imath \mathbf{k}\cdot\hat{\mathbf{R}}} \tag{1.4}$$

describes the process of a photon emission in compliance with Bohr's model. Here, the term $e^{\imath \mathbf{k}\cdot\hat{\mathbf{R}}} = |\mathbf{P} + \hbar\mathbf{k}\rangle\langle\mathbf{P}|$ describes the transition of the motional state of the atomic center-of-mass to a momentum state accelerated by the photonic recoil $\hbar\mathbf{k}$.

The operator (1.4) represents the most fundamental process in light-matter interaction, which involves three degrees of freedom: the atomic center-of-mass motion, a photon, and the internal atomic excitation. Not all three degrees of freedom are always relevant for the understanding of a phenomenon, as we will study in many examples during this lectures. On the other hand, there are possibly other degrees of freedom, which may couple to the process described by (1.4). In this lecture we will mostly disregard interaction with other atoms (van der Waals, collisions) and quantum statistical effects. Furthermore, we will mostly treat light as a classical field, which is justified whenever the light modes are macroscopically populated.

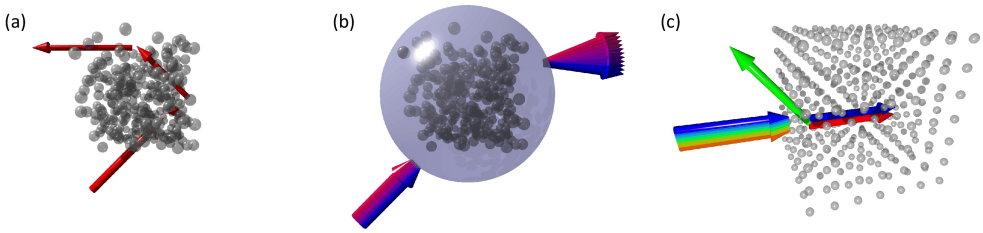

Figure 1.2: (a) Artist's view of multiple scattering of a photon through a dilute cloud. (b) Atomic cloud as a bulk object characterized by a refraction index $n(\mathbf{r})$. (c) Illustration of a photonic band in an optical lattice.

1.1.2.1 Why studying ultracold atomic gases?

Cold atoms have a lot of advantages (and no major inconvenience). Cold atomic clouds are in the same time macro- and microscopic: On one hand, a cloud of one billion atoms represents a macroscopic object so large, that it can be characterized by a refraction index and its fluorescence can be seen by eye. On the other hand, with a typical density 10 orders of magnitude lower than the air we breathe, it is so dilute that the distance between atoms is much larger than a wavelength of visible light. We can thus picture the propagation of light inside a cloud as photons bouncing off individual atoms by microscopic scattering, as illustrated in Fig. 1.2. Hence, atomic clouds allow us to study macro- and microscopic aspects of scattering in the same time.

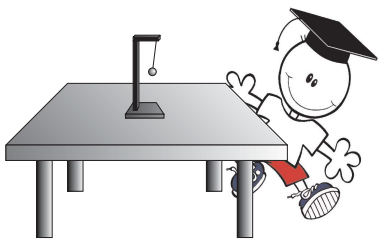

Figure 1.3: Most quantum optics experiments are table top experiment.

Second, we dispose today of incredibly powerful techniques for controlling and measuring atoms. Clouds can be isolated from all kinds of noise sources. We control energy and particle exchange with the environment over the time scale of experiments. We can manipulate all essential control parameters, such as size, temperature, and even the interatomic interaction strength. We can measure thermodynamic quantities such as the internal energy, chemical potential or heat capacity. All relevant degrees of freedom can be controlled up to a level, where the *quantum nature of the degrees of freedom dominates the dynamics*, for ex-

ample in cavity QED experiments of single atoms trapped by single photons. Moreover, we can today simulate other fields of physics, such solid state physics, with atoms trapped and periodically ordered in optical lattices and detect effects that had been predicted but never observed in solids. An interesting particularity is that most experiments are performed on trapped, i.e. inhomogeneous samples.

An important practical advantage is the fact, that atom optical experiments are table top experiments. Even though the creation of a cold atomic cloud or Bose-Einstein condensate is still difficult, it can, in principle, be done by a single medium-sized PhD student.

The general importance of the field of atom optics has been acknowledged with 23 Nobel prices in the last 25 years awarded to Dehmelt, Paul, Ramsey, Cohen-Tannoudji, Chu, Phillips, Cornell, Wieman, Ketterle, Hänsch, Glauber, Hall, Wineland, Haroche, Ahskin, plus several Nobel prices granted to closely related areas of physics (De Gennes, Leggett, Thouless, Haldane, Kosterlitz, Claussen, Aspect, Zeilinger).

1.1.2.2 The atom optical toolbox

Let us now give a brief overview on the atom optical toolbox: Typically, we work with between 1 and 10^{10} atoms (or sometimes ions). External trapping potentials compress the clouds to low or high densities of $n = 10^9 ... 10^{14}\,\mathrm{cm}^{-3}$, which however are still ten orders of magnitude below atmospheric pressure. This means that all experiments must be conducted in extreme ultrahigh vacuum (XUHV) chambers. The greatest breakthrough in atomic optics, in the eighties and nineties, was the invention of optical cooling techniques, which could bring atomic clouds to 1 μK cold and even picoKelvin ultracold temperatures.

Another important breakthrough was the observation of so-called Feshbach resonances, which allow to vary the self-interaction of the clouds over extremely wide ranges and even in real-time, with collision cross sections ranging from 0 to at least $\sigma_{collision} \simeq 10^{-9}\,\mathrm{cm}^2$. Consequently, we have separate influence over all contributions to the total energy: over the potential energy by compressing, deforming or shaking the trap, over the kinetic energy by cooling or exciting collective vibrations, and finally over the self-energy via the Feshbach resonances [33, 86],

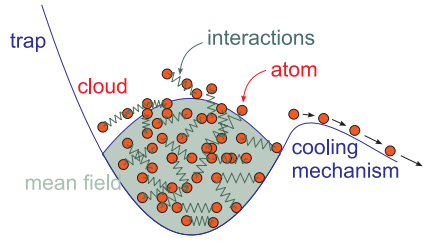

Figure 1.4: Cold trapped atoms.

$$\begin{array}{cccccc} & \text{trapping} & & \text{cooling} & & \text{Feshbach resonances} \\ & \downarrow & & \downarrow & & \downarrow \\ E & = & E_{pot} & + E_{kin} & & + E_{self} \end{array} \tag{1.5}$$

1.2 Two-level systems in quantum mechanics

In this section we will start to develop the quantum mechanical framework for treating the interaction of a single atomic two-level system with an oscillatory perturbation

coupling the two levels. Such temporal perturbations typically occur when we suddenly switch on an external field that influences the motion or spin of the particles, or when the field varies over time, for example, an electromagnetic field.

1.2.1 Time-dependent perturbations

The time-dependent Schrödinger equation is,

$$\hat{H}\psi(\mathbf{r},t) = \imath\hbar\frac{\partial\psi(\mathbf{r},t)}{\partial t} \ , \tag{1.6}$$

with $\psi(\mathbf{r},t) = \langle\mathbf{r}|\psi(t)\rangle$. We write the perturbation as [1],

$$\hat{H} = \hat{H}^{(0)} + \hat{H}^{(1)}(t) \ . \tag{1.7}$$

and the eigenenergies and -functions of the unperturbed system as,

$$\hat{H}^{(0)}|n\rangle = E_n|n\rangle \ , \tag{1.8}$$

where $|n\rangle$ are the possible states (energy levels) in which the system can be. Recalling that this stationary Schrödinger equation was obtained from the time-dependent Schrödinger equation via a separation ansatz, the temporal evolution of these eigenfunctions is given by,

$$|\psi_n^{(0)}(t)\rangle = |n\rangle e^{-\imath E_n t/\hbar} \ . \tag{1.9}$$

Since the eigenfunctions form a complete set, we may expand any solution of the Schrödinger equation as,

$$|\psi^{(1)}(t)\rangle = \sum_n a_n(t)|\psi_n^{(0)}(t)\rangle = \sum_n a_n(t)|n\rangle e^{-\imath E_n t/\hbar} \ . \tag{1.10}$$

Insertion into the Schrödinger equation and multiplying from the right with $\langle j|$, we get in first order,

$$\imath\hbar\frac{da_j(t)}{dt} = \sum_n a_n(t)\langle j|\hat{H}^{(1)}|n\rangle e^{\imath\omega_{jn}t} \ , \tag{1.11}$$

where $\hbar\omega_{jn} \equiv E_j - E_n$. Equation (1.11) is exactly equivalent to the Schrödinger equation (1.6): no approximations have been made. However, for the case of a real multilevel atom in a radiation field it is unsolvable, and so approximations are required. In perturbation theory one considers the atom to be initially in its ground state $|1\rangle$, that is, $a_n(0) = \delta_{n1}$. The approximation now consists in assuming

$$a_n(t) \ll 1 \tag{1.12}$$

for all $n \neq 1$ and doing a formal time integration of Eq. (1.11) to calculate these $a_n(t)$ values. The small components $a_n(t)$ of the excited states $|\psi_n^{(0)}\rangle$ for $n \neq 1$ that are mixed into $|\psi^{(1)}(t)\rangle$ become the transition amplitudes and their squares are the transition rates. For transitions to the continuum, such as photoionization, averaging over the density of final states results in the familiar *Fermi's golden rule* of quantum

[1] See script on *Quantum mechanics* (2023), Sec. 5.4.1.

mechanics. For transitions between discrete states driven by radiation whose spectral width is larger than the natural width of the transition, averaging over the spectral density gives the same golden rule.

This approach is not suitable for narrow-band laser excitation of atoms, however, because large excited-state populations are possible, thereby violating Eq. (1.12). Instead, a different approximation is made, which consists in truncating the summation of the exact Eq. (1.11) to just two terms, a ground and an excited state connected by the laser frequency, and solving the resulting coupled differential equations directly. Such a calculation for a two-level system was first studied by Rabi [122] in connection with magnetic resonance, and is described in many textbooks [25, 123].

The expansion now reads,

$$|\psi^{(1)}(t)\rangle = a_1(t)|\psi_1^{(0)}(t)\rangle + a_2(t)|\psi_2^{(0)}(t)\rangle \ . \tag{1.13}$$

Note that not only do eigenfunctions oscillate, but the coefficients also depend on time, because the composition of the states can change. The instantaneous probability of finding the system in state $|n\rangle$ is $|a_n(t)|^2$. Importing the above linear combination into the Schrödinger equation,

$$[\hat{H}^{(0)} + \hat{H}^{(1)}(t)]|\psi^{(1)}(t)\rangle = \imath\hbar\frac{\partial}{\partial t}|\psi^{(1)}(t)\rangle \ , \tag{1.14}$$

we find,

$$\begin{aligned} &a_1\hat{H}^{(0)}|\psi_1^{(0)}\rangle + a_2\hat{H}^{(0)}|\psi_2^{(0)}\rangle + a_1\hat{H}^{(1)}|\psi_1^{(0)}\rangle + a_2\hat{H}^{(1)}|\psi_2^{(0)}\rangle \\ &\qquad = \imath\hbar\left[\frac{\partial a_1}{\partial t}|\psi_1^{(0)}\rangle + \frac{\partial a_2}{\partial t}|\psi_2^{(0)}\rangle + a_1\frac{\partial|\psi_1^{(0)}\rangle}{\partial t} + a_2\frac{\partial|\psi_2^{(0)}\rangle}{\partial t}\right] \\ \Longrightarrow\ &a_1\hat{H}^{(1)}|\psi_1^{(0)}\rangle + a_2\hat{H}^{(1)}|\psi_2^{(0)}\rangle = \imath\hbar\dot{a}_1|\psi_1^{(0)}\rangle + \imath\hbar\dot{a}_2|\psi_2^{(0)}\rangle \ , \end{aligned} \tag{1.15}$$

because the other terms satisfy the Schrödinger equation of zero order. Replacing the stationary eigenfunctions,

$$a_1 e^{-\imath E_1 t/\hbar}\hat{H}^{(1)}|1\rangle + a_2 e^{-\imath E_2 t/\hbar}\hat{H}^{(1)}|2\rangle = \imath\hbar\dot{a}_1 e^{-\imath E_1 t/\hbar}|1\rangle + \imath\hbar\dot{a}_2 e^{-\imath E_2 t/\hbar}|2\rangle \ , \tag{1.16}$$

and multiplying this equation with $\langle 1|\times$ and $\langle 2|\times$, we find with the abbreviation $\hbar\omega_0 \equiv E_2 - E_1$,

$$\begin{aligned} \imath\hbar\dot{a}_1 &= a_1\langle 1|\hat{H}^{(1)}|1\rangle + a_2 e^{-\imath\omega_0 t}\langle 1|\hat{H}^{(1)}|2\rangle \ , \\ \imath\hbar\dot{a}_2 &= a_1 e^{\imath\omega_0 t}\langle 2|\hat{H}^{(1)}|1\rangle + a_2\langle 2|\hat{H}^{(1)}|2\rangle \ . \end{aligned} \tag{1.17}$$

Frequently, the perturbation induces only a coupling, but does not directly influence the energies, $\langle n|\hat{H}^{(1)}|n\rangle = 0$,

$$\boxed{\dot{a}_1 = a_2\frac{e^{-\imath\omega_0 t}}{\imath\hbar}\langle 1|\hat{H}^{(1)}|2\rangle \qquad \text{and} \qquad \dot{a}_2 = a_1\frac{e^{\imath\omega_0 t}}{\imath\hbar}\langle 2|\hat{H}^{(1)}|1\rangle} \ . \tag{1.18}$$

Without perturbation, $\langle m|\hat{H}^{(1)}|n\rangle = 0$, no dynamics develops; the eigenfunctions evolve independently.

Let us now consider a periodic perturbation oscillating at frequency $\omega = \omega_0 + \Delta$, where Δ is called the *detuning* from the resonance ω_0,

$$H^{(1)} = -e\vec{\mathcal{E}}(\mathbf{r},t)\cdot\mathbf{r} = -e\mathcal{E}_0\hat{\epsilon}\cos(kz-\omega t)\cdot\mathbf{r}\ . \tag{1.19}$$

Then,

$$\langle 2|H^{(1)}|1\rangle = -e\mathcal{E}_0\cos(kz-\omega t)\langle 2|r|1\rangle = \hbar\Omega\cos(kz-\omega t)\ , \tag{1.20}$$

where we call

$$\Omega \equiv \frac{-e\mathcal{E}_0\langle 2|r|1\rangle}{\hbar} \tag{1.21}$$

the *Rabi frequency*. This yields,

$$\dot{a}_1 = -\imath\Omega a_2 e^{-\imath\omega_0 t}\cos(kz-\omega t) \qquad \text{and} \qquad \dot{a}_2 = -\imath\Omega^* a_1 e^{\imath\omega_0 t}\cos(kz-\omega t)\ . \tag{1.22}$$

Neglecting fast-rotating terms doing the so-called *rotating wave approximation* (RWA) and choosing the position of the atom to be $z = 0$,

$$\dot{a}_1 \simeq -\tfrac{\imath\Omega}{2}a_2 e^{\imath\Delta t} \qquad \text{and} \qquad \dot{a}_2 \simeq -\tfrac{\imath\Omega^*}{2}a_1 e^{-\imath\Delta t}\ . \tag{1.23}$$

With the equations of motion we can, starting from initial values for $a_1(0)$ and $a_2(0)$, calculate the temporal evolution.

We solve this system of differential equations by differentiating one and substituting the other,

$$\ddot{a}_2 = -\imath\dot{a}_1\tfrac{\Omega}{2}^* e^{-\imath\Delta t} - a_1\Delta\tfrac{\Omega^*}{2}e^{-\imath\Delta t} = -\tfrac{|\Omega|^2}{4}a_2 - \imath\Delta\dot{a}_2\ . \tag{1.24}$$

We find solutions via the ansatz $a_2 = e^{-\imath\Delta t/2}(Ae^{\imath Gt/2} + Be^{-\imath Gt/2})$. The equation for a_2 yields,

$$\begin{aligned}(\tfrac{\imath}{2}G - \tfrac{\imath}{2}\Delta)^2 Ae^{\imath(G-\Delta)t/2} + (-\tfrac{\imath}{2}G - \tfrac{\imath}{2}\Delta)^2 Be^{\imath(-G-\Delta)t/2} \\ = -\tfrac{|\Omega|^2}{4}(Ae^{\imath(G-\Delta)t/2} + Be^{\imath(-G-\Delta)t/2} \\ - \imath\Delta\left[(\tfrac{\imath}{2}G - \tfrac{\imath}{2}\Delta)Ae^{\imath(G-\Delta)t/2} + (-\tfrac{\imath}{2}G - \tfrac{\imath}{2}\Delta)Be^{\imath(-G-\Delta)t/2}\right]\ .\end{aligned} \tag{1.25}$$

Separating the parts in A and in B we obtain two equations with the same result,

$$G^2 = |\Omega|^2 + \Delta^2\ . \tag{1.26}$$

G is called the *generalized Rabi frequency*. Using the initial conditions, $a_1(0) = 1$ and $a_2(0) = 0$, we can fix one of the coefficients A and B, since $a_2(0) = A + B = 0$,

$$a_2 = 2\imath Ae^{-\imath\Delta t/2}\sin\tfrac{G}{2}t\ . \tag{1.27}$$

We now import this solution into the differential equation for a_1,

$$\dot{a}_1 = -\imath\tfrac{\Omega}{2}a_2 e^{\imath\Delta t} = \Omega Ae^{\imath\Delta t/2}\sin\tfrac{G}{2}t\ . \tag{1.28}$$

The integral is,

$$a_1(t) = \int_0^t \Omega Ae^{\imath\Delta t'/2}\sin\tfrac{G}{2}t'dt' = -\frac{2A}{\Omega^*}e^{\imath\Delta t/2}\left(G\cos\tfrac{G}{2}t - \imath\Delta\sin\tfrac{G}{2}t\right)\ . \tag{1.29}$$

Using the normalization condition,

$$1 = |a_1|^2 + |a_2|^2 = \left|-\tfrac{2A}{\Omega^*}e^{\imath\Delta t/2}\left(G\cos Gt - \imath\Delta\sin\tfrac{G}{2}t\right)\right|^2 + \left|2\imath Ae^{-\imath\Delta t/2}\sin Gt\right|^2$$
$$= \frac{4A^2}{|\Omega|^2}\left(G^2\cos^2\tfrac{G}{2}t + \Delta^2\sin^2\tfrac{G}{2}t\right) + 4A^2\sin^2\tfrac{G}{2}t = 4A^2\frac{G^2}{|\Omega|^2}\ . \tag{1.30}$$

Hence, $A = |\Omega|/2G$, or $2AG/\Omega^* = \sqrt{\Omega/\Omega^*}$. In general, we can choose Ω real, and the final solution is,

$$\boxed{a_1(t) = -e^{\imath\Delta t/2}\left(\cos\tfrac{G}{2}t + \tfrac{-\imath\Delta}{G}\sin\tfrac{G}{2}t\right) \qquad \text{and} \qquad a_2(t) = \tfrac{\imath\Omega}{G}e^{-\imath\Delta t/2}\sin\tfrac{G}{2}t}\ . \tag{1.31}$$

When the detuning Δ is zero, under the influence of the perturbation, the populations of the system oscillate with the Rabi frequency Ω. When the light frequency is detuned from resonance, however, the oscillation frequency G is higher, but the amplitude decreases as well. The initially empty state never reaches unitary population. In Exc. 1.3.0.1 we calculate the time required to allow the perturbation to invert the population of a two-level system, in Exc. 1.3.0.2 we study the maximum achievable inversion as a function of detuning, and in Exc. 1.3.0.3 we analyze the dynamics of a system subject to sequences of pulses.

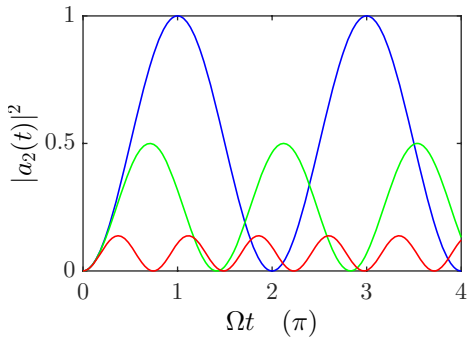

Figure 1.5: (code for download) Probability $|a_2(t)|^2$ for the atom to be in the excited state for $\Omega = \Gamma$ and $\Delta = 0$ (blue), $\Delta = \Gamma$ (green), and $\Delta = 2.5\Gamma$ (red). Time is in units of $1/\Gamma$.

1.2.2 Light-shift in the semi-classical picture

From Eqs. (1.23) written in matrix form as,

$$\begin{pmatrix}\imath\dot{a}_1\\ \imath\dot{a}_2\end{pmatrix} = \begin{pmatrix}0 & \frac{1}{2}\Omega e^{\imath\Delta t}\\ \frac{1}{2}\Omega^* e^{-\imath\Delta t} & 0\end{pmatrix}\begin{pmatrix}a_1\\ a_2\end{pmatrix} = \tfrac{1}{\hbar}\hat{H}\begin{pmatrix}a_1\\ a_2\end{pmatrix}\ , \tag{1.32}$$

via a simple transformation $\tilde{a}_2 \equiv e^{\imath\Delta t}a_2$, we arrive at an equivalent system of equations,

$$\begin{pmatrix}\imath\dot{a}_1\\ \imath\dot{\tilde{a}}_2\end{pmatrix} = \begin{pmatrix}0 & \frac{1}{2}\Omega\\ \frac{1}{2}\Omega^* & -\Delta\end{pmatrix}\begin{pmatrix}a_1\\ \tilde{a}_2\end{pmatrix} = \tfrac{1}{\hbar}\hat{H}'\begin{pmatrix}a_1\\ \tilde{a}_2\end{pmatrix}\ , \tag{1.33}$$

which has the advantage of a time-independent Hamiltonian, the time dependence having been transformed into the wavefunctions [2]. From the total Hamiltonian in Eq. (1.33), we find for the eigen-energies,

$$E_{1,2} = \frac{\hbar}{2}\Delta \pm \frac{\hbar}{2}G \ . \tag{1.34}$$

Because the light intensity is proportional to Ω^2, the energy correction $\Delta E_{1,2} \equiv E_{1,2} - \frac{\hbar\Delta}{2}$ is appropriately called the *light shift*. In the limit of large detunings, $\Omega \ll |\Delta|$ we may expand,

$$E_{1,2} \simeq \pm\frac{\hbar\Omega^2}{4\Delta} \ . \tag{1.35}$$

The eigenstates corresponding to $\Delta E_{1,2}$ are called the *dressed states* of the atom and are calculated in Sec. 2.5.3. Very often the light field is not homogeneous (e.g., in a standing light wave) producing a spatially dependent light shift $\Delta E_{1,2}(\mathbf{r})$. The force that results from this gradient of energy is called the dipole force and is discussed in more detail in Sec. 3.3.1. In Exc. 1.3.0.4 we generalize the calculation of the light-shift to the presence of spontaneous decay.

1.2.3 Numerical simulations and quantum jumps

The softwares 'Maple' or 'Mathematics' are useful for analytical calculations, that is, multiplying matrices or determining eigenvalues. For numerical calculations the softwares 'Matlab', 'Python', or 'Julia' are more adapted. For example, the time evolution of a Schrödinger equation,

$$|\psi(t)\rangle = e^{-\imath\hat{H}t/\hbar}|\psi(0)\rangle \ , \tag{1.36}$$

can be simulated in a single command line using the Matlab 'expm' function.

When the system varies in time, $\hat{H}(t)$, we may divide time into small units dt and propagate the wavefunction as,

$$|\psi(t+dt)\rangle = e^{-\imath\hat{H}(t)dt/\hbar}|\psi(t)\rangle \simeq |\psi(t)\rangle\left(1 - \imath\frac{\hat{H}}{\hbar}dt\right) \ , \tag{1.37}$$

continuously reinserting the solution into the equation. This *Newton method* does not converge quickly (dt should be chosen small enough when $\hat{H}(t)$ varies rapidly), but there are other more sophisticated procedures like the *Runge-Kutta method*.

A variation of this method is called *steepest descent method*. This method is similar to the Newton mewthod (1.37), but replaces the time dt with an imaginary time. Thus, the coherent temporal evolution of the Schrödinger equation is replaced by a dissipative evolution. The loss of energy automatically takes the system to the ground state. The method also applies to more complicated equations than the Schrödinger equation, for example, the *Gross-Pitaevskii equation*.

Another numerical method often used in quantum mechanics is called quantum *Monte Carlo simulation* of the wavefunction [111]. This method simulates trajectories

[2] The general transformation rule for time-dependent Hamiltonians is $\hat{H}' = U^\dagger\hat{H}U + \imath\hbar\dot{U}^\dagger U$ [see *Quantum mechanics* (2019), Sec. 14.1.2]. In the present case the Hamiltonians follow from each other with $U = \begin{pmatrix} 1 & 0 \\ 0 & e^{\imath\Delta t} \end{pmatrix}$.

of quantum systems treating intrinsic quantum noise as random processes disrupting the uniformity of the trajectory. The advantage of this method is that it also applies to dissipative systems. We will introduce this method in the next section.

1.2.3.1 Quantum jumps

The preceding discussions ignored the existence of spontaneous decay of the excited states resulting from their interaction with the zero-point energy of the electromagnetic field. Spontaneous emission has played an important role in atomic physics since the conception of discrete atomic states by Bohr in 1913.

The problem of radiative transitions between discrete states in atoms was discussed by Einstein in 1917 [52], where he considered three radiative processes. In the first process, an amount of optical energy $\hbar\omega$ (a 'photon') is absorbed from an applied radiation field of angular frequency ω, and atoms make transitions from the ground to the excited state. The newly introduced second process is stimulated emission, where a photon is emitted into the applied radiation field and the atoms make a transition from the excited to the ground state. Note that in both of these processes the total energy of the system consisting of the applied radiation field and the atoms is conserved. The third process is spontaneous emission, where a photon is also emitted and the atoms also make transitions from the excited to the ground state. However, unlike stimulated emission, the photon is not emitted in the mode of the radiation field, but has a random direction or polarization (see Fig. 1.6). Since the photon is emitted into the vacuum field, there is no longer conservation of energy for the system of radiation field plus atoms, since the vacuum field is outside the system. Finally, from the distribution of black-body radiation, Einstein deduced that the fourth process, spontaneous absorption, is not possible (or at least very unlikely).

The discussion in this lecture so far has properly accounted for the two stimulated processes discussed above [see Eqs. (1.31)]. The combined action of these two processes causes the oscillation in both the excited and ground state probabilities (see Fig. 1.5). For atoms initially in the ground state, the probability for absorption is large and the probability for them to go into the excited state increases. Once the atoms have a large probability to be in the excited state, however, the probability for absorption decreases and the probability for stimulated emission increases. This leads to the Rabi oscillations exhibited in Fig.1.5.

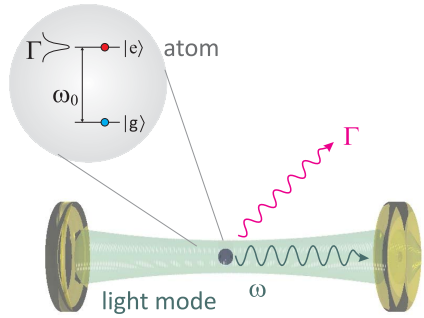

Figure 1.6: Two-level atom interacting with a cavity mode.

To include spontaneous emission, one way could be to include the vacuum field in the description of the system, which would then be closed as before. However, the task of doing so is formidable because both the spontaneous emission direction and the polarization direction are random. Thus it would be necessary to include the entire continuum of these parameters in the system, which is beyond the scope of this book. Furthermore, in most cases the properties of the emitted photon are not of

interest, and information on the atom and the applied radiation field suffices.

The usual way to treat this problem in quantum mechanics is to introduce the density matrix $\hat{\rho}$ and to discuss the excitation of the atoms in terms of populations and coherences instead of amplitudes. This follows in the next lecture. Here, an alternative view of this problem is presented.

This view is called the Monte Carlo wavefunction method and was recently described anew [111]. It is a numerical simulation that treats the evolution of the system with the same coupled equations (1.18). However, at each instant there is some probability that an atom will undergo spontaneous emission within a certain, small time interval. This probability is proportional to the probability $|a_2|^2$ for the atom of being in the excited state. In this 'Gedankenexperiment' the state of the system is observed by detecting the emitted photons with a photon counter. At each instant, the output of a random number generator is compared with the probability for a spontaneous emission, and if the random number is smaller, it is assumed that spontaneous emission has occurred (this is why this method is named after a city most famous for gambling). At that instant the evolution starts again from the values $a_1 = 1$ and $a_2 = 0$. Since there is no interest in the emitted photon, it is disregarded.

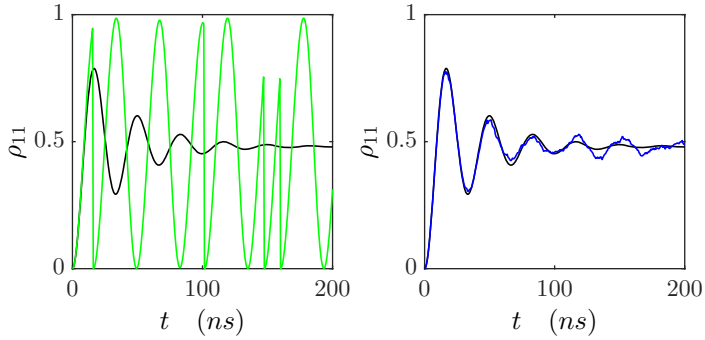

Figure 1.7: (code for download) (a) Quantum Monte Carlo wavefunction simulation. It is important to be aware, that a trajectory generated by a MCWF simulation only represents *one* of many possible trajectories of the system. (b) The evolution of the density matrix $\rho(t) = |\psi(t)\rangle\langle\psi(t)|$ (blue curve) is nothing else than the average (black curve) over all possible MCWF trajectories for the system.

Numerical results from this method, obtained in Exc. 1.3.0.5, are shown in Fig. 1.7. Note that the time when a spontaneous emission occurs is intrinsically unpredictable (otherwise the emission wouldn't be spontaneous). This randomness translates in trajectories of the wavefunction which, when we repeat the simulation procedure many times with the same starting condition, are all different. That is, a particular simulation results in a particular trajectory for a certain atom, but infinitely many different trajectories are possible. The green line in Fig. 1.7(a) shows one possible trajectory for one atom. The oscillatory behavior is evident, as suggested in Fig. 1.5; however, the oscillations are interrupted by spontaneous emission events projecting the atom into its ground state. Repeating the procedure with $N = 100$ atoms [see Fig. 1.7(b)] still results in oscillatory behavior for small time periods; however, these oscillations damp out for longer times. Also the discrete jumps, clearly visible for

$N = 1$, can are longer discernible. This results from the averaging process, since the emission times are random and thus different for different atoms. This causes the oscillations to be damped and the excitation probability reaches its steady-state value. In Exc. 1.3.0.6 we present an analytical calculation of the time evolution of a resonantly driven two-level system subject to spontaneous decay.

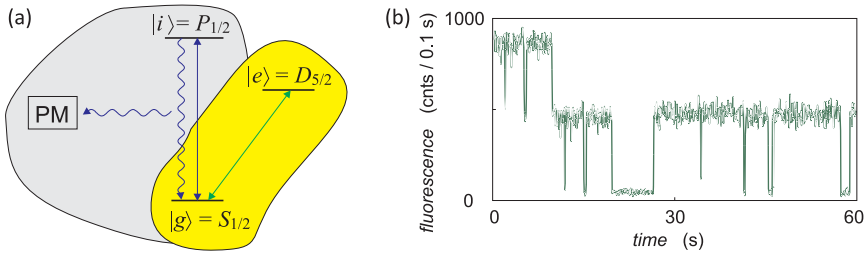

Figure 1.8: (a) Quantum measurement at the example of a three-level atom incorporating a weak (sample) transition and a strong (meter) transition. (b) Random Telegraph signal in the resonance fluorescence due to quantum jumps.

One common misconception that may arise from Fig. 1.7 is that the atoms eventually cease oscillating between the ground and excited states. In most experiments, measurement are made on a large number of atoms and indeed the oscillations are damped. However, Fig. 1.7(a) clearly shows that each individual atom still oscillates, but that these oscillations are damped out by the averaging process. This topic will reappear in the density matrix approach that describes the evolution of an ensemble of atoms [3]. Let us finally note that quantum jumps, whose existence have been the subject of longstanding controversies [138], have been observed experimentally in three-level systems (see Fig. 1.8) [115, 136, 137, 10].

1.3 Exercises

1.3.0.1 Ex: Rabi oscillation

The population of a two-level system be initially in state $|1\rangle$. What should be the duration of a perturbation to transfer the population to state $|2\rangle$?

1.3.0.2 Ex: Rabi method

Free atoms be illuminated by light pulses characterized by the Rabi frequency Ω, whose pulse area is (i) $\int_0^t \Omega \, dt = \pi$ and (ii) $= 2\pi$. For which frequency tuning $\Delta = \omega - \omega_0$ the excited state population is maximum? Draw the spectral profile of the population in the range $-5 < \Delta/\Omega < 5$.

[3] See script on *Quantum mechanics* (2023), Sec. 16.1.2.

1.3.0.3 Ex: Ramsey fringes

a. Consider a two-level atom illuminated by a $\frac{\pi}{2}$-pulse of nearly resonant light, $G \simeq \Omega$, and calculate the ground and excited state amplitudes.
b. How do the amplitudes evolve after the pulse if the detuning Δ is small but non-zero?
c. Derive the solution for $|a_2(t)|^2$ of the equations (1.23) for the resonant case ($\Delta = 0$) assuming the following initial conditions, $a_1(0) = -\frac{e^{\imath\phi/2}}{\sqrt{2}}$ and $a_2(0) = \imath\frac{e^{-\imath\phi/2}}{\sqrt{2}}$.
d. Discuss the case of two consecutive $\frac{\pi}{2}$-pulses separated by a time interval T.

1.3.0.4 Ex: Light-shift

Calculate the light-shift in a driven two-level system from the *effective Hamiltonian*,

$$\hat{H}_{eff} = \begin{pmatrix} 0 & \frac{1}{2}\Omega \\ \frac{1}{2}\Omega & \Delta - \frac{\imath}{2}\Gamma \end{pmatrix} . \tag{1.38}$$

Prepare spectra of the eigenvalues for $\Gamma/\Omega = 0$, 0.5, and 2.

1.3.0.5 Ex: Monte Carlo wavefunction simulation of quantum jumps

The possible occurrence of spontaneous emission produces a dynamics called *quantum trajectory*, which can be described by a non-hermitian *effective Hamiltonian*,

$$\hat{H}_{eff} = \hbar\Delta\sigma_z + \hbar\Omega\sigma^+ + c.c. - \tfrac{\imath}{2}\Gamma\sigma_z = \begin{pmatrix} 0 & \Omega \\ \Omega & \Delta - \frac{\imath}{2}\Gamma \end{pmatrix} ,$$

aiming at including energy dissipation processes.
a. Assuming $\Delta = 0 = \Omega$ verify that Γ is indeed the decay rate of the excited state.
b. How does the norm of an arbitrary state $|\psi(t)\rangle$ evolve in time?
c. Verify that the time evolution $|\psi'(t+dt)\rangle = e^{-\imath\hat{H}_{eff}dt}|\psi(t)\rangle$ followed by a renormalization $|\psi'(t+dt)\rangle \longrightarrow \frac{|\psi'(t+dt)\rangle}{\sqrt{\langle\psi'(t+dt)|\psi'(t+dt)\rangle}}$ conserves the norm of the wavefunction.
d. What is the probability for a spontaneous decay to occur within a time interval $[0, t]$?
e. Now, dissipative processes can be simulated by playing dices with random numbers ζ. We divide time into small intervals dt and propagate the wavefunction from $\psi(t)$ to $\psi(t+dt)$. Next, we generate a random number ζ, uniformly distributed between 0 and 1, which we compare to probability the probability p. In case, $\zeta > 1 - \langle\psi(t)|\psi(t)\rangle$, we conclude that there was no dissipative process, and we let the system proceed in peace, only renormalizing the wavefunction to compensate for the losses [109, 37]. Otherwise, if $\zeta < 1 - \langle\psi(t)|\psi(t)\rangle$, we conclude that there was a dissipative process, and the system is projected into the eigenstate ψ_0. This projection is abrupt and called *quantum jump*. Now, the evolution restarts from zero, ruled by the effective Hamiltonian. Implement a numerical simulation via,

$$|\psi(t)\rangle \curvearrowright |\psi(t+dt)\rangle \equiv \begin{pmatrix} \frac{(1-\imath\hat{H}dt)|\psi(t+dt)\rangle}{\sqrt{\langle\psi(t)|\psi(t)\rangle}} & \text{if} \quad \zeta > 1 - \langle\psi(t)|\psi(t)\rangle \\ |\psi_0\rangle \quad \text{if} \quad \zeta < 1 - \langle\psi(t)|\psi(t)\rangle \end{pmatrix} .$$

This is the method called *quantum Monte Carlo wavefunction simulation*.

1.3.0.6 Ex: Non-hermitian time evolution

We study the time evolution $|\psi(t)\rangle = e^{-\imath \hat{H}_{eff} t}|\psi(0)\rangle$ with the effective Hamiltonian (we set $\hbar = 1$),

$$\hat{H}_{eff} = \begin{pmatrix} 0 & \frac{1}{2}\Omega \\ \frac{1}{2}\Omega & -\frac{\imath}{2}\Gamma \end{pmatrix}$$

starting from the initial condition $\langle 2|\psi(0)\rangle = 1$.
a. Calculate the eigenvalues $E_\pm$ and the unitary transformation matrix U, where $U\hat{H}_{eff}U^{-1} = \hat{E}$ and

$$\hat{E} \equiv \begin{pmatrix} E_+ & 0 \\ 0 & E_- \end{pmatrix} .$$

b. Now calculate the evolution of $|\psi(t)\rangle$ and the norm $\langle\psi(t)|\psi(t)\rangle$.

1.4 Further reading

I.I. Sobelman, Springer Verlag, Berlin (1972), *Introduction to the Theory of Atomic Spectra* [ISBN]

M. Weissbluth, (Academic Press, Boston, 1989), *Photon-Atom Interactions* [ISBN]

M. Weissbluth, *Atoms and Molecules* [ISBN]

A. Corney, Clarendon Press, Oxford (1977), *Atomic and Laser Spectroscopy* [ISBN]

M. Tanifuji, World Scientific (2018), *Polarization Phenomena in Physics* [ISBN]

J. Dalibard et al., *Wave-Function Approach to Dissipative Processes in Quantum Optics* [DOI]

W. Nagourney et al., *Shelved Optical Electron Amplifier: Observation of Quantum Jumps* [DOI]

A. Schenzle et al., *Macroscopic quantum jump in a single atom* [DOI]

Chapter 2

The Bloch equations

As long as we are only interested in stimulated processes, such as the absorption of a monochromatic wave, the Schrödinger equation suffices to describe the light-atom interaction. A problem arises when we want to describe relaxation processes at the same time as excitation processes. Spontaneous emission (and any other dissipative process) must therefore be included in the physical description of the temporal evolution of our light-atom system. In this case, however, our system is no longer restricted to a single mode of the light field and the two atomic states of excitation. Spontaneous emission populates a statistical distribution of states of the light field and leaves the atom in a superposition of many momentum states. This situation can not be described by a single wavefunction, but only by a distribution of wavefunctions, and we can only expect to calculate the probability of finding the system within this distribution. The Schrödinger equation, therefore, no longer applies, and we need to trace the time evolution of a system characterized by a density operator describing a statistical mixture of quantum states. The equations which describe the time evolution of the matrix elements of this density operator are the optical Bloch equations, and we must use them instead of the Schrödinger equation. In order to appreciate the origin and the physical content of the optical Bloch equations we begin by reviewing the rudiments of the density matrix theory.

In this second lecture we will introduce the master equation for the description of the dynamics of driven atomic systems. We start in Sec. 2.1 with the definition of the density matrix, for which we will derive the two-level Bloch equations in Sec. 2.2. In Sec. 2.3 we discuss the role of spontaneous emission, in Sec. 2.3.2 line broadening mechanisms, and finally in Sec. 2.4 we give an outlook on the description of multilevel atoms driven by several laser fields.

2.1 Density operator

We define the *statistical operator* or *density operator* [1],

$$\boxed{\hat{\rho} \equiv \sum_k p_k \hat{P}_k \qquad \text{where} \qquad \hat{P}_k \equiv |\psi_k\rangle\langle\psi_k|} \ , \tag{2.1}$$

where $\{|\psi_k\rangle\}$ is a complete set of orthonormal states of the system under study. We consider a statistical distribution of these states with p_j being the probability of finding $|\psi_j\rangle$ in the set. Obviously, $\sum_k p_k = 1$. That is, the density operator acts on a member of the set $\{|\psi_k\rangle\}$ in a way to extract the probability of finding the system in $|\psi_j\rangle$,

$$\hat{\rho}|\psi_j\rangle = \sum_k p_k |\psi_k\rangle\langle\psi_k|\psi_j\rangle = p_j|\psi_j\rangle \ . \tag{2.2}$$

If all members of the set are in the same state, for example $|\psi_k\rangle$, the density operator reduces to,

$$\hat{\rho} = |\psi_k\rangle\langle\psi_k| \ , \tag{2.3}$$

and the system is in a *pure state* with $p_k = \delta_{1k}$. Each time a quantum state can be expressed by a single wave function, it is a pure state, but it does not have to be an eigenstate. Starting from the equation (2.2) we find,

$$\langle\psi_k|\hat{\rho}|\psi_j\rangle = p_j\delta_{kj} \ . \tag{2.4}$$

The diagonal elements of the density matrix are the probabilities of finding the system in $|\psi_j\rangle$, and assuming that all $|\psi_k\rangle$ are orthonormal, the non-diagonal elements of the incoherent sum (2.1) are necessarily zero [2], Besides that,

$$\sum_k \langle\psi_k|\hat{\rho}|\psi_k\rangle = 1 \ , \tag{2.5}$$

so that $\hat{\rho}$ contains all *available* information about the system, that is, our *knowledge* about its state. When the state of the system is unknown, $\hat{\rho}$ describes the probability of finding the system in each state. When the state is fully known, $\hat{\rho}$ describes a pure state, that is, a vector in the Hilbert space, which is unequivocally determined by a complete set of observables with their respective quantum numbers.

[1] In the presence of degeneracy or a continuous spectrum we can generalize the definition:

$$\hat{\rho} \equiv \sum_k p_k \hat{P}_k + \int p_\lambda \hat{P}_\lambda d\lambda \quad \text{where} \quad \hat{P}_k \equiv \sum_m |km\rangle\langle km| \quad \text{and} \quad \hat{P}_\lambda \equiv \int |\lambda\mu\rangle\langle\lambda\mu| d\mu \ .$$

Here, m and μ are degenerate quantum numbers, m, n are discrete, and λ, μ are continuous quantum numbers. The set of quantum numbers is complete, when

$$\sum\nolimits_{k,m} |km\rangle\langle km| = \hat{1} = \int |\lambda\mu\rangle\langle\lambda\mu| d\lambda d\mu \ .$$

The degree of degeneracy of a state $|k\rangle$ is $\mathrm{Tr}\ \hat{P}_k = \sum_m 1$. The probability of finding the system in the state $|k\rangle$ is $\langle\hat{P}_k\rangle = p_n \sum_m 1$.

[2] This is simply because we constructed the density operator to be diagonal in the basis $\{|\psi_k\rangle\}$. It does not mean, that the density operator cannot have non-diagonal elements in another basis.

The properties of the density operator are,

$$\boxed{\begin{array}{rcll} \hat{\rho} & = & \hat{\rho}^\dagger & \\ \langle\hat{\rho}\rangle & \geq & 0 & \\ \mathrm{Tr}\ \hat{\rho} & = & 1 & \\ \mathrm{Tr}\ \hat{\rho}^2 & \leq & 1 & \\ \det\hat{\rho} & = & 0 & \\ \hat{\rho} & = & \hat{\rho}^2 & \text{for a pure state} \end{array}} \ . \tag{2.6}$$

2.1.1 Matrix formalism

The next step is to develop matrix representations of the density operator by expanding the state vectors $|\psi_k\rangle$ in a complete orthonormal basis,

$$|\psi_k\rangle = \sum_n c_{nk}|n\rangle = \sum_n |n\rangle\langle n|\psi_k\rangle \ , \tag{2.7}$$

using the *completeness relation* $\sum_n |n\rangle\langle n| = \mathbb{I}$, and defining,

$$c_{nk} \equiv \langle n|\psi_k\rangle \tag{2.8}$$

as the projection of the state vector $|\psi_k\rangle$ on the basis vector $|n\rangle$. Now, we can write the density operator matrix representation within the basis $\{|n\rangle\}$ using the definition of $\hat{\rho}$ in Eq. (2.1) and replacing the expansions of $|\psi_k\rangle$ and $\langle\psi_k|$ of Eq. (2.7):

$$\hat{\rho} = \sum_k p_k|\psi_k\rangle\langle\psi_k| = \sum_k p_k \sum_{m,n} |n\rangle\langle n|\psi_k\rangle\langle\psi_k|m\rangle\langle m| = \sum_k p_k \sum_{m,n} c_{nk}c^*_{mk}|n\rangle\langle m| \ . \tag{2.9}$$

The matrix elements of $\hat{\rho}$ in this representation are

$$\rho_{nm} \equiv \langle n|\hat{\rho}|m\rangle = \sum_k p_k c_{nk}c^*_{mk} \tag{2.10}$$

with the diagonal elements $\langle n|\hat{\rho}|n\rangle = \sum_k p_k|c_{nk}|^2$ and $\rho^*_{nm} = \rho_{mn}$, which means that the operator $\hat{\rho}$ is Hermitian.

Example 1 (*Density operator for a mixed state*): Consider the following two possible superposition states of a two-level system,

$$|\psi_1\rangle = \sqrt{\tfrac{1}{2}}|1\rangle + \sqrt{\tfrac{1}{2}}|2\rangle \quad \text{and} \quad |\psi_2\rangle = \sqrt{\tfrac{9}{10}}|1\rangle + \sqrt{\tfrac{1}{10}}|2\rangle \ .$$

Being linearly independent, they form a basis. Let us assume that, for some reason, we do not know whether the system is in state $|\psi_1\rangle$ or state $|\psi_2\rangle$. The density operator describing our knowledge about the system is then,

$$\hat{\rho} = \tfrac{1}{2}|\psi_1\rangle\langle\psi_1| + \tfrac{1}{2}|\psi_2\rangle\langle\psi_2| \ .$$

Obviously, $\hat{\rho} \neq \hat{\rho}^2$, since

$$\hat{\rho} = \begin{pmatrix} 0.7 & 0.4 \\ 0.4 & 0.3 \end{pmatrix} \quad \text{but} \quad \hat{\rho}^2 = \begin{pmatrix} 0.65 & 0.4 \\ 0.5 & 0.25 \end{pmatrix} \ .$$

Example 2 (*Density operator for a single atom*): For a very simple system such as a single atom with several levels, that without spontaneous emission can be described by a single wavefunction $|\psi_1\rangle$, we can let $p_k = \delta_{1k}$. That is, the equations (2.9) and (2.10) reduce to,

$$\hat{\rho} = \sum_{m,n} c_{n1} c_{m1}^* |n\rangle\langle m| \quad \text{and} \quad \langle n|\rho|m\rangle = c_{n1} c_{m1}^* \ . \tag{2.11}$$

2.1.1.1 Measurement and trace

The sum of the diagonal elements of a matrix representing an operator is called the *trace*. This quantity represents a fundamental property of the density operator, since it is invariant with respect to any unitary transformation:

$$\text{Tr } \hat{\rho} \equiv \sum_n \langle n|\rho|n\rangle \ . \tag{2.12}$$

With the definition of the density operator (2.1) we can write the Eq. (2.12) as,

$$\text{Tr } \hat{\rho} \equiv \sum_{n,k} p_k \langle n|\psi_k\rangle\langle\psi_k|n\rangle \ . \tag{2.13}$$

Now, using the completeness relation,

$$\text{Tr } \hat{\rho} \equiv \sum_{n,k} p_k \langle\psi_k|n\rangle\langle n|\psi_k\rangle = \sum_k p_k \langle\psi_k|\psi_k\rangle = 1 \ , \tag{2.14}$$

which shows that the trace of the density operator representation is always 1 regardless of the basis of the matrix representation, thus justifying its interpretation as a probability density distribution.

Expectation values of observables are expressed by,

$$\langle \hat{A} \rangle = \sum_k p_k \langle\psi_k|\hat{A}|\psi_k\rangle \ . \tag{2.15}$$

On the other side,

$$\hat{\rho}\hat{A} = \sum_k p_k |\psi_k\rangle\langle\psi_k|\hat{A} \ , \tag{2.16}$$

and in the basis $\{|n\rangle\}$,

$$\langle n|\hat{\rho}\hat{A}|m\rangle = \langle n| \sum_k p_k |\psi_k\rangle\langle\psi_k|\hat{A}|m\rangle = \sum_k p_k \langle n|\psi_k\rangle\langle\psi_k|\hat{A}|m\rangle = \sum_k p_k \langle\psi_k|\hat{A}|m\rangle\langle n|\psi_k\rangle \ . \tag{2.17}$$

Now, along the diagonal, we have,

$$\langle n|\hat{\rho}\hat{A}|n\rangle = \sum_k p_k \langle\psi_k|n\rangle\langle n|\hat{A}|\psi_k\rangle \ . \tag{2.18}$$

With the completeness relation in the basis $\{|n\rangle\}$, we now have [3],

$$\boxed{\text{Tr } \hat{\rho}\hat{A} = \sum_k p_k \langle\psi_k|\hat{A}|\psi_k\rangle = \langle\hat{A}\rangle} \ . \tag{2.19}$$

The Eq. (2.19) says that the ensemble average of any dynamic observable $\hat{A}$ can be calculated from the diagonal elements of the operator matrix $\hat{\rho}\hat{A}$: Since the trace is independent of the basis (this will be shown in Exc. 2.7.0.1), each unitary transformation taking the matrix representation from a basis $\{|n\rangle\}$ to another one $\{|t\rangle\}$ leaves the trace invariant. Using the definition of a unitary transformation we can easily show that the trace of a cyclic permutation of a product is invariant. For example,

$$\text{Tr } [\hat{A}\hat{B}\hat{C}] = \text{Tr } [\hat{C}\hat{A}\hat{B}] = \text{Tr } [\hat{B}\hat{A}\hat{C}] \ , \tag{2.20}$$

and in particular

$$\text{Tr } [\hat{\rho}\hat{A}] = \text{Tr } [\hat{A}\hat{\rho}] = \langle\hat{A}\rangle \ . \tag{2.21}$$

In the Excs. 2.7.0.2 and 2.7.0.3 we apply the density operator to pure and mixed states of a two-level system. In Excs. 2.7.0.4 and 2.7.0.5 we study thermal mixtures.

2.1.2 Spontaneous emission

Statistical mixtures are not only a consequence of incomplete preparation of the system, but also occur if there is only partial detection of the final state. Suppose that for a certain quantum mechanical system there is a complete set of commuting operators and that the system is initially in a pure state. Performing a measurement on the system means *bringing it into contact with some kind of environment*, which will strongly affect *some* of the observables, in a way such as to destroy coherences between them and to project them into a distribution of eigenstates $|i\rangle$ with a probability distribution p_i. If we read out the results, we filter a single eigenstate out of the distribution, and conserve 'maximum knowledge' of the system. If we don't, then we have to describe the system by a statistical mixture of states $|i\rangle$. Note, that the system remains in a pure state with respect to the *unmeasured* observables, which did not interact with the environment.

Suppose a system consists of two parts A and B, but only part A is observed. Then information about part B is lost, and a statistical average over part B is necessary. Using the density matrix to describe the system, one has to take the trace over part B, or

$$\hat{\rho}_A = \text{Tr}_B \ \hat{\rho}_{AB} \ . \tag{2.22}$$

If the system was initially in a pure state ρ_{AB}, the incomplete detection process causes the pure state to evolve into a statistical mixture $\hat{\rho}_A$.

Now, spontaneous emission can be interpreted as a strong measurement of the excitation state of an atom, since the detection of an emitted photon would tell us

[3] In the presence of degeneracy or a continuous part of the spectrum we can generalize the definition of the expectation,

$$\langle\hat{X}\rangle \equiv \text{Tr } \hat{\rho}\hat{X} = \sum_{k,m} \langle km|\hat{\rho}\hat{X}|km\rangle \ .$$

the state of the atom shortly after the emission. However, as the emission direction is random, most spontaneous photons are never detected. Hence, spontaneous emission converts a pure state into a statistical mixture [4]. To be more specific, consider a two-level atom in its excited state. After a short time the atom has a probability to remain in the excited state, or it can make a transition to the ground state by spontaneous emission of a photon. The evolution of this system is given by,

$$|\psi\rangle = \alpha(t)|e,0\rangle + \sum_s \beta_s(t)|g,1_s\rangle \ , \tag{2.23}$$

where the state of the atom is indicated by $|g\rangle$ or $|e\rangle$. The notation $|0\rangle$ means that no photon has yet been emitted, and $|1_s\rangle$ means that one photon has been emitted into the mode denoted by $s \equiv (\mathbf{k}, \hat{\epsilon})$ with its wavevector $\mathbf{k}$ and its polarization $\hat{\epsilon}$. Note that the photon can be emitted in any direction with a certain polarization, so the sum runs over all possible modes s. If one only observes the state of the atom and not the emitted photon, then the atom will be found in either the excited state $|e\rangle$ or the ground state $|g\rangle$; nevertheless, it will no longer be in a pure state. The new state can be described by its density matrix $\hat{\rho}_{atom}$:

$$\hat{\rho}_{atom} = \mathrm{Tr}_{photon}\ |\psi\rangle\langle\psi| = |\alpha(t)|^2|e\rangle\langle e| + \sum_s |\beta_s(t)|^2|g\rangle\langle g| \ . \tag{2.24}$$

The pure state $|\psi\rangle$ has evolved to a statistical mixture of $|g\rangle$ and $|e\rangle$ since the emitted photon has not been observed. Eq. (2.24) shows that phase information has been lost from Eq. (2.23), and we immediately see that $\hat{\rho}^2_{atom} \neq \hat{\rho}_{atom}$.

The restriction to describing only the atom and the laser field and not the light spontaneously emitted in arbitrary directions with arbitrary polarizations results in a huge simplification, not to speak about the fact that spontaneous emission cannot be properly handled within the framework of a semi-classical description of the electromagnetic field as was done in Lecture 1, because it is induced by vacuum fluctuations of the field. In his famous 1917 paper [52], Einstein not only showed that stimulated emission was necessary to explain Planck's blackbody spectrum, but also derived the spontaneous emission rate using detailed balancing between spontaneous and stimulated processes. Although his result is correct, his derivation does not show the true nature of the spontaneous emission process. Its properties emerge from the Wigner-Weisskopf theory that is summarized here [149]. In this theory it is shown that an atom in the excited state decays exponentially as a result of the fluctuations of the quantized vacuum field. The rate of this decay process is just the spontaneous emission rate.

Consider an atom in the excited state at $t = 0$ and no photons in the radiation field, i.e. the system is initially in a pure state $|e,0\rangle$. Making a transition to the ground state by spontaneously emitting one photon into the radiation field, the system may evolve toward $|g,1_s\rangle$. The complete state of the system can now be described analogously to Eq. (1.10) by,

$$|\psi(t)\rangle = ae^{-\imath\omega_e t}|e,0\rangle + \sum_s b_s e^{-\imath(\omega_g+\omega)t}|g,1_s\rangle \ . \tag{2.25}$$

[4] See script on *Quantum mechanics* (2023), Sec. 14.3.1.

Note that the frequency of the photon ω in the exponent must be replaced by kc for the summation. Even though the summation runs over an infinite number of modes, this notation is sufficient for now. To describe the evolution of the wavefunction in time, the Hamiltonian of the system has to be defined. This requires the quantization of the electromagnetic field, which will be introduced in Sec. 2.5. However, the only part of the Hamiltonian that couples the two states in Eq. (2.25) is the atom-field interaction: the atomic and field parts play no role by themselves. Inserting Eq. (2.25) into the Schrödinger equation,

$$\imath\hbar\frac{d}{dt}|\psi(t)=\hat{H}|\psi(t)\rangle=\begin{pmatrix}\hbar\omega_e & \hbar\Omega_s & \hbar\Omega_s & \cdots\\ \hbar\Omega_s & \hbar\omega_g & 0 & \cdots\\ \hbar\Omega_s & 0 & \hbar\omega_g & \ddots\\ \vdots & \vdots & \ddots & \ddots\end{pmatrix}\begin{pmatrix}ae^{-\imath\omega_e t}\\ b_{s_1}e^{-\imath(\omega_g+\omega)t}\\ b_{s_2}e^{-\imath(\omega_g+\omega)t}\\ \vdots\end{pmatrix}\ , \tag{2.26}$$

that is,

$$\imath\hbar\frac{d}{dt}(ae^{-\imath\omega_e t})=\hbar\omega_e ae^{-\imath\omega_e t}+\sum_s b_s\hbar\Omega_s e^{-\imath(\omega_g+\omega)t}\ , \tag{2.27}$$

$$\imath\hbar\frac{d}{dt}(b_s e^{-\imath(\omega_g+\omega)t})=\hbar\omega_g b_s e^{-\imath(\omega_g+\omega)t}+a\hbar\Omega_s e^{-\imath\omega_e t}\ .$$

This coupling is analogous to its semi-classical counterpart discussed in Sec. 1.2.1, and the result for the time evolution of the two states is,

$$\imath\frac{da(t)}{dt}=\sum_s b_s(t)\Omega_s e^{-\imath(\omega-\omega_a)t}\qquad\text{and}\qquad\imath\frac{db_s(t)}{dt}=a(t)\Omega_s^* e^{\imath(\omega-\omega_a)t}\ , \tag{2.28}$$

where $\omega_a\equiv\omega_e-\omega_g$. These equations are similar to Eq. (1.18), where the coupling for each mode is given by $\hbar\Omega_s=-\mathbf{d}_{eg}\cdot\vec{\mathcal{E}}_\omega$ and Ω_s is called the vacuum Rabi frequency. The dipole moment is $\mathbf{d}_{eg}=e\langle e|\mathbf{r}|g\rangle$ and the electric field per mode is found from the classical expression for the energy density, $u_\omega=\varepsilon_0|\vec{\mathcal{E}}_\omega|^2$,

$$\vec{\mathcal{E}}_\omega=\hat{\epsilon}\sqrt{\frac{\hbar\omega}{2\varepsilon_0 V_m}}\ . \tag{2.29}$$

Here V_m is the volume used to quantize the field, and it will eventually drop out of the calculation. The total energy of the electromagnetic field in the volume V_m is given by $\hbar\omega/2$, corresponding to the zero point energy of the radiation field. By directly integrating the second Eq. (2.28) and substituting the result into the first Eq. (2.28), the time evolution of $a(t)$ is found to be,

$$\frac{da(t)}{dt}=-\sum_s|\Omega_s|^2\int_0^t dt'\ e^{-\imath(\omega-\omega_a)(t-t')}a(t')\ . \tag{2.30}$$

This represents an exponential decay of the excited state, and to evaluate the decay rate it is necessary to count the number of modes for the summation and then evaluate the time integral.

To count the number of modes $s = (\mathbf{k}, \hat{\epsilon})$, we represent the field by the complete set of traveling waves in a cube of side L. Since the field is periodic with a periodicity L, the components of $\mathbf{k}$ are quantized as $k_i = 2\pi n_i/L$, with $i = x, y, z$. Then $dn_i = (L/2\pi)dk_i$ and therefore $dn = (L/2\pi)^3 d^3k$. The frequency ω is given by $\omega = ck$, so [5],

$$dn = 2 \cdot \frac{V\omega^2}{8\pi^3 c^3} \sin\theta d\omega d\theta d\phi \ . \tag{2.31}$$

The factor of 2 on the right-hand side of Eq. (2.31) derives from the two independent polarizations $\hat{\epsilon}$ of the fluorescent photons. Now replace the summation in Eq. (2.30) by an integration over all possible modes, insert the result of Eq. (2.31), and then integrate over the angles θ and ϕ to find

$$\frac{da(t)}{dt} = -\frac{1}{6\varepsilon_0 \pi^2 \hbar c^3} \int d\omega \ \omega^3 d_{eg}^2 \int_0^t dt' \ e^{-\imath(\omega-\omega_a)(t-t')} a(t') \ . \tag{2.32}$$

where the volume V has dropped out, since $|\Omega_s|^2 \propto 1/V$. In this result, the orientation of the atomic dipole with respect to the emission direction has been taken into account, which yields a reduction factor of $\frac{1}{3}$ for a random emission direction.

The remaining time integral can be evaluated by assuming that the dipole moment d_{eg} varies slowly over the frequency interval of interest, so it can be evaluated at $\omega = \omega_a$. Furthermore, the time integral is peaked around $t = t'$, so that the coefficient $a(t)$ can be evaluated at time t and taken out of the integral. The upper boundary of the integral can be shifted toward infinity, and the result becomes,

$$\lim_{t\to\infty} \int_0^t dt' \ e^{-\imath(\omega-\omega_a)(t-t')} = \pi\delta(\omega-\omega_a) - \mathcal{P}\left(\frac{\imath}{\omega-\omega_a}\right) \ , \tag{2.33}$$

where $\mathcal{P}(x)$ is the principal value. The last term is purely imaginary and causes a shift of the transition frequency, which will not be discussed further. Substitution of the result of Eq. (2.33) into Eq. (2.32) yields the final result,

$$\boxed{\frac{da(t)}{dt} = -\frac{\Gamma}{2}a(t) \qquad \text{where} \qquad \Gamma \equiv \frac{\omega^3 d_{eg}^2}{3\pi\varepsilon_0\hbar c^3}} \ . \tag{2.34}$$

Since the amplitude of the excited state decays at a rate $\Gamma/2$, the population of the state decays with Γ and the lifetime of the excited state becomes $\tau = 1/\Gamma$.

The decay of the excited state is irreversible. In principle, the modes of the spontaneously emitted light also couple to the ground state in Eqs. (2.28), but there is an infinite number of modes in free space. The amplitude for the reverse process has to be summed over these modes. Since the different modes add destructively, the probability for the reverse process becomes zero. The situation can be changed by putting the atom in a reflecting cavity with dimensions of the order of the optical wavelength λ. Then the number of modes can be changed considerably compared to free space.

[5] See script on *Quantum mechanics* (2023), Sec. 1.3.2.

2.1.3 Temporal evolution of the density operator

The equations governing the temporal evolution of a quantum system depend on the choice of the picture, i.e. Schrödinger's, Heisenberg's, or the interaction picture. This, of course, also applies to a system represented by a density matrix.

Returning to the density operator definition (2.1), we can express its temporal dependence in terms of time-dependent quantum states and of the time evolution operator U,

$$\hat{\rho}(t) = \sum_k p_k |\psi_k(t)\rangle\langle\psi_k(t)| = \sum_k p_k U(t,t_0)|\psi_k(t_0)\rangle\langle\psi_k(t_0)|U^\dagger(t,t_0) \ . \tag{2.35}$$

Writing,

$$\hat{\rho}(t_0) = \sum_k p_k |\psi_k(t_0)\rangle\langle\psi_k(t_0)| \ , \tag{2.36}$$

we see immediately,

$$\hat{\rho}(t) = U(t,t_0)\hat{\rho}(t_0)U^\dagger(t,t_0) \ , \tag{2.37}$$

where, for the common case of a time-independent Hamiltonian,

$$U(t,t_0) = e^{-\imath\hat{H}(t-t_0)/\hbar} \ . \tag{2.38}$$

Now we find the time derivative of the density operator differentiating the two sides of (2.37) and substituting the Eqs.

$$\frac{dU}{dt} = \frac{1}{\imath\hbar}\hat{H}U \qquad \text{and} \qquad \frac{dU^\dagger}{dt} = -\frac{1}{\imath\hbar}U^\dagger\hat{H} \tag{2.39}$$

for the time derivatives U and $U^\dagger$. The result is

$$\boxed{\frac{d\hat{\rho}(t)}{dt} = \frac{\imath}{\hbar}[\hat{\rho}(t),\hat{H}]} \ . \tag{2.40}$$

The commutator itself can be considered as a *superoperator* acting, not any more on states but on operators, that is, we can write,

$$\boxed{\mathcal{L}\hat{\rho}(t) \equiv \frac{\imath}{\hbar}[\hat{\rho}(t),\hat{H}]} \ , \tag{2.41}$$

where $\mathcal{L}$ is called *Liouville operator*. The equation (2.40) is called *Liouville equation* or *von Neumann equation*. The Liouville equation describes the *time evolution of the density operator* which, in turn, describes the distribution of an ensemble of quantum states. Even though the form of the Liouville equation resembles the Heisenberg equation, Eq. (2.35) shows that $\hat{\rho}(t)$ is in the *Schrödinger picture*.

For a two-level system perturbatively interacting with a light field, the Hamiltonian can be decomposed into a stationary part and a time-dependent part,

$$\hat{H} = \hat{H}_{ele} + \hat{V}(t) = \hat{H}_{ele} - \hat{\mathbf{d}}\cdot\vec{\mathcal{E}}_\prime\cos\omega t \ , \tag{2.42}$$

where $\hat{H}_{ele}$ is the part of the Hamiltonian describing the atomic structure and $\hat{V}(t)$ the interaction of the dipole transition with the classical oscillating electric field.

2.2 Bloch equations for two-level atoms

Applying the Liouville operator (2.40) to a two-level atom coupled to a single-mode light field, we will now derive the optical Bloch equations, first without spontaneous emission. We will then introduce the atomic Bloch vector as a convenient and suggestive method to describe the time evolution of a coupled two-level atom. Spontaneous emission will only be incorporated into the optical Bloch equations in the subsequent section.

2.2.1 The matrix elements of the density operator

Since the optical Bloch equations are coupled differential equations relating the elements of the density operator matrix, we must examine the temporal dependence of these matrix elements, based on our knowledge of the operator's properties. We begin with the Liouville equation (2.40) and evaluate the elements of the matrix,

$$\begin{aligned}\langle m|\frac{d\hat{\rho}(t)}{dt}|n\rangle &= \tfrac{\imath}{\hbar}\langle m|[\hat{\rho}(t),\hat{H}]|n\rangle = \tfrac{\imath}{\hbar}\langle m|[\hat{\rho}(t),\hat{H}_{ele}+\hat{V}(t)]|n\rangle \\ &= \tfrac{\imath}{\hbar}(E_n-E_m)\langle m|\hat{\rho}(t)|n\rangle + \tfrac{\imath}{\hbar}\langle m|[\hat{\rho}(t),\hat{V}(t)]|n\rangle \ ,\end{aligned} \tag{2.43}$$

where $|m\rangle$ and $|n\rangle$ are members of a complete set of vectors of a basis $\{|k\rangle\}$ which are also eigen-kets of $\hat{H}_{ele}$ and span the space of $\hat{H}$. Now, we insert the completeness expression $\sum_k |k\rangle\langle k| = \mathbb{I}$ in the commutator on the right-hand side of Eq. (2.43):

$$\langle m|[\hat{\rho}(t),\hat{V}(t)]|n\rangle = \sum_k [\langle m|\hat{\rho}(t)|k\rangle\langle k|\hat{V}|n\rangle - \langle m|\hat{V}|k\rangle\langle k|\hat{\rho}(t)|n\rangle] \ . \tag{2.44}$$

For our two-level atom the complete set only includes two states: $|1(t)\rangle = |1\rangle$ and $|2(t)\rangle = e^{-i\omega_0 t}|2\rangle$. In addition, the matrix elements of the dipole coupling operator $\hat{V}$ are only non-diagonal,

$$V \equiv \langle 1|\hat{V}|2\rangle = \langle 2|\hat{V}|1\rangle \ . \tag{2.45}$$

Hence, Eq. (2.43) adopts the form,

$$\boxed{\begin{aligned}\frac{d\hat{\rho}_{11}}{dt} &= \tfrac{\imath}{\hbar}[\hat{\rho}_{12}V - \hat{\rho}_{21}V] \\ \frac{d\hat{\rho}_{22}}{dt} &= \tfrac{\imath}{\hbar}[\hat{\rho}_{21}V - \hat{\rho}_{12}V] = -\frac{d\hat{\rho}_{11}}{dt} \\ \frac{d\hat{\rho}_{12}}{dt} &= \imath\omega_0\hat{\rho}_{12} + \tfrac{\imath}{\hbar}[V(\hat{\rho}_{11}-\hat{\rho}_{22})] \\ \frac{d\hat{\rho}_{21}}{dt} &= -\imath\omega_0\hat{\rho}_{21} + \tfrac{\imath}{\hbar}[V(\hat{\rho}_{22}-\hat{\rho}_{11})] = \frac{d\hat{\rho}^*_{12}}{dt}\end{aligned}} \ , \tag{2.46}$$

remembering that the sum of the diagonal terms, called *populations*, must be unitary, and that the non-diagonal terms, called *coherences*, are complex,

$$\hat{\rho}_{11} + \hat{\rho}_{22} = 1 \quad , \quad \hat{\rho}_{21} = \hat{\rho}^*_{12} \ . \tag{2.47}$$

We have derived the optical Bloch equations from the Liouville equation, which is the fundamental equation of motion of the density operator, but so far, the Bloch equations do not include the possibility of spontaneous emission. We will learn later, how to include this phenomenon.

2.2.2 Rotating wave approximation

In the following, we will only consider exponentials rotating with the frequency $\Delta \equiv \omega - \omega_0$, and we will neglect terms rotating like $\Delta \equiv \omega + \omega_0$. This approximation, called *rotating wave approximation* (RWA) is good, when the Rabi frequency is sufficiently small, $\Omega \ll \omega$. Otherwise, we observe an energy correction of the levels called *Bloch-Siegert shift*. As we already did in deriving Eq. (1.23), the RWA can be implemented in the time dependence of the coupling operator,

$$V(t) = \hbar\Omega \cos\omega t \to \tfrac{\hbar}{2}\Omega e^{-\imath\omega t} \ , \tag{2.48}$$

neglecting the part $\frac{1}{2}\hbar\Omega e^{\imath\omega t}$.

The set of equations (2.46) constitutes the *optical Bloch equations* in the *Schrödinger picture*. Transforming to the interaction picture removes the temporal dependence of the basis vectors spanning the Hilbert space of the two-level atom. Once the RWA made, we can transform to the rotating system by the prescription,

$$\boxed{\rho_{12} \equiv \hat{\rho}_{12} e^{-\imath\omega t} \quad , \quad \rho_{22} \equiv \hat{\rho}_{22}} \ , \tag{2.49}$$

which, applied to the Bloch equations in the *Schrödinger picture* Eq. (2.46), yields,

$$\frac{d\rho_{22}}{dt} = \frac{\imath\Omega}{2}(\rho_{21} - \rho_{12}) \quad , \quad \frac{d\rho_{12}}{dt} = -\imath\Delta\rho_{12} + \frac{\imath\Omega}{2}(\rho_{11} - \rho_{22}) \ . \tag{2.50}$$

In Exc. 2.7.0.6 we derive the Bloch equations from the equations of motion for the population amplitudes a_1 and a_2.

For arbitrary starting conditions, the solution of these equations is not simple. To solve the problem we write the equations in a matrix form,

$$\boxed{\vec{\rho} \equiv \begin{pmatrix} \rho_{11} \\ \rho_{22} \\ \rho_{12} \\ \rho_{21} \end{pmatrix} \quad , \quad \mathbf{A} \equiv \begin{pmatrix} 0 & 0 & \frac{\imath}{2}\Omega & -\frac{\imath}{2}\Omega \\ 0 & 0 & -\frac{\imath}{2}\Omega & \frac{\imath}{2}\Omega \\ \frac{\imath}{2}\Omega & -\frac{\imath}{2}\Omega & -\imath\Delta & 0 \\ -\frac{\imath}{2}\Omega & \frac{\imath}{2}\Omega & 0 & \imath\Delta \end{pmatrix} \quad , \quad \dot{\vec{\rho}} = \mathbf{A}\vec{\rho}} \ . \tag{2.51}$$

To solve this system of differential equations, we calculate the eigenvalues of the matrix,

$$\begin{aligned} \det(\mathbf{A} - \lambda) = \lambda^2(\Delta^2 + \Omega^2) + \lambda^4 = 0 \\ \lambda = 0, \pm\imath G \ , \end{aligned} \tag{2.52}$$

with the *generalized Rabi frequency* $G \equiv \sqrt{\Delta^2 + \Omega^2}$. Therefore, the general solution is,

$$\begin{aligned} \rho_{22}(t) &= \rho_{22}^{(1)} + \rho_{22}^{(2)} e^{\imath G t} + \rho_{22}^{(3)} e^{-\imath G t} \\ \rho_{12}(t) &= \rho_{12}^{(1)} + \rho_{12}^{(2)} e^{\imath G t} + \rho_{12}^{(3)} e^{-\imath G t} \ . \end{aligned} \tag{2.53}$$

The coefficients follow from the Bloch equations with particular starting conditions. With a little algebra we get [6],

$$\begin{aligned}
\rho_{22}^{(1)} &= \rho_{22}(0) + \tfrac{1}{2G^2}\left[|\Omega|^2\,(1-2\rho_{22}(0)) - \Delta\,(\Omega\rho_{12}^*(0) + \Omega^*\rho_{12}(0))\right] \\
\rho_{22}^{(2)} &= \tfrac{1}{4G^2}\left[-|\Omega|^2(1-2\rho_{22}(0)) + (\Delta+G)\Omega\rho_{12}^*(0) + (\Delta-G)\Omega^*\rho_{12}(0)\right] \\
\rho_{22}^{(3)} &= \tfrac{1}{4G^2}\left[-|\Omega|^2(1-2\rho_{22}(0)) + (\Delta-G)\Omega\rho_{12}^*(0) + (\Delta+G)\Omega^*\rho_{12}(0)\right] \\
\rho_{12}^{(1)} &= \tfrac{1}{2G^2}\left[\Delta\Omega(1-2\rho_{22}(0)) + \Omega\,(\Omega\rho_{12}^*(0) + \Omega^*\rho_{12}(0))\right] \\
\rho_{12}^{(2)} &= \tfrac{\Delta-G}{4G^2}\left[-\Omega(1-2\rho_{22}(0)) + (\Delta+G)\tfrac{\Omega}{\Omega^*}\rho_{12}^*(0) + (\Delta-G)\rho_{12}(0)\right] \\
\rho_{12}^{(3)} &= \tfrac{\Delta+G}{4G^2}\left[-\Omega(1-2\rho_{22}(0)) + (\Delta-G)\tfrac{\Omega}{\Omega^*}\rho_{12}^*(0) + (\Delta+G)\rho_{12}(0)\right] \ .
\end{aligned} \tag{2.54}$$

To begin the discussion of this solution, let us consider a sample of atoms initially in the ground state when the light field is switched on at time $t = 0$,

$$\rho_{11}(0) = 1 = 1 - \rho_{22}(0) \quad , \quad \rho_{12}(0) = 0 = \rho_{21}(0) \ . \tag{2.55}$$

In this case, the conditions (2.54) simplify to,

$$\begin{aligned}
\rho_{22}^{(1)} &= \tfrac{|\Omega|^2}{2G^2} \quad , \quad \rho_{12}^{(1)} = \tfrac{1}{2G^2}\Delta\Omega \\
\rho_{22}^{(2)} &= \tfrac{-|\Omega|^2}{4G^2} \quad , \quad \rho_{12}^{(2)} = \tfrac{G-\Delta}{4G^2}\Omega \\
\rho_{22}^{(3)} &= \tfrac{-|\Omega|^2}{4G^2} \quad , \quad \rho_{12}^{(3)} = \tfrac{-G-\Delta}{4G^2}\Omega \ ,
\end{aligned} \tag{2.56}$$

such that,

$$\rho_{22} = \rho_{22}^{(1)} + \rho_{22}^{(2)}e^{\imath Gt} + \rho_{22}^{(3)}e^{-\imath Gt} = \frac{|\Omega|^2}{4G^2}(2 - e^{\imath Gt} - e^{-\imath Gt}) \tag{2.57}$$

$$\begin{aligned}
\rho_{12} &= (\rho_{12}^{(1)} + \rho_{12}^{(2)}e^{\imath Gt} + \rho_{12}^{(3)}e^{-\imath Gt})e^{\imath\Delta t} = \left(\frac{\Delta\Omega}{2G^2} - \frac{\Delta-G}{4G^2}\Omega e^{\imath Gt} - \frac{\Delta+G}{4G^2}\Omega e^{-\imath Gt}\right)e^{\imath\Delta t} \\
&= \frac{2\Omega}{4G^2}\left(\Delta - \Delta\cos Gt + \imath G\sin Gt\right)e^{\imath\Delta t} \ .
\end{aligned}$$

Using $\cos x = 1 - 2\sin^2\frac{x}{2}$ e $\sin x = 2\sin\frac{x}{2}\cos\frac{x}{2}$, we finally obtain,

$$\boxed{\rho_{22} = \frac{|\Omega|^2}{G^2}\sin^2\frac{Gt}{2} \quad , \quad \rho_{12} = \frac{\Omega}{G^2}\sin\frac{Gt}{2}\left(\Delta\sin\frac{Gt}{2} + \imath G\cos\frac{Gt}{2}\right)e^{\imath\Delta t}} \ . \tag{2.58}$$

2.2.3 Pauli matrices and the atomic Bloch vector

The internal structure of atoms is analyzed in atomic physics, where we find that the energy levels are discrete (Bohr's axiom). The center of mass motion of the atoms and collisions with other atoms are ignored, and concerning the interaction of the atoms with light, we are only interested in the aspect, that the interaction can induce transitions between internal states via absorption or emission of photons. It is the duty of atomic physics to calculate the frequencies and strengths of transitions (by

[6] See script on *Quantum mechanics* (2023), Sec. 13.4.2.

Hartree-Fock or similar methods), as well as their behavior in external electric and magnetic fields. The results of these calculations are visualized in energy level schemes called *Grotian diagrams*. In quantum optics we do not care, how the energies of the levels were calculated, but accept them as given. That is, we assume the Hamiltonian of the unperturbed atom to be diagonalized, so that according to (1.2) its internal structure can be written as,

$$\hat{H}_{ele} = \sum_j \hbar\omega_j |j\rangle\langle j| \ . \tag{2.59}$$

The electronic states are orthonormal $\langle i|j\rangle = \delta_{ij}$, and we define the transition operators by

$$\hat{\sigma}_{ij}|k\rangle = \delta_{jk}|i\rangle \ , \tag{2.60}$$

and $\hat{\sigma}^+_{ij} = \hat{\sigma}_{ji}$ satisfying the commutation relation,

$$[\hat{\sigma}_{ij}, \hat{\sigma}_{lk}] = \delta_{jl}\hat{\sigma}_{ik} - \delta_{ik}\hat{\sigma}_{lj} \ . \tag{2.61}$$

Many times we will restrict ourselves to atoms of two or three levels. For a two-level system we obtain the *Pauli spin matrix*. Every 2×2 matrix can be expanded on a Pauli matrix basis,

$$\begin{aligned}
\begin{pmatrix} \rho_{11} & \rho_{12} \\ \rho_{21} & \rho_{22} \end{pmatrix} &= |1\rangle\rho_{11}\langle 1| + |1\rangle\rho_{12}\langle 2| + |2\rangle\rho_{21}\langle 1| + |2\rangle\rho_{22}\langle 2| \\
&= \rho_{11}(\tfrac{1}{2} + \tfrac{1}{2}\hat{\sigma}_z) + \rho_{12}\hat{\sigma}^- + \rho_{21}\hat{\sigma}^+ + \rho_{22}(\tfrac{1}{2} - \tfrac{1}{2}\hat{\sigma}_z) \\
&= \rho_{11}\hat{\sigma}^+\hat{\sigma}^- + \rho_{12}\hat{\sigma}^- + \rho_{21}\hat{\sigma}^+ + \rho_{22}\hat{\sigma}^-\hat{\sigma}^+ = \begin{pmatrix} \langle\hat{\sigma}^-\hat{\sigma}^+\rangle & \langle\hat{\sigma}^-\rangle \\ \langle\hat{\sigma}^+\rangle & \langle\hat{\sigma}^+\hat{\sigma}^-\rangle \end{pmatrix} \ .
\end{aligned} \tag{2.62}$$

This formalism can easily be extended to an atom with many levels [7]. Solve the Exc. 2.7.0.7.

For the two-level case it is useful to introduce an alternative notation based on the *Bloch vector*,

$$\vec{\sigma} \equiv \begin{pmatrix} 2\mathfrak{Re}\ \rho_{12} \\ 2\mathfrak{Im}\ \rho_{12} \\ \rho_{22} - \rho_{11} \end{pmatrix} = \begin{pmatrix} \langle\sigma^-\rangle + \langle\sigma^+\rangle \\ \imath(\langle\sigma^-\rangle - \langle\sigma^+\rangle) \\ \langle\sigma^+\sigma^-\rangle - \langle\sigma^-\sigma^+\rangle \end{pmatrix} = \begin{pmatrix} \langle\sigma_x\rangle \\ \langle\sigma_y\rangle \\ \langle\sigma_z\rangle \end{pmatrix} \ . \tag{2.64}$$

We also define the torque vector,

$$\mathbf{G} \equiv \begin{pmatrix} \Omega \\ 0 \\ \Delta \end{pmatrix} \qquad \text{with} \qquad \left\|G^2\right\| = G = \sqrt{\Omega^2 + \Delta^2} \ , \tag{2.65}$$

[7] The Pauli spin matrices are,

$$\hat{\sigma}^x \equiv \begin{pmatrix} 0 & 1 \\ 1 & 0 \end{pmatrix} \quad , \quad \hat{\sigma}^y \equiv \begin{pmatrix} 0 & \imath \\ -\imath & 0 \end{pmatrix} \quad , \quad \hat{\sigma}^z \equiv \begin{pmatrix} -1 & 0 \\ 0 & 1 \end{pmatrix} \ . \tag{2.63}$$

the length of which is simply the Rabi frequency. With this, we can write the Bloch equations,

$$\boxed{\frac{d\vec{\sigma}}{dt} = \mathbf{G} \times \vec{\sigma}} \ , \tag{2.66}$$

as will be shown in Exc. 2.7.0.8. ρ_{12} describes the polarization and $\rho_{22} - \rho_{11}$ the *population inversion* of the atom. The equation is analogous to the equation of motion for a *rigid rotor* or *spinning top* (for example, a dipole in a homogeneous field). It displays phenomena such as *precession* and *nutation*. The physical content and usefulness of the Bloch vector will become clearer when we use the formalism to analyze electric and magnetic couplings. In Exc. 2.7.0.9 we verify that the Bloch vector is normalized (as long as spontaneous emission is not considered).

2.2.4 Manipulation of the state by sequences of radiation pulses

The temporal dependence of the three components of the atomic Bloch vector provides a useful illustration of the atom-field interaction. Resonant coupling, $\Delta = 0$ and $G = \Omega$, puts the solutions (2.58) into the form,

$$\rho_{22}(t) = \tfrac{1}{2}(1 - \cos\Omega t) \quad , \quad \rho_{12}(t) = \tfrac{\imath}{2}\sin\Omega t \ , \tag{2.67}$$

that is,

$$\vec{\sigma}(t) = \begin{pmatrix} 0 \\ \sin\Omega t \\ -\cos\Omega t \end{pmatrix} \ . \tag{2.68}$$

That is, a resonant pulse rotates a Bloch vector initially pointing in the direction $-z$ within the plane z-y, until it arrives, at time $t = \frac{\pi}{2\Omega}$, at the $+y$ direction and at time $t = \frac{\pi}{\Omega}$ at the $+z$ direction. This means that the entire population has been transferred to the excited state. The Bloch vector continues to rotate (the movement is called *nutation*) around the torque vector $\mathbf{G}$ which, as can be seen from Eq. (2.66), points at the $+x$ direction when $\Delta = 0$. The nutation frequency is proportional to the force Ω of the atom-field interaction. With the Eq. (2.58) we see that the population oscillates between the ground and excited state with the frequency Ω. This means that the energy $\hbar\omega$ is periodically exchanged between the atom and the field. A pulse of resonant light of duration such that $\tau = \pi/2\Omega$ is called a $\pi/2$-pulse. The nutation is illustrated in Fig. 2.1(a).

Once the coherence has been excited by a detuned radiation, $\Delta \neq 0$, the Bloch vector does not stand still, even after the radiation has been switched off. To see this, we consider again the general solution (2.54) now entering $\Omega = 0$. If the Bloch vector is initially at a point in the unitary circle of the plane z-y, it will rotate according to the formula,

$$\rho_{22}(t) = \rho_{22}(0) \quad , \quad \rho_{12}(t) = \rho_{12}(0)e^{-\imath\Delta t} \ , \tag{2.69}$$

that is,

$$\vec{\sigma}(t) = \begin{pmatrix} \rho_{12}(0)\sin\Delta t \\ \rho_{12}(0)\cos\Delta t \\ 2\rho_{22}(0) - 1 \end{pmatrix} \ . \tag{2.70}$$

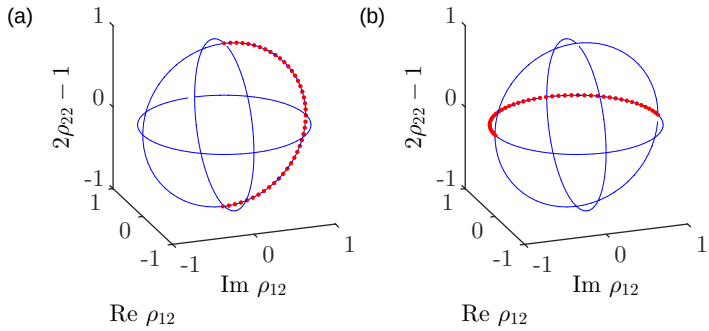

Figure 2.1: (code for download) (a) Nutation of the Bloch vector. The red circles show the evolution of the Bloch vector on the Bloch sphere for a resonant π-pulse. (b) Precession of the Bloch vector.

That is, the Bloch vector performs a motion of *precession* around the symmetry axis. The precession is illustrated in Fig. 2.1(b).

The evolution of the Bloch vector on the surface of the Bloch sphere under the influence of radiation fields can be considered a coherent trajectory of the wavefunction of the atomic state, which is therefore subject to interference phenomena [85]. Interferometers can be realized by sequences of consecutive pulses splitting populations, exciting coherences, and remixing populations.

Sensors based on interferometry of atomic excitation are nowadays among the most accurate and most sensitive. We will discuss the method of radiation pulse sequences in Exc. 2.7.0.10.

2.3 Bloch equations with spontaneous emission and line broadenings

2.3.1 Phenomenological inclusion of spontaneous emission

To find the Bloch equations including spontaneous emission, we insert the term $-\frac{\imath}{2}\Gamma a_2$ obtained in Eq. (2.34) into the Eqs. (1.18),

$$\Omega^* \cos\omega t e^{\imath\omega_0 t} a_1 - \imath\frac{\Gamma}{2}a_2 = \imath\frac{da_2}{dt} \ , \tag{2.71}$$

that is, the equations of motion can be corrected by simply replacing,

$$\frac{da_2}{dt} \curvearrowright \left(\frac{d}{dt}+\frac{\Gamma}{2}\right) a_2 \ . \tag{2.72}$$

Knowing $\rho_{mn} = a_m^* a_n$, it is easy to check,

$$\frac{d\rho_{22}}{dt} \curvearrowright \left(\frac{d}{dt}+\Gamma\right)\rho_{22} \qquad \text{and} \qquad \frac{d\rho_{12}}{dt} \curvearrowright \left(\frac{d}{dt}+\frac{\Gamma}{2}\right)\rho_{12} \ . \tag{2.73}$$

The Bloch equations become,

$$\boxed{\frac{d}{dt}\begin{pmatrix}\rho_{11}\\ \rho_{22}\\ \tilde{\rho}_{12}\\ \tilde{\rho}_{21}\end{pmatrix} = \begin{pmatrix} 0 & \Gamma & \frac{\imath}{2}\Omega & -\frac{\imath}{2}\Omega \\ 0 & -\Gamma & -\frac{\imath}{2}\Omega & \frac{\imath}{2}\Omega \\ \frac{\imath}{2}\Omega & -\frac{\imath}{2}\Omega & -\imath\Delta-\frac{\Gamma}{2} & 0 \\ -\frac{\imath}{2}\Omega & \frac{\imath}{2}\Omega & 0 & \imath\Delta-\frac{\Gamma}{2}\end{pmatrix}\begin{pmatrix}\rho_{11}\\ \rho_{22}\\ \tilde{\rho}_{12}\\ \tilde{\rho}_{21}\end{pmatrix}} \,. \tag{2.74}$$

Example 3 (*Langevin equation*): The *Heisenberg equation* for the evolution of the internal degrees of freedom, including the phenomenologically introduced decay, is also called *Langevin equation*. It can be written as,

$$i\frac{d\hat{\sigma}}{dt} = \tfrac{1}{\hbar}[\hat{\sigma},\hat{H}] - \tfrac{\imath}{2}\Gamma\hat{\sigma}\ ,$$

and analogously for $\hat{\sigma}_z$. With the Hamiltonian $\hat{H} = \hbar\Delta\hat{\sigma}^\dagger\hat{\sigma} + \frac{1}{2}\hbar\Omega(e^{\imath\omega t}\hat{\sigma} + h.c.)$ we obtain, using the Pauli spin matrices, exactly the Bloch equations,

$$i\dot{\hat{\sigma}} = \Delta[\hat{\sigma},\hat{\sigma}^\dagger\hat{\sigma}] + \tfrac{1}{2}\Omega e^{-\imath\omega t}[\hat{\sigma},\hat{\sigma}^\dagger] - \tfrac{\imath}{2}\Gamma\hat{\sigma} = -\Delta\hat{\sigma}_z - \tfrac{1}{2}\Omega e^{-\imath\omega t}\hat{\sigma}_z - \tfrac{\imath}{2}\Gamma\hat{\sigma}$$
$$i\dot{\hat{\sigma}}_z = \Delta[\hat{\sigma}_z,\hat{\sigma}^\dagger\hat{\sigma}] + \tfrac{1}{2}\Omega e^{-\imath\omega t}[\hat{\sigma}_z,\hat{\sigma}^\dagger] + \tfrac{1}{2}\Omega e^{\imath\omega t}[\hat{\sigma}_z,\hat{\sigma}] - \tfrac{\imath}{2}\Gamma\hat{\sigma}_z = -\Omega(\hat{\sigma}^\dagger - \hat{\sigma}) - \tfrac{\imath}{2}\Gamma\hat{\sigma}_z\ .$$

2.3.1.1 Stationary solution of the Bloch equations

The dissipation introduced by the spontaneous emission allows the system to reach a steady state. Letting the time derivatives be 0, we obtain the stationary solutions,

$$\boxed{\rho_{22}(\infty) = \frac{\frac{1}{4}|\Omega|^2}{\Delta^2 + \frac{1}{2}|\Omega|^2 + \frac{1}{4}\Gamma^2} \quad , \quad \rho_{12}(\infty) = e^{\imath\Delta t}\frac{\frac{1}{2}\Omega(\Delta - \frac{\imath}{2}\Gamma)}{\Delta^2 + \frac{1}{2}|\Omega|^2 + \frac{1}{4}\Gamma^2}} \,. \tag{2.75}$$

This will be shown in Exc. 2.7.0.11. The denominators have an extra term $\frac{1}{2}\Omega^2$ contributing to an *effective* widths of ρ_{22} and ρ_{12},

$$\Gamma_{\text{eff}} = \sqrt{2|\Omega|^2 + \Gamma^2}\ . \tag{2.76}$$

This effect is called *power broadening* or *saturation broadening*. The phase factor $e^{i\Delta t}$ describes the optical precession of the Bloch vector.

By introducing the *saturation parameter*,

$$s \equiv \frac{2|\Omega|^2}{4\Delta^2 + \Gamma^2}\ , \tag{2.77}$$

we can rewrite the stationary dipole moment and the excited state population (2.75) as,

$$\boxed{\rho_{22}(\infty) = \frac{s/2}{1+s} \quad , \quad \rho_{12}(\infty) = e^{\imath\Delta t}\frac{\Delta - \imath\Gamma/2}{\Omega}\frac{s}{1+s}} \,. \tag{2.78}$$

and

$$|\rho_{12}(\infty)|^2 = \frac{s/2}{(1+s)^2}\ . \tag{2.79}$$

Fig. 2.2(a) shows the Rabi oscillations damped by spontaneous emission. For long times the population of the excited state ρ_{22} converges to the asymptote (2.78). Fig. 2.2(b) shows the temporal evolution of the Bloch vector subject to spontaneous emission.

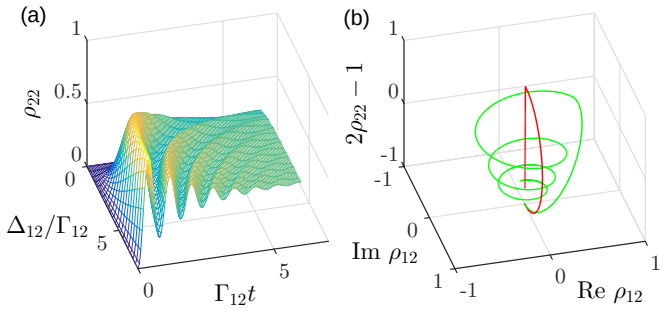

Figure 2.2: (code for download) (a) Rabi oscillations damped by spontaneous emission for Rabi frequencies between $\Omega/\Gamma = 0.2, .., 5$. (b) Evolution of the Bloch vector subject to spontaneous emission ($\Gamma_{12} = 0.05\Omega_{12}$) after of a resonant π-pulse (blue) and after a π-pulse with detuning $\Delta_{12} = \Omega_{12}/2$.

2.3.2 Line broadening mechanisms

While it is technically challenging to observe the dynamics of single atoms, it is relatively easy monitor the dynamics of ensembles of atoms, provided that they react synchronously to incident radiation. The concentration of a sufficient number of atoms in a small volume can, however, introduce additional (desirable or undesirable) effects. Collisions, for instance, induce (irreversible) decoherence. On the other hand, if the ensemble is sufficiently dense that the mean distance between atoms is less than a resonant wavelength, then the transition dipoles of the individual atoms will couple to produce a collective dipole moment and generate effects known as superradiance.

Thermal motion of the atoms is another undesired effect, because every atom will interact with the radiation on a different Doppler-shifted frequency. This leads to diffusion of the individual atomic Bloch vectors in the x-y-plane, which in turn limits the resolution of interferometric applications. We will discuss in Exc. 2.7.0.12 the *photon echo method*, which allows to circumvent this specific problem.

These perturbative effects limiting the resolution of atomic spectroscopy manifest themselves as broadening and/or shifts of atomic resonances. Free atoms, as well as atoms confined in potentials, have kinetic energy and evolve on extended phase space trajectories. If the spatial localization is less than the effective cross section of the exciting laser beam, then the interaction time is limited and the resonance lines are broadened by the Fourier effect in a process called *transit time broadening*, and the efficiency of fluorescence collection is reduced. The same happens with the *Doppler effect*: Only those atoms that have a specific velocity along the optical axis defined by the laser beam can interact. Free as well as confined atoms can only scatter when they are in specific cells of the phase space.

There are two different fundamental types of broadening. The so-called *homogeneous broadening* affects all atoms in the same way regardless of their positions or velocities. It usually give rise to Lorentzian line profiles and can be included in the Bloch equations. It correspond to an acceleration of the relaxation. Examples are the natural linewidth, saturation broadening, and collision broadening.

The so-called *inhomogeneous broadening* is due to a displacement of atomic levels, which may be different for each atom. Averaging over a large sample of atoms,

the displacements generate an *effective* broadening usually with a Gaussian line profile. It *can not* be included in the Bloch equations, but only as an average over all trajectories of all atoms. It does not correspond to an accelerated relaxation. Inhomogeneous broadening is often due to external perturbations, e.g., Doppler broadening and broadening due to temporal fluctuations or spatial inhomogeneities of external electric or magnetic fields. In Exc. 2.7.0.13 we calculate the optical density of atomic clouds. In Exc. 2.7.0.14 we present a spectroscopic technique bypassing the Doppler broadening called *Doppler-free spectroscopy* and calculate the *Lamb-dip* profile.

2.3.2.1 Saturation broadening

Eq. (2.76) shows that when the power of the incident light increases, the population of the excited state saturates at a limit value of $\rho_{22} = \frac{1}{2}$. The *saturation parameter* defined in (2.77) measures the degree of saturation. When the narrowband light source is tuned to resonance, the saturation parameter is basically a measure for the ratio between the stimulated population transfer rate Ω and the spontaneous decay rate Γ. We can rewrite the stationary population of the excited level as in (2.78). In resonance and with the saturation parameter $s = 1$, we obtain

$$\Omega = \tfrac{1}{\sqrt{2}}\Gamma \ . \tag{2.80}$$

We can use equation (2.80) to define the *saturation intensity* I_{sat} for an atom with the transition dipole d_{12}. The intensity is related to the electric field amplitude via,

$$\bar{I} = \tfrac{1}{2}\varepsilon_0 c\mathcal{E}_0^2 \ . \tag{2.81}$$

Therefore, using the definition of the Rabi frequency, $\hbar\Omega = d_{12}\mathcal{E}_0$, and the relationship between d_{12} and Γ given by Eq. (2.34), we have,

$$\boxed{I_{sat} = \frac{g_1}{g_2}\frac{2\pi^2 c\hbar}{3\lambda_0^3}\Gamma} \ , \tag{2.82}$$

taking into account the degeneracies g_j of the levels.

2.3.2.2 Collision broadening

The theory of atomic collisions covers a large area of research, including elastic and inelastic, reactive and ionizing processes. In low-pressure gases at room temperature or hotter we need only consider the simpler processes: long-range van der Waals interactions that result in *elastic collisions*. The 'low pressure' criterion requires that the average free path between collisions be greater than any linear dimension of the gas volume. Under these conditions, collisions can be modeled with straight trajectories, along which the interaction time is short and the time between collisions is long in comparison with the radiative lifetime of the excited atomic state. Then, the impact of a collision on the emission of a radiating atom causes a loss of coherence due to a phase interruption of the excited state atomic wavefunction. The term 'elastic' means that the collision does not disturb the populations of the internal states, so we only need to consider the off-diagonal elements of the density matrix,

$$\frac{d\rho_{12}}{dt} = \imath\frac{\Omega_0}{2}e^{\imath(\omega-\omega_0)t}(\rho_{11}-\rho_{22}) - \gamma'\rho_{12} \ , \tag{2.83}$$

where γ' is the sum of the spontaneous emission γ and the collision rate γ_{col},

$$\boxed{\gamma' = \gamma + \gamma_{col}} \ . \tag{2.84}$$

The inverse of the collision rate is simply the time between phase interruptions or the time between collisions. Now, for collisions between hard cores of atoms of mass m (with reduced mass $m_{red} = m/2$) and with radius ρ in a gas with density n consisting of a single species, a standard analysis based on the kinetic theory of dilute gases shows that the time between collisions is given by the *collision rate*,

$$\gamma_{col} = \tau_{col}^{-1} = \sigma n \bar{v} \ , \tag{2.85}$$

where $\bar{v} = \sqrt{\frac{8k_BT}{\pi m_{red}}}$ is the average collision velocity in a homogeneous gas at the temperature T and $\sigma = \sqrt{8}\pi\rho^2$ the collision cross section. Thereby [8] [148],

$$\boxed{\gamma_{col} = \frac{8\rho^2 n}{\sqrt{m_{red}/\pi k_B T}}} \ . \tag{2.86}$$

Substituting the generalized γ' of (2.84) for γ in the Bloch equations (2.75), we find the stationary solutions,

$$\rho_{22} = \frac{\frac{1}{4}\frac{\gamma'}{\gamma}|\Omega|^2}{\Delta^2 + \frac{1}{2}\frac{\gamma'}{\gamma}|\Omega|^2 + \gamma'^2} \quad , \quad \rho_{12} = e^{\imath(\omega-\omega_0)t}\frac{\frac{1}{2}\Omega(\Delta - \imath\gamma')}{\Delta^2 + \frac{1}{2}\frac{\gamma'}{\gamma}|\Omega|^2 + \gamma'^2} \ . \tag{2.87}$$

The effective linewidth (radiative and collisions) is,

$$\Gamma'_{\text{eff}} = 2\sqrt{\gamma'^2 + \tfrac{1}{2}\tfrac{\gamma'}{\gamma}|\Omega|^2} \ . \tag{2.88}$$

When the excitation is sufficiently weak, so that power broadening can be neglected in comparison to collision broadening, the second term can be discarded,

$$\Gamma'_{\text{eff}} = 2(\gamma + \gamma_{col}) \ . \tag{2.89}$$

The equations (2.76) and (2.89) express the linewidths in the limits of dominating power and collision broadening, respectively. Note that the susceptibility, absorption coefficient, and absorption cross-section retain their Lorentzian profile, but with a larger width due to collisions. Since each atom is subject to the same broadening mechanism, the broadening is homogeneous.

2.3.2.3 Doppler broadening

The *Doppler broadening* is simply the apparent frequency distribution of a sample of radiating atoms at temperature T. The contribution of each atom to the radiation appears detuned by the *Doppler shift* because of its velocity. The frequency shift for a non-relativistically moving particle is $\omega = \omega_0/(1 - \frac{v}{c})$, such that,

$$\Delta \equiv \omega - \omega_0 \simeq \omega_0 \frac{v}{c} = \mathbf{k}\cdot\mathbf{v} = kv_z \ , \tag{2.90}$$

[8] See script on *Quantum mechanics* (2023), Sec. 13.4.2.

where $\mathbf{k}$ is the wavevector of the light and $\mathbf{v}$ is the velocity of the atom. This distribution of Doppler shifts of a gaseous sample in thermal equilibrium follows the probability distribution of velocities,

$$P(v_z)dv_z \propto e^{-mv_z^2/2k_BT}dv_z = e^{-mc^2\Delta^2/2\omega_0^2 k_BT}\frac{c}{\omega_0}d\omega \ . \tag{2.91}$$

This frequency distribution is a Gaussian centered at $\omega = \omega_0$ and with the width,

$$\text{FWHM} = 2\omega_0\left(\frac{2k_BT\ln 2}{mc^2}\right)^2 \ . \tag{2.92}$$

A measure of the width is also the *standard deviation*,

$$2\sigma = \frac{2\omega_0}{c}\sqrt{\frac{k_BT}{m}} = \frac{\text{FWHM}}{1.177} \ . \tag{2.93}$$

From Eq. (2.91) we can see that the line profile is,

$$\mathcal{D}(\omega-\omega_0) \equiv \frac{1}{\sqrt{2\pi}}\frac{m}{k_BT}e^{-(\omega-\omega_0)^2/2\sigma^2}d\omega \ . \tag{2.94}$$

The profile compares with the Lorentzian profile Eq. (2.75) associated with natural, power, or collision broadening. Doppler broadening is a property of the atomic ensemble, each atom suffering a unique but different displacement than the other atoms. Hence, it is called *inhomogeneous broadening*.

The Heisenberg equation used to derive the Bloch equations assumes immobile atoms. However, we can easily apply the Galilei transformation to a system, where the atoms move with the given velocity $\mathbf{v}$,

$$(\partial_t + \mathbf{v}\cdot\nabla)\rho(\mathbf{r},t) = -\tfrac{\imath}{\hbar}[\hat{H},\rho(\mathbf{r},t)] \ . \tag{2.95}$$

Since the light fields propagate as $e^{\imath(\omega t-\mathbf{k}\cdot\mathbf{r})}$, the solution of the above equation simply follows from the immobile solution with the substitution $\Delta \to \Delta - \mathbf{k}\cdot\mathbf{v}$.

For a cloud obeying Maxwell's velocity distribution, $P(v) \sim e^{-mv^2k_BT}$,

$$\bar{\rho}(\Delta) = \frac{1}{\sqrt{2\pi}\delta}\int_{\mathbb{R}} e^{-(\mathbf{k}\cdot\mathbf{v})^2/2\delta^2}\rho(\Delta-\mathbf{k}\cdot\mathbf{v})d(\mathbf{k}\cdot\mathbf{v}) \ . \tag{2.96}$$

The average of the density operator over all velocities, $\bar{\rho}$, therefore follows as the convolution of the density operator ρ (obtained as the solution of the Bloch equation) and the Gaussian function $G(\Delta) = (2\pi\delta^2)^{-1/2}e^{-\Delta^2/2\delta^2}$,

$$\bar{\rho}(\Delta) = (G\star\rho)(\Delta) \ . \tag{2.97}$$

It is clear that in many practical circumstances homogeneous and inhomogeneous processes simultaneously contribute to the broadening of lines. In these cases, we can consider that the radiation of each atom, homogeneously broadened by phase-interruption processes (such as spontaneous emission or collisions), is displaced by

the Doppler effect within the Maxwell-Boltzmann distribution corresponding to the temperature T. The profile of the gaseous sample, therefore, is a convolution of homogeneous and inhomogeneous profiles. The resulting profile is called *Voigt profile*:

$$V(\omega-\omega_0) = \int_{-\infty}^{\infty} \mathcal{L}(\omega-\omega_0-\omega')\mathcal{D}(\omega-\omega_0)d\omega' \qquad (2.98)$$
$$= \frac{\gamma}{2\sigma\sqrt{2\pi}} \int_{-\infty}^{\infty} \frac{e^{-(\omega-\omega_0)^2/2\sigma^2}}{(\omega-\omega_0-\omega')^2+(\gamma/2)^2} d\omega' \ .$$

This integral has no analytical solution, but it is easy to solve numerically. Resolve Exc. 2.7.0.15.

2.4 Multi-level systems

The two-level system represents an idealization of the real atom, since at least one of the levels is usually degenerate. Many important phenomena in quantum optics are not found in this system, but depend on the existence of a third level, for example, optical pumping (essential for laser operation), quantum jumps or dark resonances [which are at the basis of the phenomenon of electromagnetically induced transparency (EIT)].

2.4.1 Liouville equation

The Liouville equation (2.40) describing the time evolution of the density operator for a two-level system has been derived from the Schrödinger equation and thus only accounts for the coherent evolution of the system. The dissipative evolution due to spontaneous emission obtained from the *Weisskopf-Wigner* theory in Sec. 2.1.2 has been introduced into the Bloch equation more or less empirically via the prescription (2.73). Now, it is possible to show (see Excs. 2.7.0.16, 2.7.0.17, and 2.7.0.18), that the two-level Bloch equations can be cast into the form,

$$\boxed{\begin{array}{lcll} \dot{\hat{\rho}}(t) & = & (\mathcal{L}_0+\mathcal{L}_{sp})\hat{\rho}(t) & \text{with} \\ \mathcal{L}_0\hat{\rho}(t) & \equiv & \frac{\imath}{\hbar}[\hat{\rho}(t),\hat{H}] \quad \text{and} & \mathcal{L}_{sp} = \frac{\Gamma}{2}(2\hat{\sigma}\hat{\rho}\hat{\sigma}^+ - \hat{\sigma}^+\hat{\sigma}\hat{\rho} - \hat{\rho}\hat{\sigma}^+\hat{\sigma}) \end{array}} \ , \qquad (2.99)$$

where $\hat{\sigma}^{\pm}$ are the Pauli matrices. This equation is called *master equation*, and the dissipative part of the Liouvillean is called *Lindbladt operator*. The Lindbladt operator can also be derived in a rigorous way directly from a Weisskopf-Wigner calculation.

The derivation can now be extended to multilevel systems excited by several lasers and coupled to the electromagnetic vacuum. The master equation (2.99) stays the same, but with a generalized Hamiltonian and Lindbladt operator,

$$\hat{H}_{ele} = \sum_i \hbar\omega_i \hat{\sigma}_{ji}\hat{\sigma}_{ij} \qquad , \qquad \hat{H}_{int} = \tfrac{\hbar}{2}\Omega_{ij}\left(e^{-\imath\omega_{ij}t}\hat{\sigma}_{ij} + e^{\imath\omega_{ij}t}\hat{\sigma}_{ji}\right) \qquad (2.100)$$

$$\mathcal{L}_{sp}\hat{\rho} = \sum_{i,j} \Gamma_{ij}\left([\hat{\sigma}_{ij},\hat{\rho}\hat{\sigma}_{ij}^+] + [\hat{\sigma}_{ij}\hat{\rho},\hat{\sigma}_{ij}^+] + 2\beta_{ij}[\hat{\sigma}_{ij}\hat{\sigma}_{ij}^+,\hat{\rho}\hat{\sigma}_{ij}\hat{\sigma}_{ij}^+] + [\hat{\sigma}_{ij}\hat{\sigma}_{ij}^+\hat{\rho},\hat{\sigma}_{ij}\hat{\sigma}_{ij}^+]\right) \ ,$$

where the $\hat{\sigma}_{ij}$ are transition operators satisfying the commutation rules (2.61). The levels have the energy $\hbar\omega_i$ above the ground level.

Let us first have a look at the coherent part of the master equation. The Hamiltonian in the semiclassical approximation (that is, the atom is quantized and consists of several levels $|i\rangle$ with energies $\hbar\omega_i$, while the light fields are described by factors $e^{i\omega_{ij}t}$, with frequencies ω_{ij} tuned near the transitions $|i\rangle$-$|j\rangle$) includes the following contributions

$$\hat{H} = \hat{H}_{ele} + \hat{H}_{int} = \sum\nolimits_i |i\rangle\hbar\omega_i\langle i| + \sum_{i<j \text{ with } E_i<E_j} |i\rangle\tfrac{\hbar}{2}\Omega_{ij}\langle j|e^{i\omega_{ij}t} + c.c. \ . \qquad (2.101)$$

The Rabi frequency Ω_{ij} is a measure for the force at which the levels $|i\rangle$ and $|j\rangle$ are coupled by the resonantly irradiated light field. The master equation can be simplified by applying the rotating wave approximation and transforming to the coordinate system which rotates with the light frequencies ω_{ij}:

$$\rho_{ij} \to \hat{\rho}_{ij}e^{\imath\omega_{ij}t} \quad , \quad \hat{H}_{atom-field} \to e^{-\imath\hat{H}t/\hbar}\hat{H}_{atom-field}e^{\imath\hat{H}t/\hbar} \ . \qquad (2.102)$$

Finally, the master equation can be reformulated by introducing a *generalized Bloch vector*, $\vec{\rho}$, and the matrix representation of the Liouville superoperator $\mathcal{L}$ as a linear system of n^2 coupled differential equations,

$$\frac{d}{dt}\vec{\rho} = \mathcal{L}\vec{\rho} \quad , \quad \vec{\rho} = (\rho_{11} \ \ .. \ \ \rho_{nn} \ \ \rho_{12} \ \ \rho_{21} \ \ .. \ \ \rho_{n-1\ n} \ \ \rho_{n\ n-1}) \ . \qquad (2.103)$$

Alternatively to the complex formulation, the differential equations can be written for the real and imaginary part of the Bloch vector. The components ρ_{ii} correspond to the population probabilities of the levels $|i\rangle$, the non-diagonal elements ρ_{ij} describe the coherences between $|i\rangle$ and $|j\rangle$. Now, we must insert the Hamiltonian (2.101) and the density operator ρ_{ij} into the Liouville equation (2.40) in order to derive the generalized Bloch equations. In practice, these calculations are simple but heavy [9].

2.4.2 Bloch equations for three levels

In principle, three-level system can exist in three possible configurations, shown in Fig. 2.3. Note that it is not possible to describe a three-level system with all levels pairwise coupled by three lasers within the formalism of Bloch's equations [10].

Defining the Bloch vector by Eq. (2.103), the Bloch equation matrix for three levels in Raman configuration (that is, in Λ-configuration) using the labeling of Fig. 2.3(a),

[9] See script on *Quantum mechanics* (2023), Sec. 13.5.4.
[10] For the same reason that the three-body problem has no general analytic solution.

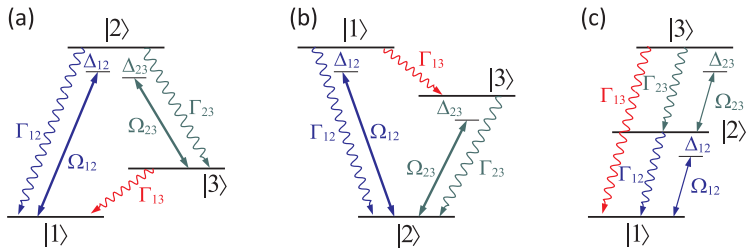

Figure 2.3: Three level system (a) in Λ-configuration, (b) in V-configuration, and (c) in cascade configuration.

is,

$$\dot{\vec{\rho}} = \mathcal{L}\vec{\rho} = \tag{2.104}$$

$$\left(\begin{array}{ccc|cccccc} 0 & \Gamma_{12} & \Gamma_{13} & \frac{\imath}{2}\Omega_{12} & -\frac{\imath}{2}\Omega_{12} & 0 & 0 & 0 & 0 \\ 0 & -\Gamma_{12}-\Gamma_{23} & 0 & -\frac{\imath}{2}\Omega_{12} & \frac{\imath}{2}\Omega_{12} & 0 & 0 & \frac{\imath}{2}\Omega_{23} & -\frac{\imath}{2}\Omega_{23} \\ 0 & \Gamma_{23} & -\Gamma_{13} & 0 & 0 & 0 & 0 & -\frac{\imath}{2}\Omega_{23} & \frac{\imath}{2}\Omega_{23} \\ \hline \frac{\imath}{2}\Omega_{12} & -\frac{\imath}{2}\Omega_{12} & 0 & -\Lambda_{12} & 0 & \frac{\imath}{2}\Omega_{23} & 0 & 0 & 0 \\ -\frac{\imath}{2}\Omega_{12} & \frac{\imath}{2}\Omega_{12} & 0 & 0 & -\Lambda_{12}^* & 0 & -\frac{\imath}{2}\Omega_{23} & 0 & 0 \\ 0 & 0 & 0 & \frac{\imath}{2}\Omega_{23} & 0 & -\Lambda_{13} & 0 & -\frac{\imath}{2}\Omega_{12} & 0 \\ 0 & 0 & 0 & 0 & -\frac{\imath}{2}\Omega_{23} & 0 & -\Lambda_{13}^* & 0 & \frac{\imath}{2}\Omega_{12} \\ 0 & \frac{\imath}{2}\Omega_{23} & -\frac{\imath}{2}\Omega_{23} & 0 & 0 & -\frac{\imath}{2}\Omega_{12} & 0 & -\Lambda_{23} & 0 \\ 0 & -\frac{\imath}{2}\Omega_{23} & \frac{\imath}{2}\Omega_{23} & 0 & 0 & 0 & \frac{\imath}{2}\Omega_{12} & 0 & -\Lambda_{23}^* \end{array}\right) \left(\begin{array}{c} \rho_{11} \\ \rho_{22} \\ \rho_{33} \\ \rho_{12} \\ \rho_{21} \\ \rho_{13} \\ \rho_{31} \\ \rho_{23} \\ \rho_{32} \end{array}\right)$$

with $\Lambda_{mn} = \imath\Delta_{mn} + \gamma_{mn}$ and,

$$\begin{aligned} \Delta_{13} &= \Delta_{12} - \Delta_{23} \qquad (2.105) \\ \gamma_{12} &= \tfrac{1}{2}(\Gamma_{12}+\Gamma_{23}) \quad , \quad \gamma_{23} = \tfrac{1}{2}(\Gamma_{12}+\Gamma_{23}+\Gamma_{13}) \quad , \quad \gamma_{13} = \tfrac{1}{2}\Gamma_{13} \ . \end{aligned}$$

In Exc. 2.7.0.19 we will derive the matrix (2.104).

The coherent terms of the same matrix can be used for the V- and the cascade configurations shown in Figs. 2.3(b,c). Obviously, the incoherent terms, that is, the submatrix 3×3 separated in the matrix (2.104) containing the population decay rates must be adjusted, as well as the decay rates of the coherences on the diagonal. Finally, the definition of the Raman detuning Δ_{13} must be adjusted. For the system in V-configuration we have,

$$\begin{aligned} \mathcal{L}_{incoh} &= \begin{pmatrix} -\Gamma_{12}-\Gamma_{13} & 0 & 0 \\ \Gamma_{12} & 0 & \Gamma_{23} \\ \Gamma_{13} & 0 & -\Gamma_{23} \end{pmatrix} \quad , \quad \Delta_{13} = \Delta_{12} - \Delta_{23} \qquad (2.106) \\ \gamma_{12} &= \tfrac{1}{2}(\Gamma_{12}+\Gamma_{13}) \quad , \quad \gamma_{23} = \tfrac{1}{2}\Gamma_{13} \quad , \quad \gamma_{13} = \tfrac{1}{2}(\Gamma_{12}+\Gamma_{13}+\Gamma_{23}) \ . \end{aligned}$$

For the cascade system we have,

$$\begin{aligned} \mathcal{L}_{incoh} &= \begin{pmatrix} 0 & \Gamma_{12} & \Gamma_{13} \\ 0 & -\Gamma_{12} & \Gamma_{23} \\ 0 & 0 & -\Gamma_{13}-\Gamma_{23} \end{pmatrix} \quad , \quad \Delta_{13} = \Delta_{12} - \Delta_{23} \qquad (2.107) \\ \gamma_{12} &= \tfrac{1}{2}\Gamma_{12} \quad , \quad \gamma_{23} = \tfrac{1}{2}(\Gamma_{12}+\Gamma_{23}+\Gamma_{13}) \quad , \quad \gamma_{13} = \tfrac{1}{2}(\Gamma_{13}+\Gamma_{23}) \ . \end{aligned}$$

These matrices serve to calculate, among others, the phenomena of *Autler-Townes splitting* treated in Exc. 2.7.0.20, of the quantum Zeno effect 2.7.0.21, of the *light-shift* treated in Exc. 2.7.0.22, the *dark resonances* treated in Exc. 2.7.0.23, the *STIRAP* method treated in Exc. 2.7.0.24, *adiabatic sweeps* treated in Exc. 2.7.0.25, and the dispersive interaction between atoms and light treated in Exc. 2.7.0.26.

2.4.3 Numerical treatment of Bloch equations

Since the differential Bloch equations are linear, they can be easily solved. For example, the prescription

$$\boxed{\vec{\rho}(t) = e^{\mathcal{L}t}\vec{\rho}(0)} \tag{2.108}$$

propagates the Bloch vector to later times.

The matrix $\mathcal{L}$ is not invertible, but by applying the condition Tr $\rho = 1$, a component of the density matrix can be eliminated, for example by letting,

$$\rho_{11} = 1 - \sum_k \rho_{kk} \ . \tag{2.109}$$

The resulting state vector, $\vec{\rho}_{red}$, has the length $n^2 - 1$, and from $\mathcal{L}$ we obtain the (trace-)reduced, now invertible matrix $\mathcal{L}_{red}$ and the inhomogeneity vector $\mathbf{b}$. The differential equation is now,

$$\frac{d}{dt}\vec{\rho}_{red} = \mathcal{L}_{red}\vec{\rho}_{red} + \mathbf{b} \ , \tag{2.110}$$

with the stationary and time-dependent solutions,

$$\boxed{\vec{\rho}_{red}(\infty) = -\mathcal{L}_{red}^{-1}\mathbf{b} \quad , \quad \vec{\rho}_{red}(t) = e^{\mathcal{L}_{red}t}\vec{\rho}_{red}(0) + (1 - e^{\mathcal{L}_{red}t})\vec{\rho}_{red}(\infty)} \ . \tag{2.111}$$

Once the matrix $\mathcal{L}$ or the matrix $\mathcal{L}_{red}$ and the inhomogeneity vector $\mathbf{b}$ are determined for a system, the state of the atom can be calculated at any time, as well as the populations and coherences. The system's free parameters are the natural transition linewidths and the detunings, as well as the intensities and emission bandwidths of the incident light fields.

2.4.3.1 Numerical simulation of the Bloch equations

When the Hamiltonian or Liouvillian depend on time, for example, when the Rabi frequencies are pulsed or the detunings are ramped, we must solve the Bloch equations iteratively. We have seen in (1.37) how to numerically solve a Schrödinger equation, when the Hamiltonian is time-independent $\hat{H}(t)$. The same can be done with the Bloch equations written in the form (2.108) or (2.111) with a time-independent Liouvillian $\mathcal{L}(t)$. That is, we chose time intervals dt sufficiently short, so that the Liouvillian can be considered constant during this interval, and we propagate the Bloch vector to later times via:

$$|\psi(t+dt)\rangle = e^{\imath\hat{H}(t)dt}|\psi(t)\rangle \qquad \text{or} \qquad \vec{\rho}(t+dt) = e^{\mathcal{L}(t)dt}\vec{\rho}(t) \ , \tag{2.112}$$

and insert the solution obtained again into equations (2.112) with the Liouvillian $\mathcal{L}(t+dt)$ adjusted to the new time.

Example 4 (*Electromagnetically induced transparency*): In some special cases, the three-level Bloch equations can be solved analytically. The system in Λ-configuration schematized in Fig. 2.3(a), where the two lasers satisfy the condition $\Delta_{12} = \Delta_{23}$ can exhibit a *dark resonance* leading to the phenomena of *electromagnetically induced transparency* (*EIT*) and *electromagnetically induced absorption*. In these resonances a dramatic change of the refractive index is observed despite the fact that the atom becomes transparent, $\mathfrak{Re}\ \chi \gg 0$ and $|\mathfrak{Im}\ \chi| \ll \mathfrak{Re}\ \chi$:

$$\mathfrak{Re}\ n = \sqrt{1 + \mathfrak{Re}\ \chi} \gg 0 \ ,$$

resulting in a high group velocity,

$$v_g = \frac{c}{n + \omega \frac{dn}{d\omega}} \ .$$

EIT is usually studied in Λ-type systems, but similar phenomena can be found in cascade-type systems [155, 154], which will be studied here. Disregarding the decay rate Γ_{13}, the Bloch equations (2.104) and (2.107) give the coherences,

$$\begin{aligned}
\dot\rho_{12} &= -\Lambda_{12}\rho_{12} + \tfrac{\imath\Omega_{12}}{2}(\rho_{11} - \rho_{22}) - \tfrac{\imath\Omega_{23}}{2}\rho_{13} \\
\dot\rho_{13} &= -\Lambda^*_{13}\rho_{13} - \tfrac{\imath\Omega_{12}}{2}\rho_{23} - \tfrac{\imath\Omega_{23}}{2}\rho_{12} \\
\dot\rho_{23} &= -\Lambda_{23}\rho_{23} + \tfrac{\imath\Omega_{23}}{2}(\rho_{22} - \rho_{33}) - \tfrac{\imath\Omega_{12}}{2}\rho_{13} \ .
\end{aligned}$$

Assuming stationarity and negligible depletion of the ground state, $\rho_{11} = 1$,

$$\begin{aligned}
0 &= -\Lambda_{12}\rho_{12} + \tfrac{\imath\Omega_{12}}{2} - \tfrac{\imath\Omega_{23}}{2}\rho_{13} \\
0 &= -\Lambda^*_{13}\rho_{13} - \tfrac{\imath\Omega_{12}}{2}\rho_{23} - \tfrac{\imath\Omega_{23}}{2}\rho_{12} \\
0 &= -\Lambda_{23}\rho_{23} - \tfrac{\imath\Omega_{12}}{2}\rho_{13} \ .
\end{aligned}$$

Substituting the third into the first equation,

$$\begin{aligned}
0 &= -\Lambda_{12}\rho_{12} + \tfrac{\imath\Omega_{12}}{2} - \tfrac{\imath\Omega_{23}}{2}\rho_{13} \\
0 &= -\Lambda^*_{13}\rho_{13} - \tfrac{\Omega_{12}^2}{4\Lambda_{23}}\rho_{13} - \tfrac{\imath\Omega_{23}}{2}\rho_{12} \ .
\end{aligned}$$

and finally,

$$\rho_{12} = \frac{\imath\Omega_{12}}{2}\frac{4\Lambda^*_{13}\Lambda_{23} + \Omega_{12}^2}{\Lambda_{12}\left(4\Lambda^*_{13}\Lambda_{23} + \Omega_{12}^2\right) + \Omega_{23}^2\Lambda_{23}} \ .$$

The macroscopic polarization is now $P = \frac{N}{V} d_{12}\rho_{21}$, with the number of atoms N. In the limit of weak probes, the *dressed* susceptibility follows from $P = \varepsilon_0\chi E_{12} = \frac{N}{V} d_{12}\rho_{21}$,

$$\chi = \frac{N d_{12}}{V\varepsilon_0 E_{12}}\rho_{21} = \frac{N|d_{12}|^2}{V\varepsilon_0\hbar\Omega_{12}}\rho_{21} \ .$$

For a resonant probe laser, $\Delta_{23} = 0$ and with $\Gamma_{13} \simeq 0$, we have $\Lambda_{13} = \frac{1}{2}\Gamma_{23} + \imath\Delta_{12}$ and $\Lambda_{23} = \frac{1}{2}(\Gamma_{23} + \Gamma_{12})$. The susceptibility in the probe transition is now, using $\Theta \equiv \Gamma_{23} + \frac{\Omega_{12}^2}{2\Lambda_{23}}$,

$$\begin{aligned}
\chi &= \frac{N|d_{12}|^2}{V\varepsilon_0\hbar\Omega_{12}}\imath\Omega_{12}\frac{\Gamma_{23} + \frac{\Omega_{12}^2}{2\Lambda_{23}} - 2\imath\Delta_{12}}{\left(\Gamma_{23} + \frac{\Omega_{12}^2}{2\Lambda_{23}} - 2\imath\Delta_{12}\right)(\Gamma_{12} + 2\imath\Delta_{12}) + \Omega_{23}^2} \\
&= \frac{N|d_{12}|^2}{V\varepsilon_0\hbar\Omega_{12}}\imath\Omega_{12}\frac{\Theta - 2\imath\Delta_{12}}{(\Theta - 2\imath\Delta_{12})(\Gamma_{12} + 2\imath\Delta_{12}) + \Omega_{23}^2} = \chi' + \imath\chi'' \ .
\end{aligned}$$

We consider, for example, the intercombination line of atomic strontium $^1S_0$-$^3P_1$ ($\lambda_{12} = 689\,\mathrm{nm}$ and $\Gamma_{12} = (2\pi)\ 7.6\,\mathrm{kHz}$) be the 'dressing' transition $^3P_1$-(5s4d)$^3D_1$ ($\lambda_{23} = 2700\,\mathrm{nm}$ and $\Gamma_{23} = (2\pi)\ 90.3\,\mathrm{kHz}$), be the 'dressing' transition $^3P_1$-(5s5d)$^3D_1$ ($\lambda_{23} = 497\,\mathrm{nm}$ and $\Gamma_{23} = (2\pi)\ 2.3\,\mathrm{MHz}$), both characterized by $\Gamma_{23} \gg \Omega_{12}, \Gamma_{12}, |\Delta_{12}|$, such that $\Theta \simeq \Gamma_{23}$. Hence,

$$\chi' + \imath\chi'' = \frac{N|d_{12}|^2}{V\varepsilon_0\hbar} \frac{2\Delta_{12} + \imath\Gamma_{23}}{\Omega_{23}} \ .$$

The refraction index follows with,

$$n = \sqrt{1+\chi} \simeq 1 + \frac{1}{2}\chi \ .$$

Its imaginary part originates from the decay term of the atom: it is here responsible for the absorbing nature of the cloud. EIT is characterized by a pronounced dispersion and a small concomitant absorption.

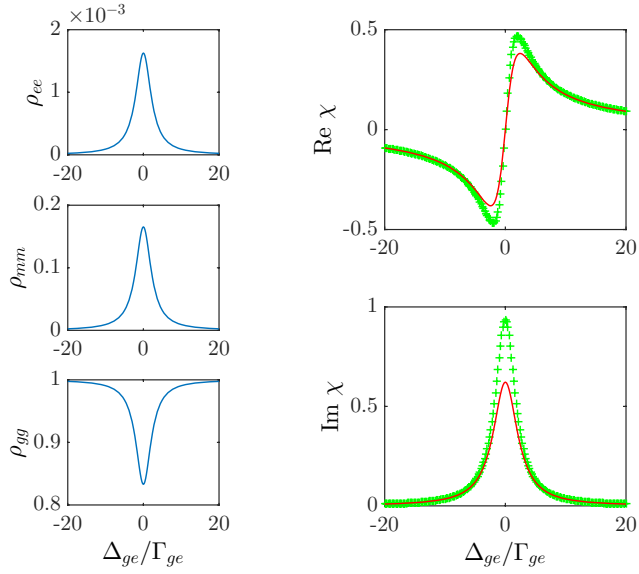

Figure 2.4: (code for download) EIT signal for the cascade system of strontium with the transitions at 689 nm and 497 nm with $\Omega_{12} = \Gamma_{12}$, $\Omega_{23} = \Gamma_{23}$ and $\Delta_{23} = 0$. The red lines are calculated by numerical integration of the Bloch equations. The dotted lines are obtained from analytical formulas based on the assumptions of weak ground state depletion (which is not really correct in the chosen parameter regime.

2.5 Quantization of the electromagnetic field

So far we have treated the optical field only as a stationary or propagating classical wave, while our two-level atom has been regarded as an entity obedient to the laws of quantum mechanics and subject to an induced perturbation by an oscillatory electromagnetic field. This procedure naturally leads to oscillations of the atomic states'

populations and the coherences between them. However, in strong fields, when atomic energy spectrum is significantly modified, a non-perturbative, time-independent approach can be fruitful. Time-independent solutions for the Schrödinger equation for atoms coupled to fields is called *dressed states*. They were used for the first time to interpret the *splitting* of rotational molecular spectra in the presence of intense classical radiofrequency fields. While the semiclassical treatment is suitable for a wide variety of phenomena and has the virtue of mathematical simplicity and familiarity, it is sometimes worth considering the field as a quantum entity as well. In the dressed states picture, the atom-field interaction corresponds to an exchange of energy quanta between the field (photons) and the atom. This approach allows us to express photonic *number states*, also called *Fock states*, on equal footings with the discrete states of atom excitation and to write the state functions of the coupled atom-field system in a basis of photonic and atomic product states. Diagonalization of the dipole coupling terms in the system's Hamiltonian generates time-independent solutions of dressed states in a completely quantum Schrödinger equation.

We begin this lecture with the quantization of the light field and then express the atom-field interaction in a fully quantized form. We will examine some examples illustrating how the dressed states picture can provide useful information on the light-matter interactions.

We have already seen that the energy of a monochromatic light field with frequency ω is quantized in small equal portions, such that the total energy is $N\hbar\omega$, where N is an integer number. The energy spectrum is the same as the one of the harmonic oscillator. Therefore, we can identify a light mode with an oscillator and adopt the entire formalism developed for the harmonic oscillator. The formalism will be assumed as known in the following. We will, for simplicity use the term *photon* (respectively *phonon*) for excitations of a harmonic oscillator mode. It is however important to be aware that a photon is not a particle, as it simply *disappears when performing the transition from quantum to classical mechanics* [100].

2.5.1 Field operators

The basic idea behind field quantization is the replacement of the classical harmonic oscillators by quantum oscillators. The simplest approach to perform this quantization is to introduce the scalar potential Φ and the potential vector $\mathbf{A}$ as done in electrodynamic theory [11]. In free space, without charges nor currents, and within the *Coulomb gauge* we have the solution of the Helmholtz wave equation generalized to a distribution of wavevectors $\mathbf{k}$ [12],

$$\mathbf{A}(\mathbf{r},t) = \sum_{\mathbf{k}} \vec{\epsilon}_{\mathbf{k}} [A^{+}_{0\mathbf{k}} e^{-\imath(\mathbf{k}\cdot\mathbf{r}-\omega_{\mathbf{k}}t)} + A^{-}_{0\mathbf{k}} e^{\imath(\mathbf{k}\cdot\mathbf{r}-\omega_{\mathbf{k}}t)}] \,, \tag{2.113}$$

where we already isolated the vectorial character due to the polarization $\vec{\epsilon}_{\mathbf{k}}$ of the light mode $\mathbf{k}$. Obviously, $A^{-}_{0\mathbf{k}} = (A^{+}_{0\mathbf{k}})^{*}$. As each amplitude and polarization of the wave

[11] See the script *Electrodynamics* by the same author Scripts/EletroMagnetismoScript.

[12] The atom-light interaction may depend on the polarization of the light with respect to the quantization axis of the atom, as defined e.g. by a magnetic field. In these cases we need to extend the index $\mathbf{k}$ to include the polarization state $(\mathbf{k}, \lambda)$.

given by the vector potential $\mathbf{A}_\mathbf{k}$ and $\mathbf{A}^*_\mathbf{k}$ must satisfy the wave equation separately, we arrive at the dispersion relation,

$$\omega_\mathbf{k} = ck \ . \tag{2.114}$$

We know that the energy in each radiative mode containing $n_\mathbf{k}$ photons is,

$$E_\mathbf{k} = \hbar\omega_\mathbf{k} N_\mathbf{k} = u_\mathbf{k} V = 2\varepsilon_0 V \omega_\mathbf{k}^2 \overline{\mathbf{A}_{0\mathbf{k}}^2} = 2\varepsilon_0 V \omega_\mathbf{k}^2 (A_{0\mathbf{k}}^- A_{0\mathbf{k}}^+ + A_{0\mathbf{k}}^+ A_{0\mathbf{k}}^-) \ , \tag{2.115}$$

where the bar denotes cycle-averaging. The second quantization now consists in interpreting the mode as a *quantum harmonic oscillator*, that is, we understand the observables as *operators* satisfying commutation rules, such as $[\hat{A}_{0\mathbf{k}}^-, \hat{A}_{0\mathbf{k}'}^+] \propto \delta_{\mathbf{k},\mathbf{k}'}$, and hence being affected by quantum fluctuations:

$$\hat{H}_\mathbf{k} = \hbar\omega_\mathbf{k}(\hat{n}_\mathbf{k} + \tfrac{1}{2}) = 2\varepsilon_0 V \omega_\mathbf{k}^2 (\hat{A}_{0\mathbf{k}}^- \hat{A}_{0\mathbf{k}}^+ + \hat{A}_{0\mathbf{k}}^+ \hat{A}_{0\mathbf{k}}^-) \ . \tag{2.116}$$

We introduce normalized field operators following the commutation rule via,

$$\hat{a}_\mathbf{k} \sqrt{\tfrac{\hbar}{4\varepsilon_0 V \omega_\mathbf{k}}} \equiv \hat{A}_{0\mathbf{k}}^+ \qquad \text{and} \qquad \hat{a}_\mathbf{k}^\dagger \sqrt{\tfrac{\hbar}{4\varepsilon_0 V \omega_\mathbf{k}}} \equiv \hat{A}_{0\mathbf{k}}^- \ , \tag{2.117}$$

such that,

$$\hat{H}_\mathbf{k} = \hbar\omega_\mathbf{k}(\hat{a}_\mathbf{k}^\dagger \hat{a}_\mathbf{k} + \tfrac{1}{2}) \ . \tag{2.118}$$

The analogy allows us to interpret them as *creation operator* and *annihilation operator* of photons satisfying $[\hat{a}_\mathbf{k}, \hat{a}_\mathbf{k}^\dagger] = 1$. Finally, we can rewrite (2.113) as,

$$\boxed{\hat{\mathbf{A}}_\mathbf{k}(\mathbf{r}, t) = \sqrt{\tfrac{\hbar}{4\varepsilon_0 V \omega_\mathbf{k}}} \vec{\epsilon}_\mathbf{k} \left[\hat{a}_\mathbf{k} e^{-\imath(\mathbf{k}\cdot\mathbf{r} - \omega_\mathbf{k} t)} + \hat{a}_\mathbf{k}^\dagger e^{\imath(\mathbf{k}\cdot\mathbf{r} - \omega_\mathbf{k} t)} \right]} \ . \tag{2.119}$$

We already know such combinations of operators and their complex conjugates from the quantum harmonic oscillator.

In the Coulomb gauge, the electric and magnetic field operators for the cavity modes can be constructed from,

$$\boxed{\begin{aligned} \hat{\vec{\mathcal{E}}}_\mathbf{k} &= -\frac{\partial \hat{\mathbf{A}}_\mathbf{k}}{\partial t} = \imath \sqrt{\tfrac{\hbar\omega_\mathbf{k}}{2\varepsilon_0 V}} \left(\hat{a}_\mathbf{k} e^{-\imath(\mathbf{k}\cdot\mathbf{r} - \omega_\mathbf{k} t)} - \hat{a}_\mathbf{k}^\dagger e^{\imath(\mathbf{k}\cdot\mathbf{r} - \omega_\mathbf{k} t)} \right) \vec{\epsilon}_k \\ \hat{\vec{\mathcal{B}}}_\mathbf{k} &= \nabla \times \mathbf{A}_\mathbf{k} = \imath \sqrt{\tfrac{\hbar\omega_\mathbf{k}}{2\varepsilon_0 V}} \left(\hat{a}_\mathbf{k} e^{-\imath(\mathbf{k}\cdot\mathbf{r} - \omega_\mathbf{k} t)} - \hat{a}_\mathbf{k}^\dagger e^{\imath(\mathbf{k}\cdot\mathbf{r} - \omega_\mathbf{k} t)} \right) \mathbf{k} \times \vec{\epsilon}_k \end{aligned}} \ . \tag{2.120}$$

We can calculate the cycle-averaged energy of the $\mathbf{k}$-th cavity mode from a quantum version of Eq. (2.115),

$$\bar{E}_\mathbf{k} = \tfrac{\varepsilon_0}{2} \int \langle n_\mathbf{k} | \hat{\vec{\mathcal{E}}}_\mathbf{k} \cdot \hat{\vec{\mathcal{E}}}_\mathbf{k} | n_\mathbf{k} \rangle dV \ . \tag{2.121}$$

The result (2.118) is exactly Planck's quantum hypothesis (although strictly speaking, he rather suggested a quantization of oscillators in the conducting walls of the cavity, not of the field) on the distribution of the spectral intensity radiated by a black body. We now can see that it follows naturally from the quantization of the cavity field modes. Solve Excs. 2.7.0.27 and 2.7.0.28.

2.5.2 Interaction of quantized fields with atoms

With the results of the previous section the complete field Hamiltonian reads,

$$\hat{H}_{field} = \sum_{\mathbf{k}} \hbar\omega_{\mathbf{k}} (\hat{a}^\dagger_{\mathbf{k}} \hat{a}_{\mathbf{k}} + \tfrac{1}{2}) \ . \tag{2.122}$$

Now, that we have a clear picture of the quantized field with the energies in the modes given by Eq. (2.121) and the photon number states given by the eigenstates $|n\rangle$ of the quantized harmonic oscillator, we are in a position to consider our two-level atom interacting with this quantized radiation field. If for the moment, we exclude spontaneous emission and stimulated processes, the Hamiltonian of the combined atom-field system is,

$$\hat{H} = \hat{H}_{atom} + \hat{H}_{field} + \hat{H}_{atom:field} \ . \tag{2.123}$$

We describe the atom by a two-level system,

$$\hat{H}_{atom} = \hbar\omega_g |g\rangle\langle g| + \hbar\omega_e |e\rangle\langle e| = \hbar\omega_g |g\rangle\langle g| + \hbar(\omega_g + \omega_0)|e\rangle\langle e| \ , \tag{2.124}$$

where $\hat{H}_{field}$ is the Hamiltonian of the quantized field, expressed by Eq. (2.118), and $\hat{H}_{atom:field}$ the atom-field interaction. For the Hamiltonian without interaction, $\hat{H} = \hat{H}_{atom} + \hat{H}_{field}$, the eigenstates are simply product states of the atomic states and the photon number states,

$$|g, n\rangle = |g\rangle|n\rangle \qquad \text{and} \qquad |e, n\rangle = |e\rangle|n\rangle \ . \tag{2.125}$$

The left side of Fig. 2.5 shows, how the eigenenergies of the product states consist of two ladders, being displaced by the energy difference $\hbar\Delta$, which corresponds to the detuning. We write the Hamiltonian of the atom Eq. (2.124) as the sum of projectors on unperturbed eigenstates using the completeness relation and the orthogonality of eigenstates. With the same idea we can rewrite the dipole operator defined in Eq. (3.13),

$$\begin{aligned} \hat{\mathbf{d}} &= \sum_i |\psi_i\rangle\langle\psi_i|\hat{\mathbf{d}}| \sum_j |\psi_j\rangle\langle\psi_j| = \sum_{i,j} |i\rangle\langle i| e^{\imath(\omega_i - \omega_j)t} \hat{\mathbf{d}} |j\rangle\langle j| \qquad (2.126) \\ &= \sum_{i,j} e^{\imath(\omega_i - \omega_j)t} \mathbf{d}_{ij} |i\rangle\langle j| = \sum_{i<j} e^{\imath(\omega_i - \omega_j)t} \mathbf{d}_{ij} |i\rangle\langle j| + e^{-\imath(\omega_i - \omega_j)t} \mathbf{d}_{ij} |j\rangle\langle i| \equiv \hat{\mathbf{d}}^{(+)} + \hat{\mathbf{d}}^{(-)} \ . \end{aligned}$$

using $|\psi_n(t)\rangle = e^{-\imath\omega_n t}|n\rangle$. Note that $\hat{\mathbf{d}}$ only has non-diagonal elements.

Now, let us use the electric field of Eqs. (2.120) to describe the atom-field interaction through the Hamiltonian $\hat{H}_{atom:field} = -\hat{\mathbf{d}} \cdot \hat{\vec{\mathcal{E}}}$,

$$\hat{H}_{atom:field} = \imath \sum_{\mathbf{k}} \sum_{i,j} \sqrt{\tfrac{\hbar\omega_{\mathbf{k}}}{2\varepsilon_0 V}} \mathbf{d}_{ij} e^{\imath(\omega_j - \omega_i)t} |i\rangle\langle j| \cdot \vec{\epsilon}_{\mathbf{k}} \left[\hat{a}_{\mathbf{k}} e^{-\imath(\mathbf{k}\cdot\mathbf{r} - \omega_{\mathbf{k}} t)} - \hat{a}^\dagger_{\mathbf{k}} e^{\imath(\mathbf{k}\cdot\mathbf{r} - \omega_{\mathbf{k}} t)} \right] \ . \tag{2.127}$$

For our two-level atom interacting with a single mode radiation field, we only have,

$$\begin{aligned} \hat{H}_{atom:field} = \imath \sqrt{\tfrac{\hbar\omega_{\mathbf{k}}}{2\varepsilon_0 V}} \mathbf{d}_{ge} \left[e^{\imath(\omega_e - \omega_g)t} |g\rangle\langle e| + e^{\imath(\omega_g - \omega_e)t} |e\rangle\langle g| \right] \cdot \qquad (2.128) \\ \cdot \vec{\epsilon}_{\mathbf{k}} \left[\hat{a}_{\mathbf{k}} e^{-\imath(\mathbf{k}\cdot\mathbf{r} - \omega_{\mathbf{k}} t)} - \hat{a}^\dagger_{\mathbf{k}} e^{\imath(\mathbf{k}\cdot\mathbf{r} - \omega_{\mathbf{k}} t)} \right] \ . \end{aligned}$$

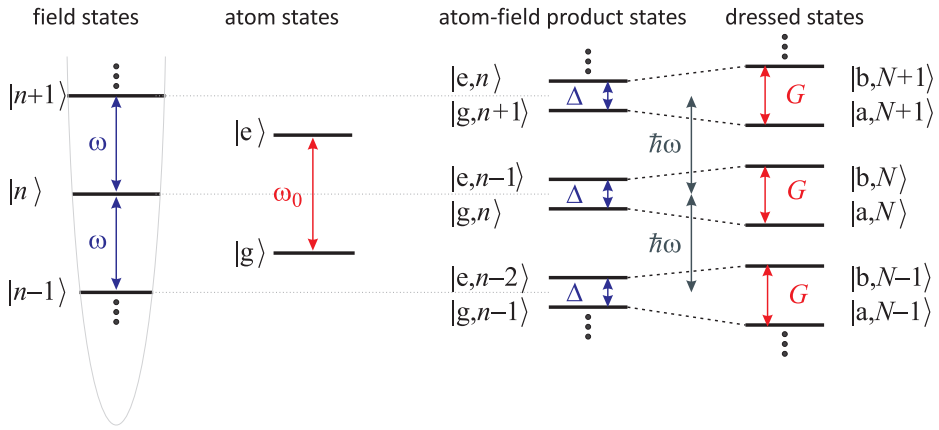

Figure 2.5: (Left) Photons number states and the two stationary states of the two-levels atom. (Center) Double ladder showing the basis of products states of photon number and atomic states. (Right) Dressed states constructed by diagonalization of the full Hamiltonian in the basis of the product states.

2.5.2.1 Rotating wave approximation for dressed states

We can simplify the notation by identifying $\hat{\sigma}^+ = |e\rangle\langle g|$ and $\hat{\sigma}^- = |g\rangle\langle e|$ and introducing as an abbreviation the *Rabi frequency*,

$$\tfrac{1}{2}\hbar\Omega_1(\mathbf{r}) \equiv \sqrt{\tfrac{\hbar\omega_{\mathbf{k}}}{2\varepsilon_0 V}}\mathbf{d}_{ge}\cdot\vec{\epsilon}_{\mathbf{k}}e^{\imath\mathbf{k}\cdot\mathbf{r}} \ . \tag{2.129}$$

The interaction Hamiltonian then becomes,

$$\begin{aligned}\hat{H}_{atom:field} = {} & \tfrac{\imath}{2}\hbar\Omega_1(\mathbf{r})e^{\imath(\omega_{\mathbf{k}}-\omega_0)t}\hat{\sigma}^+\hat{a}_{\mathbf{k}} + \tfrac{\imath}{2}\hbar\Omega_1(\mathbf{r})e^{\imath(\omega_{\mathbf{k}}+\omega_0)t}\hat{\sigma}^-\hat{a}_{\mathbf{k}} \\ & - \tfrac{\imath}{2}\hbar\Omega_1^*(\mathbf{r})e^{-\imath(\omega_{\mathbf{k}}+\omega_0)t}\hat{\sigma}^+\hat{a}_{\mathbf{k}}^\dagger - \tfrac{\imath}{2}\hbar\Omega_1^*(\mathbf{r})e^{-\imath(\omega_{\mathbf{k}}-\omega_0)t}\hat{\sigma}^-\hat{a}_{\mathbf{k}}^\dagger \ .\end{aligned} \tag{2.130}$$

This Hamiltonian contains four terms describing the following processes [13],

$|g,n\rangle \longrightarrow |e,n-1\rangle$ the atom is excited by the absorption of a photon;

$|e,n\rangle \longrightarrow |g,n-1\rangle$ the atom is deexcited by the absorption of a photon;

$|g,n\rangle \longrightarrow |e,n+1\rangle$ the atom is excited by the emission of a photon;

$|e,n\rangle \longrightarrow |g,n+1\rangle$ the atom is deexcited by the emission of a photon.

Obviously, only the first and forth terms respect energy conservation (in first-order processes) and can serve as initial and final states in real physical processes. Fig. 2.6 shows schemes of these four terms. We see, that neglecting the second and third process (i.e., terms $\propto \hat{\sigma}^{\pm}\hat{a}^{\pm}$ of the Hamiltonian) is equivalent to making the rotating wave approximation (RWA), where we despise the terms rotating with the frequency

[13] Remember that the four processes contained in the Hamiltonian are all coherent (absorption and stimulated emission), and that spontaneous emission must be treated separately.

$\pm(\omega_{\mathbf{k}} + \omega_0)$, and that we really only need to consider the coupling between the two dressed states $|g, n\rangle$ and $|e, n-1\rangle$.

Finally, within the RWA the Hamiltonian reads,

$$\boxed{\hat{H}_{atom:field} = \tfrac{\imath}{2}\hbar\Omega_1(\mathbf{r})e^{-\imath\Delta_{\mathbf{k}}t}\hat{\sigma}^+\hat{a}_k - \tfrac{\imath}{2}\hbar\Omega_1^*(\mathbf{r})e^{\imath\Delta_{\mathbf{k}}t}\hat{\sigma}^-\hat{a}_k^\dagger}\,, \tag{2.131}$$

where we introduced the detuning $\Delta_{\mathbf{k}} \equiv \omega_{\mathbf{k}} - \omega_0$ as short hand notation.

It is important to note that the first and fourth term can be important in higher order processes, such as multiphotonic absorption or Raman scattering processes, where the excited state would be a virtual level. In fact, when the Rabi frequency is very large, $\Omega_1 \simeq \omega$, the excitation and deexcitation processes follow each other so rapidly, that energy conservation can be violated for short times. The energy shift caused by terms neglected in the RWA are called *Bloch-Siegert shift* [14].

2.5.3 Dressed states

Within the new dressed states basis, the atom-light coupling problem is reduced to diagonalizing the Hamiltonian of a quasi-degenerate two-level atom ($|\Delta| \ll \omega_0$), in which the non-diagonal elements are given by $\frac{1}{2}\hbar\Omega_1$. The eigenenergies of the complete Hamiltonian $\hat{H}$ are,

$$E_\pm = \tfrac{\hbar}{2}(\omega_{g,n} + \omega_{e,n-1}) \pm \tfrac{\hbar}{2}G\,. \tag{2.132}$$

where $\hbar\omega_{g,n}$ and $\hbar\omega_{e,n-1}$ are the energies of the product states $\hbar\omega_g + n\hbar\omega_{\mathbf{k}}$ and $\hbar\omega_e + (n-1)\hbar\omega_{\mathbf{k}}$. The separation between constituents of the same dressed state is $G = \sqrt{\Omega_1^2 + \Delta^2}$.

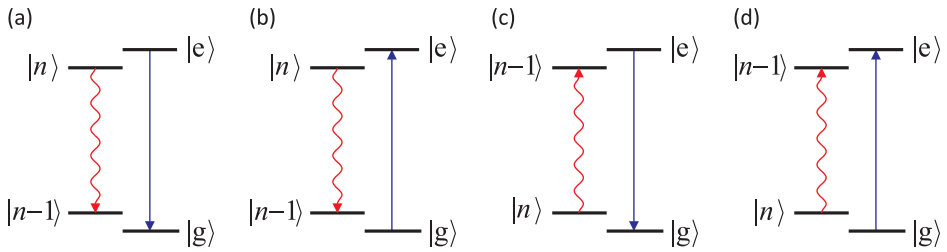

Figure 2.6: Illustration of the four processes in the atom-field interaction. Terms (b) and (c) conserve energy in first-order processes, while (a) and (d) do not conserve.

The atom-field product states offer a natural basis for the Hamiltonian of Eq. (2.123). The states resulting from the diagonalization of the Hamiltonian on this basis are called *dressed states*. As indicated in Fig. 2.5, the neighboring doublets the double ladder 'repel' each other under the influence of the interaction $\hat{H}_{atom:field}$ in Eq. (2.123). The mixed coefficients form the familiar problem of two levels, now called $|a\rangle$ and $|b\rangle$. Note that the semiclassical product state picture and the dressed

[14] The shift is not observed, when the non-rotating terms $\sigma^\pm a^\pm$ are forbidden by other conservation or selection rules. For example, when a resonance is excited by $\sigma^\pm$ light, the RWA is accurate.

states picture follow from each other via unitary transformation,

$$\boxed{\begin{pmatrix} |a,N\rangle \\ |b,N\rangle \end{pmatrix} = U \begin{pmatrix} |g,n\rangle \\ |e,n-1\rangle \end{pmatrix}}, \tag{2.133}$$

and, hence, are equivalent descriptions of the same reality. But while in the product state picture the system Hamiltonian is diagonal in the *absence* of atom-light interaction, in the dressed states picture the Hamiltonian is diagonal in the *presence* of interaction. The numbers n denote the amount of photons in the laser beam, the numbers N denote the amount of energy packets within the system, that is, the photons *plus* the possible excitation of the atom. The expression of the unitary transformation matrix will be derived in Sec. 2.6.1.

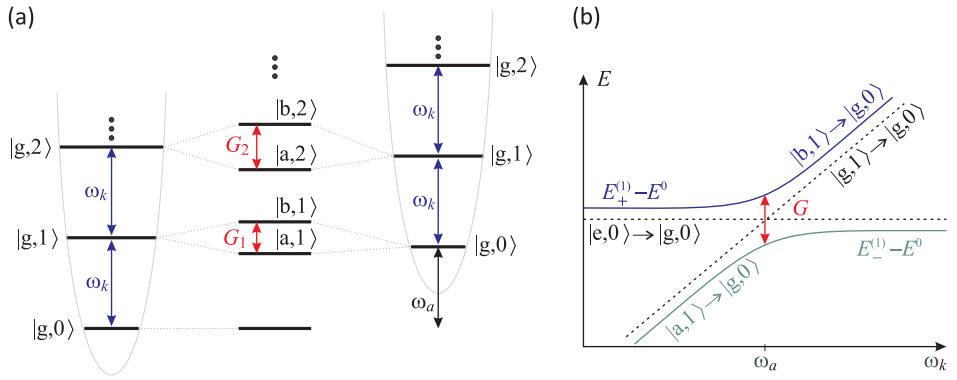

Figure 2.7: (a) Rabi splitting of the lowest dressed states. (b) Avoided crossing of dressed states.

2.6 The Jaynes-Cummings model

The *Jaynes-Cummings model* describes the dynamics of a single dressed two-level atom in a single monochromatic laser mode in the absence of spontaneous emission processes. The model, illustrated in Fig. 1.6, has become a paradigm of quantum mechanics with applications in quantum information, where it applies to the formulation of entanglement protocols of atomic states and the implementation of quantum gates. In the following, we will first study the interaction of an atom with an optical mode neglecting dissipation effects and leave the discussion on the impact of dissipation processes to later sections.

The dynamic evolution of pure states is then obtained from the Schrödinger equation. The Hamiltonian of this system is given by (2.131). Letting $\hbar = 1$ and assuming that the atom is located at the origin [such that $\Omega_1(\mathbf{r})e^{i\mathbf{k}\cdot\mathbf{r}} = \Omega_1(\mathbf{0})$], we can write

the time-dependent Hamiltonian in the *interaction picture* as,

$$\boxed{\begin{array}{rcl}\tilde{H}_I &=& \frac{\imath}{2}\Omega_1 e^{-\imath\Delta t}\hat{\sigma}^+\hat{a} - \frac{\imath}{2}\Omega_1 e^{\imath\Delta t}\hat{\sigma}^-\hat{a}^\dagger \\ &=& \begin{pmatrix} 0 & \frac{\imath}{2}\Omega_1 e^{-\imath\Delta t}\hat{a} \\ -\frac{\imath}{2}\Omega_1 e^{\imath\Delta t}\hat{a}^\dagger & 0 \end{pmatrix}\end{array}} \; . \tag{2.134}$$

where ω is the frequency of the radiation, ω_0 the frequency of the atomic transition, $\Delta \equiv \omega - \omega_0$ the detuning, and Ω_1 the Rabi frequency generated by a single photon. We use the conventions $\hat{\sigma}^z = [\hat{\sigma}^-, \hat{\sigma}^+] = |1\rangle\langle 1| - |2\rangle\langle 2| = \mathbb{I} - 2\hat{\sigma}^+\hat{\sigma}^-$ and $\omega_0 \equiv \omega_2 - \omega_1 > 0$.

Starting from this Hamiltonian the Jaynes-Cummings model is translated into the *Schrödinger picture* via the unitary transform,

$$U = e^{-\imath(\hat{n}+1/2)\omega t} e^{\imath\hat{\sigma}^z\omega_0 t/2} \; , \tag{2.135}$$

for which we find the relationships,

$$\begin{aligned} -\imath U\dot{U}^\dagger &= \omega(\hat{n} + \tfrac{1}{2}) - \tfrac{1}{2}\omega_0\hat{\sigma}^z \\ U\hat{a}U^\dagger &= \Sigma_{n'}|n'\rangle e^{-\imath n'\omega t}\langle n'|\hat{a}\Sigma_n|n\rangle e^{\imath n\omega t}\langle n| = e^{\imath\omega t}\hat{a} \\ U\hat{\sigma}^- U^\dagger &= e^{\imath\omega_0 t}\hat{\sigma}^- \; . \end{aligned} \tag{2.136}$$

Obviously, the dynamics of the states is now given by $|\psi(t)\rangle = U|\psi_I(t)\rangle$, and the new Hamiltonian in the Schrödinger picture reads,

$$\boxed{\begin{array}{rcl}\hat{H} &=& U\tilde{H}_I U^\dagger - \imath U\dot{U}^\dagger \\ &=& \omega(\hat{n} + \frac{1}{2}) - \frac{1}{2}\omega_0\hat{\sigma}^z + \frac{1}{2}\Omega_1(\hat{a}\hat{\sigma}^+ + \hat{a}^\dagger\hat{\sigma}^-) \\ &=& \begin{pmatrix} (\hat{n} + \frac{1}{2})\omega - \frac{1}{2}\omega_0 & \frac{1}{2}\Omega_1\hat{a}^\dagger \\ \frac{1}{2}\Omega_1\hat{a} & (\hat{n} + \frac{1}{2})\omega + \frac{1}{2}\omega_0 \end{pmatrix}\end{array}} \; . \tag{2.137}$$

We choose the Fock representation for the radiation mode, we represent the atomic transitions by the Pauli matrices, and we span the product space $\hat{\rho}_{field} \otimes \hat{\rho}_{atom}$ generalizing the operators $\hat{a}^\pm \curvearrowright \hat{a}^\pm \otimes \mathbb{I}$ and $\hat{\sigma}^\pm \curvearrowright \mathbb{I} \otimes \hat{\sigma}^\pm$. Explicitly we get,

$$\begin{aligned} \hat{a}^\dagger &= \sum_n \sqrt{n+1}|n+1\rangle \begin{pmatrix} 1 & 0 \\ 0 & 1 \end{pmatrix} \langle n| \quad \text{and} \quad \hat{\sigma}^+ = \sum_n |n\rangle \begin{pmatrix} 0 & 0 \\ 1 & 0 \end{pmatrix} \langle n| \\ \hat{a} &= \sum_n \sqrt{n}|n-1\rangle \begin{pmatrix} 1 & 0 \\ 0 & 1 \end{pmatrix} \langle n| \quad \text{and} \quad \hat{\sigma}^- = \sum_n |n\rangle \begin{pmatrix} 0 & 1 \\ 0 & 0 \end{pmatrix} \langle n| \; . \end{aligned} \tag{2.138}$$

2.6.1 Dressed states representation

The basis

$$|1, n\rangle = \begin{pmatrix} 1 \\ 0 \end{pmatrix} \quad , \quad |2, n-1\rangle = \begin{pmatrix} 0 \\ 1 \end{pmatrix} \tag{2.139}$$

spans a sub-space of two energetically nearly degenerate states with n photons in the system one out of which can have been absorbed by the atom. The density operator for the subspace is,

$$\hat{\rho}_n = \begin{pmatrix} |n\rangle|1\rangle\langle 1|\langle n| & |n\rangle|1\rangle\langle 2|\langle n-1| \\ |n-1\rangle|2\rangle\langle 1|\langle n| & |n-1\rangle|2\rangle\langle 2|\langle n-1| \end{pmatrix} . \tag{2.140}$$

We project the Hamiltonian onto that basis via the projectors $\hat{P} = |1,n\rangle\langle 1,n| + |2,n-1\rangle\langle 2,n-1|$,

$$\boxed{\hat{H}_n = \hat{P}\hat{H}\hat{P} = \begin{pmatrix} n\omega + \frac{\Delta}{2} & \frac{1}{2}\Omega_1\sqrt{n} \\ \frac{1}{2}\Omega_1\sqrt{n} & n\omega - \frac{\Delta}{2} \end{pmatrix}} . \tag{2.141}$$

That is, the Hamiltonian can be decomposed into sub-hyperspaces which are all orthogonal, because the Hamiltonian $\hat{H}$ only contains terms conserving the total number of photons + excitations.

Example 5 (*Orthogonality of submatrices with same numbers of excitations*): This can be seen by expanding the Hamiltonian matrix:

$$\hat{H} = \bigoplus_n \hat{H}_n \tag{2.142}$$

$$= \sum_n \left[|n\rangle \begin{pmatrix} n\omega + \frac{\Delta}{2} & 0 \\ 0 & n\omega - \frac{\Delta}{2} \end{pmatrix} + |n-1\rangle \begin{pmatrix} 0 & 0 \\ \frac{\Omega_1}{2}\sqrt{n} & 0 \end{pmatrix} + |n+1\rangle \begin{pmatrix} 0 & \frac{\Omega_1}{2}\sqrt{n+1} \\ 0 & 0 \end{pmatrix} \right] \langle n|$$

$$= \begin{pmatrix} \frac{\Delta}{2} & & & & & & \\ & \omega + \frac{\Delta}{2} & \frac{\Omega_1}{2} & & & & \\ & \frac{\Omega_1}{2} & \omega - \frac{\Delta}{2} & & & & \\ & & & 2\omega + \frac{\Delta}{2} & \frac{\Omega_1}{2}\sqrt{2} & & \\ & & & \frac{\Omega_1}{2}\sqrt{2} & 2\omega - \frac{\Delta}{2} & & \\ & & & & & 3\omega + \frac{\Delta}{2} & \cdots \\ & & & & & \vdots & \ddots \end{pmatrix} .$$

The eigenvalues can be easily calculated by [15],

$$\det \sum_n \hat{H}_n = \sum_n \det \hat{H}_n \ , \tag{2.143}$$

defining the generalized n-photon Rabi frequency, $\varpi_n \equiv \sqrt{\Delta^2 + n\Omega_1^2} = |\varpi_n| e^{\imath \mathbf{k}\cdot\mathbf{R}}$, which contains the spatial mode function of the radiation field. We find the diagonal matrix of eigenvalues,

$$\hat{E}_n = \begin{pmatrix} n\omega + \frac{\varpi_n}{2} & 0 \\ 0 & n\omega - \frac{\varpi_n}{2} \end{pmatrix} . \tag{2.144}$$

[15] The following rules apply to determinants,

$$\det(AB) = \det A \det B \qquad \text{and} \qquad (\det A)^{-1} = \det A^{-1} \ .$$

From the transformation $\hat{H}_n U_n = U_n \hat{E}_n$, under the condition that U_n is unitary and Hermitian, $U_n^\dagger U_n$, and using the abbreviation $\tan 2\phi_n \equiv \sqrt{n}\Omega/\Delta$, we obtain:

$$U_n = \begin{pmatrix} \cos\phi_n & \sin\phi_n \\ -\sin\phi_n & \cos\phi_n \end{pmatrix} . \tag{2.145}$$

The temporal evolution of the Jaynes-Cummings state, $|\psi(t)\rangle = e^{-\imath\hat{H}t}|\psi(0)\rangle$, is described by the transformation,

$$\boxed{\begin{aligned} & e^{-\imath\hat{H}_n t} = U_n e^{-\imath\hat{E}_n t} U_n^\dagger = e^{-\imath n\omega t} \times \\ & \times \begin{pmatrix} \cos^2\phi_n e^{-\imath\varpi_n t/2} + \sin^2\phi_n e^{\imath\varpi_n t/2} & \cos\phi_n \sin\phi_n (e^{\imath\varpi_n t/2} - e^{-\imath\varpi_n t/2}) \\ \cos\phi_n \sin\phi_n (e^{\imath\varpi_n t/2} - e^{-\imath\varpi_n t/2}) & \sin^2\phi_n e^{-\imath\varpi_n t/2} + \cos^2\phi_n e^{\imath\varpi_n t/2} \end{pmatrix} , \end{aligned}} \tag{2.146}$$

which is essentially the same formula as for the time evolution of a two-level atom driven by a classical light field. The transition probability between dressed states is,

$$|\langle 2, n-1|e^{-\imath\hat{H}_n t}|1, n\rangle|^2 = \frac{4n\Omega_1^2\Delta^2}{\varpi_n^2} \sin^2 \frac{\varpi_n t}{2} . \tag{2.147}$$

The temporal evolution follows with [89],

$$\hat{\rho}(t) = e^{-\imath\hat{H}_n t}\hat{\rho}(0)e^{\imath\hat{H}_n t} \equiv \mathcal{L}(t)\hat{\rho}(0) . \tag{2.148}$$

Alternatively to the master equation (2.148) we could describe the time evolution of the system by Heisenberg equations, as done in Exc. 2.7.0.29.

2.6.2 Classical and quantum limits

2.6.2.1 The limit of high laser intensities and resonant interaction

The classical limit is recovered for $n \to \infty$, where a single photon makes no difference, that is, we can treat the states $|n\rangle$ and $|n+1\rangle$ as equivalent. Then, we can approximate the Hamiltonian of the system (2.139) by the trace of this same Hamiltonian taken over the number of photons,

$$\hat{H}_{semi} = \lim_{n\to\infty} \mathrm{Tr}_{field}\hat{\rho}\hat{H} = \sum_m \langle m|\hat{\rho}\hat{H}|m\rangle . \tag{2.149}$$

This situation, as illustrated in Fig. 2.8, describes well the state of a laser as a coherent state, $|\alpha\rangle = \sum_n \frac{\alpha^n}{\sqrt{n!}}|n\rangle e^{-|\alpha|^2/2}$. For $n \to \infty$, the uncertainty of the Poisson distribution is small, $\Delta n/\bar{n} = 1/\sqrt{n} \to 0$, such that the light mode is characterized by the average number of photons, and fluctuations are negligible. This allows us to replace the Poisson distribution, $P_n = |\langle n|\alpha\rangle|^2 = \delta_{n\bar{n}}$,

$$\begin{aligned} \hat{H}_{semi} &= \hat{H}_{field} + \hat{H}_{atom} + \hat{H}_{atom:field} = \sum_m \langle m|\alpha\rangle\langle\alpha|\hat{H}|m\rangle = \langle\alpha|\hat{H}|\alpha\rangle \simeq \langle\bar{n}|\hat{H}|\bar{n}\rangle \\ &= \hat{H}_{\bar{n}} = \begin{pmatrix} \bar{n}\omega & 0 \\ 0 & (\bar{n}-1)\omega \end{pmatrix} + \begin{pmatrix} -\frac{\omega_0}{2} & 0 \\ 0 & \frac{\omega_0}{2} \end{pmatrix} + \begin{pmatrix} 0 & \frac{\varpi_{\bar{n}}}{2} \\ \frac{\varpi_{\bar{n}}^*}{2} & 0 \end{pmatrix} . \end{aligned} \tag{2.150}$$

Now, in the case of a resonant interaction, $\Delta = 0$, the Jaynes-Cummings evolution is,

$$\boxed{e^{-\imath\hat{H}_{\bar{n}}t} = \tfrac{1}{\sqrt{2}} e^{-\imath(\bar{n}-1/2)\omega t} \begin{pmatrix} \cos\frac{1}{2}\varpi_{\bar{n}}t & \imath\sin\frac{1}{2}\varpi_{\bar{n}}t \\ \imath\sin\frac{1}{2}\varpi_{\bar{n}}t & \cos\frac{1}{2}\varpi_{\bar{n}}t \end{pmatrix}} . \tag{2.151}$$

Example 6 (*Resonant* $\pi/2$*-pulse*): In this example, we consider resonant $\pi/2$-pulses, that is, $\sqrt{\bar{n}}\Omega t = \frac{1}{2}\pi$. The Jaynes-Cummings evolution now simplifies to,

$$e^{-\imath\hat{H}_{\bar{n}}t} = \tfrac{1}{2} e^{-\imath(\bar{n}-1/2)\omega t} \begin{pmatrix} 1 & \imath \\ \imath & 1 \end{pmatrix} . \tag{2.152}$$

For large $\bar{n}$, a resonant $\pi/2$-pulse does (ignoring irrelevant dynamical phases),

$$\begin{pmatrix} |1\rangle|\bar{n}\rangle \\ |2\rangle|\bar{n}-1\rangle \end{pmatrix} \overset{\pi/2}{\curvearrowright} \begin{pmatrix} (\imath|2\rangle|\bar{n}-1\rangle + |1\rangle|\bar{n}\rangle) \\ (|2\rangle|\bar{n}-1\rangle + \imath|1\rangle|\bar{n}\rangle) \end{pmatrix} , \tag{2.153}$$

that is, for a coherent field,

$$\begin{pmatrix} |1\rangle|\alpha\rangle \\ |2\rangle|\alpha\rangle \end{pmatrix} \overset{\pi/2}{\curvearrowright} \begin{pmatrix} (\imath|2\rangle + |1\rangle)|\alpha\rangle \\ (|2\rangle + \imath|1\rangle)|\alpha\rangle \end{pmatrix} . \tag{2.154}$$

Obviously, the structure of the field $|\alpha\rangle$ is not affected, and we recover the dynamics of a two-level atom excited by a resonant classical *radiation* as described by the Bloch equations (2.51). In the language of quantum computation the operation (2.152) corresponds to a Hadamard gate.

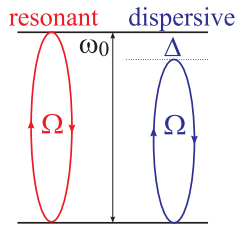

Figure 2.8: Atomic level scheme for the implementation of resonant interactions with classical radiation fields (on the lower transition) and dispersive interactions with quantum fields (on the upper transition).

2.6.2.2 Dispersive interaction, the limit of large detunings

The dispersive Jaynes-Cummings dynamics can be implemented by irradiating a light field, which is sufficiently detuned to avoid Rayleigh scattering processes, as shown in Fig. 2.8. This interaction results in a phase shift of the atomic levels. For $|\Delta| \gg \sqrt{n}\Omega$ we consider the radiative coupling as a small perturbation,

$$\hat{H}_n = \hat{H}_n^{(0)} + \hat{H}_n^{(1)} = \begin{pmatrix} n\omega - \frac{\Delta}{2} & 0 \\ 0 & n\omega + \frac{\Delta}{2} \end{pmatrix} + \begin{pmatrix} 0 & \frac{\Omega_1}{2}\sqrt{n} \\ \frac{\Omega_1}{2}\sqrt{n} & 0 \end{pmatrix} . \tag{2.155}$$

In the unperturbed case we have, $\hat{H}_n^{(0)}|\psi_{j,n}\rangle = E_{j,n}|\psi_{j,n}\rangle$, where the n-photon subspace is spanned by the basis $|j\rangle = (1\ 0)$ and $(0\ 1)$. In second perturbation order,

$$\langle\psi_{j,n}|\hat{H}_n^{(1)}|\psi_{j,n}\rangle \simeq \cancelto{0}{\langle j|\hat{H}_n^{(1)} + \hat{H}_n^{(2)}|j\rangle} + \sum_{j\neq i} \frac{\langle j|\hat{H}_n^{(1)}|i\rangle\langle i|\hat{H}_n^{(1)}|j\rangle}{E_{j,n}^{(0)} - E_{i,n}^{(0)}} = \mp\frac{n\Omega_1^2}{4\Delta} \ , \quad (2.156)$$

where the upper sign holds for $|j\rangle = (1\ 0)$. This result was already obtained in the Exc. 2.7.0.22. In matrix notation [16],

$$\hat{H}_n^{(1)} \simeq \begin{pmatrix} n\Omega_1^2/4\Delta & 0 \\ 0 & -n\Omega_1^2/4\Delta \end{pmatrix} \ . \quad (2.157)$$

The temporal propagation operator (2.146) then simplifies to,

$$\boxed{e^{-\imath\hat{H}_n^{(1)}t} = \begin{pmatrix} e^{\imath n\Omega_1^2 t/4\Delta} & 0 \\ 0 & e^{-\imath n\Omega_1^2 t/4\Delta} \end{pmatrix}} \ . \quad (2.158)$$

The fact that the ground and excited atomic states evolve with different phase factors is important, as we will show in the following example [17, 18].

Example 7 (*Dispersive π-pulse*): As in the previous example, we consider a two-level atom subject to a coherent field, but now tuned out of resonance. Introducing the abbreviation $\varphi \equiv \Omega_1^2 t/4\Delta$, the Jaynes-Cummings evolution is,

$$e^{-\imath\hat{H}_n^{(1)}t} = \begin{pmatrix} e^{\imath n\varphi} & 0 \\ 0 & e^{-\imath n\varphi} \end{pmatrix} \ . \quad (2.159)$$

The fact that the phase shift $n\varphi$ depends on the number of photons, and that it goes in opposite directions for the ground and excited states, is crucial. The dispersive interaction of the atom with a radiation field can phase-shift the Bloch vector. Now, we observe that in addition, it causes a phase shift of the probability amplitude of having n photons in the radiation field by a value proportional to n, i.e. (ignoring irrelevant dynamical phases),

$$\begin{pmatrix} |1\rangle|n\rangle \\ |2\rangle|n-1\rangle \end{pmatrix} \overset{n\varphi}{\curvearrowright} \begin{pmatrix} e^{-\imath n\varphi}|1\rangle|n\rangle \\ e^{\imath n\varphi}|2\rangle|n-1\rangle \end{pmatrix} \ . \quad (2.160)$$

[16] Note, that the same perturbation expansion applied to the complete Hamiltonian in the interaction picture yields,

$$\tilde{H}_I^{(1)} = \begin{pmatrix} 0 & \frac{1}{2}\Omega_1\hat{a}^\dagger \\ \frac{1}{2}\Omega_1\hat{a} & 0 \end{pmatrix} = \tfrac{1}{2}\Omega_1\hat{a}\hat{\sigma}^+ + \tfrac{1}{2}\Omega_1\hat{a}^\dagger\hat{\sigma}^-$$
$$\simeq \frac{\tilde{H}_I^{(1)}|2\rangle\langle 2|\tilde{H}_I^{(1)}}{\omega_2-\omega_1} + \frac{\tilde{H}_I^{(1)}|1\rangle\langle 1|\tilde{H}_I^{(1)}}{\omega_1-\omega_2} = \tfrac{\Omega_1^2}{4\Delta}(\hat{\sigma}^-\hat{\sigma}^+\hat{a}^\dagger\hat{a} - \hat{\sigma}^+\hat{\sigma}^-\hat{a}\hat{a}^\dagger) = \tfrac{\Omega_1^2}{4\Delta}\begin{pmatrix} -\hat{a}^\dagger\hat{a} & 0 \\ 0 & \hat{a}\hat{a}^\dagger \end{pmatrix} \ .$$

[17] This example assumes prior knowledge of *coherent states*, which we do not have the space to introduce here properly. Let us just state that coherent states are coherent superpositions of Fock states, which share many similarities with classical states,

$$|\alpha\rangle \equiv e^{-|\alpha|^2/2}\sum_{n=0}^{\infty}\frac{\alpha^n}{\sqrt{n!}}|n\rangle \ .$$

[18] See script on *Quantum mechanics* (2023), Sec. 3.6.

Applying this result to Glauber states,

$$\begin{pmatrix} |1\rangle|\alpha\rangle \\ |2\rangle|\alpha\rangle \end{pmatrix} \overset{n\varphi}{\curvearrowright} \begin{pmatrix} |1\rangle \sum_n \frac{\alpha^n}{\sqrt{n!}} e^{-\imath n\varphi}|n\rangle \\ |2\rangle \sum_n \frac{\alpha^n}{\sqrt{n!}} e^{\imath n\varphi}|n\rangle \end{pmatrix} = \begin{pmatrix} |1\rangle|\alpha e^{-\imath\varphi}\rangle \\ |2\rangle|\alpha e^{\imath\varphi}\rangle \end{pmatrix} . \tag{2.161}$$

Apparently, the phase of the radiation field is shifted by a value φ, which depends on the state of the atom.

We note here, that the dynamics studied in the last example provides a method of *transferring coherence from an atomic superposition to a quantum correlation of a radiation field*. All we have to do, is to bring the atom into a superposition of states $|1\rangle + |2\rangle$, and the field will automatically evolve toward a Schrödinger cat state $|\alpha e^{\imath\varphi}\rangle + |\alpha e^{-\imath\varphi}\rangle$. The transfer of quantum correlations between coupled degrees of freedom can induce a temporal complete disappearance of any signatures of quantum coherence in the light field. This phenomenon termed *quantum collapse and revival* is genuine of the Jaynes-Cummings model and will be studied in Exc. 2.7.0.30. Another phenomenon is *vacuum Rabi splitting*, which will be studied in 2.7.0.31.

2.6.3 Observables and correlations of the Jaynes-Cummings dynamics

In the limit of low laser intensities we must consider photonic distributions that are not necessarily coherent. The stationary solution of the Schrödinger equation consists of the dressed states $|1, n\rangle$ and $|2, n-1\rangle$. If we now expand a general Jaynes-Cummings state in amplitudes $c_{jn}(t)$,

$$|\psi\rangle = \sum_n (c_{1,n}|1, n\rangle + c_{2,n-1}|2, n-1\rangle) , \tag{2.162}$$

they will follow the Schrödinger equation,

$$\imath\hbar \frac{d}{dt} \begin{pmatrix} c_{1,n} \\ c_{2,n-1} \end{pmatrix} = \hat{H}_n \begin{pmatrix} c_{1,n} \\ c_{2,n-1} \end{pmatrix} . \tag{2.163}$$

The evolution of the coefficients c_{jn} completely describes the Jaynes-Cummings dynamics of the system through the formula (2.146). Obviously, the Jaynes-Cummings state is normalized because,

$$\langle\psi|\psi\rangle = \mathrm{Tr}_{field}\ |\psi\rangle\langle\psi| = \sum_{n=0}^{\infty} (|c_{1,n}|^2 + |c_{2,n}|^2) = 1 . \tag{2.164}$$

As dissipation processes are neglected, we get a pure state described by,

$$\hat{\rho} = |\psi\rangle\langle\psi| . \tag{2.165}$$

The Jaynes-Cummings dynamics involves two coupled degrees of freedom characterized by with their respective observables. If we are interested in them, we can do two things: (a) We ignore the degrees of freedom NOT under study by NOT DOING a measurement. That is, we simply remove the non-interesting degrees of freedom

from the state. For example, if our focus is on the optical mode, we ignore the atomic state,

$$|\gamma\rangle \equiv \sum_{j=1,2} \langle j|\psi\rangle = \sum_n c_{1,n}|n\rangle + c_{2,n-1}|n-1\rangle \ . \tag{2.166}$$

Our new density operator remains pure, that is,

$$\hat{\rho}_{field}^{(pure)} = \sum_{i,j=1,2} \langle j|\hat{\rho}|i\rangle = \sum_{i,j=1,2} \langle j|\psi\rangle\langle\psi|i\rangle = |\gamma\rangle\langle\gamma| \ . \tag{2.167}$$

On the other hand, ignoring the optical mode via,

$$|j\rangle = \sum_n \langle n|\psi\rangle = \sum_n c_{1,n}|1\rangle + c_{2,n-1}|2\rangle \ . \tag{2.168}$$

Again, our new density operator remains pure, that is,

$$\hat{\rho}_{atom}^{(pure)} = \sum_{m,n} \langle m|\hat{\rho}|n\rangle = |j\rangle\langle j| \ . \tag{2.169}$$

(b) We trace over the degrees of freedom NOT under study by DOING a measurement. For example, if again our focus is on the optical mode, we trace over the atomic states,

$$\begin{aligned} \hat{\rho}_{field}^{(mix)} &= \mathrm{Tr}_{atom}\ \hat{\rho} = \sum_{j=1,2} \langle j|\hat{\rho}|j\rangle = \sum_{j=1,2} \langle j|\psi\rangle\langle\psi|j\rangle \\ &= \sum_{n,m} c_{1,m}^* c_{1,n}|n\rangle\langle m| + c_{2,m-1}^* c_{2,n-1}|n-1\rangle\langle m-1| \neq \hat{\rho}_{field}^{(pure)} \ . \end{aligned} \tag{2.170}$$

It is clear, that this incomplete measurement converts the reduced density operator into a statistical mixture, which is free of inneratomic correlations of the type $c_{2,m}^* c_{1,n}$, but this means that we also loose possible field correlations. On the other hand, tracing over the field mode,

$$\begin{aligned} \hat{\rho}_{atom}^{(mix)} &= \mathrm{Tr}_{field}\ \hat{\rho} = \sum_{n=0}^{\infty} \langle n|\hat{\rho}|n\rangle = \sum_{n=0}^{\infty} \langle n|\psi\rangle\langle\psi|n\rangle \\ &= \sum_n \left(c_{1,n}|1\rangle + c_{2,n}|2\rangle\right)\left(c_{1,n}^*\langle 1| + c_{2,n}^*\langle 2|\right) \neq \hat{\rho}_{atom}^{(pure)} \ . \end{aligned} \tag{2.171}$$

After these preliminary remarks let us have a look a some interesting observables.

2.6.3.1 Temporal evolution of the Bloch vector

The expectation value for field observables $\hat{A}|n\rangle = A_n|n\rangle$ is,

$$\langle\psi|\hat{A}|\psi\rangle = \mathrm{Tr}\ \hat{\rho}\hat{A} \sum_{i,n} \langle i|\langle n|\psi\rangle\langle\psi|\hat{A}|n\rangle|i\rangle = \sum_n A_n(|c_{1,n}|^2 + |c_{2,n}|^2) \ . \tag{2.172}$$

An example for a field observable is the photon number operator $\hat{n}$. And for the annihilation operator $\hat{a}|n\rangle = \sqrt{n}|n\rangle$ we have,

$$\langle\psi|\hat{a}|\psi\rangle = \sum_n \sqrt{n}(c_{1,n-1}^* c_{1,n} + c_{2,n-1}^* c_{2,n}) \ . \tag{2.173}$$

To determine the internal state of the atom, we must trace over the light field. The populations and coherences are, therefore,

$$\boxed{\rho_{ij} = \langle i|\mathrm{Tr}_{field}\ \hat{\rho}|j\rangle = \langle i|\sum_n \langle n|\psi\rangle\langle\psi|n\rangle|j\rangle = \sum_n c_{i,n}c^*_{j,n}} \ . \tag{2.174}$$

The projection onto the atomic state is done by,

$$\frac{|j\rangle\langle j|\psi\rangle}{\langle\psi|j\rangle\langle j|\psi\rangle} = \frac{\sum_m c_{j,n}|j,n\rangle}{\sum_m |c_{j,m}|^2} \ . \tag{2.175}$$

With (2.174), we can calculate the atomic Bloch vector (2.64), whose norm is interestingly NOT preserved, since,

$$\begin{aligned} |\vec{\rho}| = \left\| \begin{pmatrix} 2\ \mathfrak{Re}\ \rho_{12} \\ 2\ \mathfrak{Im}\ \rho_{12} \\ \rho_{22}-\rho_{11} \end{pmatrix} \right\| &= 2|\rho_{12}|^2 - 2\rho_{11}\rho_{22} = -2\det\hat{\rho} \\ &= 2\sum_n c_{1,n}c^*_{2,n}\sum_n c^*_{1,n}c_{2,n} - 2\sum_n |c_{2,n}|^2\sum_n |c_{1,n}|^2 \neq 1 \ . \end{aligned} \tag{2.176}$$

2.6.3.2 The photon number distribution

To determine the state of the light field, we must trace over the atomic state. For example, the probability amplitude of encountering the state $|\psi\rangle$ in $|n\rangle$ is,

$$\langle n|\psi\rangle = c_{1,n}|1\rangle + c_{2,n}|2\rangle \ , \tag{2.177}$$

such that,

$$\boxed{p_n = \langle n|\mathrm{Tr}_{atom}\ \hat{\rho}|n\rangle = \langle n|\sum_{i=1,2}\langle i|\psi\rangle\langle\psi|i\rangle|n\rangle = |\langle n|\psi\rangle|^2 = |c_{1,n}|^2 + |c_{2,n}|^2} \ . \tag{2.178}$$

Example 8 (*The Glauber-Sudarshan Q-function*): To characterize the optical field separately from the atomic state, we can try, by a calculation similar to (2.172), to project the Jaynes-Cummings state onto a basis of coherent states [19] Thus, the probability amplitude of encountering the state $|\psi\rangle$ in $|\alpha\rangle$ is,

$$\begin{aligned} \langle\alpha|\psi\rangle &= e^{-|\alpha|^2/2}\sum_n \frac{\alpha^{*n}}{\sqrt{n!}}(c_{1,n}|1\rangle + c_{2,n}|2\rangle) \\ |\langle\alpha|\psi\rangle|^2 &= e^{-|\alpha|^2}\sum_n \frac{\alpha^{*n}\alpha^m}{\sqrt{n!}\sqrt{m!}}(c^*_{1,m}c_{1,n} + c^*_{2,m}c_{2,n}) \ , \end{aligned}$$

such that,

$$\boxed{\pi Q(\alpha) \equiv \langle\alpha|\mathrm{Tr}_{atom}\ \hat{\rho}|\alpha\rangle = e^{-|\alpha|^2}\left(\left|\sum_n c_{1,n}\frac{\alpha^n}{\sqrt{n!}}\right|^2 + \left|\sum_n c_{2,n}\frac{\alpha^n}{\sqrt{n!}}\right|^2\right)} \ .$$

[19] See previous footnote.

We will derive this result in Exc. 2.7.0.32. This quantity, called *Q-function*, allows the illustration of the state in a coordinate system spanned by $\mathfrak{Re}\ \alpha$ and $\mathfrak{Im}\ \alpha$ [13]. It is generally easy to calculate, but does not exhibit much information, e.g., on interference phenomena caused by quantum correlations. In the following section, we will calculate the Wigner function, which can also be evaluated from the Jaynes-Cummings coefficients [54]. The Jaynes-Cummings

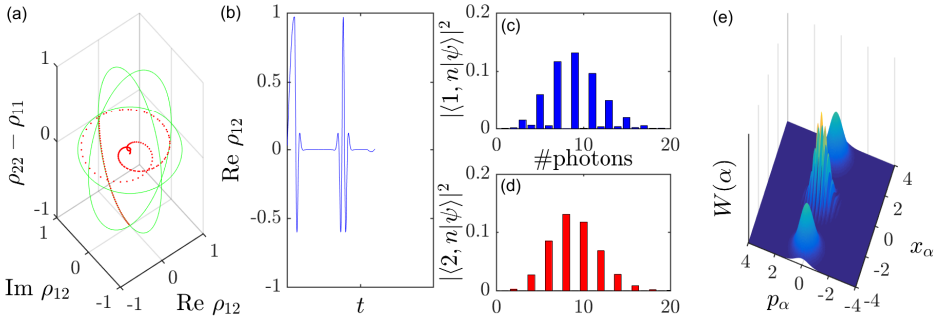

Figure 2.9: (code for download) Evolution of the state during a Jaynes-Cummings type interaction: (a) Bloch vector, (b,c) photon distribution after projection on the ground and excited atomic state, (d) time evolution of the coherence ρ_{12} showing the phenomenon of collapse and revival, and (e) $W(\alpha)$ function.

dynamics illustrated in Fig. 2.9 demonstrates the transfer of coherence between an atom and a light field. In Exc. 2.7.0.33 we study how to create, via a sequence of Ramsey pulses, a Schrödinger cat state in a light field.

2.7 Exercises

2.7.0.1 Ex: Trace of an operator

The trace of an operator $\hat{A}$ is defined by Tr $\hat{A} = \sum_n \langle n|\hat{A}|n\rangle$.
a. Show that the trace is independent of the chosen basis!
b. Show that Tr $\hat{A}\hat{B}$ = Tr $\hat{B}\hat{A}$!

2.7.0.2 Ex: Pure states and mixtures

Consider a system of two levels coupled by a light mode. The Hamiltonian can be written ($\hbar \equiv 1$),

$$\hat{H} = \begin{pmatrix} 0 & \Omega \\ \Omega & \omega_0 \end{pmatrix} .$$

Calculate $\hat{\rho}$, $\hat{\rho}^2$ and $\langle \hat{H} \rangle$ for the following two cases:
a. The atom is in a superposition state, $|\psi\rangle = \alpha|1\rangle + \beta|2\rangle$ e
b. The atom is a statistical mixture of eigenstates, $\hat{\rho} = \mu|1\rangle\langle 1| + \nu|2\rangle\langle 2|$.

2.7.0.3 Ex: Mixture of states

A two-level atom is initially in a superposition of two states $|\psi\rangle = \frac{1}{\sqrt{2}}|1\rangle + \frac{1}{\sqrt{2}}|2\rangle$. An apparatus measures the populations of the states, but the experimenter forgot to read the indicated result.
a. Describes the state the atom by the density operator.
b. Now the experimenter returns to the device. Calculate with which probability he reads the state $|1\rangle$.

2.7.0.4 Ex: Thermal population of a harmonic oscillator

In thermal equilibrium the energy states of a system are populated following Boltzmann's law,

$$P_n = \frac{e^{-n\beta\hbar\omega}}{\sum_m e^{-m\beta\hbar\omega}} \qquad \text{with} \qquad \beta \equiv \frac{1}{k_B T} \ .$$

Consider a one-dimensional harmonic oscillator characterized by the secular frequency ω and, using the density operator, calculate the mean quantum number of the population and the mean energy.

2.7.0.5 Ex: Thermal mixture

We consider a thermal non-interacting atomic gas in one dimension. Instead of describing the state of the atomic ensemble, we can consider a single atom with a distributed probability of having a given velocity v. The density operator of the continuous degree of freedom can be written,

$$\hat{\rho} = \int dv \sqrt{\frac{m}{2\pi k_B T}} e^{-mv^2/2k_B T} |v\rangle\langle v| \ ,$$

and the trace of an arbitrary observable $\hat{A}$,

$$\langle \hat{A} \rangle = \text{Tr } \hat{\rho} A = \int du \langle u|\hat{\rho}\hat{A}|u\rangle \ .$$

Now imagine a device capable of measuring the speed of a single atom randomly chosen within the cloud.
a. Express the probability of measuring a specific velocity v' for this atom using the density operator.
b. Express the expectation value of the average velocity by the density operator.

2.7.0.6 Ex: Derivation of Bloch equations

Derive the Bloch equations explicitly based on the temporal evolutions of the coefficients $a_{1,2}$ (1.18) knowing that $\rho_{ij} = a_i^* a_j$.

2.7.0.7 Ex: Expansion in Pauli matrices

Show explicitly Tr $\hat{\rho}\hat{\sigma}^-\hat{\sigma}^+ = \rho_{11}$.

2.7.0.8 Ex: Bloch vector and Bloch equations

Show that Eq. (2.66) is equivalent to the Bloch equations (2.51).

2.7.0.9 Ex: Normalization of the Bloch vector

Verify $\|\hat{\vec{\rho}}\| = 1$.

2.7.0.10 Ex: Sequence of Ramsey pulses

Many atomic clocks work according to the Ramsey spectroscopy method: The two-level atom is resonantly excited by a microwave $\pi/2$-pulse. Then, the phase of atomic coherence precesses freely over a period of time T accumulating an angle ϕ. Finally, a second $\pi/2$-pulse is applied and the population of the upper-level is measured. Calculate this population as a function of the angle ϕ. Neglect spontaneous emission.

2.7.0.11 Ex: Stationary solution of the Bloch equations

Derive the stationary solution of the Bloch equations including spontaneous emission. How does the spectrum $\rho_{22}(\Delta)$ change in the presence of phase noise, $\gamma = \frac{\Gamma}{2} + \beta$, in particular if $\beta \gg \frac{\Gamma}{2}$?

2.7.0.12 Ex: Photon echo

'Photon echo' is a powerful spectroscopic technique that allows circumvention of certain dephasing processes, for example, the Doppler shift due to the atomic motion in a thermal sample of atoms. The technique resembles the Ramsey method with the difference, that between the two Ramsey $\pi/2$-pulses, that is, during the free precession time, we apply an additional π-pulse, which inverts the imaginary part of the coherence. We will study this method by numerical simulation of the Schrödinger equation and the Bloch equations for a two-level system with and without spontaneous emission:
a. Write down the Hamiltonian of the system and do a numerical simulation of the Schrödinger equation (concatenating the pulses as explained in Eq. (2.112)) for the following temporal pulse sequence:
(i) resonant $\pi/2$-pulse ($\Delta_{12} = 0$) choosing $\Omega_{12} = 2$,
(ii) evolution for a time T without radiation ($\Omega_{12} = 0$),
(ii) resonant $\pi/2$-pulse using the same parameters as in (i),
(iv) evolution for a time T without radiation, and
(v) resonant $\pi/2$-pulse identical to the first pulse.
Prepare a graph of type 2.1 illustrating the temporal evolution of the Bloch vector during the sequence. Now, repeat the sequence taking into account a possible Doppler shift leading to $\Delta_{12} \neq 0$.
b. Repeat the calculation of (a), now numerically solving the Bloch equations, which allow the occurrence of spontaneous emission ($\Gamma_{12} = 0.03\Omega_{12}$). Interpret the results.

2.7.0.13 Ex: Optical density of a cold cloud

The cross section of an atom with the resonant frequency ω_0 moving with velocity v and irradiated by a laser beam of frequency ω is,

$$\sigma(v) = \frac{6\pi}{k^2}\frac{\Gamma^2}{4(\omega-\omega_0-kv)^2+\Gamma^2} \ .$$

The normalized one-dimensional Maxwell distribution,

$$\rho(v)dv = \sqrt{\frac{m}{2\pi k_B T}}e^{-mv^2/2k_BT}dv \ .$$

a. Calculate the absorption profile of the resonance line at 461 nm ($\Gamma_{461} = (2\pi)\ 30.5\,\text{MHz}$) of a strontium gas cooled to the Doppler limit ($k_BT_D = \hbar\Gamma$) of this transition.
b. Calculate the absorption profile of the resonance line at 689 nm ($\Gamma_{689} = (2\pi)\ 7.6\,\text{kHz}$) of a strontium gas cooled to the Doppler limit of the transition at 461 nm.
c. Compare the optical densities in case of resonance.
Help: To evaluate the convolution integral approximate the narrower distribution by a δ-function maintaining the integral over the distribution normalized.

2.7.0.14 Ex: Saturated absorption spectroscopy

Saturated absorption spectroscopy is a technique to avoid Doppler enlargement. The diagram, shown in Fig. 2.10, consists of a cell filled with a rubidium gas (resonance frequency $\omega_0 = ck = 2\pi c/780\,\text{nm}$, decay rate $\Gamma = (2\pi)\ 6\,\text{MHz}$) and two laser beams with the same frequency ω but counterpropagating, one called saturation and another called proof. The one-dimensional and normalized Maxwell velocity distribution is,

$$\rho(v)dv = \sqrt{\frac{m}{2\pi k_B T}}e^{-mv^2/2k_BT}dv \ .$$

The gas is at $T = 300$ K, where the partial pressure of rubidium is around $P = 10^{-1}\,\text{mbar}$. The length of the cell is $L = 10\,\text{cm}$. The laser has an intensity below the saturation limit, such that the cross section of an atom moving at velocity v is,

$$\sigma(v) = \frac{6\pi}{k^2}\frac{\Gamma^2}{4(\omega-\omega_0-kv)^2+\Gamma^2} \ .$$

The saturation laser has high intensity. We suppose here, $\Omega \equiv 10\Gamma$, where Ω is the frequency of Rabi caused by the saturation beam. In this way it creates a population N_and of atoms in the excited state. As this population lacks in the ground state, $N_g = N - N_e$, the absorption of the proof beam is decreased by the factor,

$$\frac{N_e}{N} = \frac{\Omega^2}{4(\omega-\omega_0+kv)^2+2\Omega^2+\Gamma^2} \ .$$

Calculate for laser proof spectrum of optical density, $OD(\omega) = Ln\int_{-\infty}^{\infty}\frac{N_g-N_e}{N}\sigma(v)\rho(v)dv$, and the intensity of light transmitted through the cell, $\frac{I}{I_0} = e^{-OD}$.

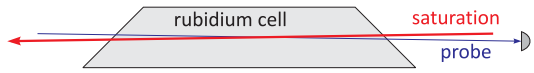

Figure 2.10: Scheme of saturation spectroscopy.

2.7.0.15 Ex: Rate equations as a limiting case of Bloch equations

We show in this exercise that, in the limit $\Gamma \gg \Omega$, we can derive, from the Bloch equations, the Einstein rate equations. Proceed as follows:
Apply the condition $\dot{\rho}_{12} = 0$ to the Bloch equations for a two-level system (2.75), determine $\rho_{12}(\infty)$, and replace this stationary value in the equations for the populations $\rho_{kk}(t)$ using, as an abbreviation, the transition rate $R \equiv \gamma s$, where s is the saturation parameter (2.77).

2.7.0.16 Ex: Purity of two-level atoms with spontaneous emission

Calculate for a driven two-level atom in the stationary limit Tr $\hat{\rho}$ and Tr $\hat{\rho}^2$.

2.7.0.17 Ex: Atomic beam

An atomic beam is illuminated perpendicular to its propagation direction by (quasi-)monochromatic, collimated laser pulses having the intensity $I = 1\,\mathrm{W/cm^2}$, the wavelength $\lambda = 780\,\mathrm{nm}$, and the duration 200 ns. The laser is tuned to the center of an atomic resonance line ($\Gamma/2\pi = 6\,\mathrm{MHz}$).
a. How does the population of the upper atomic state develop?
b. How does the dynamics change, when the light is detuned by 100 MHz?

2.7.0.18 Ex: General form of the master equation

Show that the general form of the master equation: $\dot{\hat{\rho}} = -\frac{i}{\hbar}[\hat{H}, \hat{\rho}] - \frac{\Gamma}{2}(2\hat{\sigma}\hat{\rho}\hat{\sigma}^+ - \hat{\sigma}^+\hat{\sigma}\hat{\rho} - \hat{\rho}\hat{\sigma}^+\hat{\sigma})$, reproduces the Bloch equations including spontaneous emission.

2.7.0.19 Ex: Bloch equations for three levels

An excited Λ-shaped atom consists of two ground states $|1\rangle$ and $|3\rangle$, which are coupled by two lasers with Rabi frequencies and detunings Ω_{12} and Δ_{12} respectively Ω_{23} and Δ_{23} through an excited level $|2\rangle$. Derive the Bloch equations from this system from the general master equation.

2.7.0.20 Ex: Saturation broadening and Autler-Townes splitting

In this exercise we study the Autler-Townes effect in a two-level system $|1\rangle$ and $|2\rangle$ resonantly excited ($\Delta_{12} = 0$) by a laser with the Rabi frequency Ω_{12}:
a. From the eigenvalues $E_{1,2}$ of the effective Hamiltonian (1.38) of the system, describe the behavior of the real part (energy shift) and the imaginary part (linewidth) as a function of the Rabi frequency. Prepare diagrams Ω_{12} versus $\mathfrak{Re}\ E_{1,2}$ and versus $\mathfrak{Im}\ E_{1,2}$ and discuss the limits $\Omega_{12} > \frac{1}{2}\Gamma_{12}$ and $\Omega_{12} < \frac{1}{2}\Gamma_{12}$.
The Autler-Townes effect can be measured experimentally by probing the population of level $|2\rangle$ via excitation of a third (higher) level by a second laser with the Rabi

frequency Ω_{23}. Thus, we obtain a three-level system in cascade configuration, as shown in Fig. 2.3(c). In order to reproduce the experiment by numerical simulations of the Bloch equations (2.104),
b. write down the Liouville matrix $\mathcal{L}_{red}$ reduced by the trace condition (2.109) and
c. compute the stationary Bloch vector from equation (2.111) varying the detuning of the probe laser Δ_{23} and the Rabi frequency Ω_{12} of the system under study ($|1\rangle$ and $|2\rangle$). Choosing the parameters $\Gamma_{23} = 0.5\Gamma_{12}$, $\Gamma_{13} = 0.01\Gamma_{12}$, $\Omega_{23} = 0.1\Gamma_{12}$, prepare a 3D curve (similar to Fig. 2.2(a)) of the stationary population $\rho_{22}(\infty)$. Interpret the results.

2.7.0.21 Ex: Quantum Zeno effect and saturation broadening

In this exercise we study saturation broadening effect in a three-level system $|1\rangle$, $|2\rangle$, and $|3\rangle$ in V-configuration, as shown in Fig. 2.3(b), excited by two resonant lasers with the Rabi frequencies Ω_{12} and Ω_{23}.
a. From the eigenvalues $E_{1,2}$ of the effective Hamiltonian (1.38) of the system, describe the behavior of the real part (energy shift) and the imaginary part (linewidth) as a function of the Rabi frequency. Prepare diagrams Ω_{12} versus $\mathfrak{Re}\ E_{1,2}$ and versus $\mathfrak{Im}\ E_{1,2}$ and discuss the limits $\Omega_{12} > \frac{1}{2}\Gamma_{12}$ and $\Omega_{12} < \frac{1}{2}\Gamma_{12}$.
Saturation broadening can be measured experimentally in a three-level system in V-configuration. To reproduce the experiment by numerical simulations of the Bloch equations (2.104),
b. write down the Liouville matrix $\mathcal{L}$ of the system and calculate the time evolution of the Bloch vector via equation (2.108) varying the Rabi frequency Ω_{23}. Choosing the parameters $\Gamma_{23} = \Gamma_{12}$, $\Gamma_{13} = 0.001\Gamma_{12}$, $\Omega_{12} = 0.2\Gamma_{12}$, and $\Delta_{12} = 0 = \Delta_{23}$, prepare a 3D curve (similar to Fig. 2.2(a)) of the population $\rho_{33}(t)$.
c. Interpret the results in terms of broadening by saturation. The broadening can also be understood in terms of the quantum Zeno effect, where the transition $|1\rangle$-$|2\rangle$ plays the role of the 'observed system' and the transition $|2\rangle$-$|3\rangle$ the role of the measuring device or 'meter' (for example, we can observe the light scattered on the 'meter transition' to infer the evolution of the 'system transition').

2.7.0.22 Ex: Light-shift

In this exercise we study the effect of the dynamic Stark shift (or light shift) of the energy levels of a two-level system $|1\rangle$ and $|2\rangle$ excited by a laser with the Rabi frequency Ω_{12} and the detuning Δ_{12}:
a. From the eigenvalues $E_{1,2}$ of the effective Hamiltonian (1.38) system, find approximations for weak coupling ($\Omega_{12} \ll \Gamma_{12}$) and strong coupling ($\Omega_{12} \gg \Gamma_{12}$). Prepare a graph showing the eigenvalue spectrum (separating the parts $\mathfrak{Re}\ E_{1,2}$ and $\mathfrak{Im}\ E_{1,2}$) as a function of detuning Δ_{12} for various values of Ω_{12}. Also search for approximations valid for large detunings $\Delta_{12} \gg \Gamma_{12}, \Omega_{12}$ and add them to the graph.
The light shift can be experimentally measured in a three-level system in Λ-configuration, as illustrated in Fig. 2.3(a). To reproduce the experiment by numerical simulations of the Bloch equations (2.104),
b. write the Liouville matrix $\mathcal{L}_{red}$ reduced by the condition to the trace (2.109) and calculate the stationary Bloch vector from equation (2.111) varying the detunings of the two lasers Δ_{12} and Δ_{23}. Choosing the parameters $\Gamma_{23} = \Gamma_{12}$, $\Gamma_{13} = 0.01\Gamma_{12}$,

$\Omega_{12} = 2\Gamma_{12}$, and $\Omega_{23} = 0.2\Gamma_{12}$, prepare a 3D curve (similar to Fig. 2.2(a)) of the stationary population $\rho_{22}(\infty)$. Interpret the results.

2.7.0.23 Ex: EIT & dark resonances

In this exercise we study so-called *dark resonances*, which are responsible for the phenomenon of *electromagnetically induced transparency* (EIT). Such resonances are observed in three-level systems $|1\rangle$-$|2\rangle$-$|3\rangle$ in Λ-configuration, as shown in Fig. 2.3(a), when the laser detunings are chosen so as to satisfy $\Delta_{12} = \Delta_{23}$.
a. From the Bloch equations (2.104) show analytically that, in a stationary situation, the population of the excited state is $\rho_{22}(\infty) = 0$ in the center of the dark resonance. Dark resonances can be observed experimentally. To reproduce the experiment by numerical simulations of the Bloch equations (2.104), write down the Liouville matrix $\mathcal{L}_{red}$ reduced by the trace condition (2.108) and calculate the stationary Bloch vector from equation (2.109) varying the detunings of the two lasers Δ_{12} and Δ_{23}. Choosing the parameters such that $\Gamma_{23} = \Gamma_{12}$, $\Gamma_{13} = 0.01\Gamma_{12}$, $\Omega_{12} = 2\Gamma_{12}$, and $\Omega_{23} = 0.2\Gamma_{12}$, prepare a 3D curve [similar to Fig. 2.2(a)] of the population $\rho_{22}(\infty)$. Interpret the results.

2.7.0.24 Ex: STIRAP

In experiments with cold atoms it is often necessary to transfer populations between ground states, for example, between specific levels of a hyperfine structure. One possible procedure is the method of optical pumping, from the initial ground state to an excited state, which subsequently decays to the final state by spontaneous emission. The problem with this incoherent procedure is, that one can control into which ground state level the atom will decay, and that it heats atoms due to the photonic recoil associated with the scattering of light. In this exercise we studied an alternative method, called *Stimulated Raman Adiabatic Passage* (STIRAP), which allows the coherent transfer of population between two states by counter-intuitive pulse sequences:
a. Consider a three-level system in Λ-configuration, as shown in Fig. 2.3(a), initially being in the state $|1\rangle$. Write the system's Hamiltonian in the interaction picture. Now, choose $\Delta_{12} = 0 = \Delta_{23}$, and a temporal variation of the Rabi frequencies described by $\Omega_{12}(t) = \Gamma_{12}(\frac{1}{2} + \frac{1}{\pi}\arctan\Gamma_{12}t)$ and $\Omega_{23}(t) = \Gamma_{12}(\frac{1}{2} - \frac{1}{\pi}\arctan\Gamma_{12}t)$. With this, solve the Schrödinger equation (2.112) iteratively within the time interval $t \in [-40/\Gamma_{12}, 40/\Gamma_{12}]$, while continuously adjusting the Rabi frequencies.
b. The dynamics can also be calculated via a numerical simulations of the Bloch equations (2.104). Write down the Liouville matrix and prepare a simulation using the same parameters as in (b) and additionally $\Gamma_{23} = \Gamma_{12}/2$, $\Gamma_{13} = \Gamma_{12}/500$.
c. Interpret the results.

2.7.0.25 Ex: Adiabatic sweeps

In experiments with cold atoms it is often necessary to transfer populations between ground states, for example, between specific levels of a Zeeman structure. One possible procedure is the method of optical pumping, from the initial ground state to an excited state, which subsequently decays to the final state by spontaneous emission. The

problem with this incoherent procedure is, that one can control into which ground state level the atom will decay, and that it heats atoms due to the photonic recoil associated with the scattering of light. In this exercise we study an alternative method, called *adiabatic sweep*, which allows the coherent transfer of population between the two outer states of a degenerate multiplet, as shown in Fig. 2.11, via an adiabatic ramp of the frequency of the incident radiation:
a. Write down the Hamiltonian of the system in the interaction picture. Now, choose $\Omega/2\pi = 8\,\text{kHz}$ and apply a linear ramp of the radiation detuning between $-50\,\text{kHz} < \Delta(t)/2\pi < 50\,\text{kHz}$ during a time interval of 2 ms. With this, solve the Schrödinger equation (2.104) iteratively varying the detuning.
b. Write down the Liouville matrix of the system and do a numerical simulation of the Bloch equations (2.104) using the same parameters as in (a). Interpret the results. What you observe when you introduce a decay rate between adjacent levels of $\Gamma/2\pi = 200\,\text{Hz}$?

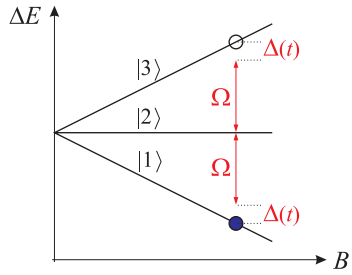

Figure 2.11: Energy levels of an atom in the ground state with Zeeman structure (for example, $|J = 1, m_J = -1, 0, +1\rangle$) as a function of the applied magnetic field.

2.7.0.26 Ex: Dispersive interaction between an atom and light

Radiation which is tuned far from a resonance can change the phase of an atomic dipole moment without changing the populations [20]. We study this effect in a three-level system in cascade configuration excited by two radiation fields, as illustrated in Fig. 2.3(c), simulating the Schrödinger equation and the Bloch equations.
a. Write down the Hamiltonian $\hat{H}$ for this system letting $\Delta_{12} = 0$.
b. Now, consider the subsystem $|2\rangle$-$|3\rangle$, write down its Hamiltonian $\hat{H}_{23}$, determine the eigenvalues, and assume that this transition be excited very far-off resonance. That is, for $\Delta_{23} \gg \Omega_{23}, \Gamma_{23}$ expand the eigenvalues of $\hat{H}_{23}$ up to second order in Ω_{23}. Finally, replace the submatrix $\hat{H}_{23}$ in the complete Hamiltonian $\hat{H}$ by the matrix of the expanded eigenvalues. This procedure corresponds to treating the transition $|2\rangle$-$|3\rangle$ as a perturbation of the transition $|1\rangle$-$|2\rangle$ until second order.
c. Assume that the atom is initially in the ground state and compute the time evolution of the state via the Schrödinger equation (2.112) using (a) the perturbed Hamiltonian and (b) the exact Hamiltonian for the following *sequence of pulses*:
(i) a $\pi/2$-pulse on the transition $|1\rangle$-$|2\rangle$,
(ii) a pulse with a variable duration between 0 and $\Delta t = \Omega_{23}^2/4\pi\Delta_{23}$ applied to the

[20] This type of interaction is used in the implementation of quantum gates in quantum computing.

transition $|2\rangle$-$|3\rangle$,
(iii) a $\pi/2$-pulse on the transition $|1\rangle$-$|2\rangle$. What you observe?
d. Establish the Liouville matrix $\mathcal{L}$ for the same system and calculate the time evolution of the Bloch vector during the sequence by the Bloch equations (2.112) choosing the same parameters as in (c) and additionally $\Gamma_{23} = 1$, $\Gamma_{13} = \Gamma_{23}$, $\Gamma_{12} = 0.01\Gamma_{23}$, and $\Omega_{12} \ggg \Delta_{23}, \Gamma_{23}$. Prepare a 3D curve [similar to Fig. 2.2(b)] of the population $\rho_{22}(t)$. Interpret the results.

2.7.0.27 Ex: Photon statistics

An optical resonator contains on average 10 photons in the mode TEM_{00q}. What is the probability of finding, at any time, 1 photon resp. 10 photons, when the light is (a) thermal, (b) coherent? For case (a), what is the temperature of the light for $\lambda = 633\,\mathrm{nm}$?

2.7.0.28 Ex: Converting a pure state into a mixture by incomplete measurement

Consider a dressed two-level atom with the atomic states $|1\rangle$ and $|2\rangle$ and the photon number state $|n\rangle$.
a. Write down the general normalized dressed state and the density operator.
b. Now, perform a measurement of the atomic state tracing over the atomic degree of freedom and verify whether the resulting density operator represents a pure state.
c. Now, perform a measurement of the photon number and verify whether the resulting density operator represents a pure state.

2.7.0.29 Ex: Time-evolution in the Jaynes-Cummings model

Derive the equations of motion for $\hat{\sigma}^-$, $\hat{\sigma}_z$, and $\hat{a}$ in the Jaynes-Cummings model. Show that the number of photons is not a constant of motion, but the total number of excitations.

2.7.0.30 Ex: Quantum collapse and revival in the Jaynes-Cummings model

Consider the Jaynes-Cummings Hamiltonian and show that the quantum coherence between the two atomic levels can disappear altogether for long periods and reappear later. Explain how this is possible.

2.7.0.31 Ex: Vacuum Rabi splitting

Calculate the Autler-Townes splitting for an excited atom interacting with an empty cavity, i.e. no light injected.

2.7.0.32 Ex: The Q-function in a Jaynes-Cummings state

Calculate the Q-function for a Jaynes-Cummings state from its definition (??).

2.7.0.33 Ex: Creation of quantum correlations in an optical mode

a. We will show in this exercise how, via coherent operations in a three-level system, we can create Schrödinger-type quantum-type correlations in an optical mode. In the system shown in Fig. 2.12 we imagine the lower transition excited by $\pi/2$-pulses of a classical resonant microwave radiation (as described by the operation (2.151)). The upper transition is excited by quantum laser pulses tuned very far out of resonance, thus creating a dispersive dynamics (as described by the operation (2.151)). At time $t = 0$ the atom is in state $|1\rangle$. Now, we apply the following pulse sequence: (i) a microwave pulse with $\sqrt{\bar{n}}\Omega_{12}t = \pi/2$, (ii) an optical pulse with $\Omega_{23}^2 t/4\Delta_{23} = \pi$, (iii) another microwave $\pi/2$-pulse, and finally (iv) an optical pulse of light which is resonant with the transition $|2\rangle$-$|3\rangle$ and projects the population of the atom into one of the states of the microwave transition. Describe the evolution of the state of the system during the sequence and determine the final state of the optical mode.
b. Calculate the number of photons for the two cases that, after a measurement, the atom is found in (i) the lower state and (ii) the upper state. Interprete the results.
(a) Level scheme and (b) pulse sequence.

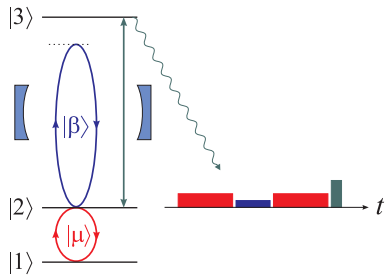

Figure 2.12: OpticatScheme

2.8 Further reading

J. Weiner and P-T. Ho, Springer-Verlag, Berlin (2003), *Light-Matter Interaction: Fundamentals and Applications* [ISBN]

R. Loudon, Oxford Science Publications, Oxford (1982), *The quantum theory of light* [ISBN]

Ch.C. Gerry and P.L. Knight, Cambridge University Press (2005), *Introductory Quantum Optics* [ISBN]

P. Meystre and M. Sargent III, Springer-Verlag, Berlin (1990), *Elements of Quantum Optics* [ISBN]

M.O. Scully and M.S. Zubairy, Cambridge University Press (1997), *Quantum Optics* [ISBN]

G.S. Agarwal et al., *Inhibition of Decoherence due to Decay in a Continuum* [DOI]

M. Brune et al., *Manipulation of photons in a cavity by dispersive atom-field coupling: Quantum-nondemolition measurement and generation of "Schrödinger cat" states* [DOI]

K.E. Cahill et al., *Density Operators and Quasiprobability Distributions* [DOI]

C.M. Caves et al., *Quantum-mechanical noise in an interferometer* [DOI]

J. Dalibard et al., *Wave-Function Approach to Dissipative Processes in Quantum Optics* [DOI]

R. Dum et al., *Monte Carlo simulation of master equations in quantum optics for vacuum, thermal, and squeezed reservoirs* [DOI]

L.E. Estes et al., *Quantum-Mechanical Description of Two Coupled Harmonic Oscillators* [DOI]

M. Fleischhauer et al., *Electromagnetically induced transparency, Optics in coherent media* [DOI]

Y. Gutiérrez et al., *Mollow triplet in cold atoms* [DOI]

L.V. Hau et al., *Light Speed Reduction to 17 Metres per Second in an Ultracold Atomic Gas* [DOI]

E.T. Jaynes et al., *Comparison of quantum and semiclassical radiation theories with application to the beam maser* [DOI]

W.E.Jr. Lamb, *Anti-Photon* [DOI]

B.R. Mollow et al., *Power spectrum of light scattered by two-level systems* [DOI]

K. Mølmer et al., *Monte Carlo wave-function method in quantum optics* [DOI]

M.O. Scully, *From lasers and masers to phaseonium and phasers* [DOI]

Y. Stalgies et al., *The Spectrum of Single-Atom Resonance Fluorescence* [DOI]

C.M. Tokarsky Dieguez et al., *Os fundamentos quânticos da Ressonância Magnética Nuclear* [DOI]

Chapter 3

Atomic motion in electromagnetic fields

The third lecture is about forces exerted by electromagnetic fields on the *center-of-mass* of atoms. In the case of neutral atoms these forces are always due to an interaction of the fields with *internal degrees of freedom*, that is electronic charge and current distributions. It is thus obvious that these forces will depend very much on the structure of the orbitals involved in an interaction, which can be static as in the case of paramagnetic atoms (exhibiting orbitals with permanent electric currents) exposed to a magnetic field, or radiative as in the case of resonantly absorbed (or emitted) light. A first approach to calculating the radiative forces is the classical (i.e. mechanical plus electrodynamic) Lorentz model [1], which describes the electronic orbitals of an atom as damped harmonic oscillators driven by the Lorentz force [2] exerted by an electromagnetic wave.

While being surprisingly powerful, this model does not grasp the subtleties of the light-matter interaction dynamics, and we need to do a little bit of atomic physics in Sec. 3.1, before we turn our attention to forces on magnetic dipole moments in Sec. 3.2 and optical forces in Sec. 3.3.

3.1 Atomic level structure

Up to here we have focused on the two-level atom problem where the light field couples a single ground and excited state. In practice atoms have many levels, and in general the light field couples more than two levels at the same time. Particularly in laser cooling one must deal with the coupling of large numbers of states by light. This section discusses the nature of these states and shows their origin for specific atoms confusing on alkali-metals. The discussion is generally restricted to the ground and first excited states, since these are the only ones that play a significant role in laser cooling.

[1] See script on *Electrodynamics* (2023), Sec. 7.2.3.
[2] See script on *Quantum mechanics* (2023), Sec. 8.1.1.

3.1.1 Level structure of alkali-metal atoms

Alkali-metal atoms were the first ones to be cooled and trapped. Their popularity has several reasons. Most important is that the excitation frequency from the lowest to the first excited state is in the visible region, which makes it relatively simple to generate light for the optical transitions. Another reason is that it is easy to generate an atomic beam with alkali atoms, which have a large vapor pressure at a modest temperature of only a few hundred degrees Celsius. Heating alkali-metals in an oven with a small opening produces an effusive beam of atoms that can be readily manipulated by laser light.

The ground states of all alkali-metal atoms have a closed shell with one valence electron. For example for sodium (Na) the electron configuration is given by ^{23}Na $(1s)^2(2s)^2(2p)^6(3s)$ = [Ne] $(3s)$. The closed shell does not contribute to the total orbital angular momentum of the electrons. The state of the valence electron is completely determined by its orbital angular momentum ℓ and spin angular momentum s. These two momenta couple in the usual way to form the total angular momentum j of the electron:

$$|\ell - s| \leq j \leq \ell + s \ . \tag{3.1}$$

Since the only contribution to the total angular momentum of the atom comes from the valence electron, the total orbital angular momentum is $\mathbf{L} = \vec{\ell}$, spin angular momentum $\mathbf{S} = \mathbf{s}$, and total angular momentum $\mathbf{J} = \mathbf{j}$ of the entire electronic shell. Different values of $\mathbf{J}$ lead to different energies of the states, since the spin-orbit interaction $V_{so} = A\mathbf{L} \cdot \mathbf{S}$ (also called LS-coupling) depends on the orientation of $\mathbf{S}$ with respect to $\mathbf{L}$. This splitting of the states by the spin-orbit interaction is called the fine structure of the atom. The interpretation of the fine structure as a perturbation due to LS-coupling is only valid if the spin-orbit interaction is small compared to the level separation of the electronic states.

For valid LS-coupling, which is the case for low-lying levels of alkali-metal atoms, the electronic states are fully specified in the Russell-Saunders notation as $n^{(2S+I)}L_J$, where n is the principal quantum number of the valence electron. The lowest state of Na is the $3^2S_{1/2}$ state, whereas the first excited states are the $3^2P_{1/2,3/2}$ states, where the valence electron is excited to the $(3p)$-state. In this case the angular momentum $L = 1$ can couple with the total spin $S = \frac{1}{2}$ to form either $J_e = \frac{1}{2}$ or $J_e = \frac{3}{2}$. The fine structure splitting between these two states is $\approx 515\,\mathrm{GHz}$ in Na.

The structure of the alkali-metal atoms becomes somewhat more complicated when the interaction of the nuclear spin $\mathbf{I}$ with the total angular momentum of the electron $\mathbf{J}$ is included. These angular momenta couple in the usual way to form the total angular momentum as $\mathbf{F} = \mathbf{I} + \mathbf{J}$. Different values of $\mathbf{F}$ for the same values of both $\mathbf{I}$ and $\mathbf{J}$ are split by the $A\mathbf{I} \cdot \mathbf{J}$ interaction between the nuclear spin and the electronic angular momentum. The resulting energy structure is called the hyperfine structure (hfs). This hfs is generally much smaller than the fine structure because of the much smaller size of the nuclear magnetic moment. For Na, with a nuclear spin of $I = \frac{3}{2}$, the ground state has $F_g = 1$ and 2, and the hfs is $\approx 1.77\,\mathrm{GHz}$. The excited state has $F_e = 0, 1, 2, 3$, and the resulting hfs is only on the order of 100 MHz. In general, the

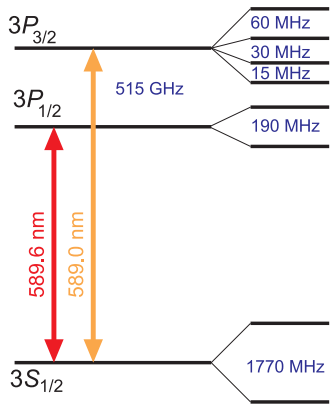

Figure 3.1: The ground S state and lowest lying P states of atomic Na, showing the hfs schematically.

shift of the energy levels due to the hyperfine interaction can be written as [3] [123, 5],

$$\Delta E_{hfs} = \tfrac{1}{2}hAK + hB\frac{\frac{3}{2}K(K+1) - 2I(I+1)J(J+1)}{2I(2I-1)2J(2J-1)} \ , \tag{3.2}$$

where $K = F(F+1) - I(I+1) - J(J+1)$ and A and B are two parameters, that are adjusted using experimental data [5]. The splitting between adjacent levels becomes,

$$\Delta E_{hfs}(F) - \Delta E_{hfs}(F-1) = hAF + 3hBF\frac{F^2 - I(I+1) - J(J+1) + \frac{1}{2}}{2I(2I-1)J(2J-1)} \ , \tag{3.3}$$

where F denotes the highest value of the total angular momentum of the two adjacent levels. A schematic diagram for the fine and hyperfine structure of Na, or other alkalis with $I = 3/2$, is given in Fig. 3.1 [4].

Each of these states of alkali-metal atoms is further split into $(2I+1)(2J+1)$ Zeeman sublevels. In the case of Na with $I = \frac{3}{2}$, this leads to 8 Zeeman sublevels in the ground state ($J_g = \frac{1}{2}$), 8 sublevels in the first excited state ($J_e = \frac{1}{2}$), and 16 sublevels in the next excited state ($J_e = \frac{3}{2}$). In principle, the light can drive all transitions between ground and excited sublevels. However, certain selection rules have to be obeyed, and these limit the number of possible transitions considerably. These selection rules are discussed in more detail in Sec. 3.1.2.

In the absence of any perturbations, many of these Zeeman sublevels are degenerate, but application of an external field lifts the degeneracy. It has already been shown in Sec. 1.2.2 that the presence of a light field not only induces transitions, but also shifts the energy levels. Later in this lecture it is shown that the transition strengths vary among the Zeeman sublevels, and thus a laser field can lift the degeneracy through the different light shifts. In fact, this feature is at the heart of the sub-Doppler cooling schemes to be described in Lecture 4.

[3] See script on *Quantum mechanics* (2023), Sec. 8.2.4.
[4] See script on *Quantum mechanics* (2023), Sec. 7.3.2.

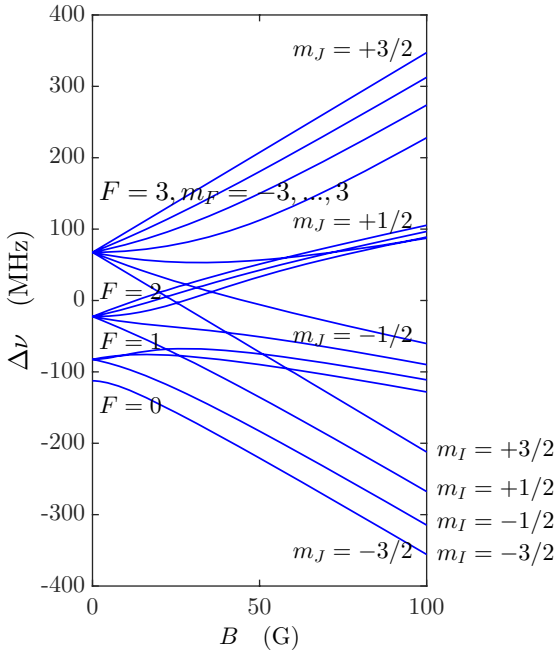

Figure 3.2: (code for download) Hyperfine splitting of the $^2P_{3/2}$-state of Na (see Fig. 3.1). m_F is the projection of the total angular momentum of the atom on the magnetic field axis.

An applied magnetic field $\mathcal{B}$ can also lift these degeneracies, producing the well-known Zeeman effect, as shown in Fig. 3.2. At low fields the energy level shifts ΔE are proportional to the field strengths according to,

$$\Delta E_{zeem} = g\mu_B m\mathcal{B} \ , \tag{3.4}$$

where $\mu_N \equiv e\hbar/2m_e c$ is the Bohr magneton, m is the projection of the angular momentum along $\mathcal{B}$, and g is the Lande g-factor (here m_e is the electron mass). The presence of the nuclear spin changes the g-factor from its usual g_J value given by

$$g_J = 1 + \frac{J(J+1) + S(S+1) - L(L+1)}{2J(J+l)} \tag{3.5}$$

to

$$g_F = g_J \frac{F(F+1) + J(J+1) - I(I+1)}{2F(F+1)} \ . \tag{3.6}$$

Here L, S, and J refer to the electron's angular momenta, I is the nuclear spin, and F is the total atomic angular momentum that ranges from $F = |J - I|$ to $F = J + I$ in integer steps. Thus the different manifolds of Fig. 3.2 have different slopes at small field values. In Exc. 3.4.0.1 we verify that the Zeeman shift depends only on the absolute value of the magnetic field.

3.1.2 Angular momentum and selection rules

For strong optical transitions the coupling between the atomic states is given by the dipole moment, and selection rules exist for such transitions. Selection rules can be inferred from the equations derived in the next section, but they can also be quite simply calculated from the commutation relations [70], as we will demonstrate now. For the z-component of the orbital angular momentum $\hat{L}_z$ of the atom, the following commutation rules apply:

$$[\hat{L}_z, \hat{x}] = \imath\hbar\hat{y} \ , \qquad [\hat{L}_z, \hat{y}] = -\imath\hbar\hat{x} \ , \qquad [\hat{L}_z, \hat{z}] = 0 \tag{3.7}$$

The eigenfunctions of the atoms are denoted by $|\alpha LM\rangle$, where α represents all the other properties of the state besides its orbital angular momentum. The third relation of Eqs. (3.7) leads to,

$$(m' - m)\langle\alpha' L' m'|\hat{z}|\alpha L m\rangle = \langle\alpha' L' m'|[\hat{L}_z, \hat{z}]|\alpha L m\rangle = 0 \ , \tag{3.8}$$

where the last equality holds because the last commutator in Eq. (3.7) is 0. As the next section shows, the coupling between two states by linearly polarized light is proportional to the matrix element for $\hat{z}$, so linearly polarized light can couple two states only if $\Delta m = 0$. Using the same procedure for $\hat{x}$ and $\hat{y}$ leads to,

$$\begin{aligned} \hbar(m' - m)\langle\alpha' L' m'|\hat{x}|\alpha L m\rangle &= \langle\alpha' L' m'|[\hat{L}_z, \hat{x}]|\alpha L m\rangle = \imath\hbar\langle\alpha' L' m'|\hat{y}|\alpha L m\rangle \\ \hbar(m' - m)\langle\alpha' L' m'|\hat{y}|\alpha L m\rangle &= \langle\alpha' L' m'|[\hat{L}_z, \hat{y}]|\alpha L m\rangle = -\imath\hbar\langle\alpha' L' m'|\hat{x}|\alpha L m\rangle \ . \end{aligned} \tag{3.9}$$

The combination of these two relations requires that either $\Delta m = \pm 1$ or that the matrix element for $\hat{x}$ or for $\hat{y}$ must vanish. Again, the next section shows that for circularly polarized light the appropriate matrix element is a combination of $\hat{x}$ and $\hat{y}$. The selection rules for circularly polarized light are thus $\Delta m = \pm 1$, where the $(+)$-sign is for right-handed and the $(-)$-sign for left-handed circular polarization.

Note that these selection rules reflect the conservation of angular momentum. Since each photon carries an angular momentum 1, the projection of this angular momentum on the z-axis can be $0, \pm 1$. Conservation of angular momentum requires that absorption of a photon be accompanied by a corresponding change of the projection of the angular momentum of an atom. In the case of fine or hyperfine interaction, the orbital angular momentum L can be replaced by the total angular momentum J of the electron or F of the atom, respectively. The same selection rules thus apply for m_J and m_F.

For the selection rules for $\hat{\mathbf{L}}^2$, we consider the commutation relation,

$$\left[\hat{L}^2, [\hat{L}^2, \hat{\mathbf{r}}]\right] = 2\hbar^2(\hat{\mathbf{r}}\hat{L}^2 + \hat{L}^2\hat{\mathbf{r}}) \ , \tag{3.10}$$

which can be obtained from the usual algebra for commutators [70]. Eq. (3.10) explicitly depends on the fact that $\mathbf{L} = \mathbf{r} \times \mathbf{p}$ is the orbital angular momentum of the atom, and this relation *cannot be generalized* for either $\mathbf{J}$ or $\mathbf{F}$. Calculating the matrix element for both sides of Eq. (3.10) results in

$$\begin{aligned} \langle\alpha' L' m'|\left[\hat{L}^2, [\hat{L}^2, \hat{\mathbf{r}}]\right]|\alpha L m\rangle &= 2\hbar^4[L(L+1) + L'(L'+1)]\langle\alpha' L' m'|\hat{\mathbf{r}}|\alpha L m\rangle \\ &= \hbar^4[L(L+1) - L'(L'+1)]^2\langle\alpha' L' m'|\hat{\mathbf{r}}|\alpha L m\rangle \ . \end{aligned} \tag{3.11}$$

Thus the coupling between two states is zero for any polarization, unless the two factors in front of the matrix elements in Eq. (3.11) are equal. Rearrangement of this requirement leads to [70],

$$[(L' + L + 1)^2 - 1][(L' - L)^2 - 1] = 0 \; . \tag{3.12}$$

The first term can only be zero if $L = L' = 0$, but this is prohibited since L' is the vector sum of L and $\kappa = 1$ for the photon, and thus cannot be zero. The second term is zero only if $\Delta L = \pm 1$, so this is the selection rule for $\hat{\mathbf{L}}^2$. Again, this selection rule reflects the conservation of angular momentum for absorption of one photon.

Furthermore, for $\Delta L = 0$ the final state angular momentum L' can be the vector sum of L and κ. But the parity of the state for a one-electron system is given by $(-1)^L$ and $\mathbf{r}$ is antisymmetric, so symmetry demands that the matrix element be zero between states where L and L' are both either odd or even. The selection rules for J and F are $\Delta J = 0, \pm 1$ and $\Delta F = 0, \pm 1$. In contrast with the case for $\Delta L, \Delta J = 0$ is allowed, since L and S couple to J, so $\Delta J = 0$ does not imply $\Delta L = 0$. Only for $J = J' = 0$ is $\Delta L = 0$ a necessary consequence, and therefore transitions with $J = 0 \; \rightarrow \; J' = 0$ are forbidden. The same rule applies to F, namely, $F = 0 \; \rightarrow \; F' = 0$ is also forbidden.

In laser cooling, selection rules play a very important role. In order to slow atoms from their thermal velocity down to zero velocity, a large number of photons have to be scattered. Therefore, the coupling strength between the two levels involved in the laser cooling has to be sufficiently high. Furthermore, since the atoms have to undergo a very large number of cycles, the decay from the excited to the ground state must be to only the sublevel coupled by the light. This restricts the number of possible cooling transitions. The selection rules can be used to determine whether two states are coupled by the laser light without extensive calculations.

For the alkali-metal atoms, the hfs complicates the level structure and most of the optically accessible transitions do not meet these criteria. Since the same selection rules for excitation are valid for spontaneous emission, the $\Delta F = 0, \pm 1$ selection rule allows the decay of one excited state to many ground states, and some of these may not be coupled by the laser to an excited state, if the laser's spectral width is considerably smaller than the ground-state hfs-splitting. However, for the states with $J = L + \frac{1}{2}$, the decay from the highest F_e-state can only occur to the highest F_g-state, since the other ground state has $F_g = F_e - 2$ (see Fig. 3.1). Therefore these two states form a closed two-level system. A similar system exists between the lowest F_e and F_g states. However, since the hfs splitting between the two lowest excited states is usually very small, exciting the lowest F_e-state can often also partially excite the next F_e state, which can then decay to the other hyperfine ground-state sublevels. Laser cooling in the alkalis is therefore usually carried out on the highest F_g and F_e states.

These complications do not appear in the metastable noble gas atoms, where the splitting between the states is caused by the spin-orbit interaction instead of the hyperfine interaction. For Ne* only the $^3P_{0,2}$ states are truly metastable. The only closed system can be formed by the $^3P_2 \; \rightarrow \; ^3D_3$ transition, which is the one most often used for laser cooling. Similar transitions exist for the other metastable noble gases and for the earth-alkali metals.

3.1.3 Optical transitions in multilevel atoms

The optical transitions considered in Lecture 1 were restricted to the particularly simple case of a two-level atom, and these transitions can be described by a single Rabi frequency. Real atoms have more than two levels that can be coupled by the optical field, and furthermore, the relative strengths of their multiple transitions depend on the orientation of the atomic dipole moment with respect to the polarization of the light. The single Rabi frequency of Lecture 1 that describes the coupling is given by $\hbar\Omega = -d_{eg}\mathcal{E}_0$ [see Eq. (1.22)], where,

$$d_{eg} = e\langle e|\hat{\epsilon}\cdot\hat{\mathbf{r}}|g\rangle \ . \tag{3.13}$$

The value of the dipole moment of Eq. (3.13) depends on the wavefunctions of the ground and excited states, and is generally complicated to calculate. It is often convenient to introduce the spherical unit vectors given by [5],

$$\hat{\mathbf{e}}_{-1} \equiv \tfrac{1}{\sqrt{2}}(\hat{\mathbf{e}}_x - \imath\hat{\mathbf{e}}_y) \quad , \quad \hat{\mathbf{e}}_{+1} \equiv -\tfrac{1}{\sqrt{2}}(\hat{\mathbf{e}}_x + \imath\hat{\mathbf{e}}_y) \quad , \quad \hat{\mathbf{e}}_0 \equiv \hat{\mathbf{e}}_z \tag{3.14}$$

and to expand the polarization vector $\hat{\epsilon}$ in terms of these vectors. Note that $\hat{\mathbf{e}}_\pm$ corresponds to circularly polarized light, whereas $\hat{\mathbf{e}}_z$ corresponds to linearly polarized light. For simplicity, only cases where the polarization of the light field is given by just one of these vectors will be considered, and this will be indicated by the symbol q ($q = 0, \pm'$ is the subscript of $\hat{\mathbf{e}}_q$). In this notation the components of the dipole moment can be written as,

$$\hat{\epsilon}\cdot\hat{\mathbf{r}} = \hat{\mathbf{e}}_q\cdot\hat{\mathbf{r}} = \sqrt{\tfrac{4\pi}{3}}\hat{r}Y_{1q}(\theta,\phi) \ , \tag{3.15}$$

where the Y_{1q}'s represent the simplest of the spherical harmonic functions.

The matrix element of Eq. (3.13) can be broken up into two parts, one depending on all the various quantum numbers of the coupled states and the other completely independent of M, the projection of l on the quantization axis. This separation is embodied in the well-known Wigner-Eckart theorem discussed in many quantum mechanics texts [11]. Here, the treatment will be somewhat different, since this section treats the simplest case, namely, that fine and hyperfine structure are absent. The more general case will be treated in Sec. 3.1.4. Thus the hydrogenic wavefunctions for the ground and excited state can be used,

$$|g\rangle = |n\ell m\rangle = R_{n\ell}Y_{\ell m}(\theta,\phi) \qquad \text{and} \qquad |e\rangle = |n'\ell'm'\rangle = R_{n'\ell'}Y_{\ell'm'}(\theta,\phi) \ , \tag{3.16}$$

Substitution of Eqs. (3.15) and (3.16) into Eq. (3.13) leads to,

$$= e\langle n'\ell'm'|\hat{\epsilon}\cdot\hat{\mathbf{r}}|n\ell m\rangle = e\langle n'\ell'||r||n\ell\rangle\langle\ell'm'|\sqrt{\tfrac{4\pi}{3}}\hat{r}Y_{1q}|\ell m\rangle \equiv eR_{n'\ell',n\ell}A_{\ell'm',\ell m} \ . \tag{3.17}$$

The following sections first treat the radial or physical part $R_{n'\ell',n\ell}$, also known as the reduced or double-bar matrix element, and then the angular or geometric part $A_{\ell'm',\ell m}$.

[5] See script on *Quantum mechanics* (2023), Sec. 12.2.2.

3.1.3.1 Radial part of the dipole matrix element

The radial part of the matrix element is generally less important in laser cooling because experiments typically use an optical transition joining a set of states that all share the same ground- and excited-state radial wavefunctions. Therefore it becomes an overall multiplicative factor that determines only the magnitude of the coupling (e.g., the overall Rabi frequency). It is given by,

$$R_{n'\ell',n\ell} = \langle R_{n'\ell'}(r)|\hat{r}|R_{n\ell}(r)\rangle = \int_0^\infty r^2 dr\ R_{n'\ell'}(r) r R_{n\ell}(r)\ , \tag{3.18}$$

with $R_{n\ell}$ the radial wavefunction of the state. Here the r^2dr term in the integral originates from the radial part of d^3r. The radial part can be evaluated if the eigenfunctions are known. For all atoms except hydrogen, the eigenfunctions can only be calculated approximately and therefore only approximate values for the radial part can be found. However, for the hydrogen atom the eigenfunctions of the bound states are known and the radial matrix elements can be calculated exactly [11]. For instance, for the first optical allowed transition in H, the $1s \rightarrow -2p$ transition, the radial wavefunctions involved are $R_{1s}(r) = 2e^{-r/a_B}/a_B^{3/2}$ and $R_{2p}(r) = (r/a_B)e^{-r/2a_B}/\sqrt{3}(2a_B)^{3/2}$. Thus the integral becomes,

$$R_{2p,1s} = \int_0^\infty R_{2p}(r) r R_{1s}(r) r^2 dr = 2^7\sqrt{6}a_B/3^5 \approx 1.290 a_B\ . \tag{3.19}$$

For other transitions in hydrogen similar integrals can be evaluated. The hydrogenic wavefunctions are given by [11],

$$R_{n'\ell',n\ell} = N_{n\ell}\rho^\ell e^{-\rho/2} L_{n-\ell-1}^{2\ell+1}(\rho)\ , \tag{3.20}$$

where $\rho \equiv 2r/na_B$ and $L_n^M(r)$ are the Laguerre polynomials, and $N_{n\ell}$ is a normalization constant.

Substitution of Eq. (3.20) into Eq. (3.18) and integrating over r with the help of standard integrals, the matrix element for any transition can be found. Note that the radial matrix elements increase with increasing n, since the radius of the electron orbit increases with n.

For all other atoms, the situation is more complicated. In the case of alkali-metal atoms with only one active electron, the matrix elements can be quite accurately expressed in terms of the effective principal quantum number $n_\ell^* = n - \delta_\ell$ of the valence electron, where δ_ℓ is called the quantum defect and depends on the orbital quantum number ℓ [19]. The same analysis as in the hydrogen case can be applied for the alkali-metal atoms; however, in the summation n is now replaced by n^* [9].

3.1.3.2 Angular part of the dipole matrix element

The angular part $A_{\ell' m\,\ell m}$ of the dipole moment for atoms with $S = 0 = I$ is defined by Eq. (3.17):

$$A_{\ell' m\,\ell m} = \sqrt{\frac{4\pi}{3}}\langle Y_{\ell' m'}|Y_{1q}|Y_{\ell m}\rangle\ , \tag{3.21}$$

where the integration limits are over 4π. The integral can be expressed in terms of the $\{3j\}$-symbols as,

$$A_{\ell' m\, \ell m} = (1)^{\ell'-m'} \sqrt{\max(\ell, \ell')} \begin{pmatrix} \ell' & 1 & \ell \\ -m' & q & m \end{pmatrix} . \tag{3.22}$$

The $\{3j\}$-symbols are related to the Clebsch-Gordan coefficients and are tabulated in [129] [see Eq. (3.25)]. The symmetry of the $\{3j\}$-symbols dictates that they are only nonzero when the sum of the entries in the bottom row is zero, which means $m + q = m'$. Thus circularly polarized light only couples states that differ in m by ± 1, whereas linearly polarized light only couples states that have equal m's. This result is thus identical to the result obtained in Sec. 3.1.2.

3.1.4 Fine and hyperfine interactions

In case of fine and hyperfine interaction the situation changes considerably. For the fine structure, the energy levels are split by the spin-orbit interaction and $\mathbf{L}$ is no longer a good quantum number. Here ℓ is replaced with $\mathbf{L}$ to be more general. The states are now specified by $\mathbf{J}$, the vector sum of $\mathbf{L}$ and $\mathbf{S}$. However, the optical electric field still couples only to the orbital angular momentum $\mathbf{L} = \mathbf{r} \times \mathbf{p}$ of the states. In this situation the Wigner-Eckart theorem could also be applied to calculate the transition strength [51], but again this section will follow a different route that provides more insight in the problem. Although the formulas below may appear rather complicated, the principle is simple.

The atomic eigenstates are denoted by $|\alpha J m_J\rangle$ in the J-basis, and m_J explicitly indicates for which angular momentum the magnetic quantum number M is the projection. In most cases, this is obvious from the notation, but in this section it is not. The dipole transition matrix element is therefore given by,

$$d_{eg} = e\langle \alpha' J' m' | \hat{\epsilon} \cdot \hat{\mathbf{r}} | \alpha J m_J \rangle . \tag{3.23}$$

Since the optical electric field only couples the $\mathbf{L}$ component of these $\mathbf{J}$ states, these eigenfunctions must be first expanded in terms of the L and S wavefunctions:

$$|\alpha J m_J\rangle = \sum_i C_i |\alpha L m_L\rangle |S m_S\rangle , \tag{3.24}$$

where i represents an appropriate set of angular momentum quantum numbers. The C_i's are Clebsch-Gordan coefficients that can also be expressed in terms of the more symmetrical $\{3j\}$-symbols as,

$$C_i = \langle L m_L, S M_S | J m_J \rangle = (-1)^{-L+S-m_J} \sqrt{2J+1} \begin{pmatrix} L & S & J \\ m_L & m_S & -m_J \end{pmatrix} . \tag{3.25}$$

The fact that Eq. (3.22) for the integral of the product of three spherical harmonics and Eq. (3.25) both contain the $\{3j\}$-symbols is a result of the important connection between the $Y_{\ell m}$'s and atomic angular momenta.

Substitution of Eq. (3.24) in Eq. (3.23) twice leads to a double summation, which contains matrix elements in the (L, S) basis of the form,

$$\langle \alpha' L' m'_L | \langle S' m'_S | \hat{r} | \alpha L M_L \rangle | S m_S \rangle = \langle \alpha' L' m'_L | \hat{r} | \alpha L m_L \rangle \delta_{SS'} \delta_{m_S m'_S} . \tag{3.26}$$

The first term on the right-hand side is the matrix element that has been evaluated before (see Eq. (3.17)). The δ-functions reflect the notion that the light couples the orbital angular momenta of the states, and not the spin. The spin and its projection are not changed by the transition. Substitution of Eq. (3.26) into Eq. (3.23), expansion of the matrix elements in the L-basis, and recoupling of all the Clebsch-Gordan coefficients leads to,

$$d_{eg} = e(-1)^{L'-m'_J}\sqrt{(2J+1)(2J'+1)}\,\langle \alpha' L'||\hat{r}||\alpha L\rangle \begin{Bmatrix} L' & J' & S \\ J & L & 1 \end{Bmatrix} \begin{pmatrix} J & 1 & J' \\ m_J & q & -m'_J \end{pmatrix}. \tag{3.27}$$

The array of quantum numbers in the curly braces is not a $\{3j\}$-symbol, but is called a $\{6j\}$-symbol. It summarizes the recoupling of six angular momenta. Values for the $\{6j\}$-symbols are also tabulated in Ref. [129]. Note that the radial part of the dipole moment has remained unchanged, and so the results of the previous section can still be used.

In case of hyperfine interactions the situation becomes even more complicated. However, the procedure is the same. First the eigenfunctions in the F-basis are expanded in the (J, I)-basis, where I is the nuclear spin, and a $\{6j\}$-symbol involving I, J, and F appears. Then the eigenfunctions of the J-basis are further reduced into the (L, S)-basis. Since the procedure is similar to the procedure for the fine structure interaction, only the result is shown:

$$d_{eg} = e(-1)^{1+L'+S+J+J'+I-M'_F}\,\langle \alpha' L'||\hat{r}||\alpha L\rangle\sqrt{(2J+1)(2J'+1)(2F+1)(2F'+1)} \begin{Bmatrix} L' & J' & S \\ J & L & 1 \end{Bmatrix} \begin{Bmatrix} J' & F' & I \\ F & J & 1 \end{Bmatrix} \begin{pmatrix} F & 1 & F' \\ m_F & q & -m'_F \end{pmatrix}. \tag{3.28}$$

Since S can be parallel or anti-parallel to $L, J' = 1/2, 3/2$ and the fine-structure interaction is usually large compared to the hyperfine interaction.

3.1.5 Selection rules for emission in certain directions

As seen by Eq. (3.23), the excitation rate induced by a light field depends on the relative orientation of the laser polarization $\hat{\epsilon}$ and the magnetic field $\mathbf{B}$. To take this dependence into account, we decompose the polarization vector (which can be linear or elliptical) on a coordinate basis, as shown in Eq. (3.14). Thus, the relative amplitude of the transitions $\Delta m_J = 0$ is proportional to the projection of the polarization vector onto the magnetic field axis, $\epsilon_0 \equiv \hat{\epsilon}\cdot\hat{\mathbf{e}}_0$. To estimate the amplitude of the transitions $\Delta m_J = \pm 1$, we must project onto the coordinates $\epsilon_{\pm 1} \equiv \hat{\epsilon}\cdot\hat{\mathbf{e}}_\pm$. Note that the direction of incidence of the beam, given by the wavevector $\mathbf{k}$, does not influence the transition probability directly (after all, the spatial dependence $e^{i\mathbf{k}\cdot\mathbf{r}}$ was removed by the dipolar approximation; only through the fact, that the polarization is perpendicular to the propagation vector, $\hat{\epsilon} \perp \mathbf{k}$.

3.2 Magnetic traps

With the level atomic structure of alkalis unraveled in Sec. 3.1 we are able to set up the atomic Hamiltonian (1.2), and knowing the transition strengths between different

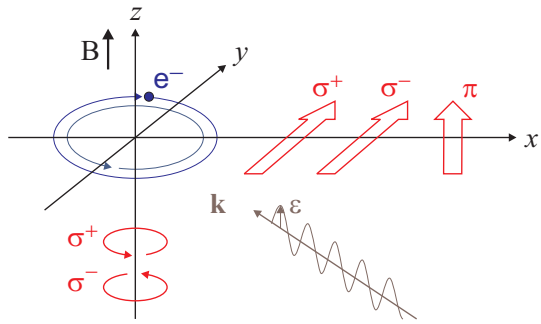

Figure 3.3: Selection rules due to polarization $\hat{\epsilon}$ of the incident light. The projection of this vector onto the axes $\pi = \hat{\epsilon} \cdot \hat{\mathbf{e}}_0$ and $\sigma_\pm = \hat{\epsilon} \cdot \hat{\mathbf{e}}_\pm$ is proportional to the excitation probability (and, obviously, also to the emission probability).

atomic levels we can write down the Bloch equation governing the internal dynamics of an atom driven by laser light. As promised in the preamble of this third lecture, we must derive from this atom-light dynamics the forces acting on the atomic center-of-mass.

3.2.1 Forces on magnetic dipole moments

The orbital motion of the electrons corresponds to a circular current generating a permanent magnetic dipole moment $\vec{\mu}_J$, which can interact with external magnetic fields. We have already shown in (3.4) that the interaction potential can be written as,

$$\hat{U} = -\hat{\vec{\mu}}_J \cdot \vec{\mathcal{B}} = -\frac{g_J \mu_B}{\hbar} \hat{\mathbf{J}} \cdot \vec{\mathcal{B}} \longrightarrow -\frac{g_J \mu_B}{\hbar} |\mathbf{J}||\vec{\mathcal{B}}| = -\frac{g_J \mu_B}{\hbar} m_J \mathcal{B} = U \ , \tag{3.29}$$

where the *Landé factor* g_J is given by the formula (3.5). Here, $\mathbf{J} = \mathbf{L} + \mathbf{S}$ is the total angular momentum resulting from the coupling of the total angular orbital momentum and the total spin of all electrons. If the atom has a nuclear spin I other than zero, then $\mathbf{F} = \mathbf{J} + \mathbf{I}$ replaces $\mathbf{J}$ in Eq. (3.29), and the g-factor generalizes to the one given in Eq. (3.6) [6]. The interaction generates a force acting on the atomic center-of-mass,

$$\boxed{\mathbf{f} = -\nabla \hat{H}_{int} = -\mu_B g_J m_J \nabla \mathcal{B}} \ , \tag{3.30}$$

which can be used for trapping purposes once we are able to arrange for inhomogeneous magnetic field configuration $\vec{\mathcal{B}} = \vec{\mathcal{B}}(\mathbf{r})$. Obviously, force is conditioned by the existence of a gradient of the absolute value of the magnetic field. It was first used in the famous *Stern-Gerlach experiment*, which led to the discovery of the electron. We discuss a Stern-Gerlach type experiment in Exc. 3.4.0.2.

Magnetic traps are widely used in atom optics, where they served, e.g. for the first realizations of Bose-Einstein condensation (BEC). An important feature of magnetic traps is that they do not need light to confine atoms. Hence, they are free of heating

[6] Note that the formula only applies to weak fields. For strong fields the Zeeman splitting changes to the Paschen-Back splitting of the hyperfine structure [7].

effects that could be caused by photonic recoil. Depending on the sign of U and $\mathbf{F}$, atoms in states whose energy increases or decreases with the magnetic field are called 'low-field seekers' or 'high-field seekers', respectively. One might think, that it should be possible to trap atoms in any of these states, generating either a magnetic field minimum or a maximum. Unfortunately, only low-field seekers can be trapped in static magnetic fields, because in free space magnetic fields can not form maxima, as we will show in Exc. 3.4.0.3. Even though low-field seekers are not in the energetically lowest hyperfine levels [see Fig. 3.4(b)], they can still be trapped because the rate of spontaneous emission through the magnetic dipole is $\sim 10^{-10}$ s^{-1}, and hence completely negligible. However, spin changing collisions can induce losses and limit the maximum densities.

3.2.2 Quadrupolar traps and Majorana spin-flips

The most basic static magnetic trap for neutral atoms is generated by a pair of current-carrying coils in anti-Helmholtz configuration producing an axially symmetric quadrupolar magnetic field, as shown in Fig. 3.4.

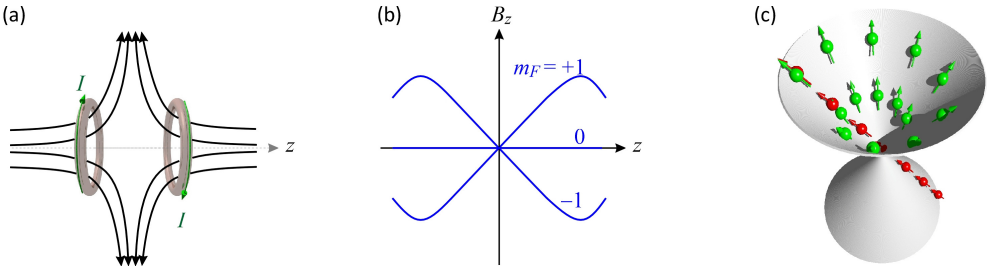

Figure 3.4: (a) Quadrupolar magnetic trap generated by a pair of current-carrying wires in anti-Helmholtz configuration. (b) Ground state energy levels of ^{23}Na, $^2S_{1/2}$, $F = 1$ as a function of axial distance from the trap center. (c) Illustration of Majorana spin-flips: The red atom passes through the hole, while the green one moves adiabatically avoiding the hole.

Close to the trap center an expansion of the magnetic field generated by anti-Helmholtz coils yields,

$$\vec{\mathcal{B}} = \begin{pmatrix} x \\ y \\ -2z \end{pmatrix} \partial_r \mathcal{B} \ , \tag{3.31}$$

where the field gradient $\partial_r \mathcal{B}$ along radial direction $r^2 \equiv x^2 + y^2$ in the trap center depends on the applied current and the geometry of the coils. However, the 1:2 aspect ratio is generic for all quadrupolar potentials, as we will see in Exc. 3.4.0.4. We easily verify that,

$$\nabla \cdot \vec{\mathcal{B}} = 0 \qquad \text{but} \qquad \nabla |\vec{\mathcal{B}}| = \frac{\partial_r \mathcal{B}}{\sqrt{r^2 + 4z^2}} \begin{pmatrix} x \\ y \\ 4z \end{pmatrix} \ . \tag{3.32}$$

Thus, the quadrupolar magnetic potential is linear in the spatial coordinates,

$$\boxed{U(\mathbf{r}) = -|\vec{\mu}||\vec{\mathcal{B}}| = \mu_B g_J m_J \ \partial_r \mathcal{B} \ \sqrt{r^2 + 4z^2}} \ , \tag{3.33}$$

where $2\partial_r\mathcal{B} = \partial_z\mathcal{B}$.

To calculate the *rms*-radius $\bar{r}$ of a cloud of temperature T confined to this potential, we set,

$$k_BT \equiv U(\bar{r},0) = \mu_B\bar{r}\partial_r\mathcal{B} \ , \tag{3.34}$$

and obtain the density distribution [8],

$$n(\mathbf{r}) = n_0 e^{-U(\mathbf{r})/k_BT} = n_0 e^{-\sqrt{r^2+4z^2}/\bar{r}} \ . \tag{3.35}$$

Normalization requires,

$$\begin{aligned} N &= \int_{R^3} n(\mathbf{r})\ d^3r = n_0 \int_{-\infty}^{\infty}\int_0^{\infty} e^{-\sqrt{r^2+4z^2}/\bar{r}} 2\pi r\ drdz \\ &= n_0 2\pi\bar{r}^2 \int_{-\infty}^{\infty}\int_{2|z|/\bar{r}}^{\infty} \xi e^{-\xi} d\xi dz = n_0 2\pi\bar{r}^2 \int_{-\infty}^{\infty} e^{-\frac{2|z|}{\bar{r}}}\left(1+\tfrac{2|z|}{\bar{r}}\right)\ dz \\ &= n_0 2\pi\bar{r}^3 \int_0^{\infty} e^{-\zeta}(1+\zeta)\ d\zeta = n_0 4\pi\bar{r}^3 \ . \end{aligned} \tag{3.36}$$

Therefore, the effective volume is, $V_{eff} = 4\pi\bar{r}^3$. In application example is discussed in Exc. 3.4.0.5.

3.2.2.1 Majorana spin-flips

The quadrupolar trap is the simplest one that can be technically realized. Unfortunately, this trap is not stable because of the phenomenon of *Majorana spin-flips*, which expel atoms from the trapped cloud. Since this field configuration always has a central point, where the magnetic field disappears, non-adiabatic Majorana transitions can occur when the atom passes through the zero point [see Fig. 3.4(c)]. The disappearance of the field leaves the atoms disoriented, that is, ready to reorient their spins. The transitions transfer population from a low-field seeking state to a high-field seeker, which consecutively is expelled from the trap. This problem is particularly severe for hydrogen, where it can induce a so-called *relaxation explosion* [83].

From (3.34) we get the *rms*-radius,

$$\bar{r} = \frac{k_BT}{\mu_B\partial_r\mathcal{B}} \ . \tag{3.37}$$

The average velocity of an atom is,

$$\bar{v} = \sqrt{\frac{k_BT}{m}} \ . \tag{3.38}$$

In order for the atomic motion in the magnetic potential to be adiabatic [so that Eq. (3.33) applies], the *local Larmor frequency*,

$$\omega_{Larmor}(\mathbf{r}) = \frac{\mu_B}{\hbar}\sqrt{r^2+4z^2}\partial_r\mathcal{B} \tag{3.39}$$

[8] See script on *Quantum mechanics* (2023), Sec. 24.2.4.

must be faster, than any change the atom might experience due to its motion with velocity $\mathbf{v}$. I.e. we need [119],

$$\omega_{Larmor}(\mathbf{r}) > \frac{\mathbf{v}\cdot\nabla|\vec{\mathcal{B}}|}{|\vec{\mathcal{B}}|} \ . \tag{3.40}$$

This can not be satisfied within a volume located at the trap center. This ellipsoidal volume is delimited by $\mathbf{r}_{sf}$ given by the condition,

$$\omega_{Larmor}(\mathbf{r}_{sf}) \equiv \frac{\mathbf{v}\cdot\nabla|\vec{\mathcal{B}}|}{|\vec{\mathcal{B}}|} \ . \tag{3.41}$$

For our quadrupole trap,

$$\frac{\mathbf{v}\cdot\nabla|\vec{\mathcal{B}}|}{|\vec{\mathcal{B}}|} = \frac{\mathbf{v}\cdot\frac{\partial_r\mathcal{B}}{\sqrt{r_{sf}^2+4z_{sf}^2}}}{\partial_r\mathcal{B}\sqrt{r_{sf}^2+4z_{sf}^2}}\begin{pmatrix}x_{sf}\\ y_{sf}\\ 4z_{sf}\end{pmatrix} = \frac{x_{sf}v_x+y_{sf}v_y+4z_{sf}v_z}{r_{sf}^2+4z_{sf}^2} \ . \tag{3.42}$$

Considering for simplicity only radial motion, $\mathbf{v} = v\hat{\mathbf{e}}_r$, then by equating (3.39) and (3.41),

$$\frac{\mu_B}{\hbar}r_{sf}\partial_r\mathcal{B} = \omega_{Larmor}(r_{sf}) = \frac{v}{r_{sf}} \ , \tag{3.43}$$

that is, the spin-flip volume is on the order of,

$$r_{sf} = \sqrt{\frac{\hbar v}{\mu_B\partial_r\mathcal{B}}} \ . \tag{3.44}$$

Let us now estimate the spin relaxation rate from the flow of atoms through the volume,

$$\frac{1}{\tau_{sf}} = N\frac{r_{sf}^3}{V_{eff}}\frac{\bar{v}}{r_{sf}} \ , \tag{3.45}$$

where r_{sf}^3/V_{eff} is simply the fraction of the cloud's volume overlapping with the spin-flip volume. Then,

$$\frac{1}{\tau_{sf}} = \frac{N}{4\pi\bar{r}^3}r_{sf}^2\bar{v} = \frac{N}{4\pi\left(\frac{k_BT}{\mu_B\partial_r\mathcal{B}}\right)^3}\frac{\hbar\bar{v}}{\mu_B\partial_r\mathcal{B}}\bar{v} = \frac{N\hbar}{4\pi(k_BT)^3}(\mu_B\partial_r\mathcal{B})^2\frac{k_BT}{m} = \frac{N\hbar(\mu_B\partial_r\mathcal{B})^2}{4\pi m(k_BT)^2} \ . \tag{3.46}$$

That is, the problem gets worse when the cloud is cooled to low temperatures.

3.2.3 Magnetic Ioffe-type traps

The spin-flip problem can be overcome by using a different magnetic field geometries. One example is the so-called *magnetic bottle*, also called the *Ioffe-Pritchard trap* illustrated in Fig. 3.5(a), where the minimum field amplitude has a finite value different from zero. Other methods to eliminate the zero-field point are time-varying potentials, such as the time-orbiting potential (TOP) trap illustrated in Fig. 3.5(b) and discussed in Exc. 3.4.0.6 [57, 75], or the application of an 'optical plug', which consist

in an intense dipolar optical laser beam, tuned to the blue of an atomic transition, focused into the center of a quadrupole trap where the magnetic field is zero, and repelling the atoms from this area (see Fig. 3.6). The advantage of Ioffe-Pritchard-type traps is that they are always harmonic sufficiently close to the trap center, which simplifies the theoretical treatment in many respects, as shown in Exc. 3.4.0.7.

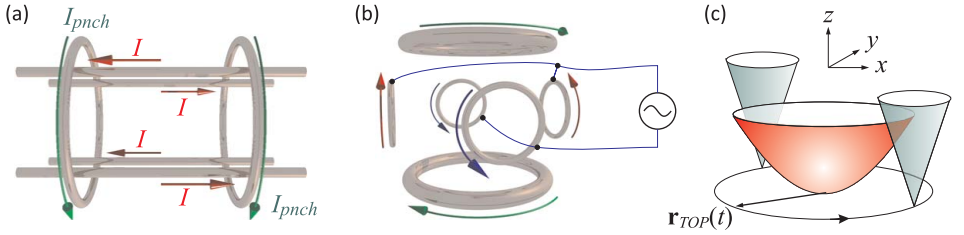

Figure 3.5: (a) Magnetic trap in Ioffe-Pritchard configuration. (b) Realization of the Time-Orbiting Potential (TOP) trap. (c) Formation of a time-averaged 'effective' harmonic potential.

Close to the trap center Ioffe-Pritchard-type traps are described by,

$$\boxed{U(\mathbf{r}) = \mu_B g_F m_F \sqrt{\mathcal{B}_0^2 + (r\partial_r \mathcal{B})^2 + (z\partial_z \mathcal{B})^2}}\ , \tag{3.47}$$

and this magnetic trapping potential can be harmonically approximated by,

$$\begin{aligned} U(\mathbf{r}) &\simeq \mu_B g_F m_F \left(\mathcal{B}_0 + \frac{(r\partial_r \mathcal{B})^2}{2\mathcal{B}_0} + \frac{(z\partial_z \mathcal{B})^2}{2\mathcal{B}_0} \right) \\ &\equiv const + \frac{m}{2}\omega_r^2 r^2 + \frac{m}{2}\omega_z^2 z^2 \equiv k_B T \left(const + \frac{r^2}{2\bar{r}^2} + \frac{z^2}{2\bar{z}^2} \right)\ , \end{aligned} \tag{3.48}$$

where the *rms*-radius $\bar{r} = \omega_r^{-1}\sqrt{k_B T/m}$ follow from the normalization of the density $n(\mathbf{r}) = n_0 e^{-U(\mathbf{r})/k_B T}$ to the number of atoms,

$$N = \int n(\mathbf{r}) d^3 r = n_0 \int_0^\infty e^{-r^2/2\bar{r}^2} 2\pi dr \int_{-\infty}^\infty e^{-z^2/2\bar{z}^2} dz = n_0 (2\pi)^{3/2} \bar{r}^2 \bar{z} \equiv n_0 V_{eff}\ . \tag{3.49}$$

The trap frequencies can be calculated as,

$$\omega_{r,z} = \sqrt{\frac{\mu_B (\partial_r \mathcal{B}_{r,z})^2}{m B_0}}\ . \tag{3.50}$$

The Earth's gravitational field deforms the trapping potential and, in the case of a harmonic potential, causes a gravitational sag without changing the secular frequencies of the potential. Assuming the potential to be given by,

$$U = \frac{m}{2}\omega_r^2 r^2 + \frac{m}{2}\omega_z^2 z^2 - mgz = \frac{m}{2}\omega_r^2 r^2 + \frac{m}{2}\omega_z^2 (z - g/\omega_z^2)^2 - \frac{m}{2} g^2/\omega_z^2\ , \tag{3.51}$$

the atoms sag to a height of g/ω_z^2. In time-dependent traps, gravity causes a more complex behavior [74]. Important works have been done by [23, 120, 58, 72, 1, 40, 101, 46]. We study the impact of gravitation in Exc. 3.4.0.8.

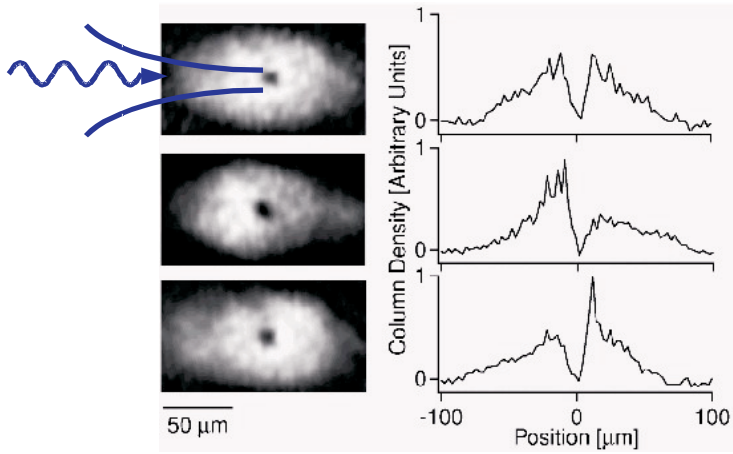

Figure 3.6: Creation of a repulsive hole by light tuned to the blue of an atomic transition.

3.2.4 Adiabatic potentials

Adiabatic potentials can be used to realize more complicated trapping geometries from magnetic potentials [32]. To study adiabatic potentials we consider for simplicity the two-level system $|\frac{1}{2},\frac{1}{2}\rangle \leftrightarrow |\frac{1}{2},-\frac{1}{2}\rangle$ coupled by an incident radiation (e.g. a radiofrequency) [9]. The dressed states Hamiltonian of our two-level system is a 2×2 matrix, as shown in Sec. 1.2.2,

$$\hat{H}(z) = \begin{pmatrix} \frac{1}{2}\mu_B g_F \mathcal{B}(z) - \frac{1}{2}\hbar\omega & \frac{1}{2}\hbar\Omega \\ \frac{1}{2}\hbar\Omega & -\frac{1}{2}\mu_B g_F \mathcal{B}(z) + \frac{1}{2}\hbar\omega \end{pmatrix} . \tag{3.52}$$

Also for simplicity, we assume a one-dimensional geometry, $\mathcal{B} = \mathcal{B}(z)$, but it is easy to generalize to three dimensions. The eigenvalues of $\hat{H}$ are,

$$E_{\pm}(z) = \pm\tfrac{1}{2}\sqrt{\hbar^2\Omega^2 + [\mu_B g_F \mathcal{B}(z) - \hbar\omega]^2} . \tag{3.53}$$

Sufficiently far from resonance, $\hbar\Omega \ll |\mu_B g_F \mathcal{B}(z) - \hbar\omega|$, we obtain,

$$E_{\pm}(z) \simeq \pm\tfrac{1}{2}[\mu_B g_F \mathcal{B}(z) - \hbar\omega] \pm \frac{\hbar^2\Omega^2}{4[\mu_B g_F \mathcal{B}(z) - \hbar\omega]} , \tag{3.54}$$

where the second term can be interpreted as the dynamic Stark shift of the energy levels. On the other hand, sufficiently close to resonance, $\hbar\Omega \ll |\mu_B g_F \mathcal{B}(z) - \hbar\omega|$,

$$E_{\pm}(z) \simeq \tfrac{1}{2}\hbar\Omega + \tfrac{1}{4\hbar\Omega}[\mu_B g_F \mathcal{B}(z) - \hbar\omega]^2 . \tag{3.55}$$

Assuming, for simplicity, a linear $1D$ magnetic field gradient $\mathcal{B}(z) \equiv zb$, we see that near the *avoided crossing* the energy levels form an approximately harmonic adiabatic potential displaced from the origin by a distance $z = \frac{\hbar\omega}{\mu_B g_F b}$.

To illustrate the influence of the radiofrequency, we calculate the potential energy and the dressed states for ^{6}Li atoms. Fig. 3.7(a) illustrates the radiofrequency coupling and Fig. 3.7(b) the dressed states for two magnetic substates coupled by a radiofrequency. The minimum emerging in the upper curve of Fig. 3.7(a) may serve

[9] A generalization to multilevel systems $F > \frac{1}{2}$ is straightforward.

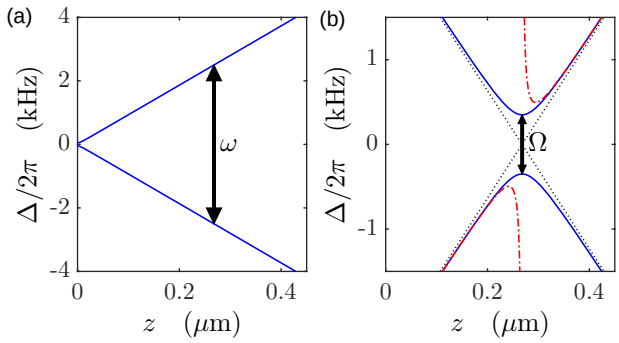

Figure 3.7: (code for download) (a) Potential energies for a hyperfine structure $F = \frac{1}{2}$ with a g-factor of $g = -\frac{2}{3}$ (as e.g. in the ground state $^2S_{1/2}$ of ^{6}Li). A radiofrequency (arrow) couples the substates $m_F = \pm\frac{1}{2}$. Here, $b = 200\,\mathrm{G/cm}$ and $\omega = 2\pi \times 5\,\mathrm{kHz}$. (b) Uncoupled dressed states (dotted line), coupled dressed states (solid line), and dynamic Stark shifts (dash-dotted) approximated far away from resonance. The Rabi frequency is $\Omega = 2\pi \times 700\,\mathrm{Hz}$.

as a confinement potential. Obviously, the atomic motion must be sufficiently slow in order to adiabatically follow the potential curve. Otherwise, they can undergo Landau-Zener transitions to other (possibly untrapped) states. This is analogous to the Majorana transitions discussed above. We will come back to this issue when discussing evaporation techniques in Sec. 4.4.1.

Note that, using an rf-radiation composed by several frequencies, potential minima can be realized at several distances Z. In Exc. 3.4.0.9 we calculate an example.

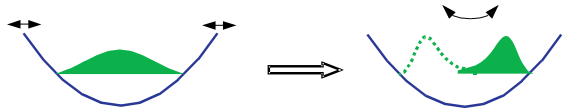

Figure 3.8: Effective potential due to a rapid modulation of the trap's location.

Another way of generating adiabatic potentials consists in directly manipulating the trapping potential, e.g. by shaking it as illustrated in Fig. 3.8. Obviously, the shaking must be fast enough to guarantee that the atoms do not notice it, but perceive a time-averaged effective potential.

3.3 Optical forces

In order to understand the optical force experienced by an atom absorbing light from a laser beam, we need to come back to the full Hamiltonian composed of all contribution identified in the beginning of the first lecture (1.1) to (1.4),

$$\hat{H} = \hat{H}_{cm} + \hat{H}_{ele} + \hat{H}_{rad} + \hat{H}_{int} \ . \tag{3.56}$$

Disregarding only the laser-field Hamiltonian considered to be classical, the only remaining degrees of freedom are the center-of-mass motion and the electronic dy-

namics. The time scale of the electronic motion is usually very rapid compared to the motion of the nucleus, where (almost) the entire mass of the atom is concentrated. Therefore, the external (nuclear) dynamics decouples from the internal (electronic) one, which allows the separation of the total wavefunction in two parts,

$$|\psi\rangle = |\psi\rangle_{ext}|\psi\rangle_{ele} \ , \tag{3.57}$$

where for a simple two-level atom, $|\psi(t)\rangle_{ele} = a_g(t)|g\rangle + a_e(t)|e\rangle$, with the atomic ground state $|g\rangle$ and the excited state $|e\rangle$. The external states are eigenstates of the momentum in the case of a free particle, $|\psi\rangle_{ext} = |\mathbf{p}\rangle$. For particles confined in a potential the external states are the vibrational eigenstates, $|\psi\rangle_{ext} = |n\rangle$. The temporal evolutions of the internal and external degrees of freedom are governed by independent Schrödinger equations. For cold atomic clouds the kinetic energy is much smaller than the excitation energy, which allows the separation of the energy scales, as illustrated in Fig. 3.9. That is, the internal degrees of freedom are frozen in the ground state. Many phenomena, for example, Bose-Einstein condensation and the dynamics of condensates are described in this regime [10].

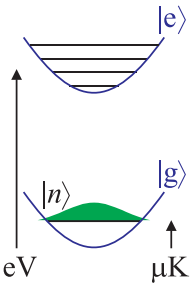

Figure 3.9: The internal degrees of freedom of cold atoms are thermally frozen.

Again, the force on the center-of-mass is exerted by the gradient of electromagnetic potentials:

$$\mathbf{F} = -\nabla \hat{H}_{int} \ . \tag{3.58}$$

The coupling of external and internal degrees of freedom is mediated by the photonic recoil transferred to the atom during absorption and emission processes. That is, the feature that the interaction with light simultaneously *excites* the atom and exerts a *force* couples the degrees of freedom. This fact manifests itself in the Hamiltonian of the atom interacting with a light field by the appearance of terms joining operators acting on different degrees of freedom,

$$\hat{H}_{int} = \hbar\Omega(\hat{\mathbf{r}})e^{\imath\mathbf{k}\cdot\hat{\mathbf{r}}}\hat{a}^{\dagger}e^{\imath\omega t}\hat{\sigma}e^{-\imath\omega_0 t} + c.c. \ , \tag{3.59}$$

where $\hat{\sigma} \equiv |g\rangle\langle e|$ and $\hat{a} \equiv \sum_n |n\rangle\langle n+1|$ and $\hbar\Omega(\hat{\mathbf{r}}) \equiv \mathbf{d}_{12}\cdot\vec{\mathcal{E}}$ is the coupling constant or *Rabi frequency*. The Hamiltonian is that of the Jaynes-Cummings model, except that in addition to the field operators $\hat{a}$ and the atom transition operators $\hat{\sigma}$, appears an operator for the position of the atom $\hat{\mathbf{r}}$, whose quantum features we have not taken very seriously so far. It appears in the Rabi frequency and also in the term $e^{\imath\mathbf{k}\cdot\hat{\mathbf{r}}}$. Now, we must remember, that

$$U_{kick} = e^{\imath\mathbf{k}\cdot\hat{\mathbf{r}}} = |\mathbf{p} + \hbar k\rangle\langle\mathbf{p}| \tag{3.60}$$

is the unitary operator of the photonic recoil in the absorption process. We shall shortly see, that it is precisely this term in the Hamiltonian that gives rise to all phenomena related to light forces on atoms.

[10] Nonetheless, the fact that it is thermally frozen does not prevent the intentional excitation of the internal degree of freedom by irradiating electromagnetic fields tuned close to resonances and coupling electronic energy levels. In the case of coupling, the external and internal degrees of freedom must both be considered.

3.3.1 The dipolar gradient force and the radiation pressure force

To compute the forces of light on an atom, we describe the atom as a two-level system: A fundamental level $|1\rangle$ and an excited level $|2\rangle$ decaying to the fundamental level with the rate Γ. The energy difference between the levels is $\hbar\omega_0 \equiv E_2 - E_1$. The light with frequency ω is derived from a laser beam, which can be detuned from the atomic transition, $\Delta \equiv \omega - \omega_0$. We consider the interaction part (3.59) of the total Hamiltonian [38]. Using the density operator $\hat{\rho}$ [11], we can calculate the force that the light field exerts on the atom,

$$\begin{aligned}\mathbf{F}(\mathbf{r}) = \langle\hat{\mathbf{F}}(\mathbf{r})\rangle &= -\mathrm{Tr}_{at}\ \hat{\rho}\nabla_{\mathbf{r}} H_{int} \\ &= -\tfrac{1}{2}\hbar\sum_j \langle j|\hat{\rho}|\nabla_{\mathbf{r}}\left(\Omega(\mathbf{r})e^{\imath\mathbf{k}\cdot\mathbf{r}-\imath\Delta t}|2\rangle\langle 1| + \Omega(\mathbf{r})e^{-\imath\mathbf{kr}+\imath\Delta t}|1\rangle\langle 2|\right)|j\rangle \\ &= -\tfrac{1}{2}\hbar\nabla_{\mathbf{r}}\Omega(\mathbf{r})\left(\langle 1|\hat{\rho}e^{\imath\mathbf{k}\cdot\mathbf{r}-\imath\Delta t}|2\rangle + \langle 2|\hat{\rho}e^{-\imath\mathbf{k}\cdot\mathbf{r}+\imath\Delta t}|1\rangle\right) \\ &\quad - \tfrac{\imath}{2}\hbar\mathbf{k}\Omega(\mathbf{r})\left(\langle 1|\hat{\rho}e^{\imath\mathbf{k}\cdot\mathbf{r}-\imath\Delta t}|2\rangle - \langle 2|\hat{\rho}e^{-\imath\mathbf{k}\cdot\mathbf{r}+\imath\Delta t}|1\rangle\right)\ .\end{aligned} \tag{3.61}$$

Now, we let the atom be at the position $\mathbf{r} = 0$, then,

$$\mathbf{F}(\mathbf{0}) = -\hbar\nabla_{\mathbf{r}}\Omega(\mathbf{0})\ \Re\mathfrak{e}\ (\rho_{12}e^{-\imath\Delta t}) + \hbar\mathbf{k}\Omega(\mathbf{0})\ \Im\mathfrak{m}\ (\rho_{12}e^{-\imath\Delta t})\ . \tag{3.62}$$

The quantities $\rho_{12} \equiv \langle 1|\hat{\rho}|2\rangle = \rho_{21}^*$ are the coherences, which develop in a two-level system excited by a laser beam. Inserting the stationary solutions of the Bloch equations (2.75), we obtain

$$\mathbf{F}(\mathbf{0}) = -\tfrac{1}{2}\hbar\frac{4\Delta\Omega}{4\Delta^2 + 2\Omega^2 + \Gamma^2}\nabla_{\mathbf{r}}\Omega + \hbar\mathbf{k}\frac{\Gamma\Omega^2}{4\Delta^2 + 2\Omega^2 + \Gamma^2}\ . \tag{3.63}$$

With the definition of the *optical cross section*,

$$\sigma_a(\Delta) \equiv \sigma_{a0}\frac{\Gamma^2}{4\Delta^2 + 2\Omega^2 + \Gamma^2} \qquad \text{where} \qquad \sigma_{a0} = \frac{3\lambda^2}{2\pi} \tag{3.64}$$

is the resonant cross section, we can write,

$$\mathbf{F}(\mathbf{0}) = -\tfrac{1}{2}\hbar\Delta\nabla_{\mathbf{r}}\ln\left(1 + \frac{2\Omega^2}{4\Delta^2 + \Gamma^2}\right) + \hbar\mathbf{k}\frac{\Omega^2}{\Gamma}\frac{\sigma_a(\Delta)}{\sigma_{a0}}\ . \tag{3.65}$$

Apparently, the force comprises two contributions. The *dipolar gradient force* can be derived from a potential. It is proportional to the intensity gradient and can be interpreted as resulting from absorption processes immediately followed by self-stimulated emission. Near resonance it is dispersive. Far from resonance it can be approximated by,

$$\boxed{\mathbf{F}_{dp} = \nabla_{\mathbf{r}}\frac{-\hbar\Delta\Omega^2}{4\Delta^2 + \Gamma^2} \overset{|\Delta|\gg\Gamma}{\longrightarrow} -\nabla_{\mathbf{r}}\frac{\hbar\Omega^2}{4\Delta}\ .} \tag{3.66}$$

The *radiation pressure force* is dissipative. Close to resonance it is absorbing. It is proportional to the phase gradient and the only force exerted by plane waves. It

[11] The total density operator consists of an inner part (atomic excitation), a radiation part, and a the part describing the motion $\hat{\rho} = \hat{\rho}_{atom} \otimes \hat{\rho}_{laser} \times \hat{\rho}_{motion}$, but the latter two are disregarded.

can be interpreted as resulting from absorption processes followed by spontaneous emission. With $\Omega^2 = \sigma_{a0}\Gamma I/\hbar\omega$ we get a formula,

$$\boxed{\mathbf{F}_{rp} = \hbar\mathbf{k}\frac{I}{\hbar\omega}\sigma_a(\Delta) = \hbar\mathbf{k}\gamma_{sct}}\ , \tag{3.67}$$

which describes the force as a product of the number of photons in the incident beam, $I/\hbar\omega$, the absorption cross section, $\sigma_a(\Delta)$, and the recoil momentum per photon, $\hbar\mathbf{k}$. γ_{sct} is the scattering rate. The dipole gradient force (and the associated potential) is

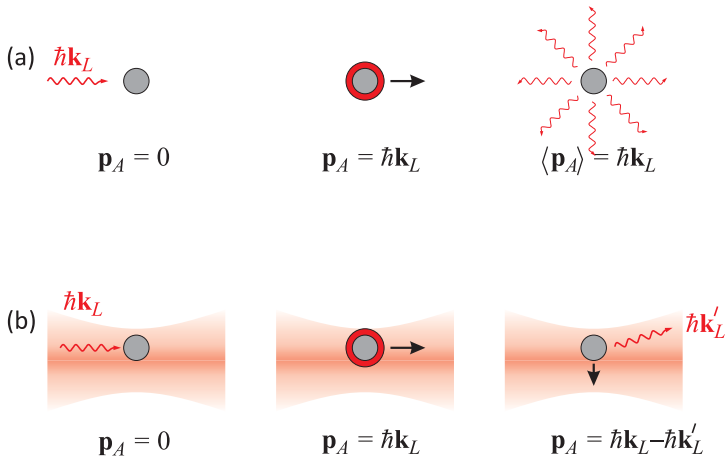

Figure 3.10: (a) An atom with mass m and velocity v_{at} moves to the right and absorbs a photon propagating to the left with momentum $\hbar k_{rd}$. Center: An excited atom suffers a change of momentum $p_{at} = mv_{at} - k_{rd}$. (b) The isotropic re-emission of a photon results, averaged over many absorption-emission cycles, in a momentum change for the atom of $\langle p_{at}\rangle = mv_{at} - k_{rd}$.

often used to spatially confine atoms, and the radiation pressure force is often used to cool them down. Note that we still need to correct Eqs. (3.66) and (3.67) to take into account the square of the average over the possible spatial orientations of the transition matrix element $d_{12}/3$.

The saturation parameter defined as

$$s = \frac{\frac{1}{2}\Omega^2}{\Delta^2 + \frac{1}{4}\Gamma^2}\ , \tag{3.68}$$

allows to write the dipolar gradient force and the radiative pressure force as,

$$\mathbf{F}_{dp} = -\frac{\hbar\Delta}{6}\frac{1}{1+s}\nabla s \qquad \text{and} \qquad \mathbf{F}_{rp} = \frac{\hbar\mathbf{k}\Gamma}{6}\frac{s}{1+s}\ . \tag{3.69}$$

Eq. (3.69) shows that the radiation pressure force 'saturates' as s increases, and is therefore limited by the spontaneous emission rate. The saturation parameter essentially describes the relative importance of terms appearing in the denominator of the line profile function for the light forces. The spontaneous emission rate is an

intrinsic property of the atom, proportional to the square of the atomic transition dipole moment, whereas the square of the Rabi frequency is a function of the incident laser intensity. If $s \ll 1$, the spontaneous emission is fast compared to any stimulated process, and the light field is said to be weak. If $s \gg 1$, the Rabi oscillation is fast compared to spontaneous emission and the field is considered as strong. The line profile factor indicates a 'power broadening' by saturation of a factor of $\sqrt{2}$. Note that the dipolar gradient force and potential, Eqs. (3.69), do not saturate when the intensity of the light field is increased. Usually $\mathbf{F}_{dp}$ and U_{dp} are used to manipulate and trap atoms in a laser beam tuned far away from resonance in order to avoid absorption.

Often, the transition moment can be oriented using circularly polarized light. In this case, all previous expressions for $\mathbf{F}_{dp}$, $\mathbf{F}_{rp}$, and U_{dp} should be multiplied by 3. From now on we will abandon the average over the orientations and only use d_{12}^2 for the square of the transition dipole moment. Solve Exc. 3.4.0.10.

3.3.1.1 Lorentz model of the dipole force

The interaction Hamiltonian (3.59) containing the coupling of the degrees of internal and external degrees of freedom allows us to easily calculate the optical forces. But it does not provide us with an intuitive picture on how a manipulation of the electronic structure can induce a force on the atomic center-of-mass. For this we need stress a classical model, called the Lorentz model. Let us have a look at Fig. 3.11(a). For the two dipoles oriented parallel and anti-parallel to the electric field to minimize their energy, they need to walk into (respectively, out of) the magnetic field. That is they feel forces attracting them to (respectively, repelling them from) electric field maxima. When the dipole has been *induced* by the electric field itself, it will necessarily be parallel.

Now, let us interpret the nucleus-electron system composing the atom as a harmonic oscillator with resonance frequency ω_0 and suppose that the electric field is generated by an electromagnetic wave oscillating at a frequency ω. We know that, driven below resonance frequency, $\omega < \omega_0$, the oscillator will vibrate in phase with the driving field, as illustrated in Fig. 3.11(b). Driven above resonance frequency, $\omega > \omega_0$, the oscillator will vibrate in anti-phase with the driving field [see Fig. 3.11(c)]. This means, that below resonance (red detuning) at any instant of time the atomic dipole induced by the electromagnetic field will be oriented parallel to the field and be attracted toward the field maximum. Above resonance (blue detuning) the atom will be repelled from the field maximum.

3.3.2 Recoil- and Doppler-shift

3.3.2.1 Recoil- and Doppler-shift in classical mechanics

In classical mechanics we speak of *elastic scattering* when no energy is transferred to internal degrees of freedom of the collision partners, so that *kinetic* energy and momentum stay conserved. This concept can be transferred to quantum particles (e.g. atoms) and photons. In elastic Compton scattering, if the atoms keep their initial internal excitation, the law of momentum conservation requires the transfer of photonic momentum to the scattering atom which, consequently, changes its kinetic

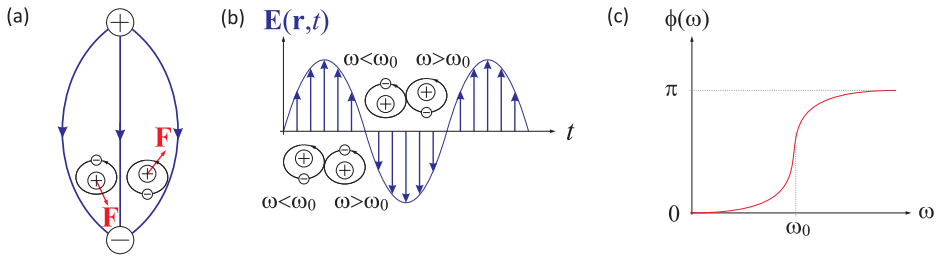

Figure 3.11: (a) Lorentz force on electric dipoles in an electrostatic field gradient. (b) Orientation of induced dipoles in an electromagnetic field. (c) Phase-shift of a harmonic oscillator with a resonance frequency at ω_0 driven at frequency ω.

energy. To compensate for this kinetic energy change, the frequency of the scattered light must change in order to preserve the total energy, as illustrated in Fig. 3.12(b).

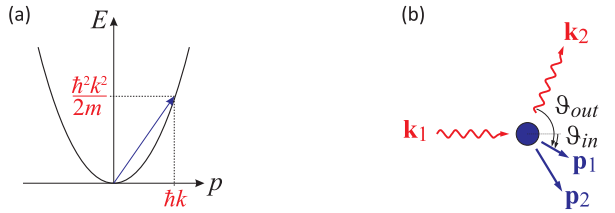

Figure 3.12: (a) Kicking an atom along its dispersion relation. (b) Scheme of the Compton-scattering of light.

We will calculate in the following the frequency distribution of the light scattered by an atom as a function of its initial velocity $\mathbf{p}_1$, of the frequency ω_1 of the incident light and of the scattering angle, that is, the angle between the modes $\mathbf{k}_1$ and $\mathbf{k}_2$. We begin by writing the laws of conservation of energy and momentum,

$$\begin{aligned} \hbar\mathbf{k}_1 + \mathbf{p}_1 &= \hbar\mathbf{k}_2 + \mathbf{p}_2 \\ \hbar\omega_1 + \frac{p_1^2}{2m} &= \hbar\omega_2 + \frac{p_2^2}{2m} \ . \end{aligned} \tag{3.70}$$

Eliminating $\mathbf{p}_2$ from the second equations, we obtain,

$$\hbar\omega_1 - \frac{\hbar^2 k_1^2}{2m} - \frac{\hbar\mathbf{k}_1 \cdot \mathbf{p}_1}{m} = \hbar\omega_2 + \frac{\hbar^2 k_2^2}{2m} - \frac{(\hbar\mathbf{k}_1 + \mathbf{p}_1) \cdot \hbar\mathbf{k}_2}{m} \ . \tag{3.71}$$

The photonic recoils of the incident and of the scattered light are almost equal,

$$\omega_{rec} \equiv \frac{\hbar^2 k_1^2}{2m} \simeq \frac{\hbar^2 k_2^2}{2m} \ , \tag{3.72}$$

such we can approximate,

$$\omega_2 = \omega_1 \frac{1 - \frac{\hbar\omega_1}{mc^2} - \frac{p_1}{mc}\cos\sphericalangle(k_1, p_1)}{1 - \frac{\hbar\omega_1}{mc^2}\cos\sphericalangle(k_1, k_2) - \frac{p_1}{mc}\cos\sphericalangle(p_1, k_2)} \ , \tag{3.73}$$

using $\omega_1 = ck_1$, or also,

$$\omega_2 - \omega_1 = \omega_1 \frac{\frac{\hbar\omega_1}{mc^2}\left[-1+\cos(\vartheta_{in}-\vartheta_{out})\right] + \frac{p_1}{mc}(\cos\vartheta_{out}+\cos\vartheta_{in})}{1-\frac{\hbar\omega_1}{mc^2}\cos(\vartheta_{in}-\vartheta_{out}) - \frac{p_1}{mc}\cos\vartheta_{out}} \ , \tag{3.74}$$

where we call the angles $\vartheta_{in} = \sphericalangle(k_1, p_1)$, $\vartheta_{out} = \sphericalangle(k_2, p_1)$, and $\vartheta = \vartheta_{in} - \vartheta_{out} = \sphericalangle(k_1, k_2)$. For non-relativistic velocities, the denominator is approximately 1:

$$\boxed{\omega_2 - \omega_1 = 2\omega_{rec}(-1+\cos\vartheta) + k_1 v_1(\cos\vartheta_{out}+\cos\vartheta_{in})} \ , \tag{3.75}$$

with $\mathbf{p}_1 = m\mathbf{v}_1$. The first term describes the recoil shift and the second term the Doppler shift. This scattering is known as *Compton scattering* from free atoms.

The second term vanishes for initially at resting atoms, $\mathbf{p}_1 = 0$, and Eq. (3.75) simplifies to,

$$\omega_2 - \omega_1 = 2\omega_{rec}(-1+\cos\vartheta) \ . \tag{3.76}$$

It also vanishes for atoms which have no velocity component in the scattering plane spanned by the wavevectors $\mathbf{k}_1$ and $\mathbf{k}_2$, that is $\vartheta_{out} = 180° - \vartheta_{in}$ [12], for which case we get the maximum recoil shift,

$$\omega_2 - \omega_1 = -4\omega_{rec} \ . \tag{3.77}$$

The recoil shift is a consequence of momentum conservation.

The recoil shift is typically on the order of $\omega_2 - \omega_1 \approx (2\pi)$ 10 kHz, which in many situations is negligible (e.g. when we deal with thermal atomic clouds), such that we can consider the scattering as elastic., i.e. the first term can be disregarded. Considering, for simplicity, only backscattering, $\cos\vartheta_{out} = \cos\vartheta_{in} = 1$, then Eq. (3.75) simplifies to,

$$\omega_2 - \omega_1 = 2k_1 v_1 \ . \tag{3.78}$$

Obviously, the frequency shift depends on the initial velocity through the Doppler shift $k_1 v_1$. In a thermal gas, the velocities are distributed according to the Maxwell-Boltzmann distribution. Therefore, Rayleigh scattering of light off a cloud of free thermal atoms is subject to Doppler broadening [13].

3.3.2.2 Recoil- and Doppler-shift in quantum mechanics

Disregarding the internal degree of freedom, we describe the photonic recoil by simply adding the corresponding momentum $\hbar k$ to the system. Before the absorption of the photon, the Hamiltonian of a free atom is,

$$\hat{H}_{cm}(t<0) = \frac{\hat{\mathbf{p}}^2}{2m} \ . \tag{3.79}$$

Afterward, it is,

$$\hat{H}_{cm}(t>0) = \hat{H}_{cm}(t<0) + \frac{\hbar\mathbf{k}}{m}\hat{\mathbf{p}} = \frac{(\hat{\mathbf{p}}+\hbar\mathbf{k})^2}{2m} - \frac{\hbar^2\mathbf{k}^2}{2m} \ , \tag{3.80}$$

[12] This situation is often realized in Bragg scattering from optical lattices [141, 143, 142].

[13] This Doppler broadening is explored e.g. in RIR spectroscopy, where the momentum distribution in p_1 reveals as a frequency distribution $\Delta\omega = \omega_2 - \omega_1$ of Bragg-scattered light, which can be measured by beating with an irradiated idler mode, which can be chosen as being identical to $\mathbf{k}_2$.

where the last term describing the recoil-shift is irrelevant, here. We define the acceleration operator $e^{-\imath\mathbf{k}\cdot\hat{\mathbf{r}}}$, which has the following properties. Using the relationship $e^{\hat{A}}\hat{B}e^{-\hat{A}} = \hat{B} + [\hat{A},\hat{B}] + \frac{1}{2!}[\hat{A},[\hat{A},\hat{B}]]$ [14] it is easy to verify,

$$\boxed{\begin{aligned} e^{\imath\mathbf{k}\cdot\hat{\mathbf{r}}}|\mathbf{r}\rangle &= |\mathbf{r}\rangle \\ e^{\imath\mathbf{k}\cdot\hat{\mathbf{r}}}|\mathbf{p}\rangle &= |\hat{\mathbf{p}}+\hbar\mathbf{k}\rangle \\ e^{-\imath\mathbf{k}\cdot\hat{\mathbf{r}}}\hat{\mathbf{r}}e^{\imath\mathbf{k}\cdot\hat{\mathbf{r}}} &= \hat{\mathbf{r}} \\ e^{-\imath\mathbf{k}\cdot\hat{\mathbf{r}}}\hat{\mathbf{p}}e^{\imath\mathbf{k}\cdot\hat{\mathbf{r}}} &= \hat{\mathbf{p}}+\hbar\mathbf{k} \\ e^{-\imath\mathbf{k}\cdot\hat{\mathbf{r}}}\frac{\mathbf{p}^2}{2m}e^{\imath\mathbf{k}\cdot\hat{\mathbf{r}}} &= \frac{(\hat{\mathbf{p}}+\hbar\mathbf{k})^2}{2m} \end{aligned}}\,, \tag{3.81}$$

implying $[e^{\imath\mathbf{k}\cdot\hat{\mathbf{r}}},\hat{H}] \neq 0$.

3.4 Exercises

3.4.0.1 Ex: Zeeman shift and quantization axes

Choosing the fixed quantization axis $\hat{\mathbf{e}}_z$ and a magnetic field $\vec{\mathcal{B}}$ in an arbitrary direction, calculate the Hamiltonian of the Zeeman interaction with an angular momentum $J = 1$ and show that the energy shift depends only on the absolute value $|\vec{\mathcal{B}}|$.

3.4.0.2 Ex: The Stern-Gerlach effect

Consider a Bose-Einstein condensate of ^{87}Rb trapped in a superposition of two the trappable Zeeman states $|F, m_F\rangle = |2,+2\rangle$ and $|1,-1\rangle$. Suddenly a magnetic gradient of $\partial_z\mathcal{B} = 100\,\mathrm{G/cm}$ is applied for 2 ms. Calculate the separation of the centers-of-masses of the two parts of the condensate after 10 ms of ballistic expansion.

3.4.0.3 Ex: Lack of trapping potentials for strong field seekers

Show that it is not possible to create magnetic trapping potentials for atoms in low-field seeking Zeeman states.

3.4.0.4 Ex: Quadrupolar potential

Show that for a quadrupolar trap always holds $2\partial_r\mathcal{B}_{qua} = \partial_z\mathcal{B}_{qua}$.

3.4.0.5 Ex: Magnetic quadrupole trap for ^{87}Rb

a. Consider ^{87}Rb atoms confined in a magnetic trap with $\vec{\mathcal{B}}(x,y,z) = \begin{pmatrix} x & y & -2z \end{pmatrix} \times 200\,\mathrm{G/cm}$. The atoms are in the state $|F = 1, m_F = -1\rangle$ with the g-factor $g_F = 1/2$. Check whether it is reasonable to assume constant vibration frequencies for such traps.
b. Assume that the trapped atomic cloud consists of $N = 10^8$ atoms at temperature

[14] See script on *Quantum mechanics* (2023), Exc. 2.6.5.1.

$T = 100\,\mathrm{K}$. Calculate the atomic density n_0 at the center of the cloud.
c. The cross section for elastic collisions is $\sigma = 10^{-12}\,\mathrm{cm}^2$. How many times do atoms meet in the middle of the trap?

3.4.0.6 Ex: TOP trap

The TOP trap (time-orbiting potential) was the first design to allow for Bose-Einstein condensation in 1995. It consists of the superposition of a quadrupolar magnetic field, with the radial and axial gradients $2\partial_r \mathcal{B}_{qua} = \partial_z \mathcal{B}_{qua}$), and a homogeneous magnetic field $\mathcal{B}_{top}$ rotating in the symmetry plane of the quadrupole field. Atoms which oscillate with an amplitude beyond a given radius r_d, called the 'circle of death', undergo Majorana transitions and are expelled from the trap. Calculate the radius of the death circle.

3.4.0.7 Ex: Harmonic trap

Calculate the vibration frequencies of ^{87}Rb atoms trapped in a harmonic trap, when the atoms are in the $|F = 1, m_F = -1\rangle$ hyperfine level of the ground state.

3.4.0.8 Ex: Gravitational sag in a trap

Consider (a) a quadrupolar trap and (b) an isotropic harmonic trap. What is the gradient, respectively the curvature of the trapping potential required to suspend a cloud of rubidium subject to gravitation? What is the sag of the cloud in the potential due to gravitation?

3.4.0.9 Ex: Adiabatic potentials

An *adiabatic potential* can be used to create more complicated trapping potentials [32]. To study these potentials we consider a system of two Zeeman states $m = \frac{1}{2}$ coupled by a radiofrequency radiation $\hbar\omega$. The dressed states Hamiltonian of our two-level system is a 2×2 matrix,

$$\hat{H} = \begin{pmatrix} \frac{1}{2}\mu_B \mathcal{B} - \frac{1}{2}\hbar\omega & \frac{1}{2}\hbar\Omega \\ \frac{1}{2}\hbar\Omega & -\frac{1}{2}\mu_B \mathcal{B} + \frac{1}{2}\hbar\omega \end{pmatrix},$$

defining the energetic zero in the middle between the states. Now, assume that the magnetic field grows linearly along the axis z, $\mathcal{B}(z) = z\partial_z \mathcal{B}$, where $\partial_z \mathcal{B}$ is the gradient. Also assume that the radiofrequency is tuned in resonance with the difference of the energies of the Zeeman states at some distance z_0 such that, $\hbar\omega = \mu_B z_0 \partial_z \mathcal{B}$.
a. Calculate the eigenenergies of the coupled system as a function of z.
b. Expands eigenenergies around the position z_0.
c. What would be the oscillation frequency of the trapped atoms inside the adiabatic potential?
d. Expands the eigenenergies in $\hbar\Omega$ for locations away from resonance.

3.4.0.10 Ex: Radiation pressure

Calculate the radiation pressure force exerted on a strontium atom by a laser beam in plane wave geometry ($I = 10\,\mathrm{mW/cm^2}$) tuned 50 MHz below the resonance at 461 nm ($\Gamma/2\pi = 30.5\,\mathrm{MHz}$).

3.5 Further reading

H.J. Metcalf, P. van der Straten, Graduate Texts in Contemporary Physics, Springer (1999), *Laser Cooling and Trapping* [http]

Ch.J. Foot, (Oxford Master Series in Atomic, Optical and Laser Physics, 2005), *Atomic physics* [http]

A. Ashkin, *Trapping of atoms by resonance radiation pressure* [DOI]

T.W. Hänsch et al., *Cooling of Gases by Laser Radiation* [DOI]

G. Vandegrift, *The Moessbauer effect explained* [DOI]

D.J. Wineland et al, *Laser Cooling of Atoms* [DOI]

Chapter 4

Manipulation of atomic gases

We learned in Lecture 3 that electromagnetic fields and radiation exert various types of forces on atoms, e.g. magnetic fields interacting with paramagnetic atoms or light fields accelerating atoms via photonic recoil. These forces can be harnessed for applications in cooling and trapping atoms, and the field of research dealing with the technical control of the motion of atoms is called *atom optics*. Indeed, at high velocities with no external forces, the atoms follow straight paths, similar to light beams in *classical optics*. At low speeds, they propagate as waves, similarly to wave optics in Maxwell's theory of *electrodynamics*. The term *atom optics* emphasizes the analogy and the duality in the behavior of microscopic particles.

In a laser, light particles are forced to oscillate synchronously, that is, coherently. By analogy, we can raise the question whether a similar phenomenon can occur with massive particles, and whether it is possible to construct an *atom laser*. Such a device would emit coherent matter waves just as the laser emits coherent light. When a gas is cooled to very low temperatures, the Broglie waves of the atoms become very long and, if the gas is sufficiently dense, eventually overlap. If the gas consists of a single species of bosonic particles with all atoms being in the same quantum state, their Broglie waves interfere constructively thus and form a huge wave of coherent matter. This matter wave is described by a single wavefunction exhibiting long range order and having a single phase. If this wavefunction is formed inside a trap, all atoms accumulate in its ground state. Thus, we obtain a pure quantum state of many bodies in the kinetic degree of freedom, while the internal excitation occurs on a very different energy scale, where the corresponding degree freedom is frozen and does not influence the atomic motion. The transition of a gas from individual atoms to a degenerate mesoscopic many-body quantum state occurs as a phase transition named *Bose-Einstein condensation* (BEC) as a homage to Bose

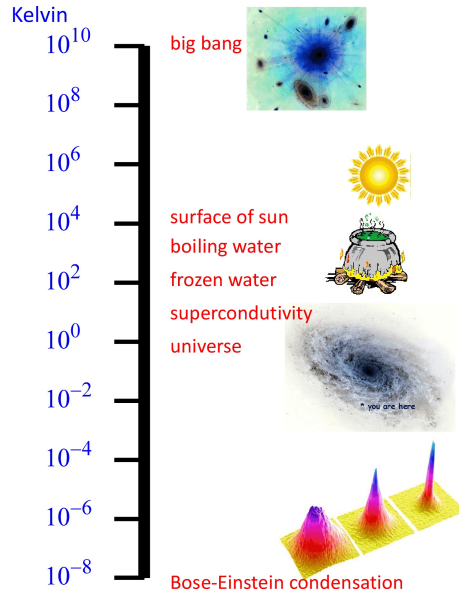

Figure 4.1: Temperature scale.

and Einstein who predicted the effect already in 1924 [16, 53].

The experimental verification of Bose and Einstein's prediction was for a long time a cherished dream of many physicists. On the one hand, several phenomena have been related to BEC in the past, for example, the phenomenon of superfluidity in liquid helium and superconductivity. On the other hand, these strongly interacting systems are not pure enough to clearly identify the role of BEC. In 1995, however, Bose-Einstein condensation of weakly interacting confined atomic gases was achieved in several laboratories [2, 42, 18, 75]. This success gave rise to a revolution in atom optics documented in an enormous amount of theoretical and experimental work [1].

In this lecture, after some introductory words on the motion of atoms in Sec. 4.1, we will present some optical cooling techniques in Sec. 4.2 and some trapping techniques using light beams in Sec. 4.3. We end this lecture with a brief discussion on how to measure the density and the velocity distribution of atomic clouds in Sec. 4.5.

4.1 The atomic motion

4.1.1 The atom as a matter wave

We have already emphasized that atomic optics deals with the motion of atoms in a gas, that is, we are interested only in the external degrees of freedom of the atoms. To describe the motion of a free massive particle in one dimension, we solve the stationary Schrödinger equation with the free space Hamiltonian [2], yielding the general solution,

$$\psi(x) = Ae^{\imath kx} + Be^{-\imath kx} \qquad \text{with} \qquad k = \sqrt{\frac{2mE}{\hbar^2}} \,. \tag{4.1}$$

Note, that the wavefunctions $e^{\imath kx}$ are not quadratically integrable. On the other hand, they do not represent real physical systems. In practice, we need to consider wavepackets or specify a finite volume for the particle.

Note also that the eigenvalue spectrum of a matter wave is continuous. To warrant the interpretation of the wavefunction as a probability density we will require quadratic integrability, $\int |\psi|^2 d^3r = 1$. This means that the wavefunction can not be infinite in a finite volume, but it can be infinite in an infinitely small volume.

The description of the atomic motion by a wave equation emphasizes the fact that microscopic particles have wave properties with each atom corresponding to a velocity-dependent *de Broglie wave*,

$$\boxed{\lambda_{dB} = \frac{h}{p}} \,, \tag{4.2}$$

which describes the coherence length of the atom.

[1] See script on *Quantum mechanics* (2023), Sec. 23.
[2] See script on *Quantum mechanics* (2023), Sec. 3.1.

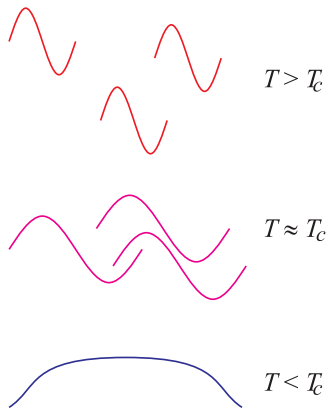

Figure 4.2: De Broglie waves at different temperatures.

4.1.2 Characteristic velocities

The behavior of an atom described by the Schrödinger equation depends very much on its kinetic energy. At high velocities (or short de Broglie waves), it will behave like a classical particle with a well-defined trajectory. At low velocities (or long de Broglie waves), it will propagate like a wave and exhibit phenomena such as diffraction and interference. Therefore, it is important to highlight some characteristic velocity regimes.

Most optical cooling techniques are based on the removal of kinetic energy upon light scattering on electronic transitions. It is, therefore, interesting to compare the kinetic energy (or temperature) of an ensemble of atoms with the width Γ of the transition. The *Doppler limit* is given by (see Exc. 4.6.0.1),

$$k_B T_D = \frac{\hbar}{2}\Gamma \ . \tag{4.3}$$

We can also compare the kinetic energy with the energy transferred to an atom by the absorption of a single photon. The *photonic recoil* energy is given by,

$$k_B T_{rec} = \frac{\hbar^2 k^2}{2m} \ . \tag{4.4}$$

Atomic clouds with temperatures around $T_D = 1..1000\,\mu\text{K}$ are called *cold*. Clouds with temperatures below $T_{rec} = 1\,\mu\text{K}$ are called *ultracold*.

In most atom optical experiments we do not work with individual atoms (or ions), but with relatively dilute ensembles of atoms, called *clouds*. In general, clouds can not be described by a single wavefunction. Either we describe every atom by a separate and independent wavefunction (which only works when the atoms do not interact), or we describe the cloud by probability distributions (such as the 'density matrix'). Let us now consider a thermal cloud. The *Maxwell-Boltzmann distribution* of velocities is,

$$g(\mathbf{v}) = \sqrt{\frac{m}{2\pi k_B T}}^3 e^{-m\mathbf{v}^2/2k_B T} \ . \tag{4.5}$$

This distribution is normalized, $\int g(\mathbf{v})d^3\mathbf{v} = \int_0^\infty 4\pi v^2 g(v)dv = 1$. Average velocity is now

$$\bar{v} = \int v g(v) dv = \sqrt{\frac{k_B T}{m}} \ . \tag{4.6}$$

We define the *thermal de Broglie wavelength* of an atomic ensemble as,

$$\boxed{\lambda_{therm} \equiv \frac{h}{m\bar{v}} = \sqrt{\frac{2\pi\hbar^2}{m k_B T}}} \ . \tag{4.7}$$

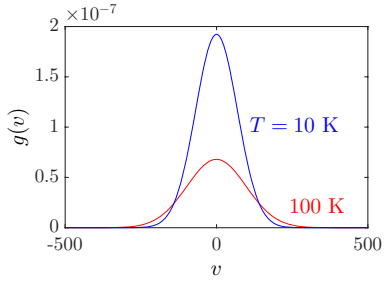

Figure 4.3: (code for download) Maxwell-Boltzmann distribution.

It represents an average over the de Broglie wavelengths of all atoms of the sample. When a dense gas is sufficiently dense, so that this quantity exceeds the average distance between atoms,

$$\rho \equiv n\lambda_{therm}^3 > 1 \ , \tag{4.8}$$

where n is the atomic density, we enter a new regime, where the *Maxwell-Boltzmann law* ceases to be valid. Since $\lambda_{therm} \propto T^{-1/2}$, this regime corresponds to low temperatures. The quantity ρ is called *phase space density*. A phase space density approaching 1 means an increased probability of finding *more than one atom per elementary phase space cell*. We then enter the regime of quantum degeneracy, where the Boltzmann statistics must be replaced by the Bose-Einstein statistics, in the case of bosons, or the Fermi-Dirac statistics, in the case of fermions [3]. From the condition $n\lambda_{therm}^3 \simeq 1$, we obtain

$$k_B T_c = \frac{1}{m}\left(\frac{2\pi\hbar}{\lambda_{therm}}\right)^2 = \frac{(2\pi\hbar)^2}{m} n^{2/3} \ . \tag{4.9}$$

4.1.2.1 Why is it difficult to make BEC?

Cooling an atomic gas to temperatures sufficiently cold for Bose-Einstein condensation is not easy! The reason is that a gas of free atoms, let's take Rb, is not in its ground state [29]. Indeed, the system could reduce its energy by going a gas of Rb_2 molecules. For pairs of atoms to stick together they would need to undergo inelastic collisions, which means that the excess energy (the distance of the bound vibrational level from the dissociation threshold) must be removed in some way. It cannot be converted into an excitation of the atomic structure (unless there is a Feshbach resonance) and it cannot be converted into kinetic energy of the molecule (this is prohibited by momentum conservation). The only way is to have the excess energy removed by a third collision partner in a three-body collision. So, if we want to maintain the atomic gas stable, we only need to keep the rate for three-body collisions low, i.e. by reducing the density.

It turns out that the maximum affordable density in the case of Rb is on the order of $10^{14}\,\mathrm{cm}^3$. Consequently, the critical temperature for Bose-Einstein condensation is, according to (4.9) on the order of a few 100 nK. Cooling to such low temperatures

[3] See script on *Quantum mechanics* (2023), Sec. 24.

are technically challenging, and various consecutive steps are necessary to reach that point.

4.2 Optical cooling

As discussed in Sec. 3.3.1, the force exerted by a light field on an atom can be of two types: a dissipative force arising called *radiation pressure*, which is often used for optical cooling purposes, and a conservative *dipolar force* which often serves for the engineering of optical trapping potentials. Both applications of optical forces will be detailed in the following sections.

4.2.1 Optical molasses

In the *Doppler cooling* model, we treat the phenomenology of optical forces quantitatively by considering the amplitude, phase and frequency of a classical field interacting with the dipole of an atomic transition in a two-level atom. From Eq. (3.63) we can write,

$$\mathbf{F}_{rp} = \hbar\mathbf{k}\Gamma\frac{\Omega^2}{4\Delta^2 + 2\Omega^2 + \Gamma^2} \ . \tag{4.10}$$

Now, if we consider an atom propagating in $+z$ direction with the velocity v_z counterpropagating to a light wave detuned by Δ from the resonance, the total detuning will be

$$\Delta \longrightarrow \Delta + kv_z \ . \tag{4.11}$$

where the term kv_z is the Doppler shift. The force F_- acting on the atom will be in the direction opposite to the motion. In general,

$$\mathbf{F}_\pm = \pm\hbar\mathbf{k}\Gamma\frac{\Omega^2}{4(\Delta \mp kv_z)^2 + 2\Omega^2 + \Gamma^2} \ . \tag{4.12}$$

Supposing now, that we have two light fields propagating in directions $\pm z$, the total force will be $\mathbf{F} = \mathbf{F}_+ + \mathbf{F}_-$. If kv_z is small compared to Γ and Δ, we find through a Taylor expansion,

$$F_z \simeq 4\hbar ks\frac{kv_z(2\Delta/\Gamma)}{[4\Delta^2 + 2\Omega^2 + \Gamma^2]^2} \equiv -\alpha_d v_z \ . \tag{4.13}$$

This expression shows that, if the detuning Δ is negative (that is, on the red side of the resonance), then the cooling force will oppose the motion and be proportional to the atomic velocity. Fig. 4.4 shows this restoring dissipative force as a function of v_z at a detuning $\Delta = -\Gamma$ with $I = I_{sat}/2$. The one-dimensional motion of the atom, subject to a restoring force which is proportional to the atomic velocity, is that of a damped harmonic oscillator. The proportionality factor,

$$\alpha_d = s\frac{-4k^2(2\Delta/\Gamma)}{4\Delta^2 + 2\Omega^2 + \Gamma^2} \tag{4.14}$$

is just the *friction coefficient*.

However, the atom will not cool down indefinitely. At some point, the Doppler cooling rate will be balanced by the heating rate coming from the momentum fluctuations of the atom absorbing and remitting photons. The *Doppler cooling limit* is given by,

$$k_B T = \hbar \frac{\Gamma}{2} \,. \tag{4.15}$$

This limit is generally, for alkaline atoms, on the order of dozens of micro-Kelvin. In the early years of cooling and trapping, the Doppler limit was thought to be a real physical barrier. But in 1988, several groups have shown that, in fact, atoms could be cooled well below the Doppler limit. The effect arises in atoms, whose ground state exhibits a hyperfine structure. We will show simplified one-dimensional models for sub-Doppler cooling in the next section.

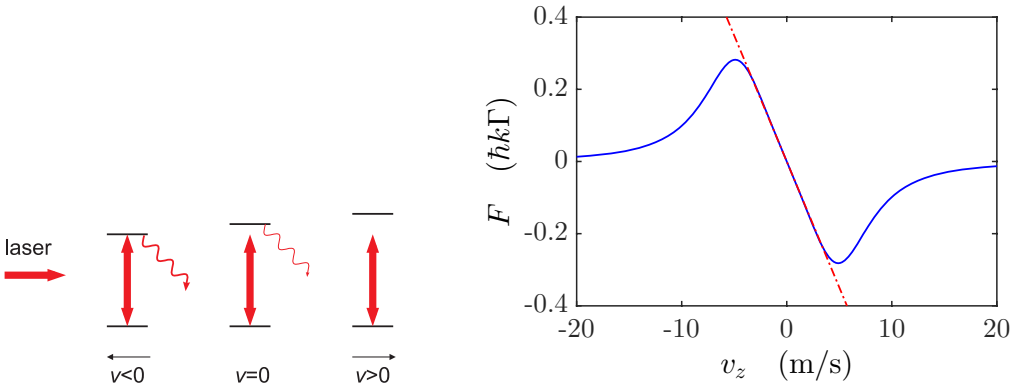

Figure 4.4: (code for download) (left) Illustration of the Doppler-shift due to atomic motion. (right) Doppler force due to one-dimensional radiative pressure as a function of atomic velocity along the z-axis for red detuning $\Delta = -\Gamma$ at a light intensity of $I = 2I_{sat}$. The blue solid line shows the exact expression for the restoring force [Eq (4.12)]. The red broken line shows the approximate linear expression of the velocity dependence according to Eq. (4.13).

Resolve the Excs. 4.6.0.2 and 4.6.0.3.

4.2.2 Sub-Doppler cooling

It turns out that atoms with a hyperfine structure in the ground state can be cooled below the Doppler limit (4.3). To explain this unexpected observation, models involving a slow motion of the atoms in polarization gradients of a standing light wave have been invoked. The phenomenon is now known as *polarization gradient cooling*.

Two principal mechanisms for cooling atoms to temperatures below the Doppler limit are based on spatial polarization gradients. These two mechanisms, however, invoke very different physical processes and are distinct by the spatial dependence of the light polarization. A key point is that these sub-Doppler mechanisms only work on atoms with multiple ground state levels. Two parameters, the friction coefficient and the capture velocity, determine the importance of these cooling processes. In this section we compare the expressions for these quantities in the sub-Doppler regime to

those found by the conventional one-dimensional Doppler cooling model for optical molasses.

4.2.2.1 Polarization and interference

In the treatment of the interaction of two-level atoms and a laser field, the discussion of the polarization has been deferred. In the case of multilevel atoms, this is no longer possible because the orientation of the dipole moment of the atoms with respect to the polarization of the light is important. Since the atoms can be in different ground states, their coupling to the light field in these states will in general be different. Another aspect is that the interference of two laser beams depends on their mutual polarization. Since the light field used in laser cooling may consist of many laser beams, their polarizations often playa key role.

A laser beam has a high degree of polarization. Although its polarization is in general elliptical, only the extreme cases of linear and circular polarization will be considered here. Because of the transverse nature of the electromagnetic field of a laser beam, the unit polarization vector $\hat{\varepsilon}$ of the field is always perpendicular to the propagation direction $\mathbf{k}$.

Consider the light field of two counterpropagating plane-wave laser beams with the same frequency ω. If the polarizations of the two laser beams are identical, then the polarization of the resulting light field is everywhere the same as that of the incoming laser beams. However, the two plane waves interfere and produce a standing wave. The resulting electric field for a linear polarization $\hat{\varepsilon}$ can be written,

$$\mathcal{E} = \mathcal{E}_0\hat{\varepsilon}\cos(\omega t - kz) + \mathcal{E}_0\cos(\omega t + kz) = 2\mathcal{E}_0\hat{\varepsilon}\cos kz\cos\omega t \ . \tag{4.16}$$

The intensity of the light field has a $\cos^2 kz$ spatial dependence with a period of $\lambda/2$. This situation of a standing wave is very common in laser cooling, and it will reappear in the discussion of optical traps and lattices.

If the polarization of the laser beams is not identical, then the situation becomes rather complicated. Only the two special cases that play important roles in laser cooling will be considered here. The first is where the two counterpropagating laser beams are both linearly polarized, but their e vectors are perpendicular (e.g. $\hat{\mathbf{e}}_x$ and $\hat{\mathbf{e}}_y$, which is called lin-perp-lin). Then the total field is the sum of the two counterpropagating beams given by,

$$\begin{aligned}\mathcal{E} &= \mathcal{E}_0\hat{\mathbf{e}}_x\cos(\omega t - kz) + \mathcal{E}_0\hat{\mathbf{e}}_y\cos(\omega t + kz) \\ &= \mathcal{E}_0\left[(\hat{\mathbf{e}}_x + \hat{\mathbf{e}}_y)\cos\omega t\cos kz + (\hat{\mathbf{e}}_x - \hat{\mathbf{e}}_y)\sin\omega t\sin kz\right] \ .\end{aligned} \tag{4.17}$$

At the origin, where $z = 0$, this becomes,

$$\mathcal{E} = \mathcal{E}_0(\hat{\mathbf{e}}_x + \hat{\mathbf{e}}_y)\cos\omega t \ . \tag{4.18}$$

which corresponds to linearly polarized light at an angle $+\pi/4$ to the x-axis. The amplitude of this field is $\sqrt{2}\mathcal{E}_0$. Similarly, for $z = \lambda/4$, where $kz = \pi/2$, the field is also linearly polarized but at an angle $-\pi/4$ to the x-axis.

Between these two points, at $z = \lambda/8$, where $kz = \lambda/4$, the total field is,

$$\vec{\mathcal{E}} = \mathcal{E}_0\left[\hat{\mathbf{e}}_x\sin(\omega t + \pi/4) + \hat{\mathbf{e}}_y\cos(\omega t + \pi/4)\right] \ . \tag{4.19}$$

Since the $\hat{\mathbf{e}}_x$ and $\hat{\mathbf{e}}_y$ components have sine and cosine dependence, they are $\pi/2$ out of phase, and so Eq. (4.19) represents circularly polarized light rotating about the z-axis in the negative sense. Similarly, at $z = 3\lambda/8$, where $kz = 3\pi/4$, the polarization is circular but in the positive sense. Thus in this lin $\perp$ lin scheme the polarization cycles from linear to circular to orthogonal linear to opposite circular in the space of only half a wavelength of light, as shown in Fig. 4.5(a). It truly has a very strong polarization gradient.

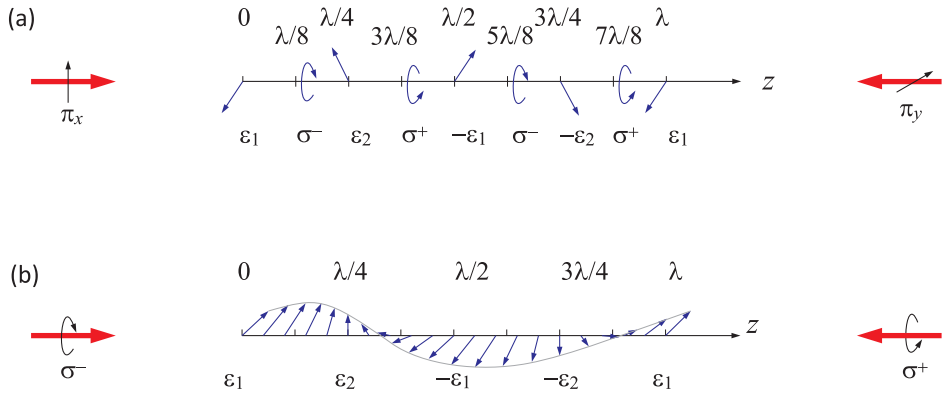

Figure 4.5: Polarization gradient field for (a) the lin$\perp$lin configuration and (b) the σ^+-σ^- configuration.

The other important polarization configuration is that of counterpropagating, oppositely circularly polarized light beams. The total electric field is,

$$\begin{aligned}\mathcal{E} &= \mathcal{E}_0\left[\hat{\mathbf{e}}_x\cos(\omega t - kz) + \hat{\mathbf{e}}_y\sin(\omega t - kz)\right] + \mathcal{E}_0\left[\hat{\mathbf{e}}_x\cos(\omega t + kz) - \hat{\mathbf{e}}_y\sin(\omega t + kz)\right] \\ &= 2\mathcal{E}_0\cos\omega t\left[\hat{\mathbf{e}}_x\cos kz + \hat{\mathbf{e}}_y\sin kz\right] \ . \end{aligned} \tag{4.20}$$

Since there is no temporal phase difference between the two polarization directions $\hat{\mathbf{e}}_x$ and $\hat{\mathbf{e}}_y$ at any position, this represents a linearly polarized field whose $\hat{\varepsilon}$ vector is fixed in time but rotates uniformly in space along z, rotating through 180° as z changes by $\lambda/2$ [see Fig. 4.5(b)]. This arrangement is called the σ^+-σ^- polarization scheme.

These two cases of lin $\perp$ lin and σ^+-σ^- polarization schemes play an important role in laser cooling. Since the coupling of the atoms to the light field depends on the polarization of the field, atoms moving in a polarization gradient will be coupled differently at different positions. Furthermore, since in a multilevel atom different states are coupled differently to the light field depending on the polarization, this will have important consequences for the laser cooling.

4.2.2.2 Lin $\perp$ lin molasses

In the first case, two counterpropagating light waves with orthogonal linear polarizations form a standing wave. This configuration is familiarly called lin-perp-lin. Fig. 4.6 illustrates the change of polarization every period of $\lambda/8$ from linear to circular to linear again, but rotated by 90°, and so on [39]. Along the same distance,

the light-atom coupling produces a periodic energy shift (light-shift) of the ground state Zeeman levels. To illustrate the cooling mechanism, we assume the simplest case, a transition $J_g = \frac{1}{2} \longrightarrow J_e = \frac{3}{2}$. As shown in Fig. 4.6 an atom moving through the region $z \simeq \lambda/8$, where the polarization is σ_-, will see its population pumped to $J_g = -\frac{1}{2}$. In addition, the Clebsch-Gordan coefficients that control the dipolar coupling of the $J_e = \frac{3}{2}$ require that the $J_g = -\frac{1}{2}$ couples to σ_- with a force three times larger than the $J_g = +\frac{1}{2}$ does. The difference of the coupling forces leads to the light-shift between the two fundamental states shown in Fig. 4.6. As the atom continues to move toward $+z$, the relative coupling forces are reversed near $3\lambda/8$, where the polarization is essentially σ_+. Thus, the relative energy levels of the two hyperfine fundamental states oscillate 'out of phase' when the atom moves through the standing wave.

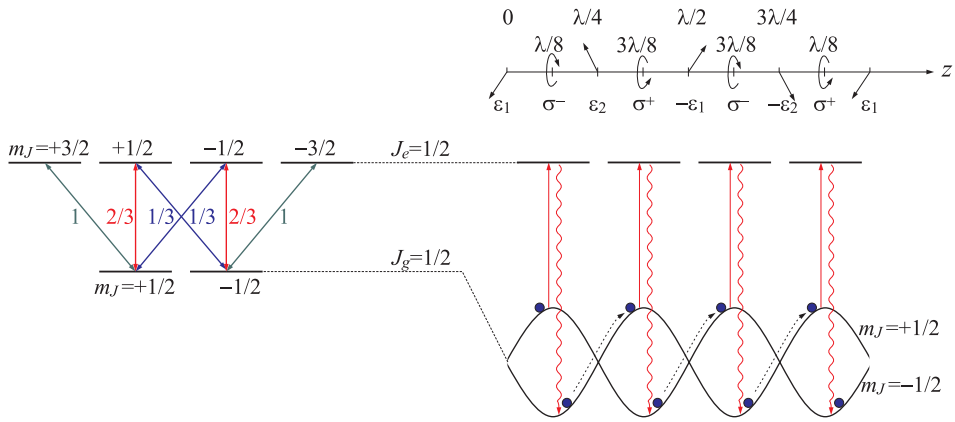

Figure 4.6: The upper line shows, how the polarization changes as a function of position (in units of a wavelength) for the 'lin-perp-lin' standing wave configuration. The figure below shows a simplified picture of the Sisyphus cooling mechanism for an atom with two levels, $J_g \leftrightarrow J_e$.

The fundamental idea is that the optical pumping rate, which always redistributes population to the lower hyperfine level, delays the light-shift of the atom moving through the field. The result is a 'Sisyphus effect', where the atom spends most of its time in sub-levels climbing a potential hill and thus converting kinetic energy into potential energy. This accumulated potential energy is subsequently dissipated by spontaneous emission to the electromagnetic modes of the vacuum. Simultaneously, the spontaneous emission transfers the population back to the lower one of two ground state levels. The lower diagram of Fig. 4.6 illustrates the phase delay of optical pumping. For this cooling mechanism to work, the optical pumping time, which is controlled by the intensity of the light, must be sufficiently slow to give the atom enough time to climb a noticeable part of the light-shift potential. This time essentially depends on the speed of the atom. As the atom is moving slowly, having previously been cooled by the Doppler mechanism, the light field must be weak in order to decrease the optical pumping rate. Interestingly, this physical picture combines the conservative dipole optical force, whose spatial integral gives rise to the mounts and valleys of the potential on which the atom moves, and the irreversible dissipation

of energy by spontaneous emission, which is necessary for any type of cooling.

We can obtain simple expressions for the friction coefficient and the capture velocity after some definitions. As in the Doppler cooling model we define the friction coefficient α_{lpl} as the proportionality constant between the force F and the atomic velocity v,

$$F = -\alpha_{lpl} v \ . \tag{4.21}$$

We assume that the light field is tuned to the red of the transition J_g - J_e,

$$\Delta = \omega - \omega_0 \ , \tag{4.22}$$

and we denote the light-shifts of the levels $J_g = \pm\frac{1}{2}$ as $\Delta_\pm$, respectively. At the position $z = \lambda/8$, we find $\Delta_- = 3\Delta_+$ and at $z = 3\lambda/8$, $\Delta_+ = 3\Delta_-$. As the applied field is tuned to red, all $\Delta_\pm$ have negative values. Now, for the cooling mechanism to be efficient, the optical pumping time τ_p should be similar to the time needed for an atom with velocity v to move from the bottom to the top of the potential, $\frac{\lambda/4}{v}$,

$$\tau_p = \frac{\lambda/4}{v} \tag{4.23}$$

or

$$\Gamma' \simeq kv \ , \tag{4.24}$$

where $\Gamma' = 1/\tau_p$ and $\lambda/4 \simeq 1/k$. Now, the energy W dissipated during a cycle of escalation and spontaneous emission is essentially the average energy difference between the light-shifted ground states, $\Delta_{ls} \equiv \Delta_+ + \Delta_-$, that is $W \simeq -\hbar\Delta_{ls}$. Therefore, the rate for energy dissipation is,

$$\frac{dW}{dt} = \Gamma'\hbar\Delta_{ls} \ . \tag{4.25}$$

At the same time, every temporal energy change of a system can always be expressed as $\frac{dW}{dt} = \mathbf{F}\cdot\mathbf{v}$. Therefore, in this one-dimensional model, considering Eq. (4.22), we can write,

$$\frac{dW}{dt} = -\alpha_{lpl} v^2 = -\Gamma'\hbar\Delta_{ls} \ , \tag{4.26}$$

such that with (4.24),

$$\alpha_{lpl} = -\frac{\Gamma'\hbar\Delta_{ls}}{v^2} \simeq -kv\frac{\hbar\Delta_{ls}}{v^2} \simeq -\frac{\hbar k^2\Delta_{ls}}{\Gamma'} \ . \tag{4.27}$$

Note that since $\Delta < 0$, α_{lpl} is a positive quantity. Also note, that for large detunings, ($\Delta \gg \Gamma$) Eq. (3.66) gives,

$$\frac{U}{\hbar} = \frac{\Delta_{ls}}{4} = \frac{\Omega^2}{4\Delta} \ . \tag{4.28}$$

It is also true that for light-shifts, which are large compared to the natural width of ground state ($\Delta_{ls} \gg \Gamma'$), and for large red detunings ($\Delta \gtrsim 4\Gamma$),

$$\frac{\Gamma}{\Gamma'} \simeq \frac{\Delta^2}{4\Omega^2} \ . \tag{4.29}$$

Therefore, the sub-Doppler friction coefficient can also be written,

$$\alpha_{lpl} = -\frac{\hbar k^2\Delta}{4\Gamma} \tag{4.30}$$

Eq. (4.30) makes two remarkable predictions: Firstly, in the 'lin-perp-lin' configuration the sub-Doppler friction coefficient can be a large number in comparison to α_d. Note that from Eq. (4.14), with $I \lesssim I_{sat}$ and $\Delta \gg \Gamma$,

$$\alpha_d \simeq \hbar k^2 \left(\frac{\Gamma}{\Delta}\right)^3 , \tag{4.31}$$

and

$$\frac{\alpha_{lpl}}{\alpha_d} \simeq \left(\frac{\Delta}{\Gamma}\right)^4 . \tag{4.32}$$

Secondly, α_{lpl} is independent of the intensity of the applied field. This last result is different from the friction coefficient, which is proportional to the field intensity up to until saturation [see Eq. (4.14)]. However, although α_{lpl} seems impressive, the range of atomic velocities where it can operate is constrained by the condition,

$$\Gamma' \simeq kv . \tag{4.33}$$

The ratio of the capture velocities for sub-Doppler versus Doppler cooling is therefore only,

$$\frac{v_{lpl}}{v_d} \simeq \frac{4\Delta_{ls}}{\Delta} . \tag{4.34}$$

Fig. 4.7 graphically illustrates the comparison between the Doppler and the 'lin-perp-lin' sub-Doppler cooling mechanisms. The dramatic difference of the capture ranges is evident. Note also that the slopes of the curves give the friction coefficients and that, within the capture range, the slope is much steeper for the sub-Doppler mechanism.

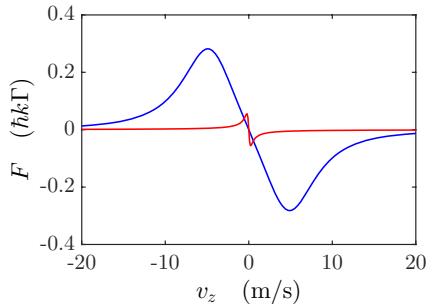

Figure 4.7: (code for download) Comparison of slopes, amplitudes, and capture ranges for Doppler and Sisyphus cooling.

σ^+-σ^- molasses exhibit sub-Doppler cooling as well, but the underlying mechanism is different [4] and will not be discussed here.

[4] See script on *Quantum mechanics* (2023), Sec. 23.2.2.2.

4.2.3 Cooling trapped particles

Other cooling techniques have been developed for confined particles, such as trapped atoms and ions [151]. As long as the oscillation frequency is so slow, that many absorption-emission cycles with the time constant Γ^{-1} can occur during one oscillation period (weak confinement), the cooling process is understood as Doppler cooling, only that a single red-detuned cooling beams suffices, because the oscillating atom periodically changes its direction. The cooling limit in this case is approximately the same as for free particles.

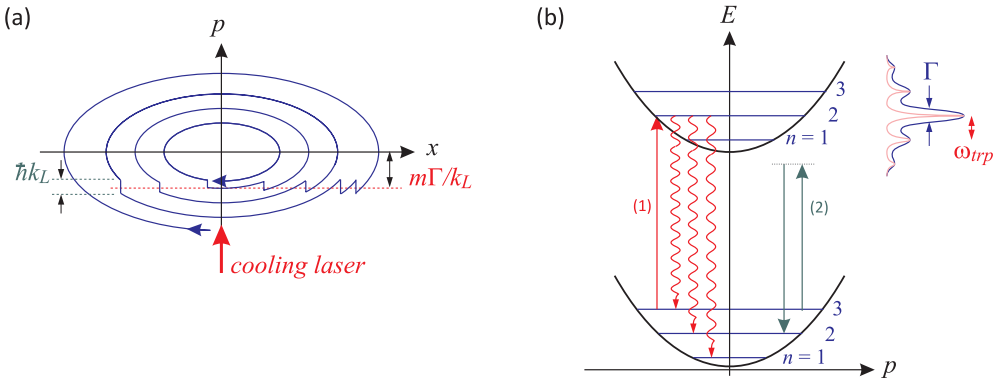

Figure 4.8: (a) Illustration of Doppler cooling of weakly trapped atoms via a shrinking of the phase-space ellipse, (b) Illustration of spontaneous (a) and stimulated (b) Raman sideband cooling of strongly trapped ions in the resolved sidebands regime.

In the case of *strong confinement*, for the description of the cooling process we must consider the quantization of the motional energy in the harmonic potential. The two levels coupled by the narrow transition split into vibrational sublevels, which are populated in thermal equilibrium according to the Boltzmann distribution.

To perform the so-called optical *Raman sideband cooling* [151] the laser is tuned to the first lower sideband. The laser light is then scattered in a Raman-Anti-Stokes process at the excited electronic state with a vibrational quantum number lower by 1. The subsequent spontaneous decay occurs most probably to the same vibrational substate of the ground state. The net effect of such a scattering process therefore is a transition to the next lower vibrational quantum number. The zero point energy of the ion in the trapping potential cannot be underscored by cooling. However, the uncertainty of the kinetic energy, and the temperature T have no lower limit [49].

4.3 Optical and magneto-optical traps

4.3.1 The magneto-optical trap

An apparently fatal obstacle to the confinement of particles by optical forces is Earnshaw's optical theorem. This theorem states that, if a force is proportional to the light intensity, its divergence must be zero because the divergence of the Poynting vector expressing the directional flux of intensity is zero inside a volume without sources nor

sinks of radiation. The absence of divergence precludes the possibility of a restoring force to the interior at all places of a closed surface [7]. However, Earnshaw's optical theorem can be bypassed by a clever trick. The internal degrees of freedom of the atom (i.e., its electronic energy levels) can change the proportionality between the force and the Poynting vector in a position-dependent manner, such that the optical Earnshaw's theorem does not apply. Spatial confinement is then possible using the radiative pressure force generated by counterpropagating light beams. The most common trap configuration is based on a radial magnetic field gradient produced by a quadrupolar field and three pairs of counterpropagating circularly polarized laser beams tuned to the red of an atomic transition and intersecting at right angles at the point where the field is zero. This *magneto-optical trap* (*MOT*) uses the position-dependent Zeeman shift of the electronic levels as the atom moves in the radially increasing magnetic field. The use of circularly polarized light which is red-detuned by about Γ results in a spatially varying transition probability, whose effect is to produce a restoring force that pulls the atom back to the origin.

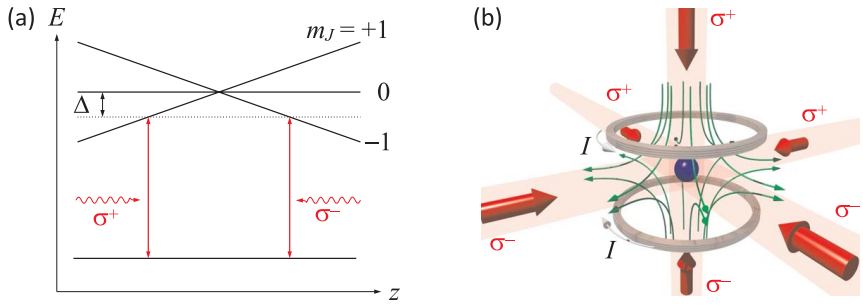

Figure 4.9: (left) Diagram of the energy level shift in an MOT, when an atom moves out of the center of the trap. A restoring force is observed around the indicated resonance positions. (right) Scheme of a typical MOT set up showing the six laser beams and the current-carrying coils in anti-Helmholtz configuration producing the quadrupolar magnetic field.

To understand better how the trapping scheme works, we consider a two-level atom with a transition $J = 0 \to J = 1$ moving along the z-direction. We apply a magnetic field $B(z)$ growing linearly with the distance from the origin. The Zeeman shifts of the electronic levels depend on the position,

$$\frac{\Delta E_{zeem}}{\hbar} = \frac{\mu_B g_F m_F}{\hbar} \frac{d\mathcal{B}}{dz} z \equiv z \partial_z \omega_{zeem} \ , \tag{4.35}$$

see Fig. 4.9. We also apply counterpropagating laser beams along the directions $\pm z$ with circular polarizations of opposite signs and tuned to the red of the atomic transition. It is clear from Fig. 4.9 that an atom moving in $\pm z$ direction will scatter $\sigma_\mp$ type photons at a faster rate than $\sigma_\pm$ type photons, because the Zeeman effect will pull the $\Delta m_J = \mp 1$ transition closer to the laser frequency. The expression for the radiation pressure force extends Eq. (4.12) to include the Doppler effect kv_z and the Zeeman effect,

$$F_{\pm z} = -\hbar k \Gamma \frac{\Omega^2}{4(\Delta \pm k v_z \pm z \partial_z \omega_{zeem})^2 + 2\Omega^2 + \Gamma^2} \ . \tag{4.36}$$

The atom will, therefore, feel a restoring force which pushes it back to the origin. If the laser beams are red-detuned by an amount $\Delta = -\Gamma$, the Doppler shift of the atomic motion adda velocity-depending term to the restoring force, such that for small displacements and velocities the total restoring force can be expressed by the sum of a term which is linear in the velocity and a term which is linear in the displacement,

$$F_{MOT} = F_{1z} + F_{2z} = -\alpha\dot{z} - \kappa z \ . \tag{4.37}$$

From Eq. (4.37) we can derive the equation of motion of a damped harmonic oscillator with mass m,

$$\ddot{z} + \frac{2\alpha}{m}\dot{z} + \frac{\kappa}{m}z = 0 \ . \tag{4.38}$$

The damping constant α and the spring constant κ can be written compactly in terms of atomic parameters and the field as,

$$\kappa = \frac{16\hbar k\Gamma\Omega^2\Delta\partial_z\omega_{zeem}}{4\Delta^2 + 2\cdot 6\Omega^2 + \Gamma^2} \ . \tag{4.39}$$

and

$$\alpha = \kappa\frac{k}{\partial_z\omega_{zeem}} \ . \tag{4.40}$$

Typical conditions for MOT are $\Omega = \Gamma/2$, $\Delta = -\Gamma$. For typical MOTs,

$$\alpha \simeq 2\cdot 10^{-22}\,\mathrm{Ns/m} \qquad \text{and} \qquad \kappa \simeq 3.7\cdot 10^{-19}\,\mathrm{N/m} \ . \tag{4.41}$$

We can also estimate the curvature of the MOT,

$$\omega = \sqrt{\frac{\kappa}{m}} \simeq (2\pi)\cdot 200\,\mathrm{Hz} \ . \tag{4.42}$$

Solve Exc. 4.6.0.4.

MOTs are realized with current-carrying coils in anti-Helmholtz configuration which generates a quadrupolar geometry potential. Near the center, the magnetic field and its absolute value are well approximated by,

$$\vec{\mathcal{B}} = q\begin{pmatrix} x \\ y \\ -2z \end{pmatrix} \qquad \text{and} \qquad |\vec{\mathcal{E}}| = q\mathcal{B}\sqrt{r^2 + 4z^2} \ , \tag{4.43}$$

with $r^2 = x^2 + y^2$ and the gradient $q \equiv \partial_r\mathcal{B}$ is a constant, which depends only on the geometry of the coils and the current in them. Thus, the extension of the above results to three dimensions is simple if we consider the fact that the gradient of the quadrupolar field in the z-direction is twice the gradient in the radial directions x and y, such that $\kappa_z = 2\kappa_x = 2\kappa_y$.The damping term, which proportional to the velocity, implies that the kinetic energy E is dissipated from the atom (or a cloud of atoms) as,

$$E/E_0 = e^{-2\alpha t/m} \ , \tag{4.44}$$

where m is the atomic mass and E_0 the kinetic energy at the beginning of the cooling process. Therefore, the dissipative force term cools the atomic cloud and, at the same

time, combines with the position-dependent term to confine it. The time constant for the damping,

$$\tau = \frac{m}{2\alpha} \tag{4.45}$$

is typically dozens of microseconds. It is important to keep in mind that a MOT is anisotropic, since the restoring force is proportional to the anisotropic field gradients. Because of its dissipative non-conservative nature, it is is more accurate to characterize a MOT by the maximum capture rate, rather than by a 'potential depth'.

In early experiments MOTs were loaded from a decelerated atomic beam. Later it was shown, that the low-velocity tail of the Maxwell-Boltzmann distribution provides a sufficient amount of atoms that can be captured by a MOT, so that it can be loaded directly from an atomic vapor at room temperature. Now many groups in the world use these assemblies for applications ranging from precision spectroscopy to the optical control of reactive collisions; the MOT has become the working horse of atom optics. Solve Exc. 4.6.0.4.

Figure 4.10: Picture of a strontium MOT operated at 461 nm. The atomic cloud, which consists of about 10^6 atoms at 10 mK temperature is visible as a diffuse spot located inside a three-mirror ring cavity (courtesy: Camila Beli and Michelle Moreno).

4.3.1.1 Density in a MOT

A typical MOT captures up to a billion atoms in a volume of a few $1\,\mathrm{mm}^3$ resulting in densities of $\sim 10^{10}\,\mathrm{cm}^{-3}$. Although a MOT works as a versatile and robust 'reaction cell' for many applications, the frequencies of the light beams must be tuned close to atomic transitions, which bears the disadvantage that a considerable fraction of atoms remains in excited states. This fact is at the origin of two processes limiting the density of a MOT: (1) losses of trapped atoms by collisions and (2) repulsive forces between the atoms caused by reabsorption of photons scattered within the cloud. Collisional losses arise from two sources: (i) hot atoms of the residual gas inside the chamber can elastically collide with cold atoms and kick them out of the MOT, and (ii) cold atoms in excited states can undergo inelastic binary collisions. 'Photon-induced repulsion' or *radiation trapping* arises when a trapped atom spontaneously emits a photon, which is then reabsorbed by other atoms. If the optical density of the cloud is high, it can take a long time for the photon to find its way out [5]. Since any photon exchange between two atoms will increase their relative momentum by $2\hbar k$, this leads to a repulsive force, which is proportional to the absorption cross section for the incident light beam. When this repulsive force balances the confining force exerted by the MOT, any increase in the number of trapped atoms augments its size, but its density. This effect is called *radiation trapping*.

Some techniques such as the *dark spontaneous force optical trap* (dark SPOT) have been developed to overcome radiation trapping by pumping the atoms into dark states,

[5] E.g. a photon at the center of the sun will take thousands of years to get out.

where they sit most of the time sheltered from the laser light and only reappearing once in a while to receive a cooling kick. Dark SPOTs have been able to increase the density of a trapped cloud by almost *two orders* of magnitude.

4.3.2 Optical dipole traps

When temporal variations are to be applied to a confinement potential, magnetic fields are not the best choice, because they are slow and of limited spatial resolution. On the other side, laser beams can be varied quickly and in localized well. The dipole force exerted by a far-detuned laser beam can be derived from the gradient of the Rabi frequency $\mathbf{F} = -\nabla(\mathbf{d}\cdot\vec{\mathcal{E}})$. Hence, it can be derived from an optical potential, which can be used for trapping. The force may be attractive (toward the intensity maximum) or repulsive.

Compared to MOTs, optical traps (*far off-resonance optical trap*, FORT) are tuned far away from resonances, where the population in excited states is insignificant and spontaneous forces are absent. Note from Eq. (3.64), that spontaneous forces fall off with the square of the detuning while the potential derived from the dipolar force only decreases linearly with the detuning. The off-resonant optical density is negligible, so that radiation trapping is not an issue. The most simple FORT consists of a single focussed, linearly polarized gaussian laser beam tuned far to the red of an atomic resonance. For large detunings and strong field gradients the Eqs. (3.66) and Eqs. (3.67) become [71],

$$\boxed{U(\mathbf{r}) \simeq \frac{\hbar\Omega(\mathbf{r})^2}{4\Delta} = \frac{3\pi c^2}{2\omega_0^3}\frac{\Gamma}{\Delta}I(\mathbf{r}) \qquad \text{and} \qquad \hbar\gamma_{sct}(\mathbf{r}) \simeq \sigma_a(\Delta)\frac{I(\mathbf{r})}{\omega} = \frac{3\pi c^2}{2\omega_0^3}\left(\frac{\Gamma}{\Delta}\right)^2 I(\mathbf{r})}, \tag{4.46}$$

using the Rabi frequency $\hbar\Omega = d_{12}\mathcal{E}$, the dipole moment $d = \sqrt{3\pi\varepsilon_0\hbar\Gamma/k^3}$, and the intensity $I = \frac{\varepsilon_0}{2}c|\mathcal{E}|^2$. This shows that the potential becomes directly proportional to the light intensity and inversely proportional to the detuning. Therefore, at large detuning but very high intensity, the depth of the FORT can be maintained, although the atoms do not absorb photons. Important advantages of FORTs as compared to MOTs are: (1) high densities ($\sim 10^{12}\,\mathrm{cm}^{-3}$) and (2) a well-defined polarization axis along which the atoms can be aligned or oriented (polarization of the spins).

Since lasers beams can easily be manipulated in position, intensity, and frequency, they can realize a large wide variety of possible geometries. For example, with a focused laser beam, one may influence the local density of a condensate and stir it around by moving the position of the laser beam. Strongly focussed laser beams are often used for transporting or manipulating microscopic objects in arrangements called *optical tweezer*s. And with standing light waves, it is possible to form periodic optical lattices in one, two or three dimensions [6].

4.3.2.1 Spin relaxation

When the atomic ground state has a hyperfine structure, another relaxation mechanism cam be observed: Near-resonance Raman scattering can induce transitions

[6] See script on *Quantum mechanics* (2023), Sec. 26.4.2.

between hyperfine states causing a population redistribution of between Zeeman substates called *spin relaxation*. In magnetic traps, this can lead to losses, because not all Zeeman substates are trapped.

The rate of an arbitrary scattering process starting from an initial state $|F, m\rangle$ through several possible excited states $|F'_j, m'_j\rangle$ to a final state $|F''m''\rangle$ is, according to the formula of Kramers-Heisenberg [110],

$$\gamma_{Fm\to F'm'} \propto \left| \sum_j \frac{\alpha^{(F'_j m'_j)}_{Fm\to F'm'}}{\Delta_{F'_j m'_j}} \right|^2 . \tag{4.47}$$

Far from resonance the scattering decreases as Δ^2 for Rayleigh scattering, $Fm = F'm'$. Raman scattering, $Fm \neq F'm'$, is further suppressed by destructive interference of the different scattering paths.

In the case of rubidium, we calculate,

$$\gamma_{spin} = \frac{3c^2\omega^4}{8\pi}\frac{70}{81}\Gamma^2 \left| \left(\frac{1}{\omega_{D1}}\right)^3 \frac{1}{\Delta_{D1}} - \left(\frac{1}{\omega_{D2}}\right)^3 \frac{1}{\Delta_{D2}} \right|^2 \frac{I_0}{\hbar\omega} . \tag{4.48}$$

4.3.2.2 Potential generated by a Gaussian beam

The *far-off resonance optical trap* (FORT) is an example of an optical trap based on dipole forces [71] (see also Excs. 4.6.0.5 and 4.6.0.6). The intensity distribution of a Gaussian beam with a diameter of w_0 at its waist is [7],

$$I(\mathbf{r}) = \frac{2P}{\pi w_0^2} e^{(-2x^2-2y^2)/w_0^2} e^{-z^2/z_R^2} , \tag{4.49}$$

where P is the total power of the beam and $z_R \equiv \pi w_0^2/\lambda_{dip}$ the *Rayleigh length* at a given wavelength λ_{dip}. The dipolar potential is given by (4.46). Using the potential depth,

$$\boxed{U_0 \equiv \frac{3\pi c^2}{2\omega_0^3}\frac{\Gamma}{\Delta}\frac{2P}{\pi w_0^2} < 0} , \tag{4.50}$$

we can approach the potential near its center, that is, near the optical axis, $r \ll \frac{1}{2}w_0$, and within the range of the Rayleigh length, $z \ll \pi w_0^2/\lambda$, by a harmonic potential [8],

$$\begin{aligned} U(\mathbf{r}) &\simeq U_0 e^{(-2x^2-2y^2)/w_0^2} e^{-z^2/z_R^2} \simeq U_0 \left(1 - \frac{2x^2+2y^2}{w_0^2} - \frac{z^2}{z_R^2}\right) \\ &\equiv U_0 + \frac{m}{2}\omega_r^2 r^2 + \frac{m}{2}\omega_z^2 z^2 \equiv k_B T \left(\frac{U_0}{k_B T} + \frac{r^2}{2\bar{r}^2} + \frac{z^2}{2\bar{z}^2}\right) . \end{aligned} \tag{4.51}$$

[7] See script on *Electrodynamics* (2023).

[8] The diameter of a Gaussian beam can be characterized in several ways,

$$\bar{r}_{1/\sqrt{e}\text{-radius}} = \frac{\bar{r}_{1/e^2\text{-radius}}}{\sqrt{2}} = \sqrt{2}\,\bar{r}_{1/e^2\text{-radius}} = \frac{\bar{r}_{1/2\text{-radius}}}{2\ln 2} ,$$

and $\bar{r}_{\text{-rms}} \equiv \bar{r}_{1/\sqrt{e}\text{-diam}}$ and $\bar{r}_{\text{-hwhm}} \equiv \bar{r}_{1/2\text{-diam}}$ and $\bar{r}_{\text{-diam}} = 2\bar{r}_{\text{-radius}}$.

This leads to the equivalences,

$$\boxed{\begin{array}{rclcrcl} \omega_r & = & \frac{2}{w_0}\sqrt{\frac{U_0}{m}} & \text{and} & \omega_z & = & \frac{\sqrt{2}}{z_R}\sqrt{\frac{U_0}{m}} \\ \bar{r} & = & \frac{w_0}{2}\sqrt{\frac{k_B T}{U_0}} & \text{and} & \bar{z} & = & \frac{z_R}{\sqrt{2}}\sqrt{\frac{k_B T}{U_0}} \end{array}} \ . \tag{4.52}$$

Example 9 (*Dipole trap for rubidium*): The formulas (4.46) hold for a two-level system. In case of the $D1$- and $D2$-lines of rubidium, we must consider all contributions weighted by the respective detunings,

$$U_0 \equiv \sigma_0 \frac{\hbar\Gamma}{4}\left(\frac{1}{\Delta_{D1}} + \frac{g_{D2}/g_{D1}}{\Delta_{D2}}\right)\frac{I_0}{\hbar\omega} \simeq \frac{3\hbar\pi c^2}{2\omega^2}\frac{\Gamma}{\Delta}\frac{I_0}{\hbar\omega} \ ,$$

where $g_{D2}/g_{D1} = 2$.
Similarly, the spontaneous emission rate is,

$$\gamma_{sct} \simeq \frac{\pi c^2 \Gamma^2}{2\omega^2}\left(\frac{1}{\Delta_{D1}^2} + \frac{g_{D2}/g_{D1}}{\Delta_{D2}^2}\right)\frac{I_0}{\hbar\omega} \ .$$

The spontaneous emission rate decays faster with detuning than the potential depth. Thus, heating can be avoided by working at large detunings and providing higher laser intensities. Defining the recoil temperature by,

$$T_{rec} = \frac{\hbar^2 k^2}{k_B m} \ ,$$

the *heating rate* is [71],

$$\dot{T} = \frac{1}{3} T_{rec} \gamma_{sct} = \frac{\hbar^2 k^2}{3 m k_B} \gamma_{sct} \ .$$

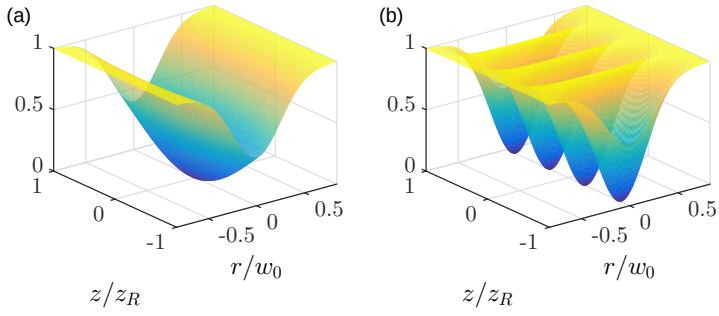

Figure 4.11: (code for download) (a) Atoms trapped in a focussed Gaussian laser beam and (b) in a standing light wave. (c) Dipole potential created by a Gaussian beam and (d) by a standing light wave.

4.3.2.3 Trapping in standing light waves

If both counterpropagating modes are pumped at different powers, $P_{\pm}$, the intensity distribution is,

$$I(\mathbf{r}) = \frac{2}{\pi w_0^2} e^{(-2x^2-2y^2)/w_0^2} e^{-z^2/z_R^2} \left| \sqrt{P_+} e^{\imath kz} + \sqrt{P_-} e^{-\imath kz} \right|^2 . \tag{4.53}$$

The potential depth is,

$$\boxed{U_0 = \frac{3\pi c^2}{2\omega_0^3} \frac{\Gamma}{\Delta} \frac{2(\sqrt{P_+} + \sqrt{P_-})^2}{\pi w_0^2} < 0} . \tag{4.54}$$

Therefore, within the Rayleigh length, the potential is,

$$U(\mathbf{r}) \simeq U_0 e^{(-2x^2-2y^2)/w_0^2} \frac{P_+ + P_- + 2\sqrt{P_+ P_-} \cos kz}{P_+ + P_- + 2\sqrt{P_+ P_-}} . \tag{4.55}$$

Letting the powers be equal,

$$\begin{aligned} U(\mathbf{r}) &\overset{P_+ = P_-}{\longrightarrow} U_0 e^{(-2x^2-2y^2)/w_0^2} \sin^2 \tfrac{kz}{2} \\ &\overset{r \ll w_0, kz \ll 1}{\longrightarrow} U_0 \left(1 - \tfrac{2x^2+2y^2}{w_0^2} - \tfrac{k^2 z^2}{4}\right) . \end{aligned} \tag{4.56}$$

This leads to the identities,

$$\boxed{\begin{array}{rclcrcl} \omega_r & = & \frac{2}{w_0}\sqrt{\frac{U_0}{m}} & \text{and} & \omega_z & = & k\sqrt{\frac{U_0}{2m}} \\ \bar{r} & = & \frac{w_0}{2}\sqrt{\frac{k_B T}{U_0}} & \text{and} & \bar{z} & = & \frac{\sqrt{2}}{k} \end{array}} . \tag{4.57}$$

4.4 Radiative coupling and evaporative cooling

As we saw in the last section, optical cooling becomes ineffective when the density of the gas is high. Hence, we need another dissipation mechanism to cool trapped atoms. A method called *evaporation* has been proposed by Hess [82] for spin-polarized hydrogen (H↑) and was observed by Masuhara et al. [106]. Later, evaporation was used on alkali metals [1, 119, 41]. A detailed review of the subject was published by Ketterle and van Druten [93].

Another collision-based cooling mechanism is *sympathetic cooling*. The technique was originally used in ion traps. Later it was applied to neutral atoms confined in magnetic traps. The idea is to get the cloud under study into thermal contact with a cold buffer gas. In some cases, the buffer gas may be optically or evaporatively cooled. Sympathetic cooling has been used in magnetic traps to create double condensates [114] and to cool fermions until the regime of quantum degeneracy [45].

4.4.1 Evaporative cooling

Evaporation always occurs when energetic particles abandon a system with finite bonding energy, removing more than their share of average energy per particle. Here,

we consider the case of a finite-sized trapping potential, that is, the potential has an edge or a beak through which hot atoms, with sufficient kinetic energy to reach that region, may leave the trap. In the ideal case, this will lead to a complete truncation of the hot tail of the equilibrium Maxwell-Boltzmann velocity distribution. If the remaining system finds back to thermal equilibrium, it will do at a lower temperature. The redistribution of kinetic energy between atoms leading to *thermalization* occurs through elastic collisions.

4.4.1.1 Truncating the Boltzmann distribution

Let us first explain how the truncation leads to colder temperatures.

The objective is to calculate the *Boltzmann distribution* in a particular trap for a given atom number N and temperature T. The first step is to obtain the *density-of-states*. For an isotropic harmonic trap $\varepsilon = \frac{p^2}{2m} + V(r)$ with $V(r) = \frac{m}{2}\omega^2 r^2$, it is,

$$\eta(\varepsilon)d\varepsilon = \frac{1}{(2\pi)^3}\int_V d^3r d^3k = \frac{2\pi(2m)^{3/2}}{h^3}\int_V \sqrt{\varepsilon - V(r)}d^3r d\varepsilon = \frac{\varepsilon^2 d\varepsilon}{2(\hbar\omega)^3} \ . \tag{4.58}$$

The atom density is,

$$n(\varepsilon) = e^{(\mu-\varepsilon)/k_BT} = Ze^{-\varepsilon/k_BT} \ , \tag{4.59}$$

where μ is the *chemical potential* and Z the *fugacity*. From these expression we obtain the atom number,

$$N = \int_0^\infty n(\varepsilon)\eta(\varepsilon)d\varepsilon = \int_0^\infty e^{(\mu-\varepsilon)/k_BT}\frac{\varepsilon^2}{2(\hbar\omega)^3}d\varepsilon = Z\frac{(k_BT)^3}{(\hbar\omega)^3} \ , \tag{4.60}$$

which we may now use this to calibrate the fugacity via

$$Z = N\frac{(\hbar\omega)^3}{(k_BT)^3} \ , \tag{4.61}$$

which finally allows us to calculate the total energy,

$$E = \int_0^\infty \varepsilon n(\varepsilon)\eta(\varepsilon)d\varepsilon = \int_0^\infty \varepsilon e^{(\mu-\varepsilon)/k_BT}\frac{\varepsilon^2}{2(\hbar\omega)^3}d\varepsilon = 3Z\frac{(k_BT)^4}{(\hbar\omega)^3} = 3Nk_BT \ . \tag{4.62}$$

The evaporation consists in truncating the distribution function $n(\varepsilon)$ at some energy $\hbar\omega_{rf}$. We get with $\beta \equiv (k_BT)^{-1}$,

$$\tilde{N} = \int_0^{\hbar\omega_{rf}} n(\varepsilon)\eta(\varepsilon)d\varepsilon = N\left(1 - \frac{2 + 2\beta\hbar\omega_{rf} + (\beta\hbar\omega_{rf})^2}{2e^{\beta\hbar\omega_{rf}}}\right) \tag{4.63}$$

and

$$\tilde{E} = \int_0^{\hbar\omega_{rf}} \varepsilon n(\varepsilon)\eta(\varepsilon)d\varepsilon = E\left(1 - \frac{6 + 6\beta\hbar\omega_{rf} + 3(\beta\hbar\omega_{rf})^2 + (\beta\hbar\omega_{rf})^3}{6e^{\beta\hbar\omega_{rf}}}\right) \ . \tag{4.64}$$

As the truncation removes the hottest atoms from the cloud, we loose atom number and energy. Assuming the existence of some rethermalization mechanism, we may

now use the new values for N and T to calculate the new equilibrium Boltzmann distribution starting all over from Eq. (4.59),

$$N \longleftarrow \tilde{N} \quad \text{and} \quad T \longleftarrow \frac{\tilde{E}}{3Nk_B} \tag{4.65}$$

Repeating this over and over the temperature will gradually reduce. The cooling process can be speed up by readjusting the truncation frequency to the actual temperature. This is called forced evaporation (see Fig. 4.12).

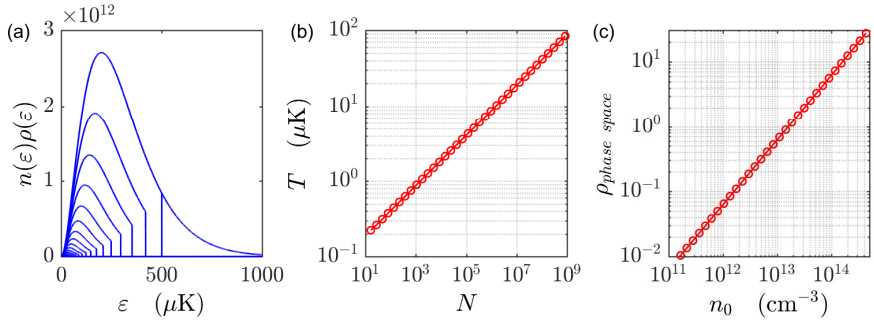

Figure 4.12: (code for download) (a) Forced evaporation by truncating the Boltzmann distribution over and over again. (b) Evolution of the temperature and (c) of the phase space density with number of remaining atoms.

4.4.1.2 Rethermalization

As already mentioned, rethermalization occurs due to elastic collisions. Numerical Monte-Carlo simulations have shown [112, 153], that it needs more or less three collisions per atom to rethermalize a cloud. Therefore, the collision rate determines the speed of the evaporation process. A large collision rate is desirable to keep the evaporation process faster than trap loss processes. Evaporation ramps between several seconds and a minute are typical.

The maximum rate of elastic collisions between trapped atoms (in the trap center) is,

$$\gamma_{coll} = n_0 \sigma_{el} \bar{v} \sqrt{2} \propto \rho^3 N^{2/3} \ , \tag{4.66}$$

where n_0 is the peak density,

$$\sigma_{el} = 8\pi a_s^2 \ , \tag{4.67}$$

is the cross-section for elastic collisions and, $\bar{v}$ being the average thermal velocity of the cloud, $\sqrt{2}\bar{v}$ is the average relative velocity between two of its atoms [92]. This formula gives the average collision rate at the *center of the cloud*, where the density is highest. To calculate the total collision rate, we need to integrate over the entire volume of the cloud,

$$\bar{\gamma}_{coll} = \tfrac{1}{N} \int \gamma_{coll}(\mathbf{r}) n(\mathbf{r}) d^3r = \frac{\int \sigma_{el} \bar{v} n^2(\mathbf{r}) d^3r}{\int n(\mathbf{r}) d^3r} \ . \tag{4.68}$$

For harmonic potential we find an average rate reduced by $2\sqrt{2}$, for linear potentials by 8. We verify this in Exc. 4.6.0.7. Finally, the rate for collision events is two times smaller, as it involves two atoms at a time. In Exc. 4.6.0.8 we show that the collision rate can be manipulated by (de-)compressing the trapping potential.

Obviously, the evaporation process slows down when the cloud cools more, unless the edge of the potential is lowered, such that the hotter atoms of the colder cloud can be evaporated. By continually lowering the edge of the potential, while the atomic cloud keeps on rethermalizing (this procedure is called *forced evaporation*) very low temperatures in the nano-Kelvin regime can be achieved, and the phase space density can be increased by many orders of magnitude (between a MOT and a BEC there are 6 orders of magnitude) up to the threshold of Bose-Einstein condensation. Of course, this is only possible by sacrificing many hot atoms. Even with a well optimized evaporation ramp (i.e. a controlled lowering of the potential edge), usually only some 0.1% of the atoms reach the condensation phase after about 500 collisions per atom.

Two aspects should be mentioned regarding the optimization of the evaporation ramp. The first aspect is, that elastic collisions with atoms from the residual background vapor of the vacuum chamber limit the lifetime of the trap. Therefore, the evaporation must be sufficiently fast, which requires either a high rate of elastic collisions or a good vacuum. A compromise must be found between a slow but efficient evaporative cooling and a minimization of the losses, which come into play when the evaporation takes too long. The second aspect is, that the dimensionality of the evaporation surface determines the effectiveness of the cooling. In the first demonstration of evaporation, H↑ atoms of a hot cloud were ejected over a saddle point. The saddle was located a small region away from the trap center, and only atoms with sufficient kinetic energy *along a certain direction*, $E_z > U_{edge}$, could leave the trap. In such cases, evaporation is called one-dimensional. Even though ergodic redistribution due to anharmonicities of the potential will drive, sooner or later, all the atoms to this region, this effect becomes less pronounced when the cloud cools down, because the atoms accumulate at the bottom of the approximately harmonic (and therefore separable) potential. This fact has inhibited efficient evaporation of H↑ below 120 μK [60].

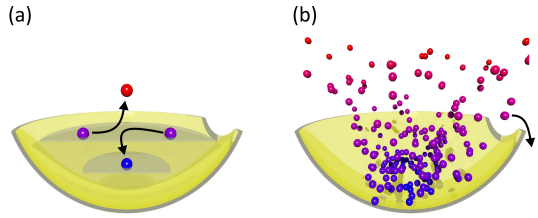

Figure 4.13: Principle of (a) rethermalization due to elastic collisions and (b) evaporation.

4.4.1.3 Radiative coupling of internal state

The most successful evaporation technique implemented so far is based on a radiative coupling of confined and free states. We discuss this technique in the following sections. See ([30], Sec. 3.1.4) for an overview.

The radiative coupling technique originates from an idea proposed by Pritchard et al. [76], who have already had some experience with radiofrequency spectroscopy in magnetically trapped neutral atoms [104, 80]. The spatial dependence of the Zeeman splitting is an intrinsic feature of magnetic traps. Irradiation of a radio wave at a

certain frequency couples trapped and untrapped Zeeman substates at a well-defined distance from the trap center. This gives rise to a 3D evaporation surface, where the passing atoms can undergo Landau-Zener transitions and be expelled from the trap. The technical advantages of this technique are substantial: The magnetic trapping potential does not have to be manipulated, for example, by the creation of a nozzle, and the potential edges can be easily controlled by the radiofrequency. If evaporation is forced via a continuous reduction of the radiofrequency and if the evaporation ramp is optimized, the density will increase as well as the collision rate. Rethermalization will accelerate and initiate a self-accelerated evaporation process (*run-away evaporation*). Rf-evaporation was first demonstrated by Ketterle and colleagues [41].

4.4.1.4 Adiabatic and diabatic limits of rf-induced evaporation

Rf-induced evaporation can be described within the formalism of the dressed atom [26], where the different states m_F of an atom with spin F are coupled to an rf-field [9], which we assume to be linearly polarized:

$$\vec{\mathcal{B}}(t) = \mathcal{B}\hat{\mathbf{e}}_{rf} \cos\omega t \ . \tag{4.69}$$

The element of the coupling matrix between the levels, $|F, m_F\rangle$ and $|F, m_F \pm 1\rangle$ is,

$$\Omega = \frac{\mu_B g}{4\hbar} \left|\vec{\mathcal{B}}_{rf} \times \hat{\mathbf{e}}_B\right| \sqrt{F(F+1) - m_F(m_F+1)} \ , \tag{4.70}$$

where g is the atomic g-factor and $\hat{e}_B$ the orientation of the local static magnetic field.

The adiabatic potentials $U(r)$ are obtained through the eigenvalues of the atomic states dressed by the local magnetic field $\mathcal{B}(r)$. In the dressed atom picture, we consider the total energy of the atom plus the field of N radiofrequency photons. Without coupling, this simply means that $N\hbar\omega$ is added to the atomic Zeeman energies, resulting in a Zeeman pattern being vertically shifted by $N\hbar\omega$ for $N = 0, \pm 1, ...$ At positions where the rf-field is in resonance, curves with $\Delta N = 1$ intersect. Here, the coupling develops an *avoided crossing*, which determines the pattern of adiabatic energy levels [see Fig. 4.15(b)].

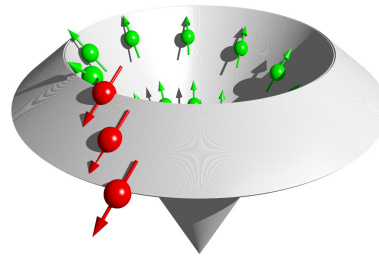

Figure 4.14: Illustration of evaporative truncation.

A slowly moving atom remains on the curve of an *adiabatic potential*. As an example, let us assume an atom in the hyperfine state $|F, F\rangle$ moving away from the center of the trap. When it comes close to resonance, the rf-field blends this state with other m_F-states, from the $|F, F-1\rangle$ down to the $|F, -F\rangle$ state, which changes the slope of the potential curve. Beyond the resonance point, the atomic state is adiabatically transformed into an untrapped high-field seeking state, and the atom is repelled from the trap. Thus, while passing the avoided crossing, the atom has emitted $2F$ rf-photons in a stimulated manner and inverted the orientation of both the electron and the nuclear spin.

[9] Alternatively, a *microwave* frequency may be used to couple *different hyperfine levels*.

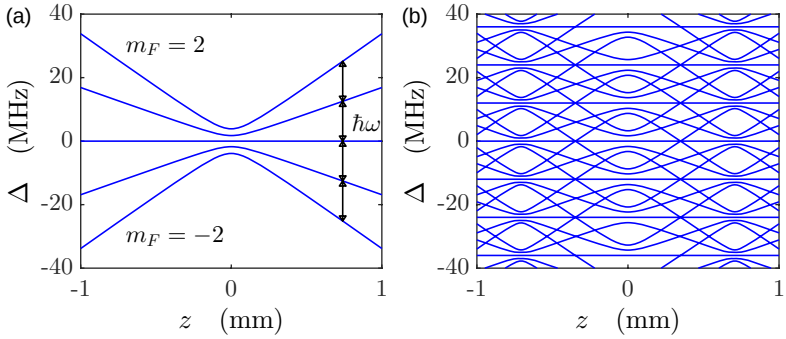

Figure 4.15: (code for download) (left) Potentials due to the Zeeman structure of an atom in the ground state with $F = 1$. (right) Adiabatic potentials resulting from the coupling of Zeeman levels via radiofrequency radiation being resonant with the difference of Zeeman levels at the position 0.7.

In this way the radiofrequency generates an adiabatic potential surface with a depth of approximately $|m_F|\hbar(\omega - \omega_0)$, where ω_0 is the resonant rf-frequency at the center of the trap. The evaporation process corresponds, then, to the removal of the most energetic atoms out of the trap.

For this adiabatic picture to be valid, an adiabaticity condition must be fulfilled. This condition requires that the energy difference at the avoided crossover be larger than the energy uncertainty related to the limited time that an atom with velocity v spends in the resonance region. For a two-level system coupled by a matrix element V_{12} and an atom moving with velocity v along the z-axis, the transition probability P between the adiabatic curves is given by the *Landau-Zener formula* [130],

$$P = 1 - e^{-\xi} \quad \text{with} \quad \xi = \frac{2\pi|V_{12}|^2}{\hbar g \mu_B \partial_z \mathcal{B} v} \,. \tag{4.71}$$

The Landau-Zener theory is strictly valid only for a two-level system, which we use here only for a qualitative discussion of two following limiting cases.

For a weak rf-field, $\xi \ll 1$, P is much smaller than 1, i.e. the atoms remain predominantly on the diabatic surface shown in Fig. 4.15(a). The probability for a *spin flip* transition is, $P \approx t$, which describes the diabatic limit of rf-induced evaporative cooling: The atomic energy levels are almost unperturbed, the atoms often spill across the resonance surface, and only after $1/P$ oscillations, they spin-flip from the hyperfine state $|F, F\rangle$ to the $|F, F-1\rangle$.

The adiabatic limit is clearly the ideal situation for evaporative cooling. However, the evaporation process in a trap (with oscillation time T_{osc}) saturates at a lower rf-power. The condition for saturation is $P \approx T_{osc}/\tau_{el}$, where τ_{el} is the average time between two collisions. This means that an energetic atom is evaporated before it collides again.

Only the component of the magnetic field of the rf-radiation which is *perpendicular* to the magnetic trapping field induces spin-flips. In certain geometries of the confinement potential, for example the quadrupole trap, the magnetic field covers the entire solid angle. Consequently, there are two points where the trapping field and

the rf-field are parallel and the elements of the transition matrix consequently zero. Within an area around these points, the coupling is diabatic. In practice however, the rf-transition can be sufficiently saturated that this area is small and does not strongly affect the evaporation efficiency.

Note also that gravitation deforms the equipotential surfaces of the confinement potential, which can reduce the evaporation efficiency [92]. Solve Exc. 4.6.0.9.

4.4.2 Sympathetic cooling

The efficiency of evaporative cooling depends on the rate of interatomic collisions. However, there are atomic species with unfavorable, that is, small or even negative scattering lengths. Also, while at low temperatures only s-wave collisions occur (higher partial waves being frozen behind the centrifugal barrier), such collisions are prohibited for fermionic gases. Fermions or species with unfavorable scattering lengths can not be cooled by evaporation. There is, however, another technique called *sympathetic cooling* by thermal contact with another species. The additional species is, in general, actively cooled (e.g. by evaporation), while the species of interest is passively cooled via elastic collisions with atoms of the additional species. Of course, for this scheme to work the *interspecies scattering length* and the mass ratio must be adequate to ensure adequate thermal coupling.

Following [113] the transfer of kinetic energy between two colliding atoms is reduced by a factor depending on the their mass difference,

$$\xi = \frac{4m_1m_2}{(m_1+m_2)^2} \ . \tag{4.72}$$

Around $3/\xi$ collisions per atom on average are required for complete thermalization of a gas. For example, for the Rb-Li mixture, we have $3/\xi = 12.4$. The collision rate is,

$$\Gamma_{coll} = \sigma_{12}\bar{v} \int n_1(\mathbf{r})n_2(\mathbf{r})d^3r \ , \tag{4.73}$$

where the average thermal velocity is,

$$\bar{v} = \sqrt{\frac{8k_B}{\pi}\left(\frac{T_1}{m_1}+\frac{T_2}{m_2}\right)} \ . \tag{4.74}$$

The instantaneous temperature is calculated by,

$$\gamma_{therm} = -\frac{1}{\Delta T}\frac{d\Delta T}{dt} \ , \tag{4.75}$$

or via simulations: $\Delta T(t+dt) = \Delta T(t) - \Delta T(t)\gamma_{therm}dt$. Following [44] the rethermalization rate is connected to the collision rate via,

$$\gamma_{therm} = \frac{\xi}{3}\left(\frac{\Delta E_{1\to2}}{N_1k_B\Delta T}+\frac{\Delta E_{2\to1}}{N_2k_B\Delta T}\right) = \frac{\xi}{3}\left(\frac{\Gamma_{coll}}{N_1}+\frac{\Gamma_{coll}}{N_2}\right) \ . \tag{4.76}$$

4.5 Analysing techniques

To analyze the kinetic state of an atomic gas and, for example, to identify the presence of a Bose-Einstein condensate, it is necessary to measure its spatial or momentum distributions. However, the only way to gather information from the atoms is to throw some kind of particles into them and to detect, where these particles are scattered. The most suitable particle to penetrate an ultra-high vacuum chamber surely is the *photon*. Therefore, apart from few exceptions where electron beams are used, all information on ultra-cold gases has been obtained so far through their reactions to incident laser beams [84, 22, 3, 88, 68].

4.5.1 Time-of-flight imaging

The most common imaging techniques measure the absorption of a laser beam by an atomic cloud after a *time-of-flight* or the dispersion of a laser beam induced by trapped cloud. The amplitude $\mathcal{E}_0$ of a light wave traversing an atomic cloud of diameter L and characterized by the refractive index η is modified by a factor $e^{\imath\omega L\eta/c}$. For an inhomogeneous cloud, we have,

$$\mathcal{E} = \mathcal{E}_0 e^{\imath\omega L/c} \exp\left(\imath\frac{\omega}{c}\int_{-\infty}^{\infty}(\eta(\mathbf{r})-1)dz\right) . \tag{4.77}$$

We can approximate the refractive index by the atomic susceptibility,

$$\eta = \sqrt{1+\chi} \approx 1+\frac{1}{2}\chi \qquad \text{with} \qquad \chi = -\frac{4\pi n(\mathbf{r})}{k^3(2\Delta/\Gamma+\imath)} , \tag{4.78}$$

where $n(\mathbf{r})$ is the density distribution of the cloud. The imaginary part of the susceptibility is related to the *absorption coefficient* α and the real part to the *dispersion coefficient* δ,

$$\mathfrak{Im}\ \chi = \frac{\alpha}{\omega/c} \qquad \text{and} \qquad \mathfrak{Re}\ \chi = \frac{2\delta}{\omega/c} . \tag{4.79}$$

Now, the absorption and dispersion coefficients can be related to the optical cross-section $\sigma(\Delta)$ defined in (3.64) [103], where Δ is the detuning of light frequency from an atomic resonance, whose linewidth is Γ. This result is called the *optical theorem*,

$$\alpha = n\sigma(\Delta) \qquad \text{and} \qquad \delta = n\sigma(\Delta)\frac{\Delta}{\Gamma} . \tag{4.80}$$

Finally, we obtain the *Lambert-Beer law*,

$$\mathcal{E} = \mathcal{E}_0 e^{\imath\omega L/c} \exp\left[\imath\sigma(\Delta)\left(\frac{\imath}{2}-\frac{\Delta}{\Gamma}\right)\int_{-\infty}^{\infty} n(\mathbf{r})dz\right] \equiv E_0 e^{\imath\omega L/c} e^{-b/2} e^{\imath\varphi} . \tag{4.81}$$

For the intensity, $I \propto |\mathcal{E}|^2$, we get,

$$\frac{I}{I_0} = \exp\left[-\sigma\int_{-\infty}^{\infty} n(\mathbf{r})dz\right] \equiv e^{-b} . \tag{4.82}$$

The *absorption* b describes the loss of intensity for the laser beam due to scattering by the (disordered) atoms. It is strong near resonance, but diminished quadratically

with the detuning Δ. The scattering is necessarily accompanied by radiation pressure accelerating and heating the atoms. The *dispersion* φ describes the refraction of the laser beam by the atomic density distribution (which for this purpose can be considered as continuous) [31, 59]. It disappears in resonance and diminishes slowly with increased detuning ($\propto \Delta$). It is connected to the dipole force and, thus, does not heat the atomic cloud. The coefficient φ describes the phase shift of the electromagnetic wave transmitted through the atomic cloud.

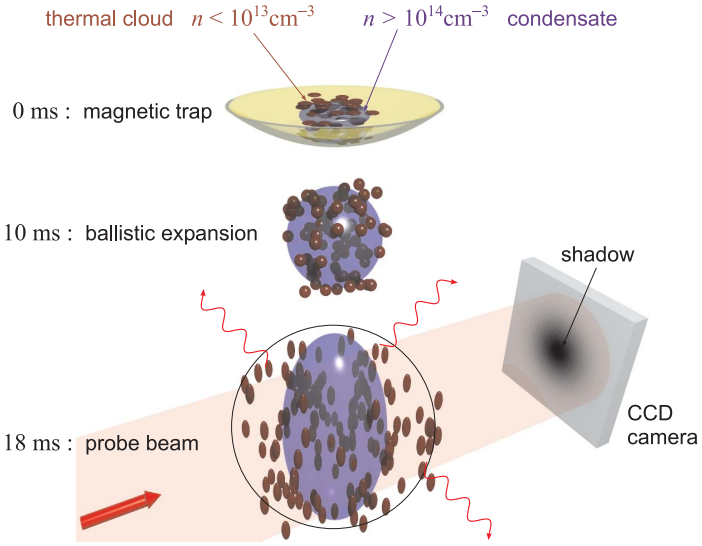

Figure 4.16: Sequence of a typical time-of-flight experiment: As soon as the trapping potential is suddenly switched off, the atomic cloud ballistically expands for 18 ms, before it is illuminated by a short resonant laser pulse. The shadow printed by the cloud onto the beam is photographed by a CCD camera.

4.5.2 Absorption imaging

Let us now detail the experimental process of *absorption imaging* (see Fig. 4.16): The trap confining the atomic cloud is suddenly turned off, thus letting the atoms, accelerated by the Earth's gravitation, fall for a flight time of a few ms. Then a pulse of a resonant laser light, whose diameter is much larger than the size of the cloud, is irradiated. The local attenuation of the beam intensity $I \sim |\mathcal{E}|^2$ can be related through the absorption b (also called *optical density* or *optical depth*) to the atomic density via,

$$-\ln \frac{I(x,y)}{I_0} = b(x,y) = \sigma(\Delta) \int n(\mathbf{r}) dz \ . \tag{4.83}$$

The shadow printed by the atomic cloud on the transverse profile of the laser beam is recorded by a CCD camera.

We have already noted that the absorption is accompanied by radiative pressure. After some scattering events, due to the photonic recoil, the atoms have accumulated a sufficiently large velocity, and therefore a sufficiently large Doppler shift, to be

out of resonance with the laser beam. Subsequent photons are no longer scattered by the atoms and only contribute to increase the illumination of the CCD camera without carrying any information about the presence of atoms. Consequently, it is advantageous to use very short laser pulses. In addition, the intensity of the laser beam should not saturate the transition in order to guarantee an optical cross-section, which is independent of the intensity, and hence to guarantee the validity of the Lambert-Beer law. Finally, the laser frequency must be tuned perfectly to resonance, $\Delta = 0$. Otherwise, the interaction between the laser beam and the atomic cloud becomes partially dispersive, which leads to a focusing or defocusing of the laser beam by refraction and a distortion of the image making it impossible to estimate the size of the cloud. See Exc. 4.6.0.10.

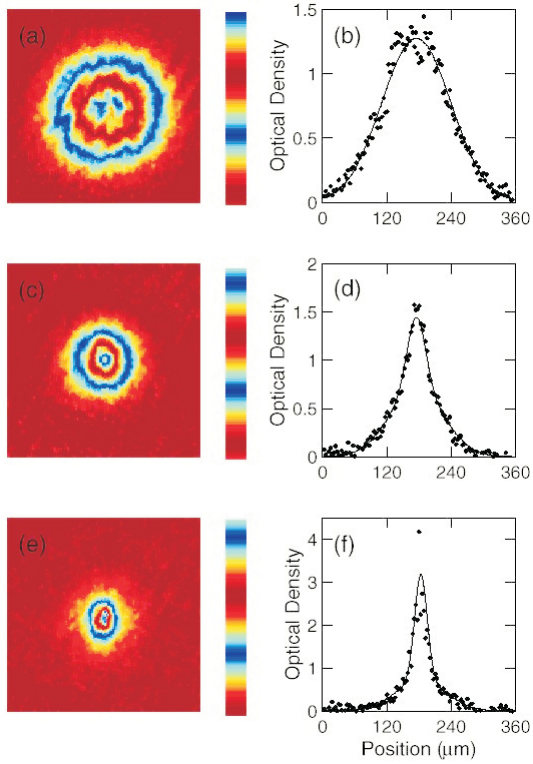

Figure 4.17: Absorption images after a time-of-flight allow to identify the presence of a Bose-condensate through its characteristic momentum distribution. Shown are images (a,b) above, (c,d) slightly below, and (e,f) well below the critical temperature for a Bose-Einstein phase transition (figures from [75]).

Fig. 4.17 shows examples of absorption images of an atomic cloud taken at different stages of the evaporation process. Fig. 4.17(a,b) was taken at a temperature of 320 nK; the cloud is large and isotropic and therefore purely thermal. At 250 nK [see Fig. 4.17(c,d)] an elliptically shaped part appears in the center of the thermal cloud. And at 180 nK [see Fig. 4.17(e,f)] the thermal cloud almost completely disappeared for the benefit of the condensate. Solve Exc. 4.6.0.11.

4.5.3 Dispersive imaging

The absorption imaging technique is destructive, because of the involved ballistic expansion and also because of the radiative pressure exerted by the resonant imaging beam, which accelerates and heats the atomic cloud. That is, the measurement process messes up the distributions of the cloud, such that a second image taken after the first one will give different results. However, there is a non-destructive imaging technique called *dispersive imaging* or *phase contrast imaging*. In this technique, the laser light is tuned sufficiently far from resonance, $|\Delta| \gg \Gamma$, for spontaneous emission and heating induced by random photonic recoil to be negligible [3]. This permits to take a series of consecutive images and create a *movie* of the temporal evolution of the cloud. Another advantage of this technique is the low off-resonant optical density, which allows to take pictures of very dense clouds *in situ*, that is, *while they are confined in a trap*.

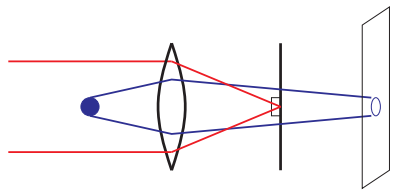

Figure 4.18: Scheme for dispersive images.

The physical quantity which is measured by this method is the local phase shift of the wavefront of the probe laser. Wavefront distortions are difficult to measure. To transform the phase profile into an intensity profile, a method known from classical optics called *Schlieren method* is used. It is based on the interference of the probe beam with its distorted wavefront and a reference plane wave. In practice, there are several possibilities. For *dark-ground imaging*, the part of the incident beam not having interacted with the atoms is blocked behind the interaction zone (see Fig. 4.18)

$$\begin{aligned} \bar{I}_{dg} = \tfrac{1}{2}|\mathcal{E} - \mathcal{E}_0|^2 = I_0 \left| e^{-b/2+\imath\varphi} - 1 \right|^2 \\ \xrightarrow{b\to 0} I_0\varphi^2 = I_0 b \frac{\Delta^2}{\Gamma^2} \ . \end{aligned} \tag{4.84}$$

The intensity signal $\bar{I}_{dg}$ is quadratic in optical density b.

For *phase contrast imaging*, the part of the beam not having interacted with the atoms receives a phase shift of $\lambda/4$ with respect to the part of the beam having interacted with the atoms:

$$\begin{aligned} \bar{I}_{pc} = \tfrac{1}{2}|\mathcal{E} - \mathcal{E}_0 + \mathcal{E}_0 e^{\pm\imath\pi/2}|^2 = I_0 \left| e^{-b/2+\imath\varphi} - 1 + e^{\pm\imath\pi/2} \right|^2 \\ \xrightarrow{b\to 0} I_0(\pm 1 + \varphi)^2 \simeq I_0 \left(1 \pm b\frac{\Delta}{\Gamma} \right) \ . \end{aligned} \tag{4.85}$$

The intensity $\bar{I}_{pc}$ is linear in b and, consequently, more sensitive to weak signals. Finally, a third technique, called *polarization contrast imaging*, detects the local birefringence of the atomic cloud [17].

The imaging techniques shown so far only allow to visualize the instantaneous density distribution of the atomic cloud $n(\mathbf{r})$. If we are interested in other quantities, we have to conceive the experiment in such a way, that the desired information leaves its signatures in the density distribution. For example, to measure the excitation frequencies of a condensate, which can perturb its shape and observe the subsequent time evolution of $n(\mathbf{r}, t)$ via dispersive imaging [90, 108, 4, 94].

4.5.4 Refraction of atoms by light and of light by atoms

Non-resonant light acts on the external degrees of freedom of atoms by a *phase shift of the Broglie wave*, $\exp\left[\imath\hbar^{-1}\int U(\mathbf{r},t)dt\right]$, and simultaneously on the internal degrees of freedom by a *dynamic Stark shift* or *light shift* of the energy levels by the value of $U(\mathbf{r})$. The Bloch vector defined by,

$$\vec{\rho} \equiv \begin{pmatrix} \frac{1}{\sqrt{2}} a_1 a_2^* \\ \frac{1}{\sqrt{2}} a_1^* a_2 \\ |a_2|^2 - |a_1|^2 \end{pmatrix} \tag{4.86}$$

describes, under the influence of the dispersive interaction, a precession around the polar axis. This was discussed in Exc. 2.7.0.26. The Stark shift causes a rotation of $\hbar^{-1}U(\mathbf{r})t$. Simultaneously, the atom is subjected to a force, which corresponds to the gradient of the potential $-\nabla U(\mathbf{r})$, as illustrated in Fig. 4.19(a). We see that the phase shifts of the Broglie wave and the Bloch vector are equal. Finally, the light mode phase is also shifted by the same amount in an effect called *refraction*. That is, the internal, external, and optical degrees of freedom are *intertwined*.

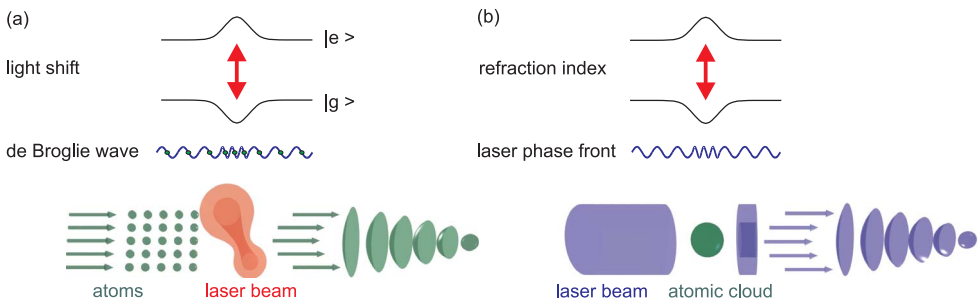

Figure 4.19: Analogy between light optics and atomic optics: (a) The de Broglie wave of atoms passing through an attractive potential is advanced. (b) The phase of a red-detuned laser beam traversing a dense atomic cloud is advanced, leading to lensing.

This fact has a practical use in atomic interferometers, because it is often easier to detect an interference of internal excitation states rather than of Broglie waves. Because of the intertwining, it is sufficient to measure *one* interference pattern to know the *other one*.

By local variations of the potential $U(\mathbf{r})$, e.g. induced by a focused laser beam, it is possible to manipulate a Broglie wavefront in the same way that, in classical optics, we manipulate the wavefront of a light beam by lenses or other objects, such

as for instance, the refractive index represented by an atomic cloud near resonance, as illustrated in Fig. 4.19(b).

The orientation of the force depends on the light frequency as compared to the resonant frequency. The dipolar force attracts the atom to regions where the light field is strong, when the frequency is tuned below ω_0, and it attracts the atom to regions of weak fields, when tuned above ω_0. Integration over the relevant spatial coordinates results in an effective potential or barrier to the atom. The qualitative behavior of the dipolar potential and its effect on the motion of atoms is easily visualized in the dressed states picture. Fig. 4.20 shows what happens when an atom enters a well defined region of an optical field, for example a focused laser beam.

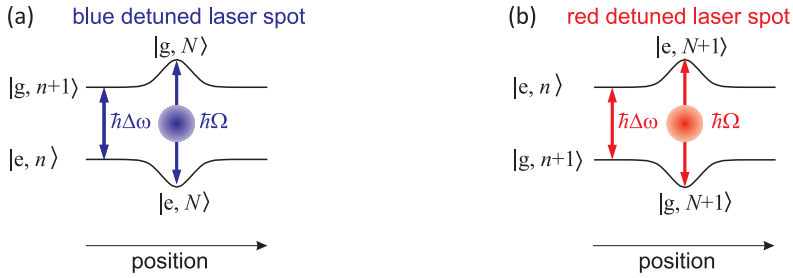

Figure 4.20: Product states and dressed states for (a) blue detuning. Note that the population is in the upper level and that the atom is subject to a repulsive weak field seeking force when it enters the laser beam. The diagram (b) is similar, but for red detuning. The population is in the lower level and the atom is subject to an attractive high field seeking force.

Outside the atom-dipole coupling zone the expression $\hbar\Omega$ is despicable and the 'dressed states' are just the atom-field product states. When the atom enters the field, this expression becomes nonzero and the atom-field states combine to produce a set of dressed states. The energy levels of the product states 'repel' each other and approach the dressed states levels. Assuming that the laser is sufficiently detuned to maintain the absorption rate negligible, the population remains in the ground state. We see that blue (red) detuning leads to a repulsive (attractive) potential for atoms remaining in the grounded state. In addition, since $\hbar\Omega$ is directly proportional to the root of the laser intensity, an increase in that intensity (optical power per unit area) obviously amplifies the force on the atom ($\mathbf{F} \simeq \nabla_R \Omega$).

4.6 Exercises

4.6.0.1 Ex: Fundamental temperature limits

Calculate the Doppler limit, the recoil limit, and the threshold to quantum degeneracy for an atomic cloud of density $n = 10^{14}\,\mathrm{cm}^{-3}$ for the sodium $D2$ transition ($\lambda = 590\,\mathrm{nm}$, $\Gamma/2\pi = 10\,\mathrm{MHz}$) and the rubidium $D2$ transition ($\lambda = 780\,\mathrm{nm}$, $\Gamma/2\pi = 6\,\mathrm{MHz}$).

4.6.0.2 Ex: Optical molasses

Optical molasses are created (in one dimension) by two beams counterpropaganting lasers tuned to red of an atomic transition. Each of the laser beams exerts on the atoms the radiative pressure force $F_{\pm} = \hbar k \frac{\Gamma}{2} \frac{s}{[2(\Delta \pm kv)/\Gamma]^2 + 1 + s}$. Δ is the detuning of the laser, ν is the velocity of an atom.
a. Show that for small velocities ($|kv| \ll \Gamma$ and $\Delta \leq \Gamma$) the optical molasses can be understood as a friction force and calculate the friction coefficient.
b. Heating processes caused by spontaneous emission limit the minimum temperature that can be reached in optical molasses. Calculate the laser tuning, where the temperature reaches its minimum value and specify the cooling limit.
Help: Suppose a one-dimensional molasses and assume, that the spontaneous emission only happens along this dimension. The heating rate follows from the scattering rate R through $\left(\frac{dE}{dt}\right)_{heat} = \frac{d}{dt}\frac{\langle p^2 \rangle}{2m} = \frac{\hbar^2 k^2}{2m} 2R$, the cooling rate follows from $\left(\frac{dE}{dt}\right)_{cool} = Fv$.

4.6.0.3 Ex: Atomic fountain

In atomic fountains atoms are accelerated upward by a 'moving optical molasses'. After the molasses has been switched off, they perform a ballistic flight in the Earth gravitational field. The moving molasses is generated by two pairs of counterpropagating laser beams intersecting at right angle and oriented both at an angle of 45° with respect to gravity. The upgoing beams are tuned to the blue, and the counterpropagating downgoing beams have the same detuning to the red side of the atomic resonance ($\lambda = 780\,\mathrm{nm}$). Supposing that the resonator is close to the position of the molasses and has with negligible length, what should be the detuning in order to achieve 1 s time period between the two passages of the atoms through the microwave resonator?

4.6.0.4 Ex: Linearization of the MOT

Derive the friction coefficient and the spring constant for a MOT.

4.6.0.5 Ex: Dipole trap with a focused beam

a. Calculate the vibration frequencies of ^{87}Rb atoms confined in an optical trap consisting of a focused laser beam with the power $P = 10\,\mathrm{W}$ and the beam diameter $w_0 = 100\,\mu\mathrm{m}$. The laser beam is tuned 5 nm to the red side of the rubidium $D1$ resonance located at $\lambda = 795\,\mathrm{nm}$.
b. Assume that the trapped atomic cloud consists of $N = 10^8$ atoms at the temperature $T = 100\,\mu\mathrm{K}$. Calculate the atomic density n_0 in the center of the cloud.
c. The cross section for elastic collisions is $\sigma = 10^{-12}\,\mathrm{cm}^2$. How many times do atoms meet on average?

4.6.0.6 Ex: Optical lattice

A laser beam with wavelength $\lambda_{dip} = 1064\,\mathrm{nm}$, power $P = 2\,\mathrm{W}$, and diameter $w_0 = 50\,\mu\mathrm{m}$ is subdivided into three retroreflected beams intersecting at right angles.

With this configuration we form a cubic optical lattice for strontium atoms, whose relevant transition lies at $\lambda_{Sr} = 461\,\text{nm}$ and has a decay width of $\Gamma_{Sr} = (2\pi)\ 32\,\text{MHz}$. Calculate the potential depth and the secular frequencies.

4.6.0.7 Ex: Mean collision rate

Assuming that the peak collision rate γ_{coll} is known, calculate the average collision rate (a) in a quadrupolar and (b) in a harmonic trap.

4.6.0.8 Ex: Adiabatic compression

How does temperature change upon adiabatic compression of (a) a quadrupole trap and (b) a harmonic trap. How do density, phase space density, and elastic collision rate vary. **Help:** Define the compression for quadrupole trap as $\eta \equiv \partial_r \mathcal{B}_{r,final}/\partial_r \mathcal{B}_{r,initial}$ and for harmonic trap as $\eta \equiv \omega_{r,final}/\omega_{r,initial}$.

4.6.0.9 Ex: Landau-Zener transitions

Consider a rubidium-88 cloud in its ground state $^2S_{1/2}, F = 1, m_F = -1$ confined in an isotropic quadrupolar potential with the gradient 200 G/cm. To initiate an efficient radiofrequency evaporation, you want atoms crossing the region where the radiofrequency couples the Zeeman states to make a transition to the untrapped Zeeman state $m_F = 0$ with 95% probability. What is the amplitude of the required magnetic field.

4.6.0.10 Ex: Lensing by cold clouds

The interaction of light with two-level atoms generates a susceptibility which gives rise to a refraction index,

$$\eta(\mathbf{r}) = \sqrt{1 - \frac{4\pi n(\mathbf{r})}{k^3(2\Delta/\Gamma + \imath)}}\ ,$$

where $n(\mathbf{r})$ is the cloud's density distribution and $\Gamma/2\pi = 30.5\,\text{MHz}$ for strontium.
a. Calculate the phase-shift suffered by a light beam crossing an ultracold atomic cloud ($N = 10^5$, $T = 1\,\mu\text{K}$) confined in an isotropic harmonic trap ($\omega_{trp} = (2\pi)\ 100\,\text{Hz}$)as a function of detuning.
b. Estimate the focal distance of the cloud for $\Delta = -\Gamma/2$.

4.6.0.11 Ex: Optical density

A cloud of $N = 10^6$ ^{87}Rb atoms is prepared in a cylindrical harmonic trap characterized by the axial vibration frequencies $\omega_z = (2\pi)\ 50\,\text{Hz}$ and the radial one $\omega_r = (2\pi)\ 200\,\text{Hz}$. The experimenter takes the absorption image after 18 ms time-of-flight, as shown in Fig. 4.17(a). A pixel of the CCD camera corresponds to 5 µm in real space.
a. At what temperature is the phase transition to Bose-Einstein condensate to be expected?
b. Determine the temperature of the sample.

c. Evaluate its density distribution.
d. Evaluate the resonant optical density for the $D2$-transition at 780 nm along the symmetry axis of the trapped cloud.

4.7 Further reading

H.J. Metcalf and P. van der Straaten, *Laser cooling and trapping* [ISBN]

S. Abend et al., *Atom-chip fountain gravimeter* [DOI]

S.C. Bell et al., *A slow atom source using a collimated effusive oven and a single-layer variable pitch coil Zeeman slower* [DOI]

Y. Castin et al., *Limit of Doppler cooling* [DOI]

R.A. Cline et al., *Spin relaxation of optically trapped atoms by light scattering* [DOI]

E.A. Cornell, *Very Cold Indeed: The Nanokelvin Physics of Bose-Einstein Condensation* [DOI]

Ph.W. Courteille et al., *Highly Versatile Atomic Micro Traps Generated by Multi-frequency Magnetic Field Modulation* [DOI]

M. Kasevich et al., *Atomic Interferometry Using Stimulated Raman Transitions* [DOI]

Y.B. Ovchinnikov et al., *A Zeeman slower based on magnetic dipoles* [DOI]

E.L. Raab et al., *Trapping of Neutral Sodium Atoms with Radiation Pressure* [DOI]

M.G. Raizen et al., *Stochastic cooling of atoms using lasers* [DOI]

D.A. Steck et al., *Rubidium 87 D Line Data* [DOI]

D.A. Steck et al., *Rubidium 85 D Line Data* [DOI]

Chapter 5

Coupling of atoms and optical cavities, collective effects

So far we have considered the coherent dynamics between atoms and radiation fields in free space, and we extended the theory to take into account the dissipative coupling to the electromagnetic vacuum by spontaneous emission and atomic motion. The vacuum represents a homogeneous and isotropic reservoir characterized by a continuous white energy spectrum. The situation changes completely when we place the atom inside an optical cavity which breaks the translational and rotational symmetries and imprints a resonance structure into the density of photonic states. Obviously, the cavity will profoundly alter the atomic coupling to the electromagnetic vacuum, and hence the way in which the atom reacts to incident light, as much with respect to light scattering as with respect to optical forces.

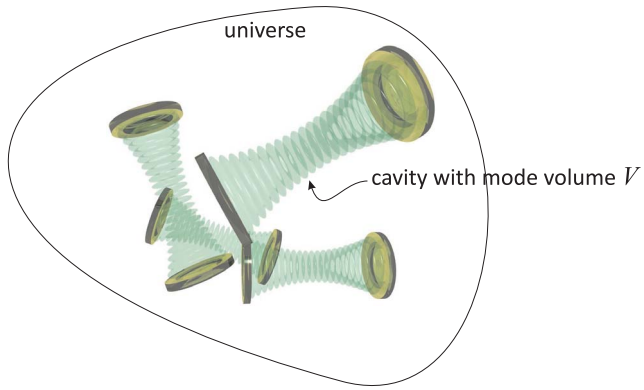

Figure 5.1: Illustration of the mode structure of empty space.

In this lecture we analyze the coupled dynamics of atoms interacting with the optical field modes of a cavity pumped by incident laser beams. We first concentrate in Sec. 5.1 on empty cavities. Then in Sec. 5.2 we turn our attention to the impact of atoms on the cavity dynamics, in particular its transmission spectrum. In Sec. 5.3 we introduce the Dicke model of light-atom interaction setting the basis for the study of collective effects within and beyond the mean-field approximation. Finally, in Secs. 5.4

and Sec. 5.5 we discuss superradiant phase transitions and collective effects induced by interatomic interactions.

5.1 Light fields in cavities without atoms

Although later on, we will consider the light field in the optical cavity as a classical entity, for reasons of consistency with later discussions we derive the equations of motion within the quantum mechanical framework. The quantization of the electromagnetic field has been introduced in Lecture 2 with the definition of the field operator $\hat{a}$ normalized to the electric field strength $\vec{\mathcal{E}}_1$ generated by a single photon, such that $|\langle\hat{a}\rangle|^2 = n$ represents the number of photons in the cavity. We will first set up the equations of motion for the cavity fields and then discuss the main quantities characterizing a cavity, such as free spectral range, mode volume, decay rate, and single-photon field strength. Finally, we will calculate the density of states of cavities.

5.1.1 Master equation

As illustrated in Fig. 5.2(a), an optical cavity isolates a single mode out of the electromagnetic vacuum, whose frequency shall be called ω_c. The corresponding Hamiltonian is then ($\hbar = 1$),

$$\hat{H}_{cavity} = \omega_c \hat{a}^\dagger \hat{a} \ . \tag{5.1}$$

If the cavity is coherently pumped by laser at a rate η, we gain another term in the Hamiltonian,

$$\hat{H}_{laser:cavity} = \imath\eta\hat{a}^\dagger + h.c. \ . \tag{5.2}$$

The laser-cavity coupling can be interpreted as beamsplitter mixing the cavity mode $\hat{a}$ with a classical laser mode $\eta \sim \langle\hat{a}_{laser}\rangle$.

Now, the modes in real cavities have limited lifetimes due to a finite transmission probability for photons through the cavity mirrors. This corresponds to an incoherent coupling between the cavity mode and entire electromagnetic spectrum outside *but collinear to* the cavity, which we will call heat bath and represent by a continuum of operators $\hat{a}_\omega$ with $[\hat{a}_\omega, \hat{a}^\dagger_{\omega'}] = \delta_{\omega,\omega'}$. In principle, we must solve the quantum Liouville equation for the total density operator $\hat{\rho}_{total} = \hat{\rho}_{cavity} \otimes \hat{\rho}_{bath}$ with all contributions to the Hamiltonian, including the coupling to the heat bath,

$$\begin{aligned} \hat{H}_{bath} &= \sum_\omega \omega \hat{a}^\dagger_\omega \hat{a}_\omega \\ \hat{H}_{cavity:bath} &= \sum_\omega g_{cavity:bath} \hat{a}^\dagger_\omega \hat{a} + h.c. \ . \end{aligned} \tag{5.3}$$

This is however impracticable, and we rather trace the over the bath's degrees of freedom [64, 27] in order to derive either a master equation for the reduced density operator $\hat{\rho}_{cavity}$ or a Heisenberg-Liouville equation for the cavity mode.

The procedure of tracing out irrelevant degrees of freedom leading to incoherence is known as the *Weisskopf-Wigner theory* [121]. Here, we only present the result for the Heisenberg-Liouville equation, which can be read as a recipe how to derive the

equations of motion for a system whose Hamiltonian is known, as well as the physical processes leading to dissipation [27],

$$\boxed{\begin{array}{l}\dot{\hat{a}} = -\imath[\hat{a}, \hat{H}_{cavity} + \hat{H}_{laser:cavity}] + \mathcal{L}^{\dagger}_{\kappa,\hat{a}}\hat{a} \\ \text{with} \quad \mathcal{L}^{\dagger}_{\kappa,\hat{L}}\hat{a} \equiv \kappa(2\hat{L}^{\dagger}\hat{a}\hat{L} - \hat{L}^{\dagger}\hat{L}\hat{a} - \hat{a}\hat{L}^{\dagger}\hat{L})\end{array}} \; . \tag{5.4}$$

The irreversible losses are described by so-called *jump operators* $\mathcal{L}$ accounting for loss processes, e.g. photon annihilation via cavity transmission described by $\hat{a}$ and occurring at a rate κ. Note, that this procedure assumes the heat bath to have $T = 0$ temperature, which is a good assumption at optical frequencies. In contrast, when microwave cavities are coupled to a heat bath, its blackbody radiation must be taken into account, as it may couple radiation into the cavity.

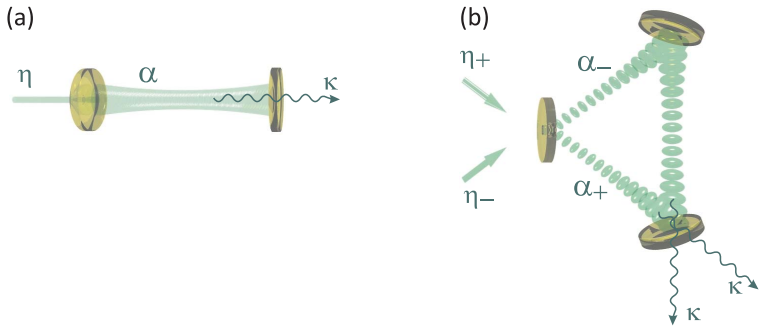

Figure 5.2: Scheme of (a) a linear cavity and (b) a ring cavity with optical modes $\alpha_{\pm}$ pumped by incident light fields $\eta_{\pm}$ and decaying into the void with rate κ.

The expectation value of Eq. (5.4) yields, after transforming into the rotating frame via $\alpha \to \alpha e^{\imath\omega t}$ with $\Delta_c \equiv \omega - \omega_c$,

$$\begin{aligned}\dot{\alpha} = \langle\dot{\hat{a}}\rangle &= \imath\langle[-\Delta_c\hat{a}^{\dagger}\hat{a} + \imath\eta(\hat{a}^{\dagger} - \hat{a}), \hat{a}]\rangle - \kappa\langle\hat{a}\rangle \\ &= (-\kappa - \imath\Delta_c)\alpha + \eta \; ,\end{aligned} \tag{5.5}$$

where we employed the usual commutation rules, $[\hat{a}, \hat{a}^{\dagger}] = 1$. The solution is easy to derive,

$$\alpha(t) = \left(\alpha(0) - \frac{\eta}{\kappa + \imath\Delta_c}\right) e^{(-\kappa - \imath\Delta_c)t} + \frac{\eta}{\kappa + \imath\Delta_c} \; . \tag{5.6}$$

The electric field in the cavity is obtained weighing the amplitude α normalized to the amplitude of the field generated by a single photon, $\vec{\mathcal{E}}^{+}_{cav} = \vec{\mathcal{E}}_1\alpha$, with the cavity mode function (e.g. a plane wave $e^{\imath kz}$in the simplest case),

$$\vec{\mathcal{E}}_{cav}(z,t) = \mathfrak{Re}\left[\vec{\mathcal{E}}_1 e^{\imath(kz-\omega t)}\alpha(t) + \vec{\mathcal{E}}_1 e^{\imath(-kz-\omega t)}\alpha(t)\right] . \tag{5.7}$$

The stationary solution of (5.5) is simply a Lorentzian,

$$|\alpha(\infty)|^2 = \frac{|\eta|^2}{\kappa^2 + \Delta_c^2} \; , \tag{5.8}$$

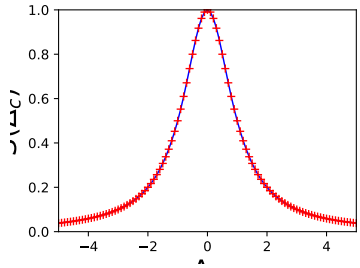

Figure 5.3: (code for download) Transmission spectrum of a cavity via numerical solution of the master equation (5.5) (solid line) and via the stationary solution (5.8) (crosses).

which represents an approximation of the Airy function.

The result (5.6) shows that, letting $\eta = 0$, the cavity field decays with the time constant κ. κ also corresponds to the HWHM of the *field intensity*, $|\alpha(|\Delta_c| = \kappa)|^2 = \frac{1}{2}|\alpha(0)|^2$. Note, that the intensity decays as 2κ, and the HWHM of the *field amplitude* is $\left|\alpha(|\Delta_c| = \sqrt{3}\kappa)\right| = \frac{1}{2}|\alpha(0)|$. We study the dynamics of laser-pumped cavities in Excs. 5.6.0.1 and 5.6.0.2.

Example 10 (*Evolution of the modes of a linear cavity*): (5.6) also shows that a cavity initially filled with a strong resonant light field $|\alpha(0)| \gg \eta/\kappa$ begins to oscillate at its own frequency ω_c, before the pump dominates and imposes its own frequency ω. This is illustrated in Fig. 5.4.

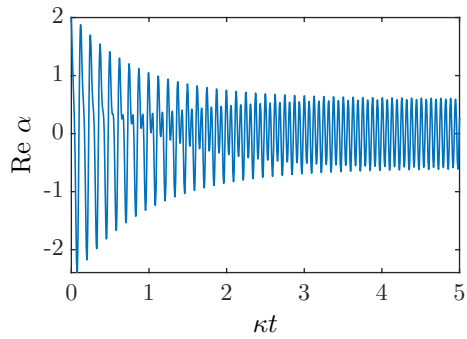

Figure 5.4: (code for download) Transient oscillations in a cavity pumped out of resonance.

Example 11 (*Dynamics of a ring cavity*): Linear cavities are characterized by the fact that they sustain standing light waves. That is, at every point of the mode volume, there are field components pointing into two counterpropagating orientations. In case of a ring cavity, we have two counterpropagating modes $\alpha_\pm$, which may be independently pumped by laser beams $\eta\pm$. Hence, the quantum Langevin equation (5.4) must be generalized to,

$$\dot{\alpha}_\pm(t) = (-\kappa - \imath\Delta_c)\alpha_\pm + \eta_\pm \ . \tag{5.9}$$

The two counterpropagating field modes will, provided they have the same polarization, interfere and form a standing light wave. In contrast to linear cavities, the phase of this standing wave is represents a degree of freedom, as it depends on the phases of the two field modes $\alpha_\pm$, which in turn can be controlled by the incident laser fields $\eta_\pm$.

5.1.2 Characterization of the bare cavity

5.1.2.1 Mode volume

We first consider a linear cavity of length L pumped by a laser without any scatterer located inside the cavity. For a cavity with a given geometry filled with a Gaussian mode of light with power P, the intensity profile is determined by Gaussian optics [1],

$$I(\mathbf{r}) = \frac{2P}{\pi w^2(z)} e^{-2\rho^2/w^2(z)} \qquad \text{and} \qquad w(z) = w_0 \sqrt{1 + \left(\frac{\lambda z}{\pi w_0^2}\right)^2} \,. \tag{5.10}$$

Defining the *mode volume* via $I(0)V_m \equiv \int I(\mathbf{r}) dV$ and evaluating the spatial integral over the Gaussian mode along the cavity, we obtain,

$$\boxed{V_m = \frac{1}{I(0)} \int_0^L \int_0^\infty \int_0^{2\pi} \frac{2P}{\pi w^2(z)} e^{-2\rho^2/w^2(z)} d\phi \rho d\rho dz = \tfrac{\pi}{2} L w_0^2} \,. \tag{5.11}$$

Defining the amplitude of the electric field generated by a *single photon* via,

$$I(\mathbf{r}) = n I_1(\mathbf{r}) = n\varepsilon_0 c |\mathcal{E}_1|^2(\mathbf{r}) \,, \tag{5.12}$$

where n is the number of photons in the cavity, we calculate for the energy stored in the cavity,

$$\tfrac{\hbar\omega}{2} = \int u_1(\mathbf{r}) dV = \tfrac{1}{c} \int I_1(\mathbf{r}) dV = \tfrac{1}{c} I_1(0) V_m \,. \tag{5.13}$$

Hence,

$$\boxed{|\vec{\mathcal{E}}_1(0)| = \sqrt{\frac{I_1(0)}{\varepsilon_0 c}} = \sqrt{\frac{\hbar\omega}{2\varepsilon_0 V_m}}} \,. \tag{5.14}$$

5.1.2.2 Resonance structure

Until now we considered the cavity only as a volume capable of containing an amount of electromagnetic energy. However, boundary conditions at the mirror surfaces only allow certain frequencies to resonate in the cavity. The cavity spectrum turns out to be an equidistant comb of eigenfrequencies $\omega = N 2\pi \delta_{fsr}$ with $N \in \mathbb{N}$ separated by,

$$\delta_{fsr} \equiv \tau_{rt}^{-1} = \frac{c}{2L} \,. \tag{5.15}$$

[1] See script on *Electrodynamics* (2023), Sec. 7.4.1 and Exc. 7.4.4.2.

Note, that the *free spectral range* δ_{fsr} is given in units of a real frequency. τ_{rt}^{-1} is the time for a photon to make a round trip in the cavity. The frequency dependence of a linear cavity is expressed by the *Airy formulas*,

$$\boxed{\mathcal{L}(\omega) \equiv \frac{I_{cav}}{I_{input}} = \frac{\sqrt{1+(2F/\pi)^2}}{1+(2F/\pi)^2 \sin^2 kL}} \,, \tag{5.16}$$

which will be derived in Exc. 5.6.0.3. The frequency ω and the optical path kL can be expressed as,

$$\omega = N2\pi\delta_{fsr} + \Delta_c \qquad \text{and} \qquad kL = \pi N + \frac{\Delta_c}{2\delta_{fsr}} \,. \tag{5.17}$$

The coefficient F is called *finesse* and depends only on the reflectivity $R = 1 - T$ of the cavity mirrors [2],

$$\frac{F}{\pi} = \frac{\sqrt{R}}{1-R} \simeq \frac{1}{T} \,, \tag{5.18}$$

where the approximation holds for high reflectivity, $\sqrt{R} \simeq 1$. From the expression (5.16) we learn, that the finesse also measures the *resonant enhancement* of the cavity, since for $\Delta_c = 0$ and $F \gg 1$ the expression yields,

$$\frac{I_{cav}}{I_{input}} = \frac{2F}{\pi} \,. \tag{5.19}$$

Near resonance the Airy function for the intensity transmission spectrum can be approximated by a Lorentzian lineshape, whose FWHM width κ_{int} is related to the finesse [3],

$$F = \frac{\delta_{fsr}}{\kappa_{int}/2\pi} \,. \tag{5.20}$$

The finesse therefore is simply the ratio between the free spectral range and the FWHM of the cavity intensity transmission curve, both measured in Hertz. Also called intensity decay rate of the cavity, κ_{int} measures the 'cavity ring-down' time τ_κ. In the following we will rather use the amplitude *decay rate of the cavity*,

$$\boxed{\kappa \equiv \frac{\kappa_{int}}{2} = \tau_\kappa^{-1} = \frac{\pi\delta_{fsr}}{F}} \,. \tag{5.21}$$

Example 12 (*Finesse of a cavity*): For example, for a linear cavity of length $L = 10\,\text{cm}$ an intensity decay time of $\tau_{int} = 20\,\mu\text{s}$ is measured, and we want to evaluate the finesse. We begin calculating the free spectral range $\delta_{fsr} = c/2L \approx 1.5\,\text{GHz}$. Since the cavity field decays like $\mathcal{E}(t) = \mathcal{E}_0 e^{-\kappa t}$ and the intensity like $I(t) = \mathcal{E}_0^2 e^{-2\kappa t}$, we get $\kappa = 1/\tau_\kappa = 1/2\tau_{int} \approx (2\pi)\,4\,\text{kHz}$. Finally, the finesse is $F = \pi\delta_{fsr}/\kappa \approx 189000$.

[2] See script on *Electrodynamics* (2023), Sec. 7.3.5.
[3] See script on *Electrodynamics* (2023), Sec. 7.3.5 and Exc. 7.3.6.16.

Now, let us assume that the cavity is resonantly pumped by a laser beam, $\Delta_c = 0$. To estimate the pump rate η, we have a look at the equation of motion (5.5). In steady-state, $\dot{\alpha} = 0$, the solution is $\alpha = \eta/\kappa$. Hence, the number n of photons inside the cavity is,

$$n = |\alpha|^2 = \frac{\eta^2}{\kappa^2} \ . \tag{5.22}$$

The light power in the linear cavity can be expressed using its free spectral range (5.15),

$$P = \frac{\pi w_0^2}{2} I(0) = \frac{V_m}{L} n I_1(0) = n \frac{c\hbar\omega}{2L} = n\delta_{fsr}\hbar\omega \ . \tag{5.23}$$

Hence, the intracavity field amplitude is resonantly amplified by the finesse,

$$\frac{\alpha}{\alpha_{input}} = \sqrt{\frac{2F}{\pi}} = \sqrt{\frac{2\delta_{fsr}}{\kappa}} \ . \tag{5.24}$$

and we may calculate the pump rate from experimental parameters,

$$\boxed{\eta = \kappa\sqrt{n} = \kappa\sqrt{\frac{P}{\delta_{fsr}\hbar\omega}} = \sqrt{\kappa_{int}\frac{P_{input}}{\hbar\omega}}} \ . \tag{5.25}$$

Neglecting losses, on resonance the injected power will be completely transmitted, $P_{output} = P_{input}$, so that the intracavity power can conveniently be inferred from transmission. In practice, however, the pump rate and the transmission will depend not only from absorption in the mirrors, but also on the quality of the phase matching of the Gaussian beams and the impedance matching.

Example 13 (*Schawlow-Townes limit of a laser*): The *Schawlow-Townes limit* results from phase fluctuation of the standing light wave in the cavity demand $\Delta\phi = \frac{1}{n}$. Using the relationships (5.23) and (5.24), we find [152],

$$\Delta\omega_{laser} = \frac{\kappa}{|\alpha|^2} = \kappa\frac{\delta_{fsr}\hbar\omega_{laser}}{P_{cav}} = \kappa\frac{\delta_{fsr}\hbar\omega_{laser}}{\frac{\delta_{fsr}}{\kappa}P_{out}} = \kappa^2\frac{\hbar\omega_{laser}}{P_{out}} \ .$$

For a typical HeNe laser, $F = 100$, $P_{out} = 1\,\mathrm{mW}$, $L = 20\,\mathrm{cm}$, we estimate,

$$\Delta\omega_{laser} = \left(\frac{\pi\delta_{fsr}}{F}\right)^2 \frac{h\nu_{laser}}{P_{out}} = \left(\frac{\pi c}{2LF}\right)^2 \frac{h\nu_{laser}}{P_{out}} \approx (2\pi)30\,\mathrm{mHz} \ .$$

5.1.2.3 Density-of-states

The density of states $\rho(\omega, \mathbf{k})$ of an optical cavity is defined by,

$$\int_{\mathcal{R}} \rho(\omega, \mathbf{k}) d\omega d\Omega = \frac{1}{(2\pi)^3} \int d^3\mathbf{x} d^3\mathbf{k} \ , \tag{5.26}$$

where $\mathcal{R}$ denotes the boundary imposed by the cavity. For free space photons we calculate,

$$4\pi \int \rho_{free}(\omega, \mathbf{k}) d\omega = \frac{V_m}{(2\pi)^3} \int k^2 \sin\theta d\theta d\phi dk = \frac{V_m k^3}{6\pi^2} = \frac{V_m \omega^3}{6\pi^2 c^3} \ , \tag{5.27}$$

such that,

$$\rho_{free}(\omega, \mathbf{k}) = \rho_{free}(\omega) = \frac{V_m \omega^2}{(2\pi c)^3} \ , \tag{5.28}$$

is isotropic.

For light in a cavity, the density of states is modified with respect to free space, because it becomes frequency-dependent and anisotropic. The frequency dependence is expressed by the Airy formula (5.16) and the anisotropy by,

$$\mathcal{R}(\hat{\mathbf{e}}_k) = 1 \qquad \forall \qquad \hat{\mathbf{e}}_k \in \Omega_{cav} \ , \tag{5.29}$$

where Ω_{cav} is the solid angle covered by the cavity mode. The formula,

$$\boxed{\rho_{cav}(\omega, \mathbf{k}) = \rho_{free}(\omega)[1 - \mathcal{R}(\hat{\mathbf{e}}_k)] + \rho_{free}(\omega)\mathcal{L}(\omega)\mathcal{R}(\hat{\mathbf{e}}_k)} \tag{5.30}$$

expresses that the density of states is nothing more than the *structure factor* of the cavity.

The modification of the density of states obviously has a strong impact on spontaneous emission. We do not have the space to derive this in detail here [78, 79] [4], but it can be shown that, with the solid angle covered by the TEM_{00} mode of the cavity,

$$\Omega_{cav} = \frac{8\pi}{k^2 w_0^2} \ , \tag{5.31}$$

the total solid angle covered by dipole radiation,

$$\Omega_{free} = \int_0^{2\pi} \int_0^{\pi} \sin^3\theta d\theta d\phi = \frac{8\pi}{3} \ , \tag{5.32}$$

and the cavity enhancement factor, which for high finesse can be approximated by (5.19), the cavity-to-free-space scattering ratio, i.e. the rate at which photons are emitted into the cavity rather than into free space, is given by,

$$\boxed{\Upsilon = \frac{\Gamma_{cav}}{\Gamma_{free}} = \frac{2F}{\pi} \frac{\Omega_{cav}}{\Omega_{free}} = \frac{F}{\pi} \frac{6}{k^2 w_0^2}} \ . \tag{5.33}$$

The ratio is also termed *Purcell factor* or cooperativity. We will see in the next section, how the cooperativity is linked to the strength at which the cavity couples to an atom.

5.2 Interaction of atoms with cavities

In Lecture 2 we have shown how to describe the dynamics of a single two-level atom driven by a quantized electromagnetic field and embedded in an electromagnetic vacuum under the assumption that the driving field be a plane wave and the vacuum be isotropic. In the following, we want to relax these conditions allowing the coupling constant $g_{\mathbf{k}}$ to depend on $\mathbf{k}$. Such a situation corresponds to placing the atom inside an optical cavity whose macroscopic boundary conditions create a cooperative

[4] See script on *Quantum mechanics* (2023), Sec. 19.2.1.

environment for the atom. We note that the role of the cavity can be understood as generating mirror images with which the atom interacts. Furthermore, both the atomic excitation and the radiation fields may decay. On the other hand, for the time being we restrict to non-interacting atoms, that is, free atoms or atoms trapped in external potentials that only interact with each other via re-scattering of an incident radiation field, i.e. no collisions and no properties requiring symmetrization of their wavefunctions.

Let us now introduce some parameters characterizing the interaction between atoms and cavities. Later on, we will relate the important notions of the *cooperativity* of several atoms (that is, the structure factor for light scattering) with the cavity-to-free space scattering ratio, the finesse and the density-of-states of a cavity, simply by pointing out that a cavity multiplies the number of atoms interacting with a light mode by the number of its mirror images.

5.2.1 Characterization of the atom-field coupling

In Sec. 5.1.2 we started introducing a number of quantities characterizing empty cavities. We will now pursue this task including their interaction with atoms. In particular, we will introduce three important quantities allowing us to measure the degree of quantization of the system: the cooperativity Υ, the saturation parameter s, and the cavity resolution r.

5.2.1.1 Atom-field coupling strength

As usual, the interaction strength of an atom with a light field is measured by the atom-field coupling constant, which is precisely HALF the single photon Rabi frequency. Using relationships derived in Sec. 5.1.2 we find,

$$g \equiv \frac{d\mathcal{E}_1}{\hbar} = \sqrt{\frac{3\pi\Gamma\omega}{2k^3 V_m}} \,, \tag{5.34}$$

where the atomic dipole moment d is given by the expression (2.34) (Γ being the spontaneous decay rate) and the electric field $\mathcal{E}_1$ produced by a single photon inside the cavity mode volume is given by (5.14). Exploiting furthermore the expressions found for the cavity mode volume V_m (5.11) and for the intracavity power (5.10) and (5.12), we can rewrite the coupling strength as,

$$g = \sqrt{\frac{3\Gamma\delta_{fsr}}{k^2 w^2}} = \sqrt{\frac{6}{k^2 w_0^2}\Gamma\frac{P}{n\hbar\omega}} \,. \tag{5.35}$$

5.2.1.2 Single atom reflection coefficient

Based on the complex atomic polarizability ,

$$\frac{\alpha_{pol}}{\varepsilon_0} \simeq \frac{6\pi}{k^3}\frac{-1}{\imath + 2\Delta/\Gamma} \,, \tag{5.36}$$

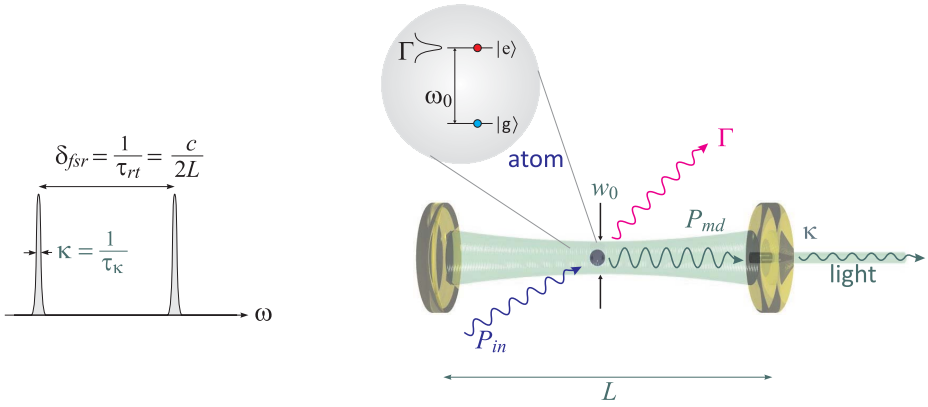

Figure 5.5: Relevant parameters for an atom interacting with a cavity.

the *single atom reflection coefficient* is defined as [5],

$$|\beta_\Delta| = \frac{k}{\pi w^2}\left|\frac{\alpha_{pol}}{\varepsilon_0}\right| = \frac{6}{k^2 w^2}\frac{1}{4\Delta_a^2 + \Gamma}\ , \tag{5.37}$$

where $\Delta_a = \omega - \omega_0$. The resonant reflection coefficient can be interpreted in terms of a phase shift that depends on the matching between the resonant optical cross-section of the atom, $\sigma_0 = 3\lambda^2/2\pi$, and the cross section of the optical mode,

$$\beta_0 = \frac{\sigma_0}{\pi w^2} = \frac{6}{k^2 w^2} = \frac{2g^2}{\delta_{fsr}\Gamma}\ . \tag{5.38}$$

5.2.1.3 Collective cooperativity

The frequency shift accumulated during a round trip in the cavity, $\delta_{fsr}\beta_0$, becomes noticeable, when it exceeds the linewidth of the cavity κ. From this condition, we obtain the optical depth for a single passage through the atomic sample multiplied by the finesse of the cavity, which is precisely the *cooperativity parameter* [6],

$$\boxed{\Upsilon = \frac{F}{\pi}\frac{6}{k^2 w^2} = \frac{\delta_{fsr}\beta_0}{\kappa} = \frac{2g^2}{\kappa\Gamma}}\ . \tag{5.39}$$

The sensitivity to the atom number can be measured in terms of a *critical atom number* N_{crt}, which the system can resolve,

$$N_{crt} = \frac{\pi}{F\beta_0} = \frac{1}{\Upsilon}\ . \tag{5.40}$$

[5] Note that the quantity $N\beta_\Delta$ with

$$\beta_\Delta = \frac{k}{\pi w_0^2}\frac{6\pi}{k^3}\frac{\alpha_{pol}}{\varepsilon_0} = \frac{2g^2}{\delta_{fsr}\Gamma}\frac{\imath - 2\Delta/\Gamma}{1 + (2\Delta/\Gamma)^2} \equiv \frac{\imath\gamma_0 - U_0}{\delta_{fsr}}$$

just represents the optical density per cavity round trip.

[6] It can be shown that the cooperativity parameter is equal to the cavity-to-free-space scattering ratio (also called Purcell factor) and to the structure factor of the coupled atom-cavity system.

While the strong coupling regime of the CQED requires $\Upsilon > 1$ with a single atom, collective cooperativity,

$$\Upsilon_N \equiv N\Upsilon \tag{5.41}$$

can be reached by simply increasing the number of atoms N interacting with the cavity [20, 28]. In this case, the atomic ensemble couples to the mode like a single 'super-atom', the coupling force being magnified to,

$$g_N = g\sqrt{N} \ . \tag{5.42}$$

5.2.1.4 Saturation parameter in cavities

The *saturation parameter* for a single photon is given by,

$$\boxed{s = \frac{2\Omega_1^2}{\Gamma^2} = \frac{8g^2}{\Gamma^2}} \ , \tag{5.43}$$

where Ω_1 is the single photon Rabi frequency. Therefore, the number of photons needed to saturate an atomic transition is,

$$n_{sat} = \frac{1}{s} \ . \tag{5.44}$$

Example 14 (*Saturation of weak transitions*): For example, in a linear cavity of mode volume $V_m = 0.5\,\mathrm{mm}^3$ interacting with strontium atoms on their $\Gamma = (2\pi)\ 7.5\,\mathrm{kHz}$ narrow intercombination line at $\lambda = 689\,\mathrm{nm}$ the atom-field interaction strength is $g = (2\pi)\ 4.5\,\mathrm{kHz}$, and so the number of photons required to saturate the transition is $n_{sat} = \Gamma^2/8g^2 \simeq 0.3$.

We see, that there is a *symmetry* between Υ and s, that is, between N_{crt} and n_{sat}. The regime $N\Upsilon > 1$ denotes the collective behavior of N atoms in the same way as $n_{sat} > 1$ indicates saturation. While Υ depends only on the phase matching between the atomic antenna and the cavity, s also depends on the cavity mode volume and the natural decay rate. See the Exc. 5.6.0.4.

5.2.1.5 Cavity resolution parameter

Comparing the photonic recoil, which is given by,

$$\omega_{rec} = \frac{\hbar k^2}{2m} \ , \tag{5.45}$$

with the resolution power of a cavity κ, we can define the *resolution parameter*,

$$\boxed{r \equiv \frac{\omega_{rec}}{\kappa}} \ . \tag{5.46}$$

With the three parameters defined in Eqs. (5.39), (5.43), and (5.46) we are able to measure the degree of quantization of the degrees of freedom involved in the matter-light interaction in a cavity. The cooperativity Υ measures the resolvability of single atoms in the atomic cloud, which depends on the phase matching between the atomic

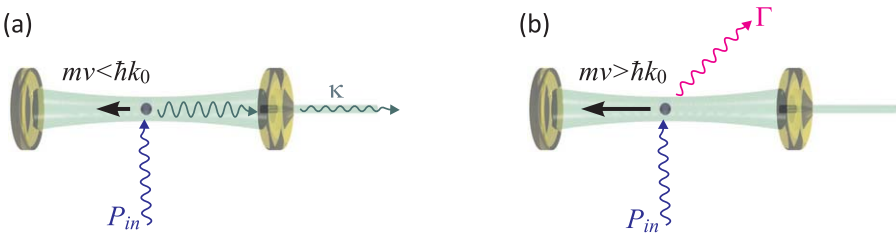

Figure 5.6: (a) If the recoil-induced Doppler shift of the atom moving along the cavity axis is smaller than the cavity linewidth, the light is preferentially scattered into the cavity mode. (b) Else it is scattered outside the mode.

antenna (i.e. its optical cross section) and the focus of the optical mode. The saturation parameter s measures the resolvability of single photons in the cavity. And the cavity resolution parameter r measures the resolvability of the Doppler-shift due to the atomic center-of-mass motion caused by the absorption of a single photon. If one wants to operate in an environment, where all degrees of freedom involved in the atom-light interactions are fully quantized, the atoms need to be placed into a cavity whose characteristic quantities are all large, $\Upsilon, s, r \gg 1$.

In Exc. 5.6.0.5 we compare the coupling force and other characteristic parameters for various combinations of atomic species and optical cavities. In Exc. 5.6.0.6 we calculate the number of photons in a cavity pumped in or out of resonance.

5.2.2 Normal mode splitting in linear cavities

To study the dynamics of the coupled atom-cavity system, we consider the Jaynes-Cummings Hamiltonian (2.134) for a more concrete situation. That is, we allow for optical pumping and decay of internal states with the rates R and Γ, respectively, and we allow for inhomogeneous mode functions, for example $g(z) = ge^{\imath kz}$ or $g(z) = g \sin kz$. On the other hand, we stick to a single atom (or N uncorrelated atoms), we disregard polarization and multi-mode excitation, and focus our attention to the phenomenon of *normal mode splitting*, which is one of the most direct witnesses of an ongoing atom-cavity interaction (see the vacuum Rabi splitting discussed in Exc. 2.7.0.31).

The Jaynes-Cummings model introduced in Sec. 2.6 represents an idealized model of the interaction of a single cavity mode with a single atom. In this section we reconsider this model taking into account the facts that the coupling strength may vary in space (via the introduction of mode functions) and that the cavity may interact with a reservoir (via the introduction of couplings to pump fields and losses. The starting point is the full Jaynes-Cummings Hamiltonian (2.134) within the RWA (see Sec. 2.2.2) for an atom located at the positions z of the optical axis and interacting with one mode of a linear optical cavity,

$$\boxed{\hat{H}_{JC} = -\Delta_a \hat{\sigma}^+\hat{\sigma}^- - \Delta_c \hat{a}^\dagger \hat{a} + g \sin kz(\hat{a}^\dagger \hat{\sigma}^- + \hat{a}\hat{\sigma}^+) - \imath\eta(\hat{a} - \hat{a}^\dagger)} \,. \tag{5.47}$$

Let us for simplicity assume, that the atom sits in an anti-node, $\sin kz = 1$. Using this Hamiltonian and exploting the usual commutation rules, $[\hat{a}, \hat{a}^\dagger] = 1$, $[\hat{\sigma}^+, \hat{\sigma}^-] = \hat{\sigma}^z$,

and $[\hat{\sigma}^z, \hat{\sigma}^\pm] = \pm 2\hat{\sigma}^\pm$, we derive the equations of motion for the individual atomic operators,

$$\begin{aligned}\dot{\hat{\sigma}}^- &= -\imath[\hat{\sigma}^-, \hat{H}_{JC}] + \mathcal{L}_\Gamma \hat{\sigma}^- \\ &= \imath\Delta_a[\hat{\sigma}^-, \hat{\sigma}^+]\hat{\sigma}^- - \imath g\hat{a}[\hat{\sigma}^-, \hat{\sigma}^+] - \tfrac{\Gamma}{2}\hat{\sigma}^- \\ &= (\imath\Delta_a - \tfrac{\Gamma}{2})\hat{\sigma}^- - \imath g\hat{a}\hat{\sigma}^z \ ,\end{aligned} \tag{5.48}$$

and

$$\begin{aligned}\dot{\hat{\sigma}}^z &= -\imath[\hat{\sigma}^z, \hat{H}_{JC}] + \mathcal{L}_\Gamma \hat{\sigma}^z \\ &= \imath\Delta_a[\hat{\sigma}^z, \hat{\sigma}^+\hat{\sigma}^-] - \imath g\hat{a}[\hat{\sigma}^z, \hat{\sigma}^+] - \imath g\hat{a}^\dagger[\hat{\sigma}^z, \hat{\sigma}^-] + 2\Gamma\hat{\sigma}^+\hat{\sigma}^- \\ &= 2\imath g(\hat{a}\hat{\sigma}^+ - \hat{a}_+^\dagger\hat{\sigma}^-) + \Gamma(\mathbb{I}_2 + \hat{\sigma}^z) \ ,\end{aligned} \tag{5.49}$$

and for the field operators,

$$\begin{aligned}\dot{\hat{a}} &= -\imath[\hat{a}, \hat{H}_{JC}] + \mathcal{L}_\kappa \hat{a} \\ &= \imath\Delta_c[\hat{a}, \hat{a}^\dagger\hat{a}] + \eta[\hat{a}, \hat{a}^\dagger] - \imath g\hat{\sigma}^-[\hat{a}, \hat{a}^\dagger] - \kappa\hat{a} \\ &= (\imath\Delta_c - \kappa)\hat{a} - \imath g\hat{\sigma}^- + \eta \ .\end{aligned} \tag{5.50}$$

The stationary solution follows from the expectation values of the Eqs. (5.50),

$$\begin{aligned}&\text{(i)} && 0 = (\imath\Delta_a - \tfrac{\Gamma}{2})\langle\hat{\sigma}^-\rangle - \imath g\langle\hat{a}\hat{\sigma}^z\rangle \\ &\text{(ii)} && 0 = 2\imath g(\langle\hat{a}\hat{\sigma}^+\rangle - \langle\hat{a}^\dagger\hat{\sigma}^-\rangle) + \Gamma(\mathbb{I}_2 - \langle\hat{\sigma}^z\rangle) \\ &\text{(iii)} && 0 = (\imath\Delta_c - \kappa)\langle\hat{a}\rangle - \imath g\langle\hat{\sigma}^-\rangle + \eta \ .\end{aligned} \tag{5.51}$$

In the mean-field approximation we neglect all correlations and derive from (i),

$$\langle\hat{\sigma}^-\rangle = \frac{-\imath g}{\frac{\Gamma}{2} - \imath\Delta_a}\alpha\langle\hat{\sigma}^z\rangle \ . \tag{5.52}$$

Substituting $\langle\hat{\sigma}^\pm\rangle$ in (ii),

$$\left(1 + \frac{2g^2}{\frac{\Gamma^2}{4} + \Delta_a^2}|\alpha|^2\right)\langle\hat{\sigma}^z\rangle = 1 \ , \tag{5.53}$$

and in (iii),

$$-(\imath\Delta_c - \kappa)\alpha + \frac{g^2}{\frac{\Gamma}{2} - \imath\Delta_a}\alpha\langle\hat{\sigma}^z\rangle = \eta \ . \tag{5.54}$$

Substituting $\langle\hat{\sigma}^z\rangle$,

$$-(\imath\Delta_c - \kappa)\alpha + \frac{g^2(\frac{\Gamma}{2} + \imath\Delta_a)\alpha}{\frac{\Gamma^2}{4} + \Delta_a^2 + 2g^2|\alpha|^2} = \eta \ . \tag{5.55}$$

or, using the abbreviations $U_\gamma \equiv U_0 - \imath\gamma_0$ and $\Delta_\kappa \equiv \Delta_c + \imath\kappa$,

$$\boxed{\frac{U_\gamma\alpha}{1 + 2|U_\gamma/g|^2|\alpha|^2} = \Delta_\kappa\alpha - \imath\eta} \ . \tag{5.56}$$

Assuming weak excitation, $g|\alpha_\pm| \ll \Gamma, \Delta_a$, expression (5.56) simplifies to,

$$U_\gamma \alpha = \Delta_\kappa \alpha - \imath\eta \ . \tag{5.57}$$

Resolving for α we finally get,

$$\alpha(\infty) \simeq \frac{-\imath\eta}{U_\gamma - \Delta_\kappa} = \frac{\eta}{\kappa + \imath(U_0 - \Delta_{ca} - \Delta_c)} \ , \tag{5.58}$$

defining $\Delta_{ca} \equiv \Delta_c - \Delta_a$. Hence, finite bunching only effects the efficient number of atoms participating in the normal mode splitting.

The excitation spectrum for $\Gamma \simeq 0$ is derived from the steady-state solution using the request, $0 = \frac{d}{d\Delta_{ca}}|\alpha(\infty)|^2$. We get,

$$\Delta_{ca} = U_0 - \Delta_a = \frac{g^2}{\Delta_a} - \Delta_a \ . \tag{5.59}$$

Assuming, $\Delta_{ca} = 0$, we obtain a cavity transmission spectrum exhibiting two peaks, as illustrated in Fig. 5.7. This phenomenon is called normal mode splitting,

$$\Delta_a = \pm g \ . \tag{5.60}$$

The calculation can be generalized to N atoms by substituting $g \to g\sqrt{N}$. We see that the normal mode spitting then reveals the number of atoms interacting with the cavity. However, in case the atoms are not perfectly *bunched*, i.e. located at anti-nodes, the coupling strengths diminishes, $g \to g|\sin kz|$.

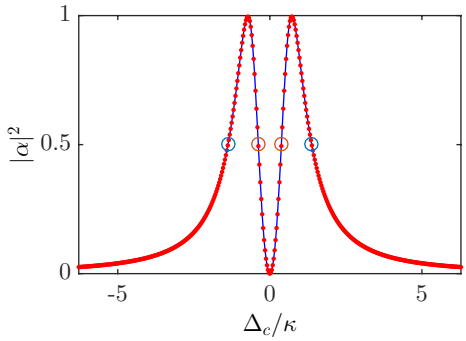

Figure 5.7: (code for download) Normal mode spectrum using the formula (5.58).

Example 15 (*Cooperativity of non-degenerate and confocal cavities*): In the case of strong excitation expression (5.56) gives,

$$\alpha = \frac{\imath\eta}{\Delta_\kappa - \frac{U_\gamma}{1+2|U_\gamma/g|^2|\alpha|^2}} \ . \tag{5.61}$$

Defining $\tilde{U}_\gamma \equiv U_\gamma/g_1$, $\tilde{\Delta}_\kappa \equiv \Delta_\kappa/g_1$, $\tilde{\eta} \equiv \eta/g_1$, and $n \equiv |\alpha|^2$,

$$\alpha = \frac{\imath\tilde{\eta}}{\tilde{\Delta}_\kappa - \frac{\tilde{U}_\gamma}{1+2|\tilde{U}_\gamma|^2 n}}. \tag{5.62}$$

From this we calculate the photon number,

$$n = \frac{\tilde{\eta}^2(1+2|\tilde{U}_\gamma|^2 n)^2}{|\tilde{\Delta}_\kappa|^2(1+2|\tilde{U}_\gamma|^2 n)^2 - \left(\tilde{\Delta}_\kappa \tilde{U}_\gamma^* + \tilde{\Delta}_\kappa^* \tilde{U}_\gamma\right)(1+2|\tilde{U}_\gamma|^2 n) + |\tilde{U}_\gamma|^2} \ . \tag{5.63}$$

Sorting the terms by powers of photon numbers we obtain a cubic equation, $0 = An^3 + Bn^2 + Cn + D$, with the coefficients,

$$\begin{aligned} A &= 4|\tilde{\Delta}_\kappa|^2|\tilde{U}_\gamma|^4 \\ B &= 4|\tilde{\Delta}_\kappa|^2|\tilde{U}_\gamma|^2 - 2\left(\tilde{\Delta}_\kappa \tilde{U}_\gamma^* + \tilde{\Delta}_\kappa^* \tilde{U}_\gamma\right)|\tilde{U}_\gamma|^2 - 4\tilde{\eta}^2|\tilde{U}_\gamma|^4 \\ C &= |\tilde{\Delta}_\kappa|^2 - \left(\tilde{\Delta}_\kappa \tilde{U}_\gamma^* + \tilde{\Delta}_\kappa^* \tilde{U}_\gamma\right) + |\tilde{U}_\gamma|^2 - 4\tilde{\eta}^2|\tilde{U}_\gamma|^2 \\ D &= -\tilde{\eta}^2 \ . \end{aligned} \tag{5.64}$$

The roots of the cubic equation are given by,

$$R \equiv \sqrt[3]{36CBA - 108DA^2 - 8B^3 + 12\sqrt{3}A\sqrt{4C^3A - C^2B^2 - 18CBAD + 27D^2A^2 + 4DB^3}} \tag{5.65}$$

and

$$X_\pm \equiv \frac{R}{6A} \pm \frac{6AC - 2B^2}{3AR} \tag{5.66}$$

so that,

$$n_0 = X_- - \frac{B}{3A} \quad , \quad n_\pm = -\frac{1}{2}X_- - \frac{B}{3A} \pm \frac{\imath\sqrt{3}}{2}X_+ \ . \tag{5.67}$$

From this expression we numerically find $n = |\alpha_+ + \alpha_-|^2$, which we ca use to finally obtain α (see also Exc. 5.6.0.7).

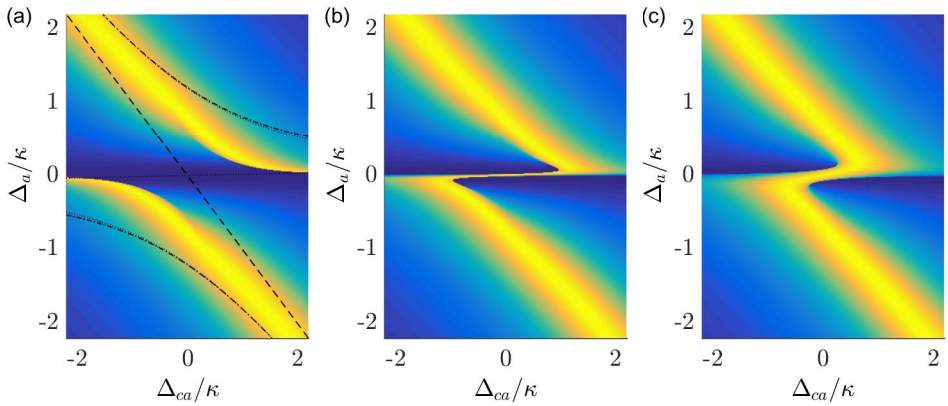

Figure 5.8: (code for download) Normal mode spectrum using the formula (5.58).

5.3 The Dicke model in the mean-field approximation

Until now we concentrated on understanding the interaction of *single* atoms with light fields, as it is described by the *Rabi* and the *Jaynes-Cummings model*. In the following

sections, we will extend these models to several and many atoms mostly considering classical light fields. It does not come as a surprise that totally new phenomena arise from the collective interaction of several atoms with a single light mode. For instance, the atomic cloud can evolve toward a spin-squeezed or an entangled state, or it can emit light in a super- and subradiant way. The interplay between collective processes and processes favoring an individualization of the atom-light interaction is subtle, and the different models used to understand the processes only grasp partial aspects. The difficulty arises from the complexity of the task of describing and numerical simulating the dynamics of many atoms evolving in huge Hilbert spaces. Indeed, the Hilbert space increases exponentially in size with the numbers of particles considered – for N particles its dimension is 2^N – and simplifying models are needed. Approximations used to reduce the complexity of the Hilbert space come at the price of eventually loosing some interesting features. On the other hand, they may also help to crystallize fundamental symmetries, which allow us to deepen our intuition on the collective behavior of the many-body system.

Famous models used in the description of collective scattering are (among others) the *Dicke model* and the *Tavis-Cummings model*. The Tavis-Cummings model operates on the full Hilbert space, and thus is the model of choice for the purpose of quantum computation. The Dicke model, on which we will focus our attention here, assumes a total indistinguishability of the atoms. The N atoms are described as spin-$\frac{1}{2}$ particles and their collective interaction with a *single mode* light field via a single collective spin $\mathbf{S}$ with $S = N/2$, i.e. the atoms cannot be addressed individually. In this model, the dimension of the Hilbert space only scales polynomially as $2S + 1$.

We will now introduce the Dicke model detailing its advantages and limitations and show how it applies to the description of spin squeezing and weak entanglement. In Sec. 5.4 we will emphasize its relations to super- and subradiance. In particular we will show that, when the coupling between the light and matter crosses a critical value, the Dicke model shows a mean-field phase transition to a superradiant phase. Finally, in Sec. 5.5 we will extend the Dicke model to atoms interacting via ground state collisions nor via direct radiation exchange.

5.3.1 Dicke states

The Hilbert space of the Dicke model [48, 81] is given by (the tensor product of) the states of the cavity and of the two-level atoms. The Hilbert space of the cavity can be spanned by Fock states $|n\rangle$. Choosing the basis $|+\rangle \equiv \binom{1}{0}$ and $|-\rangle \equiv \binom{0}{1}$, the states of each two-level atom $j = 1, 2, .., N$ are defined through the spin operators $\hat{\mathbf{s}}_j = (\hat{s}_j^x, \hat{s}_j^y, \hat{s}_j^z)$ acting only an individual atom [7],

$$\begin{aligned} \hat{s}_j^x|... \pm ...\rangle &= \tfrac{1}{2}|... \mp ...\rangle \\ \hat{s}_j^y|... \pm ...\rangle &= \pm\imath\tfrac{1}{2}|... \mp ...\rangle \\ \hat{s}_j^z|... \pm ...\rangle &= \pm\tfrac{1}{2}|... \pm ...\rangle \ , \end{aligned} \tag{5.68}$$

and satisfying the spin algebra,

$$[\hat{s}_j^x, \hat{s}_k^y] = \imath\hat{s}_j^z\delta_{j,k} \ , \tag{5.69}$$

[7] Note, that here and in the following we set $\hbar \equiv 0$ for simplicity.

and related to the Pauli spin matrices via,

$$\hat{\mathbf{s}} = \tfrac{1}{2}\vec{\hat{\sigma}} \quad , \quad \hat{s}^{\pm} = \hat{s}^x \pm \imath \hat{s}^y = \tfrac{1}{2}(\hat{\sigma}_x \pm \imath \hat{\sigma}_y) = \hat{\sigma}^{\pm} \ . \tag{5.70}$$

The Hamiltonian of the Dicke model is,

$$\hat{H} = \omega_c \hat{a}^\dagger \hat{a} + \omega_a \sum_{j=1}^{N} \hat{s}_j^z + 2g(\hat{a} + \hat{a}^\dagger) \sum_{j=1}^{N} \hat{s}_j^x \ . \tag{5.71}$$

Sometimes in literature the single-atom coupling strength (or half the single-atom single-photon Rabi frequency) is normalized to the atom number, $g \equiv \lambda/\sqrt{N}$. The coupling can be written as the sum of two terms: a co-rotating term that conserves the number of excitations and is proportional to $\hat{a}\hat{\sigma}^+ + \hat{a}^\dagger\hat{\sigma}^-$ and a counter-rotating term proportional to $\hat{a}\hat{\sigma}^- + \hat{a}^\dagger\hat{\sigma}^+$.

The above Hamiltonian assumes that all the spins are identical, i.e. they have the same transition frequency, they do not interact with each other, and they equally couple to the radiation field (e.g. a cavity mode). For the simple system of only two not mutually interacting spins, $\mathbf{s}_1$ and $\mathbf{s}_2$, simultaneously coupling to the same radiation field, the Dicke model directly follows from the SU(2) angular momentum algebra. There, we have shown that the spin operators can be added, $\hat{\mathbf{S}} = \hat{\mathbf{s}}_1 + \hat{\mathbf{s}}_2$, and the total system be represented in a coupled basis, where $[\hat{s}_1 \cdot \hat{s}_2, \hat{\mathbf{S}}^2] = 0 = [\hat{s}_1 \cdot \hat{s}_2, \hat{S}_z^2]$. This concept can be generalized to an arbitrary number of spins, that is, under the above assumption, one can define macroscopic collective spin operators,

$$\hat{S}_\alpha \equiv \sum_{j=1}^{N} \hat{s}_j^\alpha \qquad \text{with} \qquad [\hat{S}_x, \hat{S}_y] = \imath \hat{S}_z \ , \tag{5.72}$$

and $\alpha = x, y, z$. Using these operators, one can rewrite the above Hamiltonian as

$$\boxed{\hat{H} = \omega_c \hat{a}^\dagger \hat{a} + \omega_a \hat{S}_z + 2g(\hat{a} + \hat{a}^\dagger)\hat{S}_x} \ , \tag{5.73}$$

and it is easy to see that,

$$[\hat{H}, \hat{\mathbf{S}}^2] = 0 \neq [\hat{H}, \hat{S}_z] \ . \tag{5.74}$$

That is, the Dicke Hamiltonian preserves the spin $\langle \hat{\mathbf{S}}^2 \rangle$, but interaction with a light field can change the projection $\langle \hat{S}_z \rangle$. We will see in the following that this fact as important consequences for interaction dynamics of atomic ensembles coupled to a single light mode.

5.3.1.1 Degeneracies of Dicke states

Let us now look at states having the same number N of energy packets counting free photons n and atomic excitations $N - n$. For example with $N = 2$, the following states are possible.

$\lvert S, M\rangle$ $\lvert n\rangle$	$\lvert \frac{N}{2}, M\rangle$ $\# = 1$	$\lvert \frac{N}{2} - 1, M\rangle$ $\# = 1$
0	$\lvert 1,1\rangle = \lvert ++\rangle$	
1	$\lvert 1,0\rangle = \frac{1}{\sqrt{2}}(\lvert +-\rangle + \lvert -+\rangle)$	$\lvert 0,0\rangle = \frac{1}{\sqrt{2}}(\lvert +-\rangle - \lvert -+\rangle)$
2	$\lvert 1,-1\rangle = \lvert --\rangle$	

The right column of the above table contains a singlet state, which decouples from the triplet states (center column). The fact that it decouples from the deexcited triplet state makes the singlet state stable or *subradiant* [8]. See also Fig. 5.13.

For example with $N = 3$,

$\|S, M\rangle$	$\|\frac{N}{2}, M\rangle$	$\|\frac{N}{2}-1, M\rangle$
n	$\# = 1$	$\# = 2$
0	$\|\frac{3}{2}, \frac{3}{2}\rangle = \|++\!+\rangle$	
1	$\|\frac{3}{2}, \frac{1}{2}\rangle = \|++\!-\rangle + \|+-\!+\rangle + \|-++\rangle$	$\|\frac{1}{2}, \frac{1}{2}\rangle$
2	$\|\frac{3}{2}, -\frac{1}{2}\rangle = \|+--\rangle + \|-+\!-\rangle + \|--\!+\rangle$	$\|\frac{1}{2}, -\frac{1}{2}\rangle$
3	$\|\frac{3}{2}, -\frac{3}{2}\rangle = \|---\rangle$	

Example with N arbitrary,

$\|S, M\rangle$	$\|\frac{N}{2}, M\rangle$	$\|\frac{N}{2}-1, M\rangle$	$\|\frac{N}{2}-2, M\rangle$	
$\|n\rangle$	$\# = 1$	$\# = N-1$	$\# = \frac{N(N-3)}{2}$	
0	$\|\frac{N}{2}, \frac{N}{2}\rangle = \|+++\!+...\rangle$			
1	$\|\frac{N}{2}, \frac{N}{2}-1\rangle = \sum_{perm.} \|---\!+...\rangle$	$\|\frac{N}{2}-1, \frac{N}{2}-1\rangle$		
2	$\|\frac{N}{2}, \frac{N}{2}-2\rangle = \sum_{perm.} \|--\!-\!+...\rangle$	$\|\frac{N}{2}-1, \frac{N}{2}-2\rangle$	$\|\frac{N}{2}-2, \frac{N}{2}-1\rangle$	
$\vdots$	$\vdots$	$\vdots$		
N	$\|\frac{N}{2}, -\frac{N}{2}\rangle = \|----..\rangle$			

We see that the Dicke states are not made to unambiguously label degenerate states. States $|S, M\rangle$ with $S < |M|$ are largely degenerate. The degeneracy of a Dicke state with $S \leq \frac{N}{2}$, that is, the number of states $|+\rangle^{N_+}|-\rangle^{N_-}$ composing a single Dicke state labeled by $|S, M\rangle$ is [65],

$$\# = \frac{(2S+1)N!}{(\frac{N}{2}+S+1)!(\frac{N}{2}-S)!} \,. \tag{5.75}$$

Transitions between energetically degenerate states $|S, M\rangle$ and $|S', M'\rangle$ with $M = M'$ but $S \neq S'$ are prohibited.

5.3.1.2 Mean-field approximation and light field elimination

The *mean-field approximation* consists in replacing the photonic operators by their expectation values, i.e. assuming classical light. This allows us to remove the light energy term from the Hamiltonian and replace the coupling strength by the n-photon Rabi frequency, $\Omega = 2g\sqrt{n}$. The Hamiltonian then becomes just a generalization of the semiclassical one-atom Hamiltonian (2.66) to large spins,

$$\boxed{\hat{H} = \hat{\mathbf{S}} \cdot \mathbf{G} = \Delta\ \hat{S}_z + \mathfrak{Re}\ \Omega\ \hat{S}_x + \mathfrak{Im}\ \Omega\ \hat{S}_y} \,, \tag{5.76}$$

where we allow for complex Rabi frequencies.

In the absence of spontaneous emission, any pure *single-atom* state is given by,

$$|\psi\rangle = |\vartheta, \varphi\rangle = \cos\tfrac{\vartheta}{2}|+\rangle + e^{\imath\varphi}\sin\tfrac{\vartheta}{2}|-\rangle \,, \tag{5.77}$$

[8] Note that, while superradiance as well as subradiance can be explained by classical radiator models, such as the coupled dipoles model.

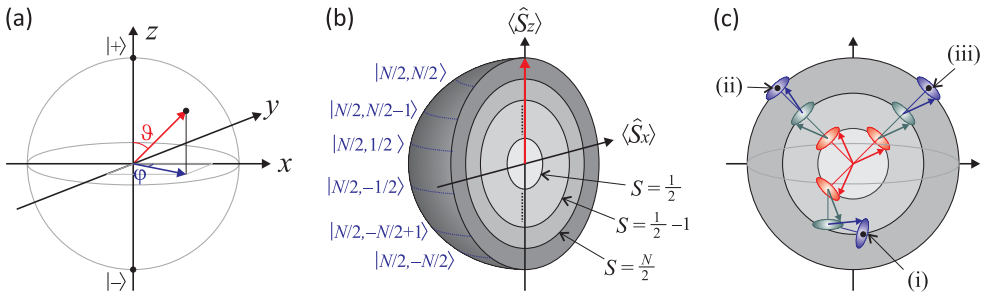

Figure 5.9: (a) Illustration of the Bloch sphere. (b) Bloch spheres of the various super/subradiant states with N atoms, here $N = 3$. (c) Illustration of (i) subradiant coupling of the atomic spins, (ii) a general coherent spin state, (iii) a spin-squeezed state.

where the angles ϑ and φ point to a location on the Bloch sphere characterizing the state of the atom. For example, a single initially deexcited atom having been subject to a $\frac{\pi}{2}$-pulse ends up in the state $|\frac{\pi}{2}, 0\rangle$. The expectation value of the spin operator in this state is simply obtained from,

$$\begin{aligned} \langle\vartheta,\varphi|\hat{S}_z|\vartheta,\varphi\rangle &= \cos^2\tfrac{\vartheta}{2}\langle+|\hat{S}_z|+\rangle + \sin^2\tfrac{\vartheta}{2}\langle-|\hat{S}_z|-\rangle = \tfrac{1}{2}\cos\vartheta \\ \langle\vartheta,\varphi|\hat{S}_+|\vartheta,\varphi\rangle &= e^{\imath\varphi}\sin\tfrac{\vartheta}{2}\cos\tfrac{\vartheta}{2}\langle+|\hat{S}_+|-\rangle = \tfrac{1}{2}e^{\imath\varphi}\sin\vartheta \ , \end{aligned} \tag{5.78}$$

yielding,

$$\langle\vartheta,\varphi|\hat{\mathbf{S}}|\vartheta,\varphi\rangle = \tfrac{1}{2}\begin{pmatrix}\cos\varphi\sin\vartheta\\ \sin\varphi\sin\vartheta\\ \cos\vartheta\end{pmatrix} \ . \tag{5.79}$$

We will also denote the probability of finding the system in state $|\pm\rangle$ by,

$$p_+ = \langle\hat{P}_\pm\rangle = |\langle+|\psi\rangle|^2 = \cos^2\tfrac{\vartheta}{2} = 1 - p_- \ . \tag{5.80}$$

5.3.1.3 Collective spin states

Let us now study the system obeying the Hamiltonian (5.76) in detail. The spin operators $\hat{\mathbf{S}}$ satisfy a SU(2) algebra, i.e. $\hat{\mathbf{S}} \times \hat{\mathbf{S}} = \imath\hat{\mathbf{S}}$. The common eigenstates of $\hat{\mathbf{S}}^2$ and $\hat{S}_z$ are denoted by $|S, M\rangle$,

$$\begin{aligned} \hat{S}_z = \hat{S}_+\hat{S}_- - \hat{S}_-\hat{S}_+ \qquad &\text{with} \qquad \hat{S}_z|S,M\rangle = M|S,M\rangle \\ \hat{N}_\pm \equiv \tfrac{N}{2}\mathbb{I} \pm \hat{S}_z \qquad &\text{with} \qquad \hat{N}_\pm|S,M\rangle = \tfrac{N}{2} \pm M|S,M\rangle \ . \end{aligned} \tag{5.81}$$

Since

$$N = N_+ + N_- \qquad \text{and} \qquad M = \tfrac{1}{2}(N_+ - N_-) \tag{5.82}$$

are, respectively, the number of atoms and the inversion, we conclude that $N_\pm = \frac{N}{2} \pm M$ is the number of atoms in each of the two states. The N atoms can occupy 2^N different collective states. However, when the atoms are identical and couple uniformly to the same light mode, all states with the same number of atoms being excited are energetically degenerate, with the total excitation energy,

$$E = M\omega_c \ . \tag{5.83}$$

The degeneracy of each many-body state with a given inversion M is given by the binomial coefficient,

$$\# = \binom{N}{\frac{N}{2}+M} = \binom{N}{N_+} = \binom{N}{N_-} \quad \text{such that} \quad \sum_{N_+=0}^{N} \binom{N}{N_+} = 2^N \ . \tag{5.84}$$

Therefore, we may set,

$$\boxed{|S,M\rangle \equiv |+\rangle^{N_+}|-\rangle^{N_-}} \ . \tag{5.85}$$

These states are called *Dicke states* [9].

For the special case $N = 2$ the transformation from the basis $|+\rangle^{N_+}|-\rangle^{N_-}$, used in the *Tavis-Cummings model*, to the basis $|S,M\rangle$, used in the Dicke model, is a unitary transformation. For $N > 2$ the situation is more complicated, since the degeneracies of both models are different. It is important to be aware that S is not simply half the atom number, but runs over $S = \frac{N}{2}, \frac{N}{2}-1, ...$, depending on how the individual spins couple together. The degeneracy of an angular momentum state $|S,M\rangle$ with a specific inversion M but undefined orbital momentum S is determined by the condition $0 \le S \le M$, and given by,

$$\# = \tfrac{N}{2} - |M| + 1 \ . \tag{5.86}$$

For example, for $N = 2$ the possible spin states are given by $|s_1 - s_2| \le S \le s_1 + s_2$, that is, $S = 0, 1$. And for $N = 5$, $M = \frac{3}{2}$ is supported by $S = \frac{3}{2}$ and $\frac{5}{2}$. Obviously, the degeneracy (5.86) is lower than (5.84) except for $N = 2$. Dicke states may be represented as vectors pointing to the surface of a so-called Bloch sphere of radius,

$$\|\langle N,S,M|\hat{\mathbf{S}}^2|N,S,M\rangle\| = S(S+1) \ , \tag{5.87}$$

as illustrated in Fig. 5.9(b).

5.3.2 Coherent spin states

By the fact that the individual spins are additive and the Hamiltonian linear in the spin operators, $\hat{H} \propto \hat{S}_z$, we know that the Schrödinger equation will be satisfied by *product states*,

$$|\Psi_N\rangle = \prod_{k=1}^{N} |\vartheta_k, \varphi_k\rangle_k \ , \tag{5.88}$$

where $|\vartheta_k, \varphi_k\rangle_k$ is the state of the k-the atom given by (5.77).

Coherent spin states now consist of N atoms, all being in the same state. In Exc. 5.6.0.8 we present another equivalent definition. Since the atoms are indistinguishable by the radiation field, we may as well drop the labeling index k,

$$|\Psi_N\rangle = |\vartheta,\varphi\rangle^N = \sum_{k=0}^{N} \sqrt{\binom{N}{k}} \cos^{N-k}\tfrac{\vartheta}{2}|+\rangle^{N-k} \ e^{\imath k\varphi} \sin^k\tfrac{\vartheta}{2}|-\rangle^k \ , \tag{5.89}$$

[9] For the coupling of two spins the notation $|(s_1,s_2)s,m\rangle$ is frequently used. For coupling N spins, we should write in analogy,

$$|(\overbrace{\tfrac{1}{2},..,\tfrac{1}{2}}^{N}),S,M\rangle \equiv |N,S,M\rangle \ .$$

Mostly, we will however drop the (constant) number N.

or equivalently, using the Dicke state notation (5.85),

$$\boxed{|\vartheta,\varphi\rangle^N = \sum_{k=0}^{2S} \sqrt{\binom{2S}{k}} \cos^{2S-k}\tfrac{\vartheta}{2}\; e^{\imath k\varphi} \sin^k\tfrac{\vartheta}{2} |S, S-k\rangle} \; . \tag{5.90}$$

Hence, similarly to the coherent state of a harmonic oscillator, which consists of a Poissonian distribution of number states, the coherent spin state consists of a binomial distribution of N_+ atoms in one state and $N - N_+$ in the other. Note also, that by construction, the coherent spin states are **stretched**, $S = N/2$. That is, they can be represented by a vector of length N equal to the radius of the (generalized) Bloch sphere. In other words, S is a conserved quantum number as already shown in (5.74), and this feature does not change under the influence of the Hamiltonian (5.76). These states are called superradiant. Nevertheless, other states $|S, M\rangle$ are possible with $S \leq \frac{N}{2}$. These are squeezed, subradiant, or entangled states.

In the following we will study some of the properties of the coherent spin states. For instance, in Exc. 5.6.0.9(a) we calculate the expectation values of coherent spin states,

$$\langle\vartheta,\varphi|^N \hat{\mathbf{S}} |\vartheta,\varphi\rangle^N = S \begin{pmatrix} \cos\varphi \sin\vartheta \\ \sin\varphi\sin\vartheta \\ \cos\vartheta \end{pmatrix} \; . \tag{5.91}$$

Hence, the spin evolves on the surface of a Bloch sphere with radius,

$$\|\langle\vartheta,\varphi|^N \hat{\mathbf{S}} |\vartheta,\varphi\rangle^N\| = S \qquad \text{while still} \qquad \|\langle\vartheta,\varphi|^N \hat{\mathbf{S}}^2 |\vartheta,\varphi\rangle^N\| = S(S+1) \; . \tag{5.92}$$

For the number of atoms in each state we expect,

$$\langle\hat{N}_+\rangle = \tfrac{N}{2} + \langle\hat{S}_z\rangle = N\cos^2\tfrac{\vartheta}{2} = Np_+ = N(1-p_-) = N - \langle\hat{N}_-\rangle \; . \tag{5.93}$$

Example 16 (*Spin excitation operator*): As an example on how to calculate with Dicke states, we calculate the expectation value of the spin excitation operator for a coherent spin state. With the expression (5.91) for a we calculate, with a little help from MAPLE,

$$\begin{aligned}
&\langle\vartheta,\varphi|^N \hat{S}_+ |\vartheta,\varphi\rangle^N \\
&= \sum_{k,l=0}^{2S} \sqrt{\binom{2S}{l}\binom{2S}{k}} p_+^{2S-l/2-k/2} e^{-\imath(l-k)\varphi} p_-^{l/2+k/2} \langle S, S-l|\hat{S}_+|S, S-k\rangle \\
&= \sum_{k,l=0}^{2S} \sqrt{\binom{2S}{l}\binom{2S}{k}} p_+^{2S-l/2-k/2} e^{-\imath(l-k)\varphi} p_-^{l/2+k/2} \sqrt{S(S+1)-(S-l)(S-k+1)}\,\delta_{k,l+1} \\
&= e^{\imath\varphi} \sum_{k=0}^{2S} \binom{2S}{k} k \cos^{4S-2k+1}\tfrac{\vartheta}{2} \sin^{2k-1}\tfrac{\vartheta}{2} = N\sqrt{p_+p_-} = Se^{\imath\varphi}\sin\vartheta \; .
\end{aligned}$$

5.3.3 Rotations, spin excitation and precession

A useful rule for the subsequent calculations is the following,

$$e^{\imath F(\hat{S}_z)} \hat{S}_+ e^{-\imath F(\hat{S}_z)} = \hat{S}_+ e^{\imath[F(\hat{S}_z+\mathbb{I})-F(\hat{S}_z)]} \; , \tag{5.94}$$

where F is an arbitrary function. For $F(\hat{S}_z) \equiv \phi\hat{S}_z$ the unitary transform $e^{\imath F(\hat{S}_z)}$ denotes a rotation about the z-axis, which we will study in the example below. For $F(\hat{S}_z) \equiv \zeta\hat{S}_z^2$ it generates squeezing along the z-axis, which we will study in the next section. Furthermore, we define the rotation matrices about the Cartesian axis,

$$R_x(\gamma) \equiv \begin{pmatrix} 1 & 0 & 0 \\ 0 & \cos\gamma & -\sin\gamma \\ 0 & \sin\gamma & \cos\gamma \end{pmatrix} , \qquad R_y(\gamma) \equiv \begin{pmatrix} \cos\gamma & 0 & -\sin\gamma \\ 0 & 1 & 0 \\ \sin\gamma & 0 & \cos\gamma \end{pmatrix} ,$$
$$R_z(\gamma) \equiv \begin{pmatrix} \cos\gamma & -\sin\gamma & 0 \\ \sin\gamma & \cos\gamma & 0 \\ 0 & 0 & 1 \end{pmatrix} , \tag{5.95}$$

for which it is possible to show (with $\alpha = x, y, z$),

$$\boxed{R_\alpha(\gamma)\hat{\mathbf{S}} = e^{\imath\gamma\hat{S}_\alpha}\hat{\mathbf{S}}e^{-\imath\gamma\hat{S}_\alpha}} . \tag{5.96}$$

Example 17 (*Rotation about* $\hat{S}_z$): Defining $F(\hat{S}_z) \equiv \phi\hat{S}_z$ the relationship (5.94) tells us,

$$e^{\imath\phi\hat{S}_z}\hat{S}_+e^{-\imath\phi\hat{S}_z} = \hat{S}_+e^{\imath\phi} ,$$

and consequently,

$$e^{\imath\phi\hat{S}_z}\hat{\mathbf{S}}e^{-\imath\phi\hat{S}_z} = \begin{pmatrix} \frac{1}{2}(e^{\imath\phi}\hat{S}_+ + e^{-\imath\phi}\hat{S}_-) \\ \frac{1}{2\imath}(e^{\imath\phi}\hat{S}_+ - e^{-\imath\phi}\hat{S}_-) \\ \hat{S}_z \end{pmatrix} = \begin{pmatrix} \cos\phi & -\sin\phi & 0 \\ \sin\phi & \cos\phi & 0 \\ 0 & 0 & 1 \end{pmatrix} \hat{\mathbf{S}} \equiv R_z(\phi)\hat{\mathbf{S}} .$$

Furthermore,

$$e^{-\imath\phi\hat{S}_z}|\vartheta,\varphi\rangle^N = \sum_{k=0}^{2S}\sqrt{\binom{2S}{k}}\cos^{N-k}\tfrac{\vartheta}{2}e^{\imath k\varphi}\sin^k\tfrac{\vartheta}{2}e^{-\imath\phi(S-k)}|S,S-k\rangle$$
$$= e^{-\imath\phi S}\left(e^{-\imath\phi}\cos\tfrac{\vartheta}{2}|+\rangle + e^{\imath(\varphi+\phi)}\sin\tfrac{\vartheta}{2}|-\rangle\right)^N = e^{-\imath\phi S}|\vartheta,\varphi+\phi\rangle^N .$$

We also find,

$$\langle\vartheta,\varphi|^N R_z(\phi)\hat{\mathbf{S}}|\vartheta,\varphi\rangle^N = \tfrac{N}{2}\begin{pmatrix} \cos(\varphi+\phi)\sin\vartheta \\ \sin(\varphi+\phi)\sin\vartheta \\ \cos\vartheta \end{pmatrix} = \langle\vartheta,\varphi+\phi|^N\hat{\mathbf{S}}|\vartheta,\varphi+\phi\rangle^N .$$

To vary the polar angle ϑ of a coherent spin state $|\vartheta,\varphi\rangle$, we first rotate the coordinate system about the z-axis until $\varphi = 0$, then rotate about the y-axis by the desired angle θ, and finally rotate back about the z-axis to reach the initial azimuth φ,

$$\langle\vartheta,\varphi|^N R_z(\varphi)R_y^{-1}(\theta)R_z^{-1}(\varphi)\hat{\mathbf{S}}|\vartheta,\varphi\rangle^N = \tfrac{N}{2}\begin{pmatrix} \cos\varphi\sin(\theta+\vartheta) \\ \sin\varphi\sin(\theta+\vartheta) \\ \cos(\theta+\vartheta) \end{pmatrix} = \langle\vartheta+\theta,\varphi|^N\hat{\mathbf{S}}|\vartheta+\theta,\varphi\rangle^N .$$

In Exc. 5.6.0.10 we write down the explicit rotation matrix for two atoms.

Rotations such as the ones described by $R_\alpha(\gamma)$ are generated by the Dicke Hamiltonian (5.76), since the solution of the Schrödinger equation is,

$$\boxed{|\Psi(t)\rangle = e^{-\imath t\hat{H}t}|\Psi(0)\rangle = e^{-\imath t\hat{S}_x\mathfrak{Re}\ \Omega_x - \imath t\hat{S}_y\mathfrak{Im}\ \Omega_y - \imath t\hat{S}_z\Delta}|\Psi(0)\rangle} \ . \tag{5.97}$$

That is, the Dicke Hamiltonian generates rotations $R_x(\mathfrak{Re}\ \Omega_x t)$, $R_y(\mathfrak{Im}\ \Omega_y t)$, and $R_z(\Delta t)$. This confirms that rotations do only transform coherent states into each other. Nevertheless, there are other unitary operations that transform coherent states into states that cannot be represented by coherent states. One example for this is squeezing.

5.3.4 Uncertainties, quantum projection noise and spin squeezing

Measuring the population of a coherently excited two-level system by projecting it onto an energy eigenstate introduces *quantum projection noise*. Although this inherent noise spoils the determination of the resonance frequency, it can to some extent be surpassed by *spin squeezing* [150]. The projection noise limit has been observed with ions [87, 85] and with atomic clouds [135]. The reduction of the noise by spin squeezing has been observed with ions [131], micromasers [124], and atomic clouds [73, 99]. Also, a weakly entangled state of two modes was observed for continuous spin variables [91]. Very strong squeezing spin can be obtained in a *Mott insulator* state, as demonstrated by [69].

First, we want to show that the Heisenberg uncertainty of a coherent spin state is nothing else than quantum projection noise. On one hand, we have,

$$\begin{aligned}\langle\vartheta,\varphi|^N(\Delta\hat{S}_z)^2|\vartheta,\varphi\rangle^N &= \langle\vartheta,\varphi|^N\hat{S}_z^2|\vartheta,\varphi\rangle^N - (\langle\vartheta,\varphi|^N\hat{S}_z|\vartheta,\varphi\rangle^N)^2 \\ &= \sum_{k=0}^{N}\binom{N}{k}(\tfrac{N}{2}-k)^2p_+^{N-k}p_-^k - \left(\sum_{k=0}^{N}\binom{N}{k}(\tfrac{N}{2}-k)p_+^{N-k}p_-^k\right)^2 \\ &= \left(\tfrac{N^2}{4} - N^2p_+p_- + Np_+p_-\right) - \left(\tfrac{N}{2}(p_+-p_-)\right)^2 = Np_+p_- \ .\end{aligned} \tag{5.98}$$

On the other hand, this results corresponds to the variance of quantum projection noise,

$$\begin{aligned}(\Delta r)^2 &= \sum_{r=0}^{N}(r-Np_\pm)^2P_{N,r,\pm} \\ &= \sum_{k=0}^{N}(\tfrac{N}{2}-k+\tfrac{N}{2}(p_+-p_-))^2\binom{N}{k}p_+^{N-k}p_-^k = Np_+p_- \ .\end{aligned} \tag{5.99}$$

The Heisenberg uncertainty relation applied to angular momentum operator satisfying $[\hat{S}_x,\hat{S}_y]=\imath\hat{S}_z$ states,

$$\Delta\hat{S}_x\Delta\hat{S}_y \geq \tfrac{1}{2}|\hat{S}_z| \ . \tag{5.100}$$

Since there are no quantum correlations between the particles, the uncertainty of coherent spin states is additive,

$$(\Delta\hat{S}_\alpha)^2 = \sum_{k=0}^{N} (\Delta\hat{s}_k^\alpha)^2 \ . \tag{5.101}$$

For a coherent spin state we can calculate explicitly [see Exc. 5.6.0.9(b)],

$$\langle\vartheta,\varphi|^N \begin{pmatrix} \Delta\hat{S}_x^2 \\ \Delta\hat{S}_y^2 \\ \Delta\hat{S}_z^2 \end{pmatrix} |\vartheta,\varphi\rangle^N = \tfrac{N}{4} \begin{pmatrix} 1-\sin^2\vartheta\cos^2\varphi \\ 1-\sin^2\vartheta\sin^2\varphi \\ \sin^2\vartheta \end{pmatrix} \ . \tag{5.102}$$

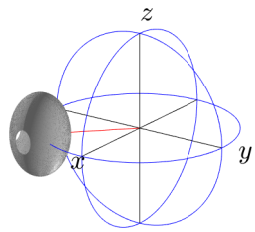

Figure 5.10: Illustration of the uncertainty of the spin components of a coherent spin state.

Example 18 (*Uncertainty of a coherent spin state after a $\frac{\pi}{2}$-pulse*): A $\frac{\pi}{2}$-pulse applied to a cloud in the collective ground state generates the state $|\vartheta,\varphi\rangle = |\frac{\pi}{2},0\rangle$. This is somewhat analogous to the beam splitting of a photonic Fock state. Interestingly, a Fock state seems more natural for an atomic cloud, while the Glauber state is more natural for a photonic mode. For example, for the particular state $|\frac{\pi}{2},0\rangle$ we find from (5.102),

$$(\Delta\hat{S}_x)^2 = 0 \qquad \text{and} \qquad (\Delta\hat{S}_y)^2 = (\Delta\hat{S}_z)^2 = \tfrac{S}{2} \ .$$

Note, that spin squeezing along the z-axis could be obtained by quantum non-demolition measurement of the inversion, that is, by measuring $\hat{S}_z$ without influencing the populations of the ground and excited state.

5.3.4.1 Spin squeezing by one-axis twisting

We have seen in the last section, that rotations influence the distribution of the uncertainty among the Cartesian coordinates in a specific way. It is, however, possible to manipulate the uncertainty distribution without rotating the collective spin state. An example with great practical importance is the concept of spin squeezing. It consists in establishing appropriate quantum correlations are between the individual spins, such as to partly cancel out fluctuations in one direction augmenting them in the other direction.

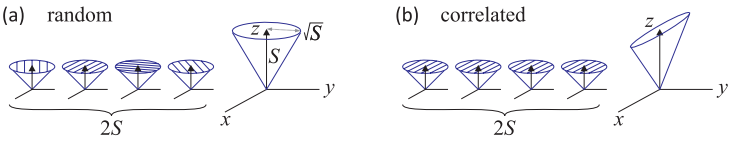

Figure 5.11: (code for download) Illustration of the uncertainty in (a) a coherent state and (b) a spin-squeezed state. See also Fig. 5.9(c).

Squeezing of spin is not as straightforward as squeezing of bosons, since the uncertainty relations are essentially different [96]. To study spin-squeezing along the z-axis let as analyze the unitary transformation,

$$\boxed{Q_z(\zeta)\hat{\mathbf{S}} \equiv e^{\imath\zeta\hat{S}_z^2}\hat{\mathbf{S}}e^{-\imath\zeta\hat{S}_z^2}} \ . \tag{5.103}$$

Specifying the rule (5.94) for the particular case $F(\hat{S}_z) \equiv \zeta\hat{S}_z^2$, we get,

$$e^{\imath\zeta\hat{S}_z^2}\hat{S}_+e^{-\imath\zeta\hat{S}_z^2} = \hat{S}_+e^{2\imath\zeta(\hat{S}_z+1/2)} \ , \tag{5.104}$$

and hence,

$$Q_z(\zeta)\hat{\mathbf{S}} = e^{\imath\zeta\hat{S}_z^2}\hat{\mathbf{S}}e^{-\imath\zeta\hat{S}_z^2} = \begin{pmatrix} \frac{1}{2}(\hat{S}_+e^{2\imath\zeta(\hat{S}_z+1/2)} + e^{-2\imath\zeta(\hat{S}_z+1/2)}\hat{S}_-) \\ \frac{1}{2\imath}(\hat{S}_+e^{2\imath\zeta(\hat{S}_z+1/2)} - e^{-2\imath\zeta(\hat{S}_z+1/2)}\hat{S}_-) \\ \hat{S}_z \end{pmatrix} \ . \tag{5.105}$$

Let us now apply the *squeezing operator* to the state $|\frac{\pi}{2},0\rangle$. In Exc. 5.6.0.11 we show that,

$$\langle\tfrac{\pi}{2},0|^N e^{\imath\zeta\hat{S}_z^2}\hat{\mathbf{S}}e^{-\imath\zeta\hat{S}_z^2}|\tfrac{\pi}{2},0\rangle^N = \begin{pmatrix}1\\0\\0\end{pmatrix}\tfrac{N}{2}\cos^{N-1}\zeta \tag{5.106}$$

$$\langle\tfrac{\pi}{2},0|^N e^{\imath\zeta\hat{S}_z^2}\begin{pmatrix}\hat{S}_x^2\\ \hat{S}_y^2\\ \hat{S}_z^2\end{pmatrix}e^{-\imath\zeta\hat{S}_z^2}|\tfrac{\pi}{2},0\rangle^N = \begin{pmatrix}N+1\\N+1\\2\end{pmatrix}\tfrac{N}{8} + \begin{pmatrix}1\\-1\\0\end{pmatrix}\tfrac{N(N-1)}{8}\cos^{N-2}2\zeta \ .$$

The dependencies of the uncertainties as a function of the squeezing parameter are plotted in Fig. 5.12. We see that the uncertainties never get smaller than the unsqueezed value. The reason is that, since the unitary transform $e^{\imath\zeta\hat{S}_z^2}$ commutes with $\hat{S}_z$, the prescription (5.103) does not immediately lead to squeezing along the z-axis.

Nevertheless, the prescription does generate quantum correlations in $\hat{S}_x$ and $\hat{S}_y$, which can be transformed to squeezing by subsequently rotating the collective spin about the x-axis [96]. A rotation by an angle ν does not modify the x-component,

$$\begin{aligned}\langle\tfrac{\pi}{2},0|^N e^{\imath\nu\hat{S}_x}e^{\imath\zeta\hat{S}_z^2}\Delta\hat{S}_x^2e^{-\imath\zeta\hat{S}_z^2}e^{-\imath\nu\hat{S}_x}|\tfrac{\pi}{2},0\rangle^N \\ = \tfrac{N(N+1)}{8} + \tfrac{N(N-1)}{8}\cos^{N-2}2\zeta - \tfrac{N^2}{4}\cos^{2N-2}\zeta \ ,\end{aligned} \tag{5.107}$$

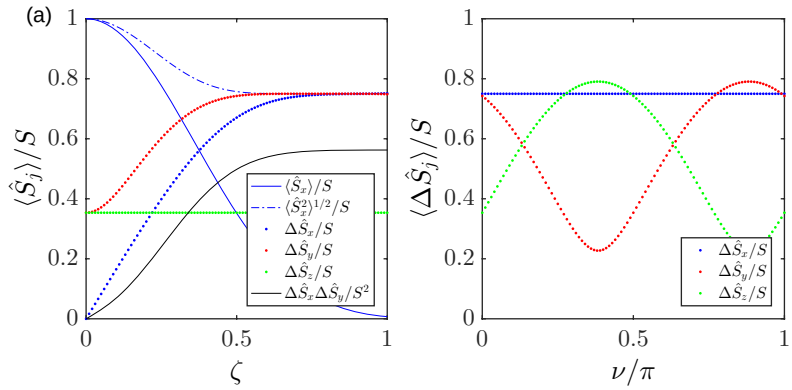

Figure 5.12: (code for download) (a) Uncertainties calculated in (5.106) as a function of the squeezing parameter. (b) Uncertainties after application of squeezing operator as a function of the rotation angle ν about the x-axis.

but it modifies the other ones,

$$\begin{aligned} &\langle \tfrac{\pi}{2}, 0|^N e^{\imath\nu \hat{S}_x} e^{\imath\zeta \hat{S}_z^2} \Delta \hat{S}_{y,z}^2 e^{-\imath\zeta \hat{S}_z^2} e^{-\imath\nu \hat{S}_x} |\tfrac{\pi}{2}, 0\rangle^N \\ &\qquad = \tfrac{N}{4}\{1 + \tfrac{N-1}{4}[A \pm \sqrt{A^2 + B^2}\cos(2\nu + \arctan \tfrac{B}{A})]\} \ , \end{aligned} \tag{5.108}$$

with $A \equiv 1 - \cos^{N-2} 2\zeta$ and $B \equiv 4 \sin\zeta \cos^{N-2}\zeta$. We study spin squeezing in Exc. 5.6.0.12. In Exc. 5.6.0.13 we study entanglement witnesses with coherent spin states.

Obviously, since squeezed states are obtained from coherent states by unitary transform, they are still normalized,

$$\langle \vartheta, \varphi|^N e^{-\imath\zeta \hat{S}_z^2} e^{\imath\zeta \hat{S}_z^2} |\vartheta, \varphi\rangle^N = 1 \ . \tag{5.109}$$

Example 19 (*Conditional spin-squeezing by non-demolition measurement*): Technically, spin-squeezed states can be generated in experiments by quantum non-demolition measurements [14, 34, 132]. Another idea would be to arrange for totally uniform spin-spin coupling, since this generates terms like,

$$H_{ss} = \sum_{i,j\neq i}^{N} \kappa_{ij} \hat{s}_i^z \hat{s}_j^z \simeq \kappa \sum_{i,j\neq i}^{N} \hat{s}_i^z \hat{s}_j^z = \kappa \hat{S}_z^2 \ . \tag{5.110}$$

In a cloud this latter idea is not realizable, because the interatomic coupling strength depends on the distance between the atoms, but if the atoms are coupled via their interaction with a common mode of an optical cavity it should be feasible.

5.4 Super- and subradiance in open systems

The abstract spin formalism developed in the last sections revealed propagators allowing us to rotate and squeeze coherent spin states, but it did not tell us how to

implement them physically. For this, we need to solve equations of motion derived from Hamiltonians realizable in the laboratory. In the following sections, we will set up the fundamental equations of motion (master or Heisenberg-Liouville) for open systems of N atoms subject to spontaneous emission collectively interacting with a single light mode subject to cavity decay and pumped by an external source.

We will discuss constants of motion of the Dicke and of the Tavis-Cummings model and phase transitions to superradiant states in the mean-field approximation. Finally, we will present recent experimental realizations of Dicke phase transitions, namely superradiant self-ordering and superradiant lasing.

5.4.1 Models for open systems and phase transitions

We have already seen, that the spin quantum number S is preserved under the effect of the Dicke Hamiltonian (5.73). The spherical harmonics $|S, M\rangle$ are orthonormal and the spin operators $\hat{S}_\pm$ and $\hat{S}_{x,y,z}$ or their combinations do not allow for transitions between states with different S,

$$[\hat{H}, \hat{\mathbf{S}}^2] = 0 \qquad \text{with} \qquad \hat{\mathbf{S}}^2 = \tfrac{1}{2}(\hat{S}_+\hat{S}_- + \hat{S}_-\hat{S}_+) + \hat{S}_z^2 \tag{5.111}$$
$$\text{but} \qquad [\hat{H}, \hat{S}_z] = \imath(\mathfrak{Im}\ \Omega\ \hat{S}_x - \mathfrak{Re}\ \Omega\ \hat{S}_y) \neq 0\ .$$

Hence, under the effect of the Dicke Hamiltonian an initial state $|N, S, M\rangle$ can only change its magnetic quantum number $|N, S, M\rangle \longrightarrow |N, S, M'\rangle$, and the manifolds with a given S form closed sub-spaces. In other words, once we start in a superradiant state $|N, S, M\rangle = |N, \frac{N}{2}, +\frac{N}{2}\rangle$, spin conservation excludes subradiant states, which allowed us to restrict to the superradiant Dicke subspace. Transitions between Dicke subspaces are only possible via physical processes that act on individual atoms, e.g. decay or phase fluctuation processes, as we will see later [66, 156].

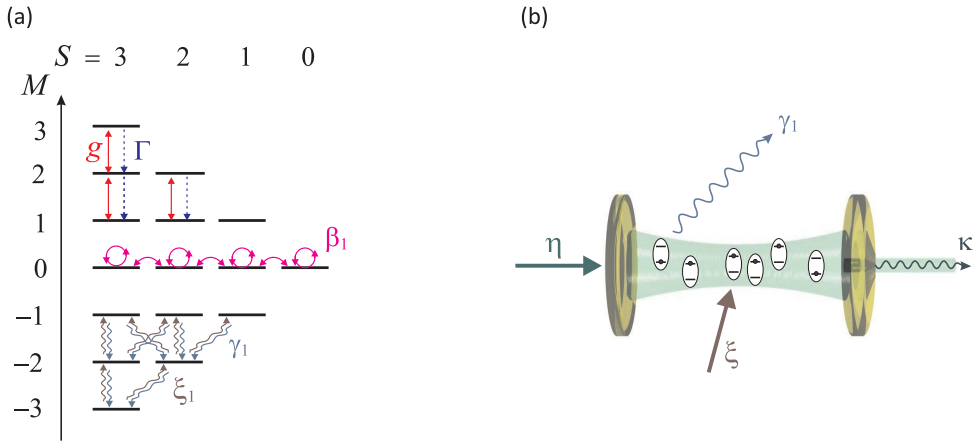

Figure 5.13: (a) Illustration of the Dicke states for $N = 6$. Hamiltonian interactions are in depicted in red. Superradiant decay occurs through a cascade from state $M = S$ to state $M = -S$. Spontaneous emission and phase noise leads to transitions along the blue arrows. The lowest states in each S subspace are dark and can only decay through a (subradiant) dark states cascade. (b) Scheme of the Dicke model.

5.4.1.1 The generalized open Dicke model

In the presence of spontaneous decay or dephasing, superradiant spin conservation is no longer guaranteed. Let us have a look at the master equation for a set of N atoms coupled with the strength g to the mode of a cavity and additionally pumped by a classical laser field η [12, 95]. After transformation into the rotating frame we have,

$$\boxed{\begin{aligned}&\dot{\hat{\rho}} = \imath[\hat{\rho}, \hat{H}_{gD}] + \textstyle\sum_\gamma \mathcal{L}_{\gamma,\hat{L}}\hat{\rho} \qquad \text{or} \qquad \dot{\hat{A}} = -\imath[\hat{A}, \hat{H}_{gD}] + \textstyle\sum_\gamma \mathcal{L}^\dagger_{\gamma,\hat{L}}\hat{A}\\ &\hat{H}_{gD} = -\Delta_c\hat{a}^\dagger\hat{a} - \Delta_a\hat{S}_z + 2g(\hat{a}\hat{S}_+ + \hat{S}_-\hat{a}^\dagger) + 2g'(\hat{a}\hat{S}_- + \hat{S}_+\hat{a}^\dagger) - \imath\eta(\hat{a} - \hat{a}^\dagger)\\ &\text{and} \quad \mathcal{L}_{\gamma,\hat{L}}\hat{\rho} \equiv \gamma(2\hat{L}\hat{\rho}\hat{L}^\dagger - \hat{L}^\dagger\hat{L}\hat{\rho} - \hat{\rho}\hat{L}^\dagger\hat{L})\\ &\text{and} \quad \mathcal{L}^\dagger_{\gamma,\hat{L}}\hat{A} \equiv \gamma(2\hat{L}^\dagger\hat{A}\hat{L} - \hat{L}^\dagger\hat{L}\hat{A} - \hat{A}\hat{L}^\dagger\hat{L})\end{aligned}} \; . \tag{5.112}$$

The different coupling strengths g and g' allow us to isolate the counter-rotating terms, in order to discuss their relevance. The usual *open Dicke model* is obtained from the generalized Dicke Hamiltonian $\hat{H}_{gD}$ by setting $g' \equiv g$, while the rotating wave approximation is done by setting $g' \equiv 0$. The rates γ describe possible decay processes to which the degrees of freedom $\hat{L}$ are subject. The most relevant decay processes are listed in the following table:

decay rate γ	dissipative operator $\hat{L}$	physical process
κ	$\hat{a}$	cavity decay
ϕ	$\hat{a}^\dagger\hat{a}$	cavity phase jitter
Γ	$\hat{S}_- = \sum_j \hat{s}_j^-$	collective (superradiant) atomic decay
γ_1	$\hat{s}_j^-$	single-atom decay
ξ_1	$\hat{s}_j^+$	single-atom optical pumping
β_1	$\hat{s}_j^z$	single-atom dephasing

Γ, κ, and ϕ describe collective decay respectively collective phase noise, while γ_1, ξ_1, and β_1 stand for spontaneous emission, optical pumping via higher-lying levels, and phase fluctuation of individual atoms. The latter decay processes are described by sums of Lindbladians over all atoms. In Exc. 5.6.0.14 we derive the Heisenberg equations for the relevant degrees of freedom,

$$\begin{aligned}\dot{\hat{a}} &= (\imath\Delta_c - \kappa - \phi)\hat{a} - 2\imath(g\hat{S}_- + g'\hat{S}_+) + \eta \\ \dot{\hat{S}}_- &= (\imath\Delta_a - \gamma_1 - \xi_1 - \beta_1 + 2\Gamma\hat{S}_z)\hat{S}_- + 4\imath\hat{S}_z(g\hat{a} + g'\hat{a}^\dagger) \\ \dot{\hat{S}}_z &= -2\imath\hat{S}_+(g\hat{a} + g'\hat{a}^\dagger) + 2\imath(g\hat{a}^\dagger + g'\hat{a})\hat{S}_- - 2\Gamma\hat{S}_+\hat{S}_- - N(\gamma_1 - \xi_1)\mathbb{I} - 2(\gamma_1 + \xi_1)\hat{S}_z \\ \dot{\hat{s}}_j^- &= (\imath\Delta_a - \gamma_1 - \xi_1 - \beta_1)\hat{s}_j^- + 4\imath(g\hat{a} + g'\hat{a}^\dagger)\hat{s}_j^z \\ \dot{\hat{s}}_j^z &= -2\imath(g\hat{a} + g'\hat{a}^\dagger)\hat{s}_j^+ + 2\imath(g\hat{a}^\dagger + g'\hat{a})\hat{s}_j^- - \gamma_1(\mathbb{I} - 2\hat{s}_j^z) + \xi_1(\mathbb{I} + 2\hat{s}_j^z) \; .\end{aligned} \tag{5.113}$$

In Exc. 5.6.0.15 we verify that these equations of motion do not change the spin $\hat{\mathbf{S}}$. Neglecting all dissipation processes but Γ, the Eqs. (5.113) can be rewritten in terms

of observables as,

$$\dot{\hat{\mathbf{S}}} = \begin{pmatrix} 2(g+g')(\hat{a}+\hat{a}^\dagger) \\ 2\imath(g-g')(\hat{a}-\hat{a}^\dagger) \\ -\Delta_a \end{pmatrix} \times \hat{\mathbf{S}} + \Gamma \begin{pmatrix} -\hat{S}_x + \hat{S}_x\hat{S}_z + \hat{S}_z\hat{S}_x \\ -\hat{S}_y + \hat{S}_y\hat{S}_z + \hat{S}_z\hat{S}_y \\ -2\hat{S}_z - 2\hat{S}_x^2 - 2\hat{S}_y^2 \end{pmatrix} . \tag{5.114}$$

Only the terms $\mathcal{L}_{\gamma_1}$, $\mathcal{L}_{\xi_1}$, and $\mathcal{L}_{\beta_1}$ can change $\hat{\mathbf{S}}^2$. The $\hat{\mathbf{S}}^2$ and $\hat{S}_z$ eigenvalues determine the coupling strength of the many-atom (Dicke) state to the cavity mode and the coherent, external drive. This coupling determines the rate of cavity photon generation as well as the pumping strength. The magnitude of the coupling strength distinguishes between superradiance and subradiance. For superradiant states the coupling strength scales superlinear in N, while for subradiant states the scaling is sublinear in N, and some subradiant states are dark. Dark means that the collective coupling to the cavity and the coherent, external drive of these states vanishes, meaning these states cannot decay via collective interactions e.g. by creating a cavity photon. However these states still decay into other states via the decay and dephasing processes $\mathcal{L}_{\gamma_1}$ and $\mathcal{L}_{\beta_1}$ acting individually on the emitters, see Fig. 5.13. Hence, spontaneous decay is an individualization process [66]. Generally, the spin preserving contributions in the master equation (5.116) generate quantum correlations leading to collective behavior (both super- and subradiance are collective effects) and the non-preserving terms destroy correlations leading to individualization (all properties scale exactly linear in N). However only the spin non-preserving contributions introduce coupling between superradiant and subradiant states, thus in order to prepare subradiant states an interplay of collectivity and individualization is necessary. Based on these considerations, we may distinguish between collective versus individual behavior and superradiant versus subradiant behavior. The latter are special cases of collective behavior. This twofold distinction seems crucial when investigating super- and subradiance in the presence of dephasing and individual decay. In Exc. 5.6.0.16 we study superradiant decay.

5.4.1.2 Symmetries of the Dicke and the Tavis-Cummings model

The total number of excitations,

$$\hat{N}_{ex} \equiv \hat{a}^\dagger\hat{a} + \hat{S}_z \tag{5.115}$$

is a constant of motion only for the Tavis-Cummings Hamiltonian, i.e. the Dicke Hamiltonian with RWA, $g' = 0$, and in the absence of pumping, $\eta = 0$,

$$[\hat{H}_{gD}, \hat{N}_{ex}] = \eta(\hat{a} - \hat{a}^\dagger) + 4g'(\hat{S}_-\hat{a} - \hat{S}_+\hat{a}^\dagger) . \tag{5.116}$$

That is, the Dicke Hamiltonian preserves the excitation number, except for the counter-rotating terms, which can only change the excitation number by ± 2.

The Dicke model without RWA, $g' = g$, has one global symmetry,

$$\mathcal{P} : (\hat{a}, \hat{\sigma}^\pm) \to (-\hat{a}, -\hat{\sigma}^\pm) . \tag{5.117}$$

Because $\mathcal{P}$ squares to unity, it has two eigenvalues, 1 and -1. This symmetry is associated with a conserved quantity: the parity of the total number of excitations, $\mathcal{P} = (-1)^{N_{ex}}$. This parity conservation is a consequence of the preserved excitation number. A state of the Dicke model is said to be normal when this symmetry is preserved, and superradiant when this symmetry is spontaneously broken.

5.4.2 Superradiant Dicke phase transition

The interesting feature of the set of equations (5.113) is, that the degrees of freedom are macroscopically populated, yet, they follow the rules of quantum mechanics. For instance, we may expect them to behave as order parameters for macroscopic phase transitions. We will study one such example in the following.

5.4.2.1 Equilibrium Dicke phase transition

The Dicke model predicts a phase transition to a superradiant state, when the coupling strength g exceeds a certain critical value. To see this we simplify the Hamiltonian (5.73) by the mean-field approximation,

$$\omega_c \hat{a}^\dagger \hat{a} = \omega_c \alpha^2 \ , \tag{5.118}$$

where the field amplitude α is a real number, and calculate the free energy as a function of α,

$$\begin{aligned} F(\alpha) \equiv -\tfrac{1}{\beta} \ln Z(\alpha) \qquad \text{with} \qquad & Z(\alpha) = \mathrm{Tr}\ e^{-\beta \hat{H}} \\ \text{and} \qquad & \hat{H} = \omega_c \alpha^2 + \sum\nolimits_j \hat{h}_j \\ \text{and} \qquad & \hat{h}_j = \omega_a \hat{s}_j^z + 4g\alpha \hat{s}_j^x \ . \end{aligned} \tag{5.119}$$

$Z(\alpha)$ is the partition function, $\hat{h}_j$ the single-atom Hamiltonian, and $\beta \equiv 1/k_B T$. Carried out in Exc. 5.6.0.17, the calculation results in,

$$\begin{aligned} F(\alpha) &= \omega_c \alpha^2 - \tfrac{N}{\beta} \ln(2 \cosh \beta E) \\ \text{where} \qquad \pm E \equiv \langle \hat{h}_j \rangle &= \pm \sqrt{\left(\tfrac{\omega_a}{2}\right)^2 + (2g\alpha)^2} \end{aligned} \tag{5.120}$$

are the single-atom energy eigenvalues. The minimum of the free energy as a function of the field amplitude, $F'(\alpha) = 0$, yields a critical coupling strength g_c,

$$g_c \sqrt{N} = \tfrac{1}{2} \sqrt{\omega_c \omega_a \coth \tfrac{\beta \omega_a}{2}} \ , \tag{5.121}$$

Below g_c the free energy minimizes for $\alpha = 0$, and beyond g_c it minimizes for $\alpha > 0$, as seen in Fig. 5.14.

Note that the critical coupling smoothly evolves down to zero temperature ($\beta \to 0$), where one obtains $g_c = \sqrt{\omega_c \omega_a / 2N}$ [10].

5.4.3 Beyond mean-field

We already applied the mean-field approximation in the derivation of the semiclassical Dicke Hamiltonian (5.76) and the Dicke phase transition (5.118). Some effects,

[10] Note, that in the thermodynamic limit, $N \to \infty$, the operators can be replaced by [95]:

$$\hat{S}_x \overset{N\to\infty}{\longrightarrow} \tfrac{1}{2} \hat{N} \cos \hat{\varphi} \qquad \text{and} \qquad \hat{S}_y \overset{N\to\infty}{\longrightarrow} \tfrac{1}{2} \hat{N} \sin \hat{\varphi} \ .$$

In this case, the operators commute $[\hat{S}_x, \hat{S}_y] \to 0$.

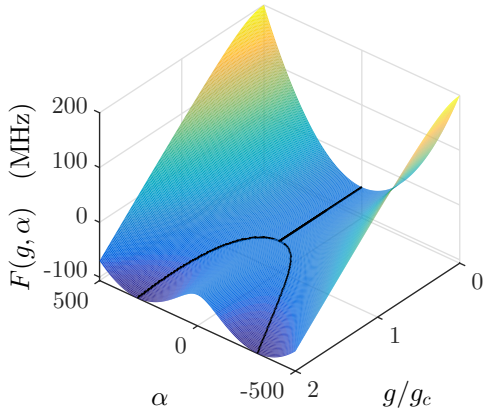

Figure 5.14: (code for download) Free energy as a function of coupling strength and photon number. Beyond the critical coupling strength g_c the minimum of the free energy splits opening the way for two possible equilibrium states of the mean-field phase.

however, are intrinsically to the existence of interatomic correlations, as for example, superradiant lasing [11]

> **Example 20 (*Superradiant lasing*):** In a conventional laser amplification and optical phase coherence are established by stimulated photon emission from a population-inverted medium. This results in the Schawlow-Townes spectral linewidth, proportional to the square of the cavity decay width and inversely proportional to the photon number in the cavity. As Dicke showed, the coherence can also be stored in the emitters that constitute the gain medium provided they interact collectively with common radiation field modes [43]. If the spontaneous decay rate is much smaller than the cavity decay rate very narrow emission bandwidths far below the cavity decay width can be achieved. In Exc. 5.6.0.18 we study *superradiant lasing* in the Dicke model [107]. Cavity-mediated superradiance can also be described within the *Tavis-Cummings model* [21]. It represents an extension of the Jaynes-Cummings model for several atoms.

5.5 Interacting atoms

When two atoms excited to an internal level of energy hc/λ are so close together that the range of their dipole moments overlap without forming a molecular bonding, $a_B \ll R \ll \lambda$, they may exhibit cooperative relaxation. The atoms are coupled via the radiation that they are susceptible to emit into the same continuum. The coupled atomic dipoles oscillate and decay in phase. The decays is accelerated one leads to an intense burst of coherent and spatially directional radiation. This phenomenon is

[11] Interestingly, spin-squeezing, which is also based on interatomic correlations, can be described within the mean-field approximation.

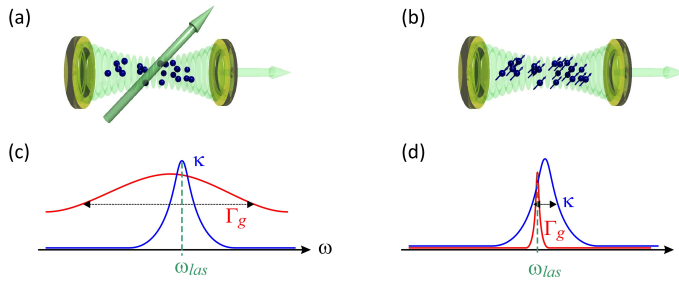

Figure 5.15: (a) Principle scheme of standard lasing. Here, the coherence is stored in the cavity field. The gain profile is much larger than the cavity width (good-cavity limit, $\kappa \ll \Gamma_g$), as shown in (c). The laser frequency follows any (technical) cavity fluctuation: $\omega_{las} = \omega_{cav} + \omega_g \frac{\kappa}{\Gamma_g}$. (b) *Superradiant lasing*. Here, the coherence is stored in the gain. We are in the bad-cavity limit, $\kappa \gg \Gamma_g$, as shown in (d). The laser frequency is robust to cavity fluctuations: $\omega_{las} = \omega_g + \omega_{cav} \frac{\Gamma_g}{\kappa}$.

termed *superradiance* [48, 125]. We may view superradiance as destructive interference of the dipolar radiation patterns of all atoms in all but one direction of space triggered by the first spontaneous decay. The superradiant enhancement is largest when half of the atoms are deexcited. The correlated atoms can be in a Dicke state (then the total dipole moment is always zero) or in a product state (then the net dipole moment is non-zero at half-deexcitation). In the second case, we also talk about *superfluorescence*. In this case, an excited initially incoherent sample develops correlations due to the emission process. One can also imagine the case that the emission patterns pairwise cancel, and the decay is thus inhibited. This is called *subradiance*. Superradiance has been used in the microwave domain as a spectroscopic method in the observation of photon echoes.

Correlated quantum jumps are, in a sense, the few-atoms precursors of superradiance. Accelerated spontaneous decay has been predicted for atoms whose distance is shorter than the wavelength of the decaying transition [139, 102]. Super- and subradiance has been observed in a system of two ion trapped in a Paul trap [47].

5.5.1 Rydberg blockade

Rydberg atoms (i.e. atoms in excited Rydberg states) exhibit huge polarizabilities inducing large interaction energies even at relatively modest densities. These can be so strong, that the presence of a single Rydberg-excited atom can drive out of resonance the frequencies of transitions connected to the Rydberg state for several neighboring atoms once the exciting laser is sufficiently narrow-band. This effect called *Rydberg blockade* can be described by the following interaction Hamiltonian [128, 144],

$$\hat{H}_{Rb} = \sum_{i>j} \kappa_{ij} \tfrac{1}{2}(\hat{\sigma}_i^z - 1)\tfrac{1}{2}(\hat{\sigma}_j^z - 1) \qquad \text{with} \qquad \kappa_{ij}/2\pi = \frac{C_6}{r_{ij}^6} \,, \tag{5.122}$$

where $\frac{1}{2}(\hat{\sigma}_i^z - 1) = |e\rangle_i\langle e|$ is the probability of finding the i-th atom in an excited state and C_6 interatomic van der Waals interaction coefficient of the transition.

Example 21 (*Two interacting Rydberg atoms*): In this example we study Rydberg blockade for two interacting Rydberg atoms. In this case, the Hamiltonian can be cast into the matrix form,

$$\hat{H}_{Rb} = \begin{pmatrix} \Delta_a & \frac{1}{2}\Omega & \frac{1}{2}\Omega^* & 0 \\ \frac{1}{2}\Omega^* & 0 & 0 & \frac{1}{2}\Omega^* \\ \frac{1}{2}\Omega & 0 & 0 & \frac{1}{2}\Omega \\ 0 & \frac{1}{2}\Omega & \frac{1}{2}\Omega^* & -\Delta_a + \kappa_{12} \end{pmatrix} .$$

The master equation can be numerically solved using the procedure outlined in example **??**. The result of such a simulation is shown in Fig. 5.16. Comparing

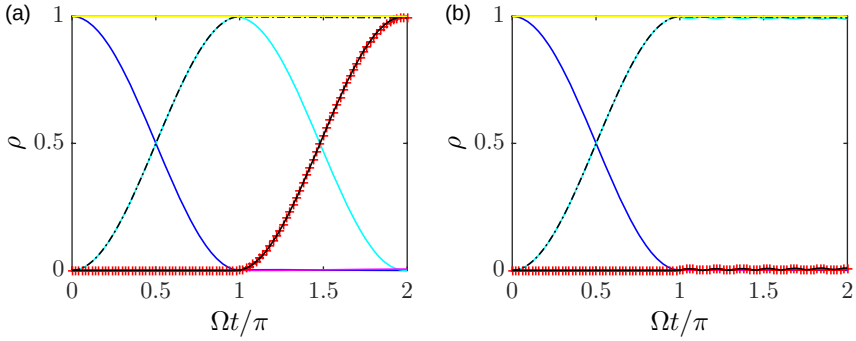

Figure 5.16: (code for download) Populations in a system of two two-level atoms interaction via van der Waals forces. Initially ($\Omega t < \pi$) only one atom is driven, after that only the other. We assume $\Omega \gg \Gamma$ and $C_6 = 4 \cdot 10^7$. The interatomic distance is (a) $kr_{12} = 0.5$, respectively, (a) $kr_{12} = 5$. (blue) $\rho_{11,11}$, (cyan) $\rho_{12,12}$, (magenta) $\rho_{21,21}$, (red) $\rho_{22,22}$, (black dotted) $\rho_{22}^{(1)}$, and (black) $\rho_{22}^{(2)}$.

the evolutions calculated in Fig. 5.16 for large and small interatomic distances, we see that the excitation of the first atom impedes the excitation of the second one when the interaction is strong.

Note, that an interesting situation occurs when the coupling is completely uniform (e.g. mediated by a cavity), $\kappa_{ij} \simeq \kappa$,

$$\hat{H}_{Rb} \simeq -\Delta_a \hat{S}_z + \Omega \hat{S}^+ + \Omega^* \hat{S}^- + \tfrac{1}{8}\kappa(\hat{S}_z^2 - 2\hat{S}_z + 1) \ , \tag{5.123}$$

as pointed out in Eq. (5.110). Such Hamiltonians may be interesting for the generation of spin-squeezing.

5.5.2 Dipole-dipole interactions in the non-linear optics regime

The mean-field Dicke model totally neglects interactions between the atoms due to the exchange of real of virtual photons, i.e. neither resonant dipole-dipole interactions nor van der Waals interactions are considered [6, 12, 50, 56, 126, 128, 140]. That is, interaction terms such as,

$$\hat{H}_{Ising} = -\sum_{i,j\neq i}^{N} V_{ij} \hat{\sigma}_j^+ \hat{\sigma}_i^- \tag{5.124}$$

are absent from the Hamiltonian. Spin-spin interactions are studied in the so-called *Ising model*, which is interesting in the context of (anti-)*ferromagnetism* [61, 62, 67, 95, 157]. The negligence of interaction is of course the price to pay for the simplicity of the model and its manageability for large atom numbers. Note that dipole-dipole interactions are easier to study in the linear optics regime allowing for at most a single photon to interact with the cloud [12].

In this section, we will consider dipole-dipole interactions in very small dilute clouds interacting with an arbitrary number of photons. The possibility for the cloud of storing as many photons as there are atoms is common to the Dicke model. Here, we will call it the *non-linear optics* regime, as several photons may team up to excite higher Dicke excitations states. In particular, we will study two interacting atoms as done by the milestone experiment of DeVoe and Brewer [47].

The starting point is the collective many-atoms Hamiltonian. After tracing over the vacuum modes, one obtains the master equation,

$$\boxed{\begin{aligned}
\dot{\hat{\rho}} &= -\imath[\hat{H},\hat{\rho}] + \mathcal{L}[\hat{\rho}] \quad \text{with} \\
\hat{H} &= -\Delta_a \textstyle\sum_j \hat{\sigma}_j^+\hat{\sigma}_j^- + \frac{1}{2}\sum_j \left[\Omega(\mathbf{r}_j)\hat{\sigma}_j^+ + h.c.\right] + \frac{1}{2}\sum_{i\neq j}\Delta_{ji}\hat{\sigma}_j^+\hat{\sigma}_i^- \\
\mathcal{L}[\hat{\rho}] &= \frac{1}{2}\sum_{i,j}\Gamma_{ij}\left(2\hat{\sigma}_j^-\hat{\rho}\hat{\sigma}_i^+ - \hat{\sigma}_i^+\hat{\sigma}_j^-\hat{\rho} - \hat{\rho}\hat{\sigma}_i^+\hat{\sigma}_j^-\right) \\
\Delta_{j\neq i} &= -\frac{\Gamma\cos kr_{ji}}{kr_{ji}} \quad \text{and} \quad \Delta_{jj} = 0 \\
\Gamma_{j\neq i} &= \frac{\Gamma\sin kr_{ji}}{kr_{ji}} \quad \text{and} \quad \Gamma_{jj} = \Gamma
\end{aligned}} \tag{5.125}$$

with $r_{ji} = |\mathbf{r}_j - \mathbf{r}_i|$.

Assuming $\Delta_{ji} = 0 = \Gamma_{ji}$ and $\Omega(\mathbf{r}_j) = \Omega$ we recover the mean-field Dicke model, where interaction terms are completely neglected,

$$\hat{H} = -\Delta_a \sum_j \hat{\sigma}_j^+\hat{\sigma}_j^- + \tfrac{1}{2}\Omega\sum_j(\hat{\sigma}_j^+ + h.c.)\ . \tag{5.126}$$

In principle, the collective many-atom system (5.125) can be mapped to a single-atom multilevel system,

$$\frac{d}{dt}\hat{\vec{\varrho}} = \mathcal{M}\vec{\varrho}\ , \tag{5.127}$$

which is more amenable to numeric simulation using the methods presented in Sec. 2.4.3. However, analytically this is only simple to do in the case of two atoms, which can be mapped to a four-level system.

Example 22 (*Two atoms with dipole-dipole interactions*): For the case of only two atoms located at $\mathbf{r}_j$, using an appropriate basis, we find the Hamiltonian [24],

$$\hat{H} = \begin{pmatrix} 0 & \frac{1}{2}\Omega^*(\mathbf{r}_2) & \frac{1}{2}\Omega^*(\mathbf{r}_1) & 0 \\ \frac{1}{2}\Omega(\mathbf{r}_2) & -\Delta_a & \frac{1}{2}\Delta_{21} & \frac{1}{2}\Omega^*(\mathbf{r}_1) \\ \frac{1}{2}\Omega(\mathbf{r}_1) & \frac{1}{2}\Delta_{12} & -\Delta_a & \frac{1}{2}\Omega^*(\mathbf{r}_2) \\ 0 & \frac{1}{2}\Omega(\mathbf{r}_1) & \frac{1}{2}\Omega(\mathbf{r}_2) & -2\Delta_a \end{pmatrix}\ , \tag{5.128}$$

[12] See script on *Quantum mechanics* (2023), Sec. 18.1.2.

with $\Omega(\mathbf{r}) = \Omega_0 e^{\imath \mathbf{k}\cdot\mathbf{r}_j}$. For two atoms the master equations (5.125) can easily be solved numerically by setting [13],

$$\hat{\sigma}_1^{\pm} = \hat{\sigma}^{\pm} \otimes \mathbb{I} \quad \text{and} \quad \hat{\sigma}_2^{\pm} = \mathbb{I} \otimes \hat{\sigma}^{\pm} \ , \tag{5.129}$$

as usual and,

$$\langle i, j|\hat{\rho}|m, n\rangle = \rho_{ij,mn} \ , \tag{5.130}$$

where the indices $i, m = 1, 2$ refer to the first atom and the indices $j, n = 1, 2$ to the second. The populations of the Dicke states $|11\rangle$, $|12\rangle$, $|21\rangle$, and $|22\rangle$ are then given by $\rho_{ij,ij}$, and the populations of the (anti-)symmetric states $|\psi\rangle^{(s,a)} = \frac{1}{\sqrt{2}}(|1, 2\rangle \pm |2, 1\rangle)$ are calculated via,

$$\langle\psi|^{(s,a)}\hat{\rho}|\psi\rangle^{(s,a)} = \tfrac{1}{2}(\rho_{12,12} \pm \rho_{12,21} \pm \rho_{21,12} + \rho_{21,21}) \ . \tag{5.131}$$

The temporal evolution of the populations in one and two atom systems, initially driven by a laser field which is then suddenly switched off, is shown in Fig. 5.17. Note that super and subradiance do occur for $\Delta_{12} = 0 = \Delta_a$ but necessitate $\Gamma_{ij} \neq 0$.

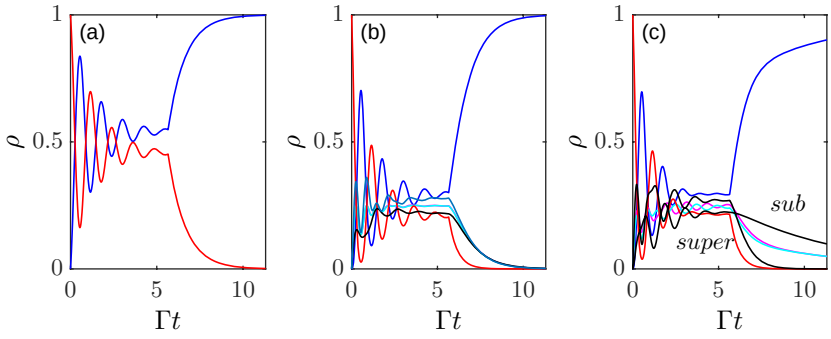

Figure 5.17: (code for download) (a) Response of a single two-level atom driven by a laser light with $\Omega = 5\Gamma$, $\Delta = -\Gamma$. The curves show (blue) the ground state and (red) the excited state populations. The light is switched off at $\Gamma t = 0.5$. (b) Response of two atoms $j = 1, 2$ located at $kz_j = \pm 5$ driven by the same laser light as in (a). (cyan and magenta) populations of the states $|eg\rangle$ and $|ge\rangle$. The two black lines show the populations of the (anti-)symmetric states $\frac{1}{\sqrt{2}}(|eg\rangle \pm |ge\rangle)$. (c) Same as (c) but with $kz_j = \pm 0.5$.

In Exc. 5.6.0.19 we study the impact of dipole-dipole interactions on super- and subradiance and in Exc. 5.6.0.20 we study three interacting two-level atoms.

5.5.3 Cavity-mediated spin-exchange interactions

In the preceding sections we got to know two fundamentally different types of interatomic interactions, that is, Rydberg and dipole-dipole type interactions. Both are generally nearest neighbor interactions and thus inhomogeneous. Let us nevertheless make the assumption of uniform coupling to simplify the discussion. Then the

[13] Remember, that the formal solution of coherent part of the master equation can be written as $\hat{\rho}(t) = \mathcal{L}(t)\hat{\rho}(0) = e^{-\imath\hat{H}t}\hat{\rho}(0)e^{\imath\hat{H}t}$.

Rydberg blockade term (5.122) reads,

$$\hat{H} = \tfrac{1}{2}\sum_{i\neq j}\kappa_{ij}\hat{\sigma}_j^z\hat{\sigma}_i^z \simeq \kappa\hat{S}_z^2 \ , \tag{5.132}$$

and the Ising interaction term (5.124), respectively (5.125), becomes,

$$\hat{H}_{Ising} = -\sum_{i\neq j}V_{ij}\hat{\sigma}_j^+\hat{\sigma}_i^- \simeq -V\hat{S}_+\hat{S}_- \ . \tag{5.133}$$

A way of achieving uniform coupling consists in coupling all atoms with the same strength to the same cavity mode. This is what we will discuss in the next subsection..

5.5.3.1 Adiabatic elimination of the modes of a bad high-finesse cavity

We consider again the Heisenberg-Liouville equations (5.114) derived from the open Dicke model and the open Tavis-Cummings model Hamiltonian, restricting to many immobile atoms and a single cavity mode. In the bad cavity limit, $\kappa \gg g$, the cavity field is effectively slaved to the internal atomic dynamics. Hence, we may assume $\dot{\hat{a}} \equiv 0$ and adiabatically eliminate the field,

$$g\hat{a} = \frac{-2\imath g^2}{\kappa - \imath\Delta_c}\hat{S}_- = -2\imath(\kappa_c + \imath U_c)\hat{S}_- \ . \tag{5.134}$$

where we additionally assumed $\eta \equiv 0$ and introduced the abbreviations,

$$U_c \equiv \frac{g^2\Delta_c}{\Delta_c^2+\kappa^2} \qquad \text{and} \qquad \kappa_c \equiv \frac{g^2\kappa}{\Delta_c^2+\kappa^2} \ .$$

U_c is the cooperative cavity Lamb-shift and κ_c is the Purcell-enhanced atomic decay rate. Inserting this into the above Heisenberg-Liouville equations of the Dicke model (5.114) without RWA, $g' = g$, we obtain neglecting Γ,

$$\dot{\hat{\mathbf{S}}} = \begin{pmatrix} -16\kappa_c\hat{S}_y + 16U_c\hat{S}_x \\ 0 \\ -\Delta_a \end{pmatrix} \times \hat{\mathbf{S}} \ . \tag{5.135}$$

Inserting this into the above Heisenberg-Liouville equations of the Tavis-Cummings model (5.114) with RWA, $g' = 0$, we obtain neglecting Γ,

$$\dot{\hat{\mathbf{S}}} = \begin{pmatrix} -8\kappa_c\hat{S}_y + 8U_c\hat{S}_x \\ 8\kappa_c\hat{S}_x + 8U_c\hat{S}_y \\ -\Delta_a \end{pmatrix} \times \hat{\mathbf{S}} \ . \tag{5.136}$$

Alternatively, as studied in Exc 5.6.0.21, we may use the adiabatic elimination to simplify the Hamiltonians of the respective models and derive the Heisenberg-Liouville equations from these Hamiltonians [116]. E.g. for the Tavis-Cummings model, we get,

$$\hat{H}_{TC} = 4U_c\hat{S}_+\hat{S}_- - \Delta_a\hat{S}_z \ . \tag{5.137}$$

This is the effective Hamiltonian of the *XX-Heisenberg model*.

5.6 Exercises

5.6.0.1 Ex: Quick ullage of an optical cavity

Consider a linear cavity resonantly pumped by a laser beam until a stationary state is reached. Suddenly, the phase of the incident light is changed by 180°. Based on equation (5.5), analyze the evolution of the light field inside the cavity.

5.6.0.2 Ex: Ringing of an optical cavity

Consider a linear cavity with resonant frequency ω_c and the decay rate κ pumped by a laser beam whose frequency is swept linearly over a range $\omega \in [-10\kappa, 10\kappa]$. Prepare a numerical simulation varying the time Δt of the sweep.

5.6.0.3 Ex: Derivation of the Airy formula

Derive the Airy formula (5.16).

5.6.0.4 Ex: Cooperative amplification for a rubidium gas in a cavity

Consider an non-degenerate cavity characterized by $\delta_{fsr} = 2\,\text{GHz}$, $F = 80$, and $w_0 = 6\,\mu\text{m}$. In order to benefit from the cooperativity of the cavity, the atoms must be within a volume axially delimited by the Rayleigh length and radially by the diameter of the mode near its waist.
a. Calculate the Rayleigh length for a wavelength of 780 nm and the mode volume.
b. For a given partial pressure of rubidium at room temperature of $p \approx 10^{-5}\,\text{Pa}$, calculate the average number of atoms within the mode volume.
c. Of these atoms only those with an axial Doppler shift below $kv_z < \kappa$ emit resonantly into the cavity. Calculate the number of these atoms from the Maxwell-Boltzmann distribution.
d. Calculate the cooperative amplification of the emission rate into the cavity.

5.6.0.5 Ex: Characteristic parameters for various atom-cavity systems

Complete the following table calculating κ, V_m, ω_r, g_1, Υ, s, and r,

	rubidium	strontium
Γ	6 MHz	6.8 kHz
F	250000	250000
L	100 µm	3 cm
w_0	20 µm	70 µm

5.6.0.6 Ex: Number of photons in a cavity

a. How many photons are in the mode of a cavity with finesse $F = 80000$ (i) in resonance and (ii) out of resonance resonantly pumped with a laser power of $P_{in} = 100\,\mu\text{W}$?
b. What power must be injected to produce 1 photon inside the cavity?
c. Resonant backscattering by the cavity mirrors can scatter photons into the reverse mode. Typically, $P_-/P_+ \simeq 0.005$. Hence, $n^{on}_{-,cav} = 1.5\times10^7$ and $n^{off}_{-,cav} = 0.01$. Using

advanced techniques it is possible to reduce the number of backscattered photons by factor of > 20. Assuming that the losses due to backscattering are $S = 1$ ppm. Can the resonant backscattering by the mirrors destroy a BEC?
d. What is the amplitude of the output signal in terms of photons?

5.6.0.7 Ex: Saturation-induced bistability in a linear cavity

a. Write down the expression (5.63) for $n = |\alpha|^2$ for the case of strong saturation and resonant excitation, $\Delta_c = 0 = \Delta_a$, in terms of the single-atom cooperativity parameter $\Upsilon \equiv 4g^2/\gamma\Gamma$ and the single-photon saturation parameter $s_1 \equiv 8g^2/\Gamma^2$.
b. How does the result generalize in the case of N uncorrelated atoms.

5.6.0.8 Ex: Coherent spin states

Show that the coherent spin state is an eigenstate of the operator $\hat{S}_{\vartheta,\varphi} \equiv \hat{S}_x \sin\vartheta\cos\varphi + \hat{S}_y \sin\vartheta\sin\varphi + \hat{S}_z\cos\vartheta$.

5.6.0.9 Ex: Collective spin of a coherent spin state

a. Calculate the expectation values for all spin components of the collective spin $\hat{\mathbf{S}}$ in a coherent spin state.
b. Calculate the uncertainties for all spin components of the collective spin $\hat{\mathbf{S}}$ in a coherent spin state and check the uncertainty relation.

5.6.0.10 Ex: Spin operators for two atoms

Calculate explicitly for the case of two atoms the rotation matrices $e^{\imath\gamma\hat{S}_\alpha}$ for $\alpha = x, y, z$. Check the relationship $e^{\imath\gamma\hat{S}_\alpha}\hat{\mathbf{S}}e^{-\imath\gamma\hat{S}_\alpha} = R_\alpha(\gamma)\hat{\mathbf{S}}$ by explicit calculation.

5.6.0.11 Ex: Spin squeezing

a. Calculate $\langle\frac{\pi}{2},0|^N e^{\imath\zeta\hat{S}_z^2}\hat{\mathbf{S}}e^{-\imath\zeta\hat{S}_z^2}|\frac{\pi}{2},0\rangle^N$.
b. Calculate $\langle\frac{\pi}{2},0|^N e^{\imath\zeta\hat{S}_z^2}\Delta\hat{S}^2_{x,y,z}e^{-\imath\zeta\hat{S}_z^2}|\frac{\pi}{2},0\rangle^N$.

5.6.0.12 Ex: Spin squeezing with two atoms

a. For a system of two atoms, write down the coherent state $|\vartheta,\varphi\rangle^2 = |\frac{\pi}{2},0\rangle^2$ in the Tavis-Cummings basis and in the Dicke state basis.
b. Derive the matrix representation for the squeezing operator along the z-axis and apply this operator to the above coherent spin state.
c. Compare spin squeezing with entanglement.

5.6.0.13 Ex: Entanglement criteria

A sufficient entanglement criterion for an N-qubit state is, that it violates one of the following inequalities [146, 147],

$$\begin{aligned}
\frac{\langle \Delta \hat{S}_z^2 \rangle}{\langle \hat{S}_x \rangle^2 + \langle \hat{S}_y \rangle^2} &\geq \frac{1}{N} \\
\langle \hat{S}_x^2 \rangle + \langle \hat{S}_y^2 \rangle + \langle \hat{S}_z^2 \rangle &\leq \tfrac{N(N+2)}{4} \\
\langle \Delta \hat{S}_x^2 \rangle + \langle \Delta \hat{S}_y^2 \rangle + \langle \Delta \hat{S}_z^2 \rangle &\geq \tfrac{N}{2} \\
\langle \hat{S}_k^2 \rangle + \langle \hat{S}_m^2 \rangle - \tfrac{N}{2} &\leq (N-1) \langle \Delta \hat{S}_n^2 \rangle \\
(N-1)[\langle \Delta \hat{S}_k^2 \rangle + \langle \Delta \hat{S}_m^2 \rangle] &\geq \langle \hat{S}_k^2 \rangle + \tfrac{N(N-2)}{4} \ ,
\end{aligned}$$

for $(kmn) = (123)$. Verify that, according to these criteria, coherent Dicke states are not entangled.

5.6.0.14 Ex: Heisenberg equation for the open Dicke model

Derive the Heisenberg equation for the open Dicke model.

5.6.0.15 Ex: Spin conservation in the open Dicke model

a. Show that the Dicke Hamiltonian (5.112) with $g' = g$ preserves the spin $\hat{\mathbf{S}}^2$.
b. Show that the Dicke Hamiltonian (5.112) with $g' = 0$ preserves the spin $\hat{\mathbf{S}}^2$.
c. Verify whether the dissipative terms of the open Dicke model preserve the spin $\hat{\mathbf{S}}^2$.

5.6.0.16 Ex: Superradiant enhancement

For the open Dicke model consider the Heisenberg equations (5.113) without coherent mean-field, $\hat{a} = 0$, and disregarding single-atom decoherence, $\gamma_1 = \xi_1 = \beta_1 = 0$. Solve the equation of motion for the collective spin projection $\hat{S}_z$ for an arbitrary coherent spin state $|S, M\rangle$ and discuss the collective decay rate as a function of the collective inversion $\langle \hat{S}_z \rangle$.

5.6.0.17 Ex: Equilibrium phase transition

a. Calculate the free energy of the Hamiltonian (5.73) in the mean-field approximation.
b. Minimize the free energy as a function of the field amplitude α for various coupling strengths g. **Help:** Expand the expression for $F'(\alpha)$ for small values of α. Derive the expression for the critical coupling strength.

5.6.0.18 Ex: Superradiant lasing

a. Consider the generalized open Dicke model Hamiltonian (5.112) neglecting counter-rotating terms, $g' \equiv 0$, as well as pumping and phase fluctuations of the cavity modes, $\eta = \phi \equiv 0$. Derive the Heisenberg equations for the operators $\hat{a}$, $\hat{s}_j^-$, $\hat{s}_j^z$, $\hat{a}^\dagger \hat{s}_j^-$, $\hat{s}_i^+ \hat{s}_j^-$, and $\hat{a}^\dagger \hat{a}$.
b. Calculate the expectation values of the equations of motion for all degrees of freedom and for the products specified in (a) assuming that all atoms are equal. Now,

assume that the phase-invariance is not broken, $\langle \hat{a} \rangle = \langle \hat{a}^\dagger \rangle = \langle \hat{s}_1^\pm \rangle = 0$, and apply a cumulant expansion up to second order.
c. Assuming the system to be in steady state solve the system of equations for the operators and products specified in (a) analytically. Assume $\gamma_1 \ll g \ll \kappa$ and plot $\hat{a}^\dagger \hat{a}$ as a function of the atom number N and the optical pumping rate ξ_1.
d. In which parameter regimes do you observe superradiant lasing?
e. Express $\langle \hat{\mathbf{S}}^2 \rangle$ and $\langle S_z \rangle$ in terms of single particle spin operators.
f. Evaluating $\langle \mathbf{S}^2 \rangle$ and $\langle S_z \rangle$ via the solution of the equations of motion, we find the steady-state quantum numbers always around $M \simeq \pm S$ [43]. Explain how this fact can induce squeezing, once $\langle S_z \rangle > 0$.

5.6.0.19 Ex: Impact of dipole-dipole interactions on super- and subradiance

Here, we use the two-atom toy model studied in Fig. 5.17 to demonstrate the emergence of subradiant modes as a consequence of dipole-dipole interaction [47]. Calculate numerically the anti-symmetric state population $\hat{\rho}_A$ given in Eq. (5.131) at very long times as a function of the saturation parameter s and the interatomic distance kr_{ij}. Interpret the results.

5.6.0.20 Ex: Three interacting atoms

Numerically integrate the master equation (5.125) for three atoms.

5.6.0.21 Ex: Open system Hamiltonians after adiabatic elimination of the cavity mode

Use the adiabatic elimination of the cavity mode to simplify the Hamiltonians of the respective models and derive the Heisenberg-Liouville equations from these Hamiltonians.

5.7 Further reading

F. Albarelli et al., *Nonlinearity as a resource for nonclassicality in anharmonic systems* [DOI]

K. Baumann et al., *Dicke quantum phase transition with a superfluid gas in an optical cavity* [DOI]

J.G. Bohnet et al., *Reduced spin measurement back-action for a phase sensitivity ten times beyond the standard quantum limit* [DOI]

Ph. Bouyer et al., *Heisenberg-Limited Spectroscopy with Degenerate Bose-Einstein Gases* [DOI]

A. Bychek et al., *Superradiant lasing in inhomogeneously broadened ensembles with spatially varying coupling* [DOI]

K. Cox et al., *Deterministic Squeezed States with Collective Measurements and Feedback* [DOI]

K. Debnath et al., *Lasing in the superradiant crossover regime* [DOI]

R.G. DeVoe et al., *Observation and Superradiant and Subradiant Spontaneous Emission of Two Trapped Ions* [DOI]

R.H. Dicke, *Coherence in Spontaneous Radiation Processes* [DOI]

J. Eschner et al., *Light interference from single atoms and their mirror images* [DOI]

Z. Ficek et al., *Effect of interatomic interactions on resonance fluorescence of two atoms coherently driven by strong resonant laser field* [DOI]

C.W. Gardiner et al., *A multimode quantum theory of a degenerate parametric amplifier in a cavity* [DOI]

B.M. Garraway, *The Dicke model in quantum optics: Dicke model revisited* [DOI]

M. Gegg et al., *Superradiant to subradiant phase transition in the open system Dicke model: dark state cascades* [DOI]

K. Gietka et al., *Quantum-enhanced interferometry with cavity QED-generated nonclassical light* [DOI]

W. Guerin, *Subradiance in a Large Cloud of Cold Atoms* [DOI]

D.J. Heinzen et al., *Enhanced and Inhibited Visible Spontaneous Emission by Atoms in a Confocal Resonator* [DOI]

D.J. Heinzen et al., *Vacuum Radiative Level Shift and Spontaneous-Emission Linewidth of an Atom in an Optical Resonator* [DOI]

A.F. Huss et al., *Phase Correlation of Laser Waves with Arbitrary Frequency Spacing* [DOI]

P. Kirton et al., *Introduction to the Dicke Model: From Equilibrium to Nonequilibrium, and Vice Versa* [DOI]

M. Kitagawa et al., *Spin-squeezed states* [DOI]

P. Lambropoulos et al., *Fundamental quantum optics in structured reservoirs* [DOI]

I.D. Leroux et al., *Implementation of Cavity Squeezing of a Collective Atomic Spin* [DOI]

U. Leonhardt et al., *Measuring the quantum state of light* [DOI]

U. Leonhardt, *Quantum physics of simple optical instruments* [DOI]

R. Loudon et al., *Squeezed light* [DOI]

B.M. Peden et al., *Nondestructive cavity QED probe of Bloch oscillations in a gas of ultracold atoms* [DOI]

D. Meiser et al., *Prospects for a Millihertz-Linewidth Laser* [DOI]

Th. Maier et al., *A superradiant clock laser on a magic wavelength optical lattice* [DOI]

M.A. Norcia et al., *Superradiance on the millihertz linewidth strontium clock transition* [DOI]

M.A. Norcia et al., *Cold-Strontium Laser in the Superradiant Crossover Regime* [DOI]

M.A. Norcia et al., *Cavity-mediated collective spin-exchange interactions in a strontium superradiant laser* [DOI]

M. Reitz et al., *Cooperative Quantum Phenomena in Light-Matter Platforms* [DOI]

L. Salvi et al., *Squeezing on Momentum States for Atom Interferometry* [DOI]

M. Schleier-Smith et al., *Squeezing the collective spin of a dilute atomic ensemble by cavity feedback* [DOI]

M. Schubert et al., *Photon antibunching and non-Poissonian fluorescence of a single three-level ion* [DOI]

M. Tavis et al., *Exact solution for an N-molecule-radiation-field Hamiltonian* [DOI]

D.J. Wineland et al., *Squeezed atomic states and projection noise in spectroscopy* [DOI]

Chapter 6

Bonus: Atomic motion in optical lattices and cavities

In this lecture, we will apply the notions acquired during the previous lectures to understand some pecularities of the motion of atoms interacting with periodically modulated light fields and/or the modes of an optical cavity pumped by lasers. We will restrict to one-dimensional systems, e.g. standing wave light fields generated by two counterpropagating laser fields.

In free space, as discussed in Lecture 3, the force of light has two components: the radiation pressure, which scatters photons isotropically into space, and the dipole force, which can be interpreted in terms of a redistribution of photons between light modes. In cavities, where the isotropic scattering is much reduced, because the density-of-modes is concentrated around the optical axis, radiative pressure can often be neglected. On the other hand, the atom will feel a dipole force originating from the backscattering of photons between counterpropagating modes, even if the light is tuned away from atomic resonances.

In Sec. 6.1, we will discuss the phenomenon of Bloch oscillations observed with ultracold atoms interacting with a standing wave light field and subject to an external force. Then, we will turn our attention to atoms interacting with an optical ring cavity, deriving the equations of motion in Sec. 6.2, studying self-organization phenomena in the regime of classical motion in Sec. 6.3, and of quantized motion in Sec. 6.4.

6.1 Atoms in an optical standing wave

We derived the optical potential for a standing wave configuration in (4.55). Neglecting the radial atomic motion, $x = 0 = y$, we may restrict ourselves to a one-dimensional periodic potential, $V(z) = V(z + a)$. Such a potential can be generated by two counterpropaganting plane wave laser beams with wavevectors k_L and $-k_L$ and tuned to the red side of an atomic transition. In this situation the atoms are attracted to the maxima of the light intensity, the antinodes. Therefore, we can write the potential as $V(z) = -\frac{V_0}{2}|e^{\imath k_L z} + e^{-\imath k_L z}|^2 = -V_0(1 + \cos 2k_L z)$ or, by letting $K = 2k_L$ [1],

$$V(z) = -2V_0 \cos^2 Kz \ . \tag{6.1}$$

[1] See script on *Quantum mechanics* (2023), Sec. 6.1.3.

In the Fourier expansion, $V(z) = \sum_K U_K e^{\imath K z}$, this potential corresponds to the Fourier coefficients $U_0 = -V_0$ and $U_{\pm K} = -\frac{V_0}{2}$,

$$V(z) = -V_0(1 + \tfrac{1}{2}e^{2\imath k_L z} + \tfrac{1}{2}e^{-2\imath k_L z}) \ . \tag{6.2}$$

We also expand the wavefunction into plane waves,

$$\psi(z) = \sum_q c_q e^{\imath q z} \ , \tag{6.3}$$

and we insert these expansions into Schrödinger's stationary equation,

$$\hat{H}\psi = \varepsilon\psi \ , \tag{6.4}$$

yielding,

$$\left[\frac{-\hbar^2}{2m}\frac{\partial^2}{\partial z^2} + \sum_K U_K e^{\imath K z}\right]\sum_q c_q e^{\imath q z} = \varepsilon\sum_q c_q e^{\imath q z} \ . \tag{6.5}$$

Defining $q = k + nK$, where $k \in [-K/2, K/2]$ and $n \in \mathbb{Z}$,

$$\left[\tfrac{\hbar^2}{2m}(nK+k)^2 - V_0\right] c_{nK+k} - \tfrac{1}{2}V_0 c_{nK+k-K} - \tfrac{1}{2}V_0 c_{nK+k+K} = \varepsilon c_{nK+k} \ . \tag{6.6}$$

In matrix notation,

$$\hat{H}\mathbf{c} = \varepsilon\mathbf{c} \ . \tag{6.7}$$

where the matrix is around $n = .., -1, 0, +1, ..$:

$$\hat{H} = \begin{pmatrix} \ddots & & & & & \\ & \frac{\hbar^2}{2m}(k-K)^2 - V_0 & -\frac{1}{2}V_0 & & & \\ & -\frac{1}{2}V_0 & \frac{\hbar^2}{2m}k^2 - V_0 & -\frac{1}{2}V_0 & & \\ & & -\frac{1}{2}V_0 & \frac{\hbar^2}{2m}(k+K)^2 - V_0 & & \\ & & & & \ddots & \end{pmatrix} \quad , \quad \mathbf{c} = \begin{pmatrix} \vdots \\ c_{k-K} \\ c_k \\ c_{k+K} \\ \vdots \end{pmatrix} . \tag{6.8}$$

For shallow potentials, $V_0 \ll \hbar^2K^2/2m$, we can neglect the coefficients V_0 in the Eq. (6.6) and we find,

$$\varepsilon \simeq \hbar^2 q^2/2m \ , \tag{6.9}$$

which corresponds to the dispersion relation for free particles. On the other hand, looking *at the bottom* of deep potentials, $V_0 \gg \hbar^2K^2/2m$, we can harmonically approximate the cosine potential by $V(z) \simeq -2V_0 + \frac{m}{2}\omega^2 z^2$ with $\omega = K\sqrt{V_0/m} = \hbar^{-1}\sqrt{2V_0E_r}$. For this case we expect,

$$\varepsilon \simeq -2V_0 + \hbar\omega\left(n + \tfrac{1}{2}\right) \ . \tag{6.10}$$

The exact spectrum of eigenvalues ε can be calculated by numerically determining the eigenvalues of the matrix (6.8) for the first Brillouin zone, $k \in [-K/2, K/2]$, and the above limits are confirmed.

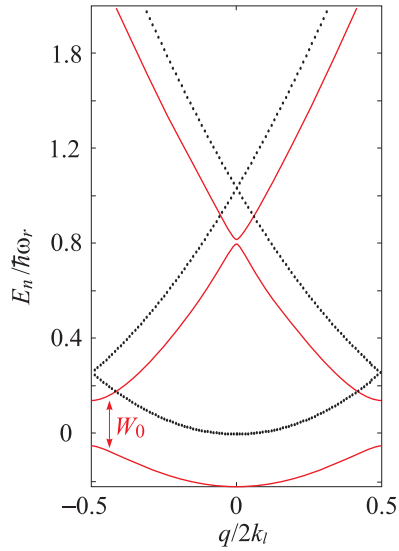

Figure 6.1: (code for download) Bloch bands with coupling potential (continuous red line) and without potential, $V_0 = 0$ (dotted black line). The parameters are $\omega_r = (2\pi)\ 20\,\text{kHz}$, $\omega_{ho} = (2\pi)\ 12\,\text{kHz}$, $\lambda_L = 689\,\text{nm}$, and $V_0 = 0.2\hbar\omega_r$.

To estimate the width of the forbidden band, we cut out a 2×2 matrix within the matrix $\hat{H}$ and neglect its coupling with the others submatrices,

$$\hat{H}_s = \begin{pmatrix} \frac{\hbar^2}{2m}(k-K)^2 - V_0 & -\frac{1}{2}V_0 \\ -\frac{1}{2}V_0 & \frac{\hbar^2}{2m}k^2 - V_0 \end{pmatrix} . \tag{6.11}$$

At the edges of the Brillouin zone, $k = \frac{1}{2}K$, we get the eigenvalues,

$$\varepsilon(\pm\tfrac{1}{2}K) = \frac{\hbar^2 K^2}{m} - V_0 \pm \frac{V_0}{2} , \tag{6.12}$$

that is, the band gap is $\Delta\varepsilon = V_0$ [2]. Bloch's theorem says that Schrödinger's equation can be solved for any *Bloch state*s. These are superpositions of plane wave momentum states [8],

$$\psi_k(z) = e^{\imath kz} u_k(z) , \tag{6.13}$$

with $u_k(z) = u_k(z + a)$.

6.1.1 Bloch oscillations

A *Bloch oscillation* is a phenomenon first predicted in solid state physics. It is the oscillation of a particle (e.g., an electron) confined to a periodic potential (e.g., a crystal), when a constant force (e.g., generated by a continuous electric field) acts on it. This phenomenon is very difficult to observe in solid crystals because, due to

[2] For Bose-Einstein condensates, the procedure should be generalized taking into account the energy of the mean field.

electron scattering by defects of the lattice [36, 117], the coherent evolution is limited to a small fraction of the Brillouin zone. However, Bloch oscillations were observed in semiconducting superlattices, in ultrathin *Josephson junction*s and with cold atoms in optical lattices [77, 105].

Neutral atoms in a lattice can be accelerated by gravitation. The Bloch oscillations can be understood in various pictures. The first one, illustrated in 6.2(a), is as *Bragg reflection*: Being constantly accelerated, the matter wave reduces its de Broglie wavelength from ∞ to a value, where it is commensurable with the periodicity of the standing light wave potential. At this moment Bragg reflection comes into play scattering the atoms back.

How does the matter wave interact with the standing light wave? This is only possible if the atom has an internal transition capable of scattering photons from the light beams. As any absorption and emission process transfers a recoil momentum to the atom, we can understand the Bragg scattering process as a Raman scattering process: a photon of the laser beam generating the optical lattice coming from the left is absorbed and re-emitted to the left. This is best illustrated in the momentum domain sketched in Fig. 6.2(b). This Raman scattering transfers twice the photonic recoil to the atom. The requirement for commensurability of the Broglie wavelength and wavelength of the standing light wave is equivalent to saying that the matter wave momentum is equal to the recoil of a single photon. In other words, the matter wave always Bragg-reflected at the edge of a Brillouin zone.

In the Bloch picture, the dispersion relation of a free particle is distorted due to the periodicity of the potential generated by the standing light wave such as to open a forbidden band. As a consequence, instead of being accelerated without limits, the atom enters the second Brillouin zone, which is to say that it is reflected to the other side of the first Brillouin zone.

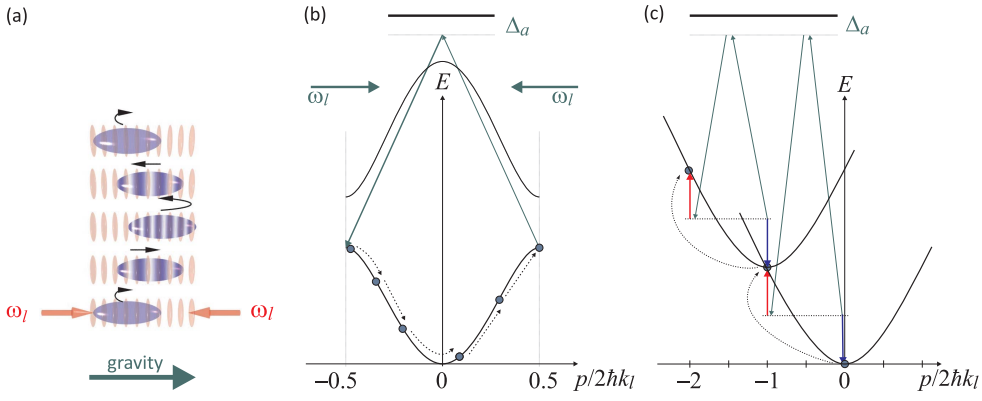

Figure 6.2: Illustration of Bloch oscillations (a) in real space, (b) in momentum space, and (c) in the moving frame.

To reproduce the dynamics of the matter wave, we start from the time-dependent Schrödinger equation with the same periodic potential, and we also allow for an

external force whose potential can be added to Schrödinger's potential,

$$i\hbar\frac{\partial\psi}{\partial t} = -\frac{\hbar^2}{2m}\frac{\partial^2\psi}{\partial x^2} + \frac{\hbar W_0}{2}\sin(2k_l x)\psi - mgx\psi \ . \tag{6.14}$$

The additional term can be removed by a Galilei transformation into the moving frame via $e^{imgxt/\hbar}$ [3]. We now expand the time-dependent wavefunction into plane waves,

$$\psi(x,t) = \sum_{n=-\infty}^{\infty} c_n(t) e^{2\imath n k_l x} \cdot e^{\imath mgxt/\hbar} \ . \tag{6.15}$$

By inserting this ansatz into the Schrödinger equation, we obtain a set of equations for the expansion coefficients c_n,

$$\frac{dc_n}{dt} = -4\imath\omega_r(n+\nu_b t)^2 c_n + \tfrac{W_0}{2}(c_{n+1} - c_{n-1}) \ , \tag{6.16}$$

with the usual definition of the recoil frequency $\omega_r = \frac{\hbar k_l^2}{2m}$. The additional term, which contains the frequency of the Bloch oscillation,

$$\nu_b = \frac{g}{\omega_r} \ , \tag{6.17}$$

increases linearly over time. A resonance is crossed each time when $t = -n\tau_b$, and the crossing is periodically repeated at every $n = -1, -2, 0, ...$

Tracing the matter wave evolution in the laboratory system, which can be done by numerical simulation, we see that whenever the resonance is crossed, the momentum undergoes a change of sign corresponding to a reflection of its motion. We expand the population of the momentum states into plane (Bloch) waves with $|c_n(t)|^2$ [133, 134] and the center-of-the mass momentum is,

$$\langle p\rangle_{lab} = \sum_n n|c_n(t)|^2 + \nu_b t \tag{6.18}$$

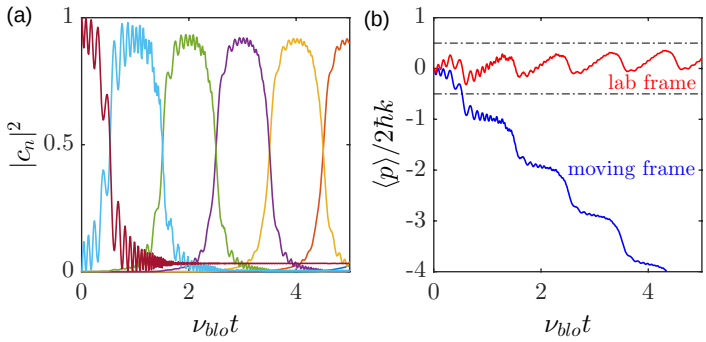

Figure 6.3: (code for download) Dynamics of Bloch's oscillations.

[3] See script on *Quantum mechanics* (2023), Sec. 2.5.2.

Of course there are some conditions that need to be met to observe Bloch oscillations. The transfer of momentum is efficient only in the rapid adiabatic passage (ARP) regime characterized by the conditions $2(\nu_b/\omega_r) \ll (W_0/4\omega_r)^2 \ll 16$. The first condition requires that the force that drives the atoms to perform the Bloch oscillations must be weak enough to avoid transitions between Bloch bands, which guarantees the adiabaticity of the process. The other condition requires that the optical lattice be weak enough so that the dynamics involves only two adjacent momentum states at the same time and the transfer between the two is successful.

6.2 Cavity interacting with a single atom

Standing light waves, such as the one discussed, above can also be realized in optical cavities. We must distinguish two types of cavities with very different behaviors: The linear cavity or (*Fabry-Pérot etalon*) illustrated in Fig. 1.6, where counterpropagating modes form a single mode, and the *ring cavity* illustrated in Fig. 6.4, where counterpropagating modes have independent photon budgets, so that we thus must distinguish the counterpropagating modes $\hat{a}_\pm$,

$$\hat{\vec{\mathcal{E}}}^+(z,t) = \mathcal{E}_1 \hat{a}_+(t) e^{\imath kz} + \mathcal{E}_1 \hat{a}_-(t) e^{-\imath kz} = (\hat{\vec{\mathcal{E}}}^-(z,t))^\dagger \ . \tag{6.19}$$

For a ring cavity (which we will focus on from now on), the total Hamiltonian $\hat{H}$ consists of the following parts ($\hbar = 1$),

$$\boxed{\begin{aligned} \hat{H}_{atom} &= -\Delta_a \hat{\sigma}^+\hat{\sigma}^- + \tfrac{\hat{p}^2}{2m} \\ \hat{H}_{cavity} &= -\Delta_c \hat{a}_+^\dagger \hat{a}_+ - \Delta_c \hat{a}_-^\dagger \hat{a}_- \\ \hat{H}_{atom-cavity} &= g\hat{a}_+^\dagger \hat{\sigma}^- e^{-\imath k\hat{z}} + h.c. + g\hat{a}_-^\dagger \hat{\sigma}^- e^{\imath k\hat{z}} + h.c. \\ \hat{H}_{laser-cavity} &= -\imath\eta_+(\hat{a}_+ - \hat{a}_+^\dagger) - \imath\eta_-(\hat{a}_- - \hat{a}_-^\dagger) \end{aligned}} \ . \tag{6.20}$$

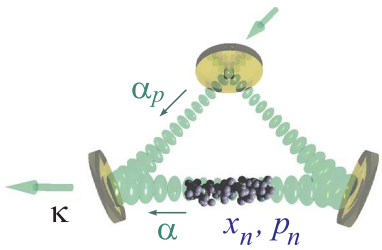

Figure 6.4: Atoms interacting with a ring cavity.

We identify the degrees of freedom of the system through the quantum observables appearing in the Hamiltonian: the counterpropagating modes of light with the amplitudes ($\hat{a}_\pm$), the internal degrees of freedom ($\hat{\sigma}^z, \sigma^\pm$), and the spatial coordinates of the atom ($\hat{z}, \hat{p}$). Each degree of freedom has its own loss mechanism. κ for the finite transmission of the resonator mirrors, Γ for the spontaneous emission, and γ_{frc}, when we exert a frictional force on the atoms.

In contrast to linear cavities, ring cavities have the following particularities: 1. The phase of the standing wave is free to move; 2. the counterpropagating modes of the cavity have independent photon budgets, each backscattering event conserves momentum; 3. the backscattering acts on the phase of the standing wave. Atoms can be trapped by the dipole force within the cavity mode volume. The dipole force corresponds to a backscattering of photons between modes.

6.2.1 Derivation of the CARL equations

Tracing over the vacuum modes responsible for the spontaneous emission and the cavity decay, the Liouville equation turns into a *master equation* with the following form,

$$\begin{aligned}\dot{\hat{\rho}} &= -\imath[\hat{H},\hat{\rho}] + \mathcal{L}_{atom} + \mathcal{L}_{cavity,+} + \mathcal{L}_{cavity,-} \\ \mathcal{L}_{atom}\hat{\rho}(t) &= -\gamma\{\hat{\sigma}^+\hat{\sigma}^-\hat{\rho}(t) - 2\hat{\sigma}^-\hat{\rho}(t)\hat{\sigma}^+ + \hat{\rho}(t)\hat{\sigma}^+\hat{\sigma}^-\} \\ \mathcal{L}_{cavity,\pm}\hat{\rho}(t) &= -\kappa\{\hat{a}_\pm^\dagger\hat{a}_\pm\hat{\rho}(t) - 2\hat{a}_\pm\hat{\rho}(t)\hat{a}_\pm^\dagger + \hat{\rho}(t)\hat{a}_\pm^\dagger\hat{a}_\pm\} \ .\end{aligned} \tag{6.21}$$

To obtain the equations of motion we insert the Hamiltonian (6.20) into the equations for the field operators, for which the following commutation rules hold, $[\hat{a}_\pm,\hat{a}_\pm^\dagger]=1$ and $[\hat{a}_\pm,\hat{a}_\mp^\dagger]=0=[\hat{a}_\pm,\hat{a}_\pm]$ [4].

Under certain conditions, the internal and external dynamics occur at very different time scales, which allows a decoupling of the differential equations [5]. When the light fields are very detuned from atomic resonances, the internal dynamics of the atoms are very fast, that is, the internal state adapts very rapidly to the boundary conditions defined by the external state and the state of the light field. Therefore, the internal state has no separate dynamics of its own, and we can *adiabatically eliminate* the internal degrees of freedom. Thus, neglecting correlations between degrees of freedom, $\hat{a}_\pm\hat{\sigma}^\pm = \hat{a}_\pm\hat{\sigma}^\pm$ etc., we can represent the operators by complex numbers $\alpha_\pm \equiv \hat{a}_\pm$ and $\rho_{eg}=\hat{\sigma}^-$ etc. [118, 63].

For the atomic coherence we solve the Bloch equations for $t\to\infty$ [see Eq. (2.75)],

$$\rho_{eg} = \frac{4g(\Delta+\imath\Gamma)}{4\Delta_a^2+2\Omega^2+\Gamma^2}(e^{\imath kz}\alpha_+ + e^{-\imath kz}\alpha_-) \ . \tag{6.22}$$

$\Omega(z)=g(e^{\imath kz}\alpha_+ + e^{-\imath kz}\alpha_-)$ is the Rabi frequency dependent on the position within the standing wave. Inserting it into the Heisenberg equation for the fields gives, with $|\Delta_a| \gg \Gamma$ [6],

$$\boxed{\begin{aligned}\dot{\alpha}_\pm &= (-\kappa+\imath\Delta_c-\imath U_0)\alpha_\pm - \imath U_0 e^{\mp 2\imath kz}\alpha_\mp + \eta_\pm \\ m\ddot{z} &= 2\imath\hbar k U_0(\alpha_+^*\alpha_- e^{-2\imath kz} - \alpha_+\alpha_-^* e^{2\imath kz})\end{aligned}} \ , \tag{6.23}$$

where we defined the detuning caused by only one photon,

$$U_0 \equiv \frac{g^2}{\Delta_a} \ . \tag{6.24}$$

Recalling that $\alpha_\pm^*\alpha_\pm$ is the number of photons in the respective mode, we can interpret this equation as a rate equation: The number of photons in a mode α_+ changes by photon losses at a rate κ from resonator, or by gain due to backscattering from the counterpropagating mode, or by pumping with an external incident light field at rate η_+.

The equations (6.23) completely describe our coupled atom-cavity system. They are totally classical and work for both, atoms and macroscopic particles.

[4] See script on *Quantum mechanics* (2023), Sec. 19.1.1.1.

[5] In good cavity the limit the degrees of freedom of atomic excitation $\hat{\sigma}^\pm$ drop out of the dynamics, in the bad cavity limit, the fields $\hat{a}^\pm$ drop out of the dynamics.

[6] See script on *Quantum mechanics* (2023), Sec. 19.1.2.

6.2.2 Solutions of the CARL equations

The equations (6.23) treat the coordinates of the atom as dynamic variables influenced by the amplitudes and phases of the light fields. But we can also consider the coordinates being fixed by imposed boundary conditions. This situation occurs, for example, for very heavy scatterers, as in the case of imperfections on the surfaces of the mirrors of the cavity. Such imperfections can scatter light both out of the cavity and into the reverse mode. In *laser gyroscopes* this backscattering may induce a locking of counterpropagating modes and hamper their proper operation.

6.2.2.1 Stationary solutions for immobile atoms

Considering the *atom fixed in space*, $\dot{x} = 0 = \dot{p}$, we can concentrate on solving the equations of motion (6.23) only for the fields. As a first approach, we look for stationary solutions, being aware that they do not always exist, as we will see later in the discussion of the proper CARL effect.

The discussion is left to exercises [7]. In the Exc. 6.5.0.1 we derive the stationary solutions of the equations and in Exc. 6.5.0.2 we calculate the *normal mode splitting* [8] of the cavity resulting from the coupling of the two cavity modes $\hat{a}_+^\dagger \hat{a}_-$. In the Exc. 6.5.0.3 we will calculate the stationary position of the atom in a unidirectionally pumped ring cavity.

6.2.2.2 Simulation of the dynamics for many perfectly bunched atoms

In experiment we generally deal with many atoms, which means that we have to extend the equations of motion (6.23) to N atoms via $z \longrightarrow z_j$ and $p \longrightarrow p_j$, where $j = 1, N$. This will be done in the next section. Here, we will assume for simplicity, that the atoms are perfectly bunched, $z_j = z$ and $p_j = p$. This means that we only need to consider a single equation of motion for the atoms. However, their coupling to the cavity modes is N times stronger, which means that we have to substitute $U_0 \longrightarrow U_N \equiv NU_0$ in the equation of motion for the cavity fields.

In general, the equations can not be solved analytically, especially when the pump varies over time. Then we have to iterate numerically the equations,

$$\begin{aligned} \alpha_\pm(t+dt) &= \alpha_\pm(t) + dt\ \left[-(\kappa + \imath NU_0 - \imath\Delta_c)\alpha_\pm - \imath NU_0 e^{\mp 2\imath kz}\alpha_\mp + \eta(t)\right] \\ z(t+dt) &= z + dt\ \tfrac{1}{m}p \\ p(t+dt) &= p - dt\ 2\imath\hbar k U_0(\alpha_+\alpha_-^* e^{2\imath kz} - \alpha_-\alpha_+^* e^{-2\imath kz})\ . \end{aligned} \tag{6.25}$$

The kinetic and potential energies are [9],

$$E_{kin} = \frac{p^2}{2m} \quad , \quad E_{pot} = U_0 I = U_0|\alpha_+ e^{\imath kz} + \alpha_- e^{-\imath kz}|^2\ . \tag{6.26}$$

[7] See script on *Quantum mechanics* (2023), Sec. 19.1.4.

[8] The splitting is not exactly the *vacuum Rabi splitting*, which occurs when the excitation can not be eliminated adiabatically. The vacuum Rabi splitting results from the Jaynes-Cummings [145, 35] and is caused by the coupling of internal and external states $\hat{a}^\dagger\hat{\sigma}$.

[9] Note, that there is also a radial motion of the atom coupled to the axial movement. The coupling happens, because the axial radial influences the number of intracavity photons of the radiation field which, in turn, determines the depth of the dipole potential.

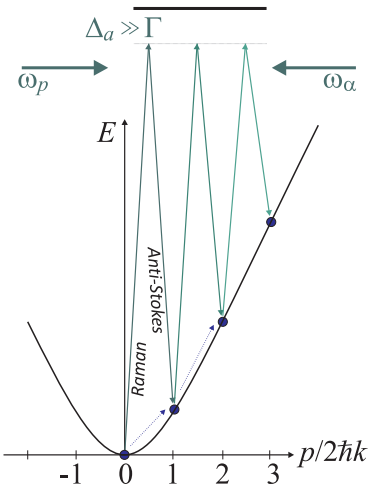

Figure 6.5: In the momentum picture the CARL acceleration process occurs as Raman-anti-Stokes processes along the free-particle dispersion relation.

6.2.2.3 Analytic approximation for perfectly bunched atoms in a unidirectionally pumped ring cavity

When only one atom is in the cavity or when the atoms are perfectly bunched together, it is possible to derive analytical solutions. Particularly interesting is the following situation: We pump the cavity from one side. The pump is supposed to be dominant and locked to a resonance, such that we can neglect the feedback of the system on the pump, that is, we can assume, $\alpha_+ = \eta/\kappa$. Using the abbreviations $\chi \equiv \kappa + iU_0 - i\Delta_c$ and the photon recoil shift [63],

$$\omega_{rec} \equiv \frac{\hbar k^2}{2m} \ , \tag{6.27}$$

the equations (6.23) then become,

$$\boxed{\begin{array}{rcl} \dot{\alpha}_- & = & -\chi\alpha_- - \imath U_N \alpha_+ e^{2\imath kz} \\ k\dot{v} & = & 4\omega_{rec}\imath U_0 \alpha_+ (\alpha_- e^{-2\imath kz} - \alpha_-^* e^{2\imath kz}) \end{array}} \ . \tag{6.28}$$

We consider the stationary case doing the ansatz,

$$\alpha_- \equiv \beta e^{2\imath kx} \qquad \text{where} \qquad \dot{\beta} = 0 \tag{6.29}$$

we assume that the atom and the standing wave have the same velocity, that is, they move in phase. We obtain as solution,

$$\beta = \frac{-\imath U_N \alpha_+}{\kappa + 2\imath kv} \qquad , \qquad k\dot{v} = 8\omega_{rec} U_0^2 \alpha_+^2 \frac{2\kappa}{\kappa^2 + 4k^2 v^2} \ . \tag{6.30}$$

If $\kappa \ll 2kv$, then the differential equation is approximately solved by,

$$(kv)^3 = 3\varepsilon\kappa U_0^2 \alpha_+^2 t \ . \tag{6.31}$$

This means that the CARL frequency, that is, the frequency difference between the emitted probe wave and the incident light, increases temporarily. The frequency corresponds to the double Doppler shift. As the frequency of the probe light gradually shifts away from the cavity resonance, the probe light finally stops being amplified, and the amplitude of the probe field decreases: CARL is only a transient phenomenon. In fact, the behavior described by the equation (6.30) was observed in experiments [97].

Example 23 (*Locking of the pump laser*): In practice the resonant frequency of a cavity fluctuates due to ambient noise. Hence, it is easier, experimentally, to lock the pump laser on a cavity mode, e.g. using the Pound-Drever-Hall method. This means,

$$\alpha_+ = \frac{\eta_+}{\kappa} \ . \tag{6.32}$$

In the presence of atoms, however, the resonant frequency can be shifted due to the refractive index of the atomic cloud [55]. Moreover, the shift depends on the atomic bunching and consequently varies during the dynamics of the CARL. The way the locking circuit works, is to continuously adjust the detuning between the laser and the cavity Δ_c (defined for the empty cavity) such as to maximize the amplitude of the field $|\alpha_+|$ and, hence, the transmission of the cavity filled with atoms. The dynamics of the detuning must be incorporated by an additional equation modeling the action of locking. Now that we know the effect, which an ideal lock should have, we can apply the boundary condition (6.32) and eliminate the pump mode α_+ from the dynamics of the system. That is, the following equations are usually sufficient to describe the CARL:

$$\boxed{\begin{aligned} \dot{\alpha}_- &= (-\kappa + \imath\Delta_c - \imath U_0)\alpha_- - \imath U_0 e^{-2\imath kz}\alpha_+ + \eta_- \\ m\ddot{z} &= 2\imath\hbar k U_0 \alpha_+ (\alpha_- e^{-2\imath kz} - \alpha_-^* e^{2\imath kz}) \end{aligned}} \ . \tag{6.33}$$

The frequency offset of the cavity resonances caused by the atom, U_0, can exceed the width of the cavity κ. From Exc. 6.5.0.1 we know, neglecting $\gamma = 0$,

$$|\alpha_+(\infty)|^2 = \frac{\chi\chi^*}{(\chi^2 + U_0^2)(\chi^{*2} + U_0^2)}\eta_+^2 \ . \tag{6.34}$$

The maxima of $|\alpha_+(\infty)|^2$ as a function of Δ_c give the shifted resonances of the modes.

6.3 CARL: The collective atomic recoil laser

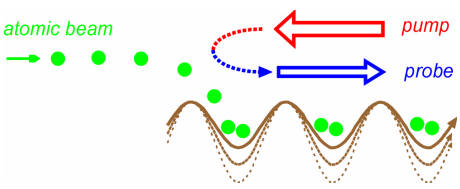

Figure 6.6: Collective atomic recoil laser.

The *collective atomic recoil laser* (*CARL*) was first predicted in 1994 [15] as an atomic analog of FEL. The idea consists of a monochromatic homogeneous beam of moving two-level atoms (all atoms have the same velocity), a strong counterpropagating pump laser beam and a weak copropagating probe beam tuned to the blue side of the resonance. The lasers form a standing

light wave that moves in the same direction as the atoms. Atoms that are faster than the velocity of the standing wave are rejected by the maxima of the dipolar potential created by the standing wave and feel a repulsive force. Atoms that are slower than the standing wave velocity are pushed by the dipole potential maxima and feel an accelerating force. These forces can be interpreted as backscattering of photons from the pump wave into the probe wave. This redistribution of energy amplifies the contrast of the stationary wave, which in turn amplifies the backscattering efficiency, etc. Therefore, the CARL converts kinetic energy into coherent radiation (or more precisely, into an increase of the energy difference between probe and pump) mediated by atomic bunching. It is a self-amplifying mechanism. The CARL signature is a transient exponential amplification for the incident probe, which defines the frequency of the 'CARL laser'.

The first experimental realization of CARL used an annular cavity [98].

6.3.1 Collective effects

To understand the dynamics of CARL we must understand how atomic ensembles commonly interact with light modes. Let us first consider two atoms: The generalization of the fundamental equations (6.23) to two atoms is,

$$\begin{aligned}\dot{\alpha}_+ &= -\kappa\alpha_+ - \imath U_0 e^{-2\imath k z_1}\alpha_- - \imath U_0 e^{-2\imath k z_2}\alpha_- + \eta_+ \\ \dot{\alpha}_- &= -\kappa\alpha_- - \imath U_0 e^{2\imath k z_1}\alpha_+ - \imath U_0 e^{2\imath k z_2}\alpha_+ .\end{aligned} \tag{6.35}$$

The equations decouple to $e^{-2\imath k z_1} = e^{-2\imath k z_2 - \imath\pi}$, such that the impact of the atoms on the light modes vanishes. This situation can be generalized to N atoms, for which the fundamental equations (6.23) are generalized to,

$$\begin{aligned}\dot{\alpha}_\pm &= (-\kappa - \imath N U_0)\alpha_\pm - \imath U_0 \sum_{m=1}^{N} e^{\mp 2\imath k z_m}\alpha_\mp + \eta_\pm \ , \\ \dot{p}_m &= -2\imath\hbar k U_0(\alpha_+\alpha_-^* e^{2\imath k z_m} - \alpha_-\alpha_+^* e^{-2\imath k z_m}) \ .\end{aligned} \tag{6.36}$$

If the quantity,

$$b \equiv \tfrac{1}{N}\sum_j e^{-2\imath k z_j} \neq 0 \ , \tag{6.37}$$

called *bunching parameter* vanishes, it means that the atomic density distribution is homogeneous. So, the phases of randomly scattered photons destructively interfere, and the impact of the scatterers on the light modes cancels out [10].

On the other hand, when atoms accumulate in the antinodes of the standing wave, this increases the contrast of their matter grating, so that light can be backscattered efficiently via Bragg scattering. The particularity of the CARL is that, during the temporal evolution, the bunching process can amplify itself leading to an exponential growth of the counterpropagating mode, accompanied by an increasingly pronounced self-bunching.

[10] See script on *Quantum mechanics* (2023), Sec. 20.1.2.

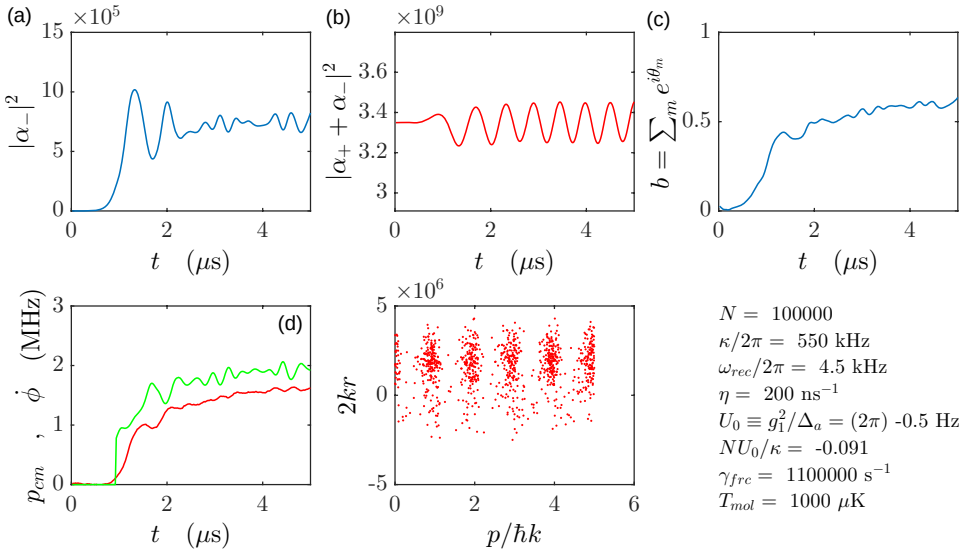

Figure 6.7: (code for download) Example for the time evolution of the dynamics of the CARL equation including an additional friction term and Langevin-type diffusion. Shown are (a) the number of photons in the probe mode, (b) the beat signal, (c) the bunching, (d) the phase of the standing wave and the position of the center-of-mass of the cloud, and (e) the dipole potential with the atomic distribution.

6.4 Quantization of the atomic motion in cavities

So far, the atomic motion in CARL has been treated classically, as well as cavity modes. In this section we will analyze effects due to the quantization of these degrees of freedom.

6.4.1 Modal expansion of the motion

Our starting point is the quantum version of the CARL equations (6.35),

$$\boxed{\begin{aligned} \dot{\hat{a}}_\pm &= (-\kappa + \imath\Delta_c - \imath U_0)\hat{a}_\pm - \imath U_0 e^{-2\imath k\hat{z}_j}\hat{a}_\mp + \eta_\pm \\ m\ddot{\hat{z}}_j &= 2\imath\hbar k U_0(\hat{a}_+^*\hat{a}_- e^{-2\imath k\hat{z}_j} - \hat{a}_+\hat{a}_-^* e^{2\imath k\hat{z}_j}) \end{aligned}} \; . \tag{6.38}$$

We note that the total momentum is a constant of motion,

$$[\hat{H}, 2\hbar k\hat{a}^\dagger\hat{a} + \sum_j \hat{p}_j] = 0 \; . \tag{6.39}$$

To treat the motion as being quantized we define a base $|n\rangle_j$,

$$\hat{p}_j|n\rangle_j = 2\hbar k n|n\rangle_j \qquad \text{and} \qquad |\psi(z_j\rangle = \sum_n c_{j,n}|n\rangle_j \; , \tag{6.40}$$

and calculate the expected value of the equations (6.38) regarding the atomic motion,

$$\begin{aligned}\frac{d\hat{a}}{dt} &= -\imath\Delta_c\hat{a} - iU_0\eta\sum_j \langle\psi(z_j)|e^{-2\imath k\hat{z}_j}|\psi(z_j)\rangle - \kappa_c\hat{a} \\ &= -\imath\Delta_c\hat{a} - \imath U_0\eta\sum_{j,m,n} c^*_{j,m}c_{j,n_j}\langle m|e^{-2\imath kz_j}|n\rangle_j - \kappa\hat{a} \\ &= -\imath\Delta_c\hat{a} - \imath U_0\eta\sum_{j,n} c^*_{j,n}c_{j,n+1} - \kappa\hat{a}\ .\end{aligned} \tag{6.41}$$

In addition, the Schrödinger equation $i\hbar\frac{d|\psi(\theta_j\rangle}{dt} = \hat{H}|\psi(z_j)\rangle$ yields,

$$\imath\hbar\sum_n \frac{dc_{j,n}}{dt}|n\rangle_j = \sum_n \frac{1}{2m}p_j^2 c_{j,n}|n\rangle_j + \frac{\hbar\Delta_c}{N}\hat{a}^\dagger\hat{a}\sum_n c_j(n)|n\rangle_j + \hbar U_0\eta\sum_n(\hat{a}^\dagger e^{-2\imath kz_j} + \hat{a}e^{2\imath kz_j})c_{j,n}|n\rangle_j\ . \tag{6.42}$$

Projecting on ${}_j\langle m|$, we obtain,

$$\boxed{\begin{aligned}\dot{c}_{j,m} &= -\imath\omega_r m^2 c_{j,m} - \imath\tfrac{\Delta_c}{N}\hat{a}^\dagger\hat{a}c_{j,m} - iU_0\eta[\hat{a}^\dagger c_{j,m+1} + ac_{j,m-1}] \\ \frac{d\tilde{a}}{dt} &= NU_m\eta\textstyle\sum_n c^*_{j,n}c_{j,n+1} - (\kappa_c + \imath\Delta_c)\tilde{a}\end{aligned}}\ . \tag{6.43}$$

where $\omega_r = \hbar 4k^2/2m$. The equations (6.43) can be used for numerical simulations [127].

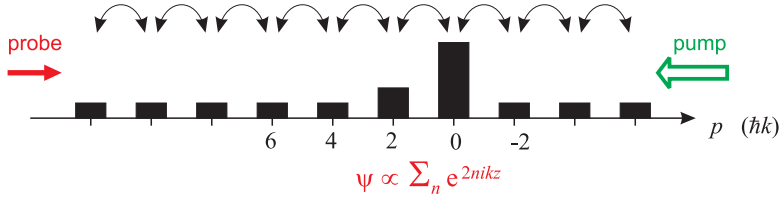

Figure 6.8: Probe light and 'bunching' when the temperature is raised.

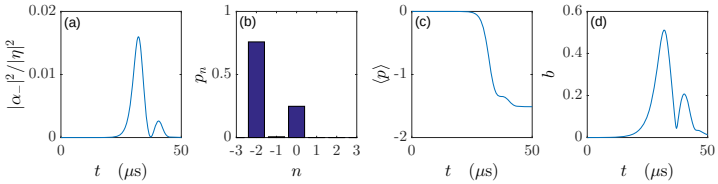

Figure 6.9: (code for download) Simulation of the CARL equation (6.43) in the superradiant, semi-classical, 'bad-cavity' regime for $\kappa_c = 4$, $\rho = 4$, $\Delta_c = 0$.

6.4.1.1 Bloch oscillations of atoms in optical lattices

Interestingly, the Bloch and the CARL dynamics can be combined [133, 134] resulting in a dynamics that can be exploited for the *in vivo* monitoring of Bloch oscillations, and the application in inertial sensing.

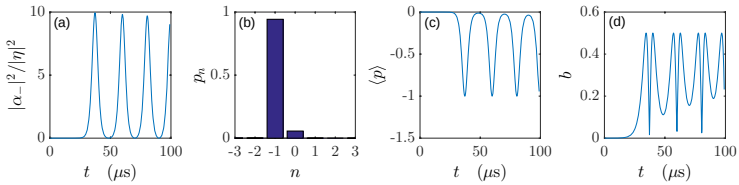

Figure 6.10: (code for download) Simulation of the CARL equation (6.43) in the superradiant, semi-classical, 'good-cavity' regime for $\kappa_c = 0.02$, $\rho = 4$, $\Delta_c = 0$.

6.5 Exercises

6.5.0.1 Ex: Stationary solution of the equations of motion

Derive the stationary solution of the equations of motion (6.23).

6.5.0.2 Ex: Normal mode splitting

From the stationary equations of Exc. 6.5.0.1, assuming one-way pumping, $\eta_- = 0$, calculate the transmission of the cavity as a function of the detunings Δ_a and Δ_c and the number of atoms.

6.5.0.3 Ex: Stationary position of the atom in a unidirectionally pumped ring cavity

What is the steady state position of an atom interacting with the modes of a unidirectionally pumped ring cavity?

6.6 Further reading

J.K. Asbóth et al., *Optomechanical coupling in a one-dimensional optical lattice* [DOI]

P.R. Berman, *Comparison of recoil-induced resonances and the collective atomic recoil laser* [DOI]

R. Bonifacio et al., *Collective atomic recoil laser (CARL) optical gain without inversion by collective atomic recoil and self-bunching of two-level atoms* [DOI]

R. Bonifacio et al., *A quantum model for collective recoil lasing* [DOI]

S. Bux et al., *Cavity-controlled matter wave superradiance at the recoil limit* [DOI]

J.-Y. Courtois et al., *Recoil-induced Resonances in Cesium: An Atomic Analog to the Free Electron Laser* [DOI]

R. Culver et al., *Collective strong coupling of cold potassium atoms in a ring cavity* [DOI]

M. Gangl et al., *Cold atoms in a high-Q ring cavity* [DOI]

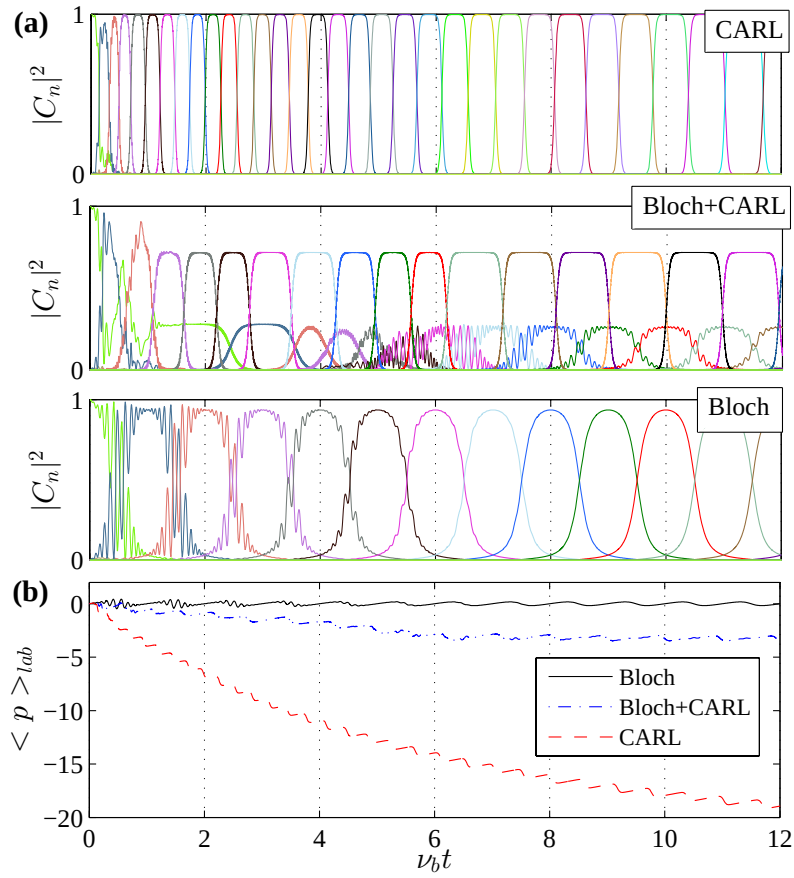

Figure 6.11: Illustration of the first Brillouin zone.

J. Guo et al., *Recoil-induced Resonances in Non-linear Spectroscopy* [DOI]

S. Gupta et al., *Cavity Nonlinear Optics at Low Photon Numbers from Collective Atomic Motion* [DOI]

P.R. Hemmer et al., *Self-Organization, Broken Symmetry, and Lasing in an Atomic Vapor: The Interdependence of Gratings and Gain* [DOI]

J. Léonard et al., *Supersolid formation in a quantum gas breaking continuous translational symmetry* [DOI]

G.-L. Lippi et al., *Spontaneous Generation of a Longitudinal Atomic Density Grating in Sodium Vapor* [DOI]

D.R. Meacher et al., *Method for Velocimetry of Cold Atoms* [DOI]

S. Ostermann et al., *Atomic self-ordering in a ring cavity with counterpropagating pump fields* [DOI]

E. Peik et al., *Bloch Oscillations of Atoms, Adiabatic Rapid Passage, and Monokinetic Atomic Beams* [DOI]

G.R.M. Robb, *Dispersive optical bistability in cold atomic vapours* [DOI]

R.J. Schulze et al., *Optomechanical approach to cooling of small polarizable particles in a strongly pumped ring cavity* [DOI]

S.C. Schuster et al., *Supersolid properties of a Bose-Einstein condensate in a ring resonator* [DOI]

M. Vengalattore et al., *Optical bistability at low light level due to collective atomic recoil* [DOI]

V. Vuletic et al., *Three-dimensional cavity Doppler cooling and cavity sideband cooling by coherent scattering* [DOI]

Bibliography

[1] C. S. Adams, H. J. Lee, N. Davidson, M. Kasevich, and S. Chu, *Evaporative cooling in a crossed dipole trap*, Phys. Rev. Lett. **74** (1995), 3577, .

[2] M. H. Anderson, J. R. Ensher, M. R. Matthews, C. E. Wieman, and E. A. Cornell, *Observation of Bose-Einstein condensation in a dilute atomic vapor*, Science **269** (1995), 198, .

[3] M. R. Andrews, M. O. Mewes, N. J. Van Druten, D. S. Durfee, D. M. Kurn, and W. Ketterle, *Direct, non-destructive observation of a bose condensate*, Science **273** (1996), 84.

[4] M. R. Andrews, D. M. Stamper-Kurn, H. J. Miesner, D. S. Durfee, C. G. Townsend, S. Inouye, and W. Ketterle, *Erratum: Propagation of sound in a Bose-Einstein condensate*, Phys. Rev. Lett. **80** (1997), 2967.

[5] E. Arimondo, M. Inguscio, and P. Violino, *Experimental determination of the hyperfine structure in the alkali atoms*, Rev. Mod. Phys. **49** (1977), 31.

[6] J. K. Asbóth, P. Domokos, H. Ritsch, and A. Vukics, *Self-organization in a cavity field: Threshold, bistability, and scaling laws*, Phys. Rev. A **72** (2005), 053417, DOI.

[7] A. Ashkin and J. P. Gordon, *Stability of radiation-pressure particle traps: an optical earnshaw theorem*, Opt. Lett. **8** (1978), 511, DOI.

[8] N. W. Ashkroft and D. N. Mermin, *Solid state physics*, Hartcourt College publishers, 1976, ISBN.

[9] D. R. Bates and A. Daamgard, *The calculation of the absolute strenghts of spectral lines*, Phil. Tr. R. Soc. A **242** (1949), 101.

[10] J. Bergquist, R. G. Hulet, W. M. Itano, and D. J. Wineland, *Observation of quantum jumps in a single atom*, Phys. Rev. Lett. **57** (1986), 1699.

[11] Hans A. Bethe and Edwin E. Salpether, *Quantum mechanics of one- and two-electron atoms*, Springer-Verlag, 1 ed., Berlin, 1957, ISBN.

[12] M. J. Bhaseen, J. Mayoh, B. D. Simons, and J. Keeling, *Dynamics of nonequilibrium Dicke models*, Phys. Rev. A **85** (2012), 013817, DOI.

[13] C. A. Blockley, D. F. Walls, and H. Risken, *Quantum collapses and revivals in a quantized trap*, Europhys. Lett. **17** (1992), 509.

[14] J. G. Bohnet, K. C. Cox, M. A. Norcia, J. M. Weiner, Z. Chen, and J. K. Thompson, *Reduced spin measurement back-action for a phase sensitivity ten times beyond the standard quantum limit*, Nature Phot. **8** (2014), 731, DOI.

[15] R. Bonifacio and L. De Salvo, *Collective atomic recoil laser (carl) optical gain without inversion by collective atomic recoil and self-bunching of two-level atoms*, Nucl. Instrum. Methods A **341** (1994), 360, DOI.

[16] Satyendra N. Bose, *Plancks gesetz und lichtquantenhypothese*, Z. Phys. **26** (1924), 178.

[17] C. C. Bradley, C. A. Sackett, and R. G. Hulet, *Analysis of in situ images of Bose-Einstein condensates of lithium*, Phys. Rev. A **55** (1997), 3951, .

[18] C. C. Bradley, C. A. Sackett, J. J. Tolett, and R. G. Hulet, *Evidence of Bose-Einstein condensation in an atomic gas with attractive interactions*, Phys. Rev. Lett. **75** (1995), 1687, .

[19] B. H. Bransden and C. J. Joachain, *Physics of atoms and molecules*, 1983, ISBN.

[20] F. Brennecke, T. Donner, S. Ritter, T. Bourdel, M. Köhl, and T. Esslinger, *Cavity QED with a Bose-Einstein condensate*, Nature **250** (2007), 268, .

[21] A. Bychek, Ch. Hotter, D. Plankensteiner, and H. Ritsch, *Superradiant lasing in inhomogeneously broadened ensembles with spatially varying coupling*, ePrints (2021), arXiv2105.11023, DOI.

[22] Y. Castin and R. Dum, *Bose-Einstein condensates in time dependent traps*, Phys. Rev. Lett. **77** (1996), 5315, .

[23] Steve Chu, J. E. Bjorkholm, A. Ashkin, and A. Cable, *Experimental observation of optically trapped atoms*, Phys. Rev. Lett. **57** (1986), 314.

[24] A. Cipris, N. A. Moreira, T. S. do Espirito Santo, P. Weiss, C. J. Villas-Boas, R. Kaiser, W. Guerin, and R. Bachelard, *Subradiance with saturated atoms: Population enhancement of the long-lived states*, Phys. Rev. Lett. **126** (2021), 103604, DOI.

[25] C. Cohen-Tannoudji, B. Diu, and F. Lao, *Quantum mechanics*, 1, vol. 1 & 2, 1977, ISBN.

[26] C. Cohen-Tannoudji, J. Dupont-Roc, and G. Grynberg, *Photons and atoms: Introduction to quantum electrodynamics*, John Wiley and Sons New York, 1992, ISBN.

[27] M. J. Collett and C. W. Gardiner, *Squeezing of intracavity and travelling-wave light fields produced in parametric amplification*, Phys. Rev. A **30** (1984), 1386, .

[28] Y. Colombe, T. Steinmetz, G. Dubois, F. Linke, D. Hunger, and J. Reichel, *Strong atom field coupling for bose Einstein condensates in an optical cavity on a chip*, Nature **250** (2005), 272, .

[29] E. A. Cornell, *Very cold indeed: The nanokelvin physics of Bose-Einstein condensation*, J. Res. Natl. Inst. Stand. Tech. **101** (1996), 419.

[30] Ph. W. Courteille, V. S. Bagnato, and V. I. Yukalov, *Bose-Einstein condensation of trapped atomic gases*, Laser Phys. **11** (2001), 659–800.

[31] Ph. W. Courteille, S. Bux, E. Lucioni, K. Lauber, T. Bienaimé, R. Kaiser, and N. Piovella, *Modification of radiation pressure due to cooperative scattering of light*, Euro. Phys. J. D **58** (2010), 69.

[32] Ph. W. Courteille, B. Deh, J. Fortágh, A. Günther, S. Kraft, C. Marzok, S. Slama, and C. Zimmermann, *Highly versatile atomic micro traps generated by multifrequency magnetic field modulation*, J. Phys. B **39** (2006), 1055.

[33] Ph. W. Courteille, D. J. Han, R. H. Wynar, and D. J. Heinzen, *New observation of Bose-Einstein condensation of* ^{87}*rb atoms in a magnetic top trap*, Proc. of SPIE **3270** (1998), 116.

[34] K. C. Cox, G. P. Greve, J. M. Weiner, and J. K. Thompson, *Deterministic squeezed states with collective measurements and feedback*, Phys. Rev. Lett. **116** (2016), 093602, DOI.

[35] R. Culver, A. Lampis, B. Megyeri, K. Pahwa, L. Mudarikwa, M. Holynski, Ph. W. Courteille, and J. Goldwin, *Collective strong coupling of cold potassium atoms in a ring cavity*, New J. Phys. **18** (2016), 113043.

[36] M. Ben Dahan, E. Peik, Y. Castin, and C. Salomon, *Bloch oscillations of atoms in an optical potential*, Phys. Rev. Lett. **76** (1996), 4508, .

[37] J. Dalibard, Y. Castin, and K. Molmer, *Wave-function approach to dissipative processes in quantum optics*, Phys. Rev. Lett. **68** (1992), 580, DOI.

[38] J. Dalibard and C. Cohen-Tannoudji, *Dressed-atom approach to atomic motion in laser light: The dipole force revisited*, J. Opt. Soc. Am. B **2** (1985), 1707.

[39] ———, *Laser cooling below the doppler limit by polarization gradients: Simple theoretical studies*, J. Opt. Soc. Am. B **6** (1989), 2023.

[40] N. Davidson, H. J. Lee, C. S. Adams, M. Kasevich, and S. Chu, *Long atomic coherence times in an optical dipole trap*, Phys. Rev. Lett. **74** (1995).

[41] K. B. Davis, M.-O. Mewes, M. A. Joffe, M. R. Andrews, and W. Ketterle, *Evaporative cooling of sodium atoms*, Phys. Rev. Lett. **74** (1995), 5202, .

[42] K. B. Davis, M.-O. Mewes, and W. Ketterle, *An analytical model for evaporative cooling of atoms*, Appl. Phys. B **60** (1995), 155, .

[43] K. Debnath, Y. Zhang, and K. Mølmer, *Lasing in the superradiant crossover regime*, Phys. Rev. A **98** (2018), 063837, DOI.

[44] G. Delannoy, S. G. Murdoch, V. Boyer, V. Josse, P. Bouyer, and A. Aspect, *Understanding the production of dual Bose-Einstein condensation with sympathetic cooling*, Phys. Rev. A **63** (2001), 051602, .

[45] B. DeMarco and D. S. Jin, *Onset of fermi-degeneracy in a trapped atomic gas*, Science **285** (1999), 1703, DOI.

[46] M. T. DePue, C. McCormick, S. L. Winoto, S. Oliver, and D. S. Weiss, *Unity occupation of sites in a 3d optical lattice*, Phys. Rev. Lett. **82** (1999), 2262, DOI.

[47] R. G. DeVoe and R. G. Brewer, *Observation and superradiant and subradiant spontaneous emission of two trapped ions*, Phys. Rev. Lett. **76** (1996), 2049, DOI.

[48] R. H. Dicke, *Coherence in spontaneous radiation processes*, Phys. Rev. **93** (1954), 99, DOI.

[49] F. Diedrich, J.C. Bergquist, W.I. Itano, and D.J. Wineland, *Laser cooling to the zero-point energy of motion*, Phys. Rev. Lett. **62** (1989), 403, .

[50] P. Domokos and H. Ritsch, *Collective cooling and self-organization of atoms in a cavity*, Phys. Rev. Lett. **89** (2002), 253003, DOI.

[51] A. R. Edmonds, *Angular momentum in quantum mechanics*, 1957.

[52] A. Einstein, *On the quantum theory of radiation*, Zeitschrift für Physik **18** (1917), 121.

[53] _____, *Quantentheorie des einatomigen idealen gases*, S. B. Kgl. Preuss. Akad. Wiss. **35** (1924).

[54] J. Eiselt and H. Risken, *Quasiprobability distributions for the Jaynes-Cummings model with cavity damping*, Phys. Rev. A **43** (1991), 346.

[55] Th. Elsässer, B. Nagorny, and A. Hemmerich, *Collective sideband cooling in an optical ring cavity*, Phys. Rev. A **67** (2003), 051401(R), .

[56] C. Emary and T. Brandes, *Quantum chaos triggered by precursors of a quantum phase transition: The Dicke model*, Phys. Rev. Lett. **90** (2003), 044101, DOI.

[57] J. R. Ensher, D. S. Jin, M. R. Matthews, C. E. Wieman, and E. A. Cornell, *Bose-Einstein condensation in a dilute gas: Measurement of energy and ground-state occupation*, Phys. Rev. Lett. **77** (1996), 4984, .

[58] W. Ertmer, R. Blatt, J. L. Hall, and M. Zhu, *Laser manipulation of atomic beam velocities: Demonstration of stopped atoms and velocity reversal*, Phys. Rev. Lett. **54** (1985), 996.

[59] DOIR. Bachelard and N. Piovella and Ph. W. Courteille, *Cooperative scattering and radiation pressure force in dense atomic clouds*, Phys. Rev. A **84** (2011), 013821.

[60] D. G. Fried, T. C. Killian, L. Willmann, D. Landhuis, S. C. Moss, D. Kleppner, and T. J. Greytak, *Bose-Einstein condensation of atomic hydrogen*, Phys. Rev. Lett. **81** (1998), 3811, .

[61] S. Gammelmark and K. Molmer, *Phase transitions and Heisenberg limited metrology in an ising chain interacting with a single-mode cavity field*, New J. Phys. **13** (2011), 053035, DOI.

[62] ———, *Interacting spins in a cavity: Finite-size effects and symmetry-breaking dynamics*, Phys. Rev. A **85** (2012), 042114, DOI.

[63] M. Gangl and H. Ritsch, *3d dissipative motion of atoms in a strongly coupled driven cavity*, Eur. Phys. J. D **8** (2000), 29, .

[64] C. W. Gardiner and M. J. Collett, *Input and output in damped quantum systems: Quantum stochastic differential equations and the master equation*, Phys. Rev. A **31** (1985), 3761, .

[65] B. M. Garraway, *The Dicke model in quantum optics: Dicke model revisited*, Phil. Trans. R. Soc. A **369** (2011), 1137, DOI.

[66] M. Gegg, A. Carmele, A. Knorr, and M. Richter, *Superradiant to subradiant phase transition in the open system Dicke model: dark state cascades*, New J. Phys. **20** (2018), 013006, DOI.

[67] J. Gelhausen, M. Buchhold, A. Rosch, and P. Strack, *Quantum-optical magnets with competing short- and long-range interactions: Rydberg-dressed spin lattice in an optical cavity*, SciPost Phys. **1** (2016), 004, DOI.

[68] R. Graham and D. Walls, *Spectrum of light scattered from a weakly interacting Bose-Einstein condensed gas*, Phys. Rev. Lett. **76** (1996), 1774.

[69] M. Greiner, O. Mandel, T. Esslinger, T. W. Hänsch, and I. Bloch, *Quantum phase transition from a superfluid to a mott insulator in a gas of ultracold atoms*, Nature **415** (2002), 39, .

[70] D. J. Griffiths, *Introduction to quantum mechanics*, Pearson Prentice Hall, New Jersey, 2005, ISBN.

[71] R. Grimm, M. Weidemüller, and Y. B. Ovchinnikov, *Optical dipole traps for neutral atoms*, Adv. At. Mol. Opt. Phys. **42** (2000), 95, .

[72] G. Grynberg, B. Lounis, P. Verkerk, J.-Y. Courtois, and C. Salomon, *Quantized motion of cold cesium atoms in two- and three-dimensional optical potentials*, Phys. Rev. Lett. **70** (1993), 2249, .

[73] J. Hald, J. L. Sorensen, C. Schori, and E. S. Polzik, *Spin squeezed atoms: A macroscopic entangled ensemble created by light*, Phys. Rev. Lett. **83** (1999), 1319, .

[74] D. S. Hall, J. R. Ensher, D. S. Jin, and et al., *Recent experiments with Bose-condensed gases at JILA*, Proc. SPIE **3270** (1998), 98, cond-mat/9903459.

[75] D. J. Han, R. H. Wynar, Ph. W. Courteille, and D. J. Heinzen, *Bose-Einstein condensation of large numbers of atoms in a magnetic time-averaged orbiting potential trap*, Phys. Rev. A **57** (1998), R4114.

[76] S. Haroche, J. C. Gay, and G. Grynberg (eds.), *Atom traps*, World Scientific, 1989.

[77] T. Hartmann, F. Keck, H. J. Korsch, and S. Mossmann, *Dynamics of Bloch oscillations*, New J. Phys. **6** (2004), 2.

[78] D. J. Heinzen, J. J. Childs, J. E. Thomas, and M. S. Feld, *Enhanced and inhibited visible spontaneous emission by atoms in a confocal resonator*, Phys. Rev. Lett. **58** (1987), 1320, DOI.

[79] D. J. Heinzen and M. S. Feld, *Vacuum radiative level shift and spontaneous-emission linewidth of an atom in an optical resonator*, Phys. Rev. Lett. **59** (1987), 2623, DOI.

[80] K. Helmerson, A. Martin, and D. E. Pritchard, *Laser and rf spectroscopy of magnetically trapped neutral atoms*, J. Opt. Soc. Am. B **9** (1992), 483.

[81] K. Hepp and E. Lieb, *On the superradiant phase transition for molecules in a quantized radiation field: the Dicke maser model*, Annals of Phys. **76** (1973), 360, DOI.

[82] H. F. Hess, *Evaporative cooling of magnetically trapped spin-polarized hydrogen*, Phys. Rev. B **34** (1986), 3476.

[83] T. W. Hijmans, Yu. Kagan, and G. V. Shlyapnikov, *Bose condensation and relaxation explosion in magnetically trapped atomic hydrogen*, Phys. Rev. B **48** (1993), 12886, .

[84] M. J. Holland, D. S. Jin, M. L. Ciafalo, and J. Cooper, *Emergence of interaction effects in Bose-Einstein condensation*, Phys. Rev. Lett. **78** (1997), 3801, .

[85] R. Huesmann, Ch. Balzer, Ph. W. Courteille, W. Neuhauser, and P. E. Toschek, *Single-atom interferometry*, Phys. Rev. Lett. **82** (1999), 1611.

[86] S. Inouye, M. R. Andrews, J. Stenger, H.-J. Miesner, D. M. Stamper-Kurn, and W. Ketterle, *Observation of Feshbach resonances in a Bose-Einstein condensate*, Nature **392** (1998), 151, DOI.

[87] W. M. Itano, J. C. Bergquist, J. J. Bollinger, J. M. Gilli-Gans, D. J. Heinzen, F. L. Moore, M. G. Raizen, and D. J. Wineland, *Quantum projection noise: Population fluctuations in two-level systems*, Phys. Rev. A **47** (1993), 3554, DOI.

[88] J. Javanainen and J. Ruostekoski, *Off-resonance light scattering from low-temperature bose and Fermi gases*, Phys. Rev. A **52** (1995), 3033, .

[89] E. T. Jaynes and F. W. Cummings, *Comparison of quantum and semiclassical radiation theories with application to the beam maser*, Proc. IEEE **51** (1963), 89.

[90] D. S. Jin, J. R. Ensher, M. R. Matthews, C. E. Wieman, and E. A. Cornell, *Collective excitations of a Bose-Einstein condensate in a dilute gas*, Phys. Rev. Lett. **77** (1996), 420, .

[91] B. Juisgaard, A. Kozhekin, and E. S. Polzik, *Experimental long-lived entanglement of two macroscopic objects*, Nature **413** (2001), 400, .

[92] W. Ketterle and N. J. Van Druten, *Bose-Einstein condensation of a finite number of particles trapped in one or three dimensions*, Phys. Rev. A **54** (1996), 656.

[93] ———, *Evaporative cooling of trapped atoms*, Adv. At. Mol. Opt. Phys. **37** (1996), 181, .

[94] W. Ketterle, D. S. Durfee, and D. M. Stamper-Kurn, *Making, probing and understanding Bose-Einstein condensates*, Proc. Int. School of Phys. Enrico Fermi **CXL** (1999), 67, .

[95] P. Kirton, M. M. Roses, J. Keeling, and E. G. Dalla Torre, *Introduction to the Dicke model: From equilibrium to nonequilibrium, and vice versa*, Adv. Quantum Technol. **2** (2019), 1800043, DOI.

[96] M. Kitagawa and M. Ueda, *Squeezed spin states*, Phys. Rev. A **47** (1993), 5138, DOI.

[97] D. Kruse, M. Ruder, J. Benhelm, C. von Cube, C. Zimmermann, Ph. W. Courteille, B. Nagorny, Th. Elsässer, and A. Hemmerich, *Cold atoms in a high-q ring-cavity*, Phys. Rev. A **67** (2003), 051802(R).

[98] D. Kruse, C. von Cube, C. Zimmermann, and Ph. W. Courteille, *Observation of lasing mediated by collective atomic recoil*, Phys. Rev. Lett. **91** (2003), 183601.

[99] A. Kuzmich, L. Mandel, and N. P. Bigelow, *Generation of spin squeezing via continuous quantum nondemolition measurement*, Phys. Rev. Lett. **85** (2000), 1594, DOI.

[100] W. E. Jr. Lamb, *Anti-photon*, Appl. Phys. B **60** (1995), 77, DOI.

[101] J. Lawall, S. Kulin, B. Saubamea, N. Bigelow, M. Leduc, and C. Cohen-Tannoudji, *Three-dimensional laser cooling of helium beyond the single-photon recoil limit*, Phys. Rev. Lett. **75** (1995), 4194.

[102] M. Lewenstein and Juha Javanainen, *Cooperative quantum jumps with two atoms*, Phys. Rev. Lett. **59** (1987), 1289, .

[103] R. Loudon, *The quantum theory of light*, Clarendon Press Oxford, 1982, ISBN.

[104] A. G. Martin, K. Helmerson, V. S. Bagnato, G. P. Lafyatis, and D. E. Pritchard, *Rf spectroscopy of trapped neutral atoms*, Phys. Rev. Lett. **61** (1988), 2431, .

[105] N. Marzari, A. A. Mostofi, J. R. Yates, I. Souza, and D. Vanderbilt, *Maximally localized wannier functions: Theory and applications*, Rev. Mod. Phys. **84** (2012), 1419, DOI.

[106] N. Masuhara, J. M. Doyle, J. C. Sandberg, D. Kleppner, T. J. Greytak, H. F. Hess, and G. P. Kochanski, *Evaporative cooling of spin-polarized atomic hydrogen*, Phys. Rev. Lett. **61** (1988).

[107] D. Meiser, Jun Ye, D. R. Carlson, and M. J. Holland, *Prospects for a millihertz-linewidth laser*, Phys. Rev. Lett. **102** (2009), 163601, DOI.

[108] M.-O. Mewes, M. R. Andrews, N. J. van Druten, D. M. Kurn, D. S. Durfee, C. G. Townsend, and W. Ketterle, *Collective excitations of a Bose-Einstein condensation in a magnetic trap*, Phys. Rev. Lett. **77** (1996), 988, .

[109] G. Milburn, *Intrinsic decoherence in quantum mechanics*, Phys. Rev. A **44** (1991), 5401, .

[110] J. D. Miller, R. A. Cline, and D. J. Heinzen, *Far-off-resonance optical trapping of atoms*, Phys. Rev. A **47** (1993), R4567, .

[111] K. Mølmer, Y. Castin, and J. Dalibard, *Monte-carlo wave-function method in quantum optics*, J. Opt. Soc. Am. B **10** (1993), 524, DOI.

[112] C. Monroe, E. A. Cornell, C. A. Sackett, C. J. Myatt, and C. E. Wieman, *Measurement of cs-cs elastic scattering at t=30uk*, Phys. Rev. Lett. **70** (1993), 414, .

[113] M. Mudrich, S. Kraft, K. Singer, R. Grimm, A. Mosk, and M. Weidemüller, *Sympathetic cooling with two atomic species in an optical trap*, Phys. Rev. Lett. **88** (2002), 253001.

[114] C. J. Myatt, E. A. Burt, R. W. Ghrist, E. A. Cornell, and C. E. Wieman, *Production of two overlapping Bose-Einstein condensates by sympathetic cooling*, Phys. Rev. Lett. **78** (1997), 586, DOI.

[115] W. Nagourney, J. Sandberg, and H. G. Dehmelt, *Shelved optical electron amplifier: Observation of quantum jumps*, Phys. Rev. Lett. **56** (1986), 2797.

[116] M. A. Norcia, R. J. Lewis-Swan, J. R. K. Cline, Bihui Zhu, A. M. Rey, and J. K. Thompson, *Cavity-mediated collective spin-exchange interactions in a strontium superradiant laser*, Science **361** (2018), 259, DOI.

[117] E. Peik, M. Ben Dahan, I. Bouchoule, Y. Castin, and C. Salomon, *Bloch oscillations of atoms, adiabatic rapid passage, and monokinetic atomic beams*, Phys. Rev. A **55** (1997), 2989, DOI.

[118] M. Perrin, G.-L. Lippi, and A. Politi, *Phase-transition in a radiation-matter interaction with recoil and collisions*, Phys. Rev. Lett. **86** (2001), 4520, .

[119] W. Petrich, M. H. Anderson, J. R. Ensher, and E. A. Cornell, *Stable, tightly confining trap for evaporative cooling of neutral atoms*, Phys. Rev. Lett. **74** (1995), 3352, .

[120] William D. Phillips and Harold Metcalf, *Laser deceleration of an atomic beam*, Physical Review Letters **48** (1982), 596.

[121] Ravinder Puri, *Mathematical methods of quantum optics*, Springer Series in Optical Sciences (2000).

[122] I. I. Rabi, *Space quantization in a gyrating magnetic field.*, Phys. Rep. **51** (1937), 652.

[123] N. F. Ramsey, *Molecular beams*, Clarendon Press, Oxford, 1985, ISBN.

[124] A. Rauschenbeutel, G. Nogues, S. Osnaghi, P. Bertet, M. Brune, J.-M. Raimond, and S. Haroche, *Step-by-step engineering of multiparticle entanglement*, Science **288** (2000), 2024.

[125] N. E. Rehler and J. H. Eberly, Phys. Rev. A **3** (1971), 1735, DOI.

[126] H. Ritsch, P. Domokos, F. Brennecke, and T. Esslinger, *Cold atoms in cavity-generated dynamical optical potentials*, Rev. Mod. Phys. **85** (2013), 553, DOI.

[127] G. R. M. Robb and B. W. J. McNeil, *Four-wave mixing with self-phase matching due to collective atomic recoil*, Phys. Rev. Lett. **94** (2005), 023901, .

[128] F. Robicheaux and J. V. Hernández, *Many-body wave function in a dipole blockade configuration*, Phys. Rev. A **72** (2005), 063403, DOI.

[129] M. Rotenberg, N. Metropolis, R. Birins, and J. Wooten Jr., *The 3j and 6j symbols*, 1959, ISBN.

[130] J. R. Rubbmark, M. M. Kash, M. G. Littman, and D. Kleppner, *Dynamical effects at avoided level crossings: A study of the Landau-Zener effect using Rydberg atoms*, Phys. Rev. A **23** (1981), 3107.

[131] S. A. Sackett, D. Kielpinski, B. E. King, C. Langer, V. Meyer, C. J. Myatt, M. Rowe, Q. A. Turchette, W. M. Itano, D. J. Wineland, and C. Monroe, *Experimental entanglement of four particles*, Nature **404** (2000), 256.

[132] L. Salvi, N. Poli, V. Vuletić, and G. M. Tino, *Squeezing on momentum states for atom interferometry*, Phys. Rev. Lett. **120** (2018), 033601, DOI.

[133] M. Samoylova, N. Piovella, M. Holynski, Ph.W. Courteille, and R. Bachelard, *One-dimensional photonic band gaps in optical lattices*, Annual Review of Cold Atoms and Molecules **2** (2014), 193.

[134] M. Samoylova, N. Piovella, G. Robb, R. Bachelard, and Ph. W. Courteille, *Synchronisation of Bloch oscillations by a ring cavity*, Opt. Exp **23** (2015), 14823.

[135] G. Santarelli, Ph. Laurent, P. Lemonde, A. Clairon, A. G. Mann, S. Chang, A. N. Luiten, and C. Salomon, *Quantum projection noise in an atomic fountain: A high stability cesium frequency standard*, Phys. Rev. Lett. **82** (1999), 4619, .

[136] Th. Sauter, R. Blatt, W. Neuhauser, and P.E. Toschek, *Observation of quantum jumps*, Phys. Rev. Lett. **57** (1986), 1696, .

[137] ———, *Quantum jumps observed in the fluorescence of a single ion*, Opt. Comm. **60** (1986), 287, .

[138] E. Schrödinger, Brit. Journ. f. the Philos. of Science III (1952).

[139] A. S. Schumovsky, R. Taras, and Tram Quang, *Collective jumps in a system of three-level atoms*, Opt. Comm. **64** (1987), 45.

[140] Jiteng Sheng, Yuanxi Chao, Santosh Kumar, Haoquan Fan, J. Sedlacek, and J. P. Shaffer, *Intracavity Rydberg-atom electromagnetically induced transparency using a high-finesse optical cavity*, Phys. Rev. A **96** (2017), 033813, DOI.

[141] S. Slama, C. von Cube, B. Deh, A. Ludewig, C. Zimmermann, and Ph. W. Courteille, *Phase-sensitive detection of bragg-scattering at 1d optical lattices*, Phys. Rev. Lett. **94** (2005), 193901.

[142] S. Slama, C. von Cube, M. Kohler, C. Zimmermann, and Ph. W. Courteille, *Multiple reflections and diffuse scattering in bragg scattering at optical lattices*, Phys. Rev. A **73** (2006), 023424.

[143] S. Slama, C. von Cube, A. Ludewig, M. Kohler, C. Zimmermann, and Ph. W. Courteille, *Dimensional crossover in bragg scattering from optical lattices*, Phys. Rev. A **72** (2005), 031402(R).

[144] J. Stanojevic and R. Côté, *Many-body Rabi oscillations of Rydberg excitation in small mesoscopic samples*, Phys. Rev. A **80** (2009), 033418, DOI.

[145] R. J. Thompson, G. Rempe, and H. J. Kimble, *Observation of normal mode splitting for an atom in an optical cavity*, Phys. Rev. Lett. **68** (1992), 1132, .

[146] G. Tóth, C. Knapp, O. Gühne, and H. J. Briegel, *Optimal spin squeezing inequalities detect bound entanglement in spin models*, Phys. Rev. Lett. **99** (2007), 250405, DOI.

[147] ———, *Spin squeezing and entanglement*, Phys. Rev. A **79** (2009), 042334, DOI.

[148] J. Weiner and P.-T. Ho, *Light-matter interaction, fundamentals and applications*, John Wiley & Sons, Hokoken, New Jersey, 2003, ISBN.

[149] V. Weisskopf and E. Wigner, *Berechnung der natiirlichen linienbreite auf grund der diracschen lichttheorie*, Zeitschrift für Physik **63** (1930), 54.

[150] D. J. Wineland, J. J. Bollinger, W. M. Itano, and D. J. Heinzen, *Squeezed atomic states and projection noise in spectroscopy*, Phys. Rev. A **50** (1994), 67, DOI.

[151] D. J. Wineland and H. G. Dehmelt, *Proposed* $10^{14}\delta n < n$ *laser fluorescence spectroscopy on* Tl^{+} *mono-ion oscillator*, Bull. Am. Phys. Soc. **20** (1975), 637.

[152] H. M. Wiseman, *Light amplification without stimulated emission: Beyond the standard quantum limit to the laser linewidth*, Phys. Rev. A **60** (1999), 4083, DOI.

[153] Huang Wu and Ch. J. Foot, *Direct simulation of evaporative cooling*, J. Phys. B **29** (1996), L321, .

[154] Jin-Hui Wu, M. Artoni, and G. C. La Rocca, *Controlling the photonic band structure of optically driven cold atoms*, J. Opt. Soc. Am. B **25** (2008), 1840, DOI.

[155] Deshui Yu, *Photonic band structure of the three-dimensional* ^{88}*sr atomic lattice*, Phys. Rev. A **84** (2011), 043833, DOI.

[156] Yuan Zhang, Yu-Xiang Zhang, and K. Mølmer, *Monte-carlo simulations of superradiant lasing*, New J. Phys. **20** (2018), 112001, DOI.

[157] Bihui Zhu, J. Marino, N. Y. Yao, M. D. Lukin, and E. A. Demler, *Dicke time crystals in driven-dissipative quantum many-body systems*, Phys. Rev. Lett. **21** (2019), 073028, DOI.

Index

absorption coefficient, 120
absorption imaging, 121
adiabatic elimination, 177
adiabatic potential, 84, 93, 117
adiabatic sweep, 40
Airy formula, 134
annihilation operator, 44
atom laser, 95
atom optics, 95
Autler-Townes splitting, 40
avoided crossing, 84, 117

Bloch equation
    optical, 27
Bloch oscillation, 173
Bloch state, 173
Bloch vector, 29
    generalized, 38
Bloch-Siegert shift, 27, 47
Bohr
    Niels, 2
Boltzmann distribution, 114
Bose-Einstein condensation, 95
Bragg reflection, 174
bunching parameter, 181

CARL, 180
chemical potential, 114
coherence, 26
coherent spin state, 148
coherent states, 53
collapse and revival
    quantum, 54
collective atomic recoil laser, 180
collision rate, 35
completeness relation, 19
Compton scattering, 91
cooperativity, 137
cooperativity parameter, 138
correlated
    quantum jump, 160
Coulomb gauge, 43
creation operator, 44
critical atom number, 138
cross section
    optical, 87

dark resonance, 40, 41
dark-ground imaging, 123
de Broglie wave, 96
de Broglie wavelength
    thermal, 98
decay rate of the cavity, 134
Democritus, 2
density operator, 18
density-of-states, 114
detuning, 9
Dicke model, 144
Dicke state, 148
dipolar force, 99
dipolar gradient force, 87
dispersion coefficient, 120
dispersive imaging, 123
Doppler broadening, 35
Doppler cooling, 99
Doppler cooling limit, 100
Doppler effect, 33
Doppler limit, 97
Doppler shift, 35
Doppler-free spectroscopy, 34
dressed state, 11, 43, 47
duality principle, 3
dynamic Stark shift, 124

effective Hamiltonian, 15
EIT, 41
elastic collisions, 34
elastic scattering, 90
electromagnetically induced absorption,
        41
electromagnetically induced transparency,
        41
Ernst
    Ising, 162
evaporation, 113

Fabry-Pérot etalon, 176
far off-resonance optical trap, 110
Fermi's golden rule, 7
ferromagnetism, 162

finesse, 134
Fock state, 43
forced evaporation, 116
FORT, 111
free spectral range, 134
fugacity, 114

Gross-Pitaevskii equation, 11
Grotian diagram, 29

heating rate, 112
Heisenberg equation, 32
homogeneous broadening, 33

inhomogeneous broadening, 33, 36
Ioffe-Pritchard trap, 82
Ising model, 162

Jaynes-Cummings model, 48, 143
Josephson junction, 174
jump operator, 131

Lamb-dip, 34
Lambert-Beer law, 120
Landé factor, 79
Landau-Zener formula, 118
Langevin equation, 32
Larmor frequency, 81
laser gyroscopes, 178
Leucippus, 2
light shift, 11, 124
light-shift, 40
Lindbladt operator, 37
Liouville equation, 25
Liouville operator, 25

magnetic bottle, 82
magneto-optical trap, 107
Majorana spin-flip, 81
master equation, 37, 177
Maxwell-Boltzmann distribution, 97
Maxwell-Boltzmann law, 98
mean-field approximation, 146
mode volume, 133
Monte Carlo simulation, 11
Monte Carlo wavefunction simulation
    quantum, 15
MOT, 107

Mott insulator, 151

Newton method, 11
normal mode splitting, 140, 178
number state, 43
nutation, 30

open
    Dicke model, 156
optical density, 121
optical theorem, 120
optical tweezer, 110

Pauli spin matrices, 29
phase contrast imaging, 123
phase space density, 98
phonon, 43
photon, 43
photon echo method, 33
photonic recoil, 97
Planck
    Max, 2
polarization contrast imaging, 123
polarization gradient cooling, 100
population, 26
population inversion, 30
power broadening, 32
precession, 30, 31
product state, 148
Purcell factor, 136
pure state, 18

Q-function, 57
quantum jump, 15
quantum projection noise, 151
quantum trajectory, 15

Rabi, 143
Rabi frequency, 9, 46, 86
    generalized, 9, 27
Rabi splitting
    vacuum, 54, 178
radiation pressure, 99
radiation pressure force, 87
radiation trapping, 109
Raman sideband cooling, 106
Rayleigh length, 111
refraction, 124

relaxation explosion, 81
resolution parameter, 139
resonant enhancement, 134
rigid rotor, 30
ring cavity, 176
rotating wave approximation, 9, 27
run-away evaporation, 117
Runge-Kutta method, 11
Rydberg blockade, 160

saturation broadening, 32
saturation intensity, 34
saturation parameter, 32, 34, 139
scattering length
    interspecies, 119
Schawlow-Townes limit, 135
Schlieren method, 123
Schrödinger picture, 25, 27
spin flip, 118
spin relaxation, 111
spinning top, 30
squeezing
    spin, 151
squeezing operator, 153
standard deviation, 36
statistical operator, 18
steepest descent method, 11
Stern-Gerlach experiment, 79
STIRAP, 40
structure factor, 136
subradiance, 160
superfluorescence, 160
superoperator, 25
superradiance, 159
superradiant laser, 160
superradiant lasing, 159
sympathetic cooling, 113, 119

Tavis-Cummings model, 144, 148, 159
thermalization, 114
time-of-flight, 120
trace, 20
transit time broadening, 33

Voigt profile, 37
von Neumann equation, 25

Weisskopf-Wigner theory, 130

XX-Heisenberg model, 164